# Eluvial Chromite Resources of the Great Dyke of Zimbabwe

**Caston T Musa**

**A Thesis submitted in partial fulfillment of the requirements for the degree of Master of Science in Economic Geology**

Geology Department
Faculty of Science
Rhodes University, 2006

Abstract

Apart from the concentrations of chromite in layers within the Great Dyke and other ultramafic complexes, chromite also occurs as interstitial grains throughout the olivine-bearing rock-types. These olivine-bearing rocks include norites, gabbros, dunites and pyroxenites. Chromite concentration in these rocks varies from 0.48 to 3.09 per cent of the rock, usually in the form of chromite (Ahrens, 1965; Worst, 1960). A small fraction of this chromite settled to form chromitite layers whilst the remainder is retained within the rock mass as finely disseminated chromite and chromite interstitial to olivine. This retained chromite is much finer grained than layer chromite and is the primary source of eluvial chromite (Cotterill, 1981). During weathering of the serpentine rock and transportation by rainwater, the heavier chromite and magnetite grains are re-deposited along watercourses and vleis or valleys as the speed of the water is retarded sufficiently for the heavier particles to settle. The lighter serpentine material is removed and the chromite concentration in the soil is increased, thus resulting in eluvial chromite (Keech et al, 1961; Worst, 1960; Prendergast, 1978). The concentration of chromite particles in soil can be up to 15 (or more) $Cr_2O_3$ %, resulting in economic and exploitable deposits, located primarily along the Great Dyke flacks. A preliminary evaluation of the eluvials indicate that the Great Dyke could be host to up to 10 million tonnes of potential chromite concentrates which could be processed from such eluvial concentrates. These chromite-rich soils can be mined more cheaply than the traditional seams mining and processed into chromite concentrates through simple mechanical processing techniques of spirals, jigs and heavy media separators. The resultant chromite concentrates are of high quality and can be used to manufacture chromite ore briquettes, which are an alternative to lumpy chromite smelter feed.

The main challenges to eluvial mining are the inevitable environmental degradation and coming up with methods that could possibly mitigate against such environmental damage. The distribution of these eluvials over vast plains as thin soil horizons, necessitate use of mobile concentrator plants and hence establishment of extensive infrastructure. These challenges, however, are not insurmountable and test mining and previous production runs have proved profitable. The eluvials are also associated with some lateritic nickel concentrations. The nickel occurs in close association with some oxide such as goethite and garnierite and is associated with iron-manganiferous soil pisolites. The analyses of these pisolites indicate high nickel grades of generally above 1.00 %Ni. Such high nickel-content of Great Dyke laterites warrant, further investigations.

Acknowledgements

I gratefully acknowledge the assistance I received from my supervisor, Professor John Moore his encouragement and constructive criticism and advice willingly given are well appreciated. I also thank Professor John Moore for his support, through visits to Zimbabwe and affording me numerous field trips and many hours of discussion over the years.

I thank my colleagues Jeff Chaumba, Arimon Ngilazi, Desire Chikutiro, Benjamin Ruzive, Maxwell Matongo and Collins Mwatahwa for reading and offering constructive criticism to sections of the original drafts to this thesis. I acknowledge help rendered by Desire Chikutiro in sample preparation and organizing some analytical data.

I thank Ronel August for her assistance and direction in the use of the Microprobe Instrument. I thank Westbury Nyahasha for cartography drawing of some of the illustrations, Knowledge Nyahoja and Glenda Kukura for their assistance in printing and binding the final thesis.

I thank Dr N. R. Shoko of Zimbabwe Alloys Limited for affording me time to attend course work modules at Rhodes University, Grahamstown, RSA.

Finally a real "big thank you" to my family, my wife Sandra and the girls Nesu, Batsi, Ano and Maka. I am indebted to you for all the encouragement and support.

Contents

List of Tables

List of Figures

List of Appendices

# CHAPTER 1

## 1.0 Introduction

### 1.1 Discovery of Chromium and Early Applications

Louis Nicolaus Vauquelin, a French Chemist, is credited with the discovery of chromium (Cr) in 1797 (Cunat, 2004). The first development in the use of the element was in the chemical industry. Potassium dichromate became available on the market in England during early $19^{th}$ century and was followed by subsequent trade in chromium pigments. Of these pigments chromium yellow become very popular. Later, chromium chemicals found application in the tanning industry and eventually application widened into textiles, colouring, pickling and etching, wood preservation and corrosion prevention. In 1879, in France, chromite was first applied as a refractory, where it was used as an intermediate source of refractory between basic magnesite brick and acid silica bricks to prevent chemical action. Finally the $20^{th}$ century saw the element gaining prominence in steel making with further developments in refractory use. The later was to become the most important development for the use of chromium during that era (Cunat, 2004; Cox, 1989; Ahrens, 1995). At present the most dominant use of chromium is in steelmaking.
http://www.webelements.com/webelements/scholar/elements/chromium/history.html
http://www.webmineral.com/data/chromite/shtml

### 1.2 Uses of Chromium and Outlook

The use of chromium in steels was highly popularized by the development of stainless steels, which began in 1905, and by the development of stellite, a cobalt-chromium alloy, just prior to the First World War. The use of chromium in the stainless steel industry gained so much importance and prominence, that chromium production and its pricing can now be directly linked to trends observed in the stainless steel industry (Mills, 2002, CRU International, 2002). Other uses of chromium include the manufacture of a variety of other alloys, nickel chromium heating elements and chrome plating. In addition chromium compounds are also utilized as corrosion inhibitors, and for aluminium anodizing and pigment manufacture. The chromite ($FeCr_2O_4$), is used as a refractory.
Possible substitutes for chromium appear limited. Most research is into new uses of chromium rather than into substitutes. Some stainless steel could be replaced by plastic vitreous enamel and glass reinforced plastic coating, but these materials tend to be more costly, less convenient and less durable (Cunat, 2004; Mills, 2002; De Wit, 2002). Cost is the main factor that presently limits the increased use of chromium, but the long development lead times for new products and the high level of capital investment in existing equipment are also important inhibiting factors. Consequently, the metallurgical role of chromium is assured for a long time to come (Mills, 2002; De Linde, 2002).

## 1.3 Chromium, a Mineral Constituent

Chromium is an important-rock forming element in the earth's crust and is ranked 20$^{th}$ in order of abundance of the elements in igneous rocks and is the 13$^{th}$ most abundant element in the earth's crust with an average concentration of the order of 400ppm (Cunat, 2004; Ahrens, 1965). Chromium occurs in crystalline rocks as spinels, simple silicates, aluminum silicates and complex salts. Chromium also occurs in minor amounts in a wide variety of silicates by virtue of its ability to proxy for aluminum and ferric iron. There are 82 known chromium-bearing minerals, but of all these chromium-bearing minerals, chromite ($FeCr_2O_4$) is the only commercial source of chromium. Chromite is a term embracing a wide range of chromium-bearing spinel-group minerals, the composition of which can be expressed as (Mg, $Fe^{2+}$) O · (Cr, Al, $Fe^{3+}$)$_2O_3$. This can further be generalized to $R^{2+}O \cdot R_2^{3+}O_3$ whose molecular RO:$R_2O_3$ ratio is generally close to one. The spinel composition may be expressed by three end members $RO.Fe_2O_3$, $RO.Al_2O_3$ and $RO.Cr_2O_3$. The MgO/RO ratio is a usefully parameter in characterizing chromites chemically (Irvine, 1965; Wilson, 1982; Barnes and Roeder, 2001). (www.mineralsnet/minerals/oxides/chromite/chomite.htm).

### 1.3.1 Chromite, a Chromium-Bearing Mineral

The mineral chromite has a theoretical chromic oxide ($Cr_2O_3$) content of up to 68% though due to impurities it seldom contains more than 50% $Cr_2O_3$. The chromite from each given locality tends to have its own characteristic composition and analyses.

### 1.3.2 Chromite, an Ore Mineral

Chromite ores consumed by industry were previously graded as metallurgical, refractory or chemical-grade, based on the ores' physical and chemical properties. However, technological advances now render these classes inter-changeable to an ever-increasing extent and the classification has now been largely abandoned. The rock consisting entirely of the mineral chromite is termed chromitite and is the principal chromite ore. Chromite is often disseminated in ultramafic rocks in sufficient and economic quantities to warrant their beneficiation and subsequent utilization as chromite concentrate ores. Similarly chromite contained in soils or ultramafic rock waste dumps released by processes of weathering and/or milling can be concentrated and utilized as ores.

### 1.3.3 Chromite Occurrence in Mineral Environments

Chromite typically occurs in ultramafic, magmatic rock types and shows a close geochemical affinity to magnesium (Mg) and nickel (Ni). Typical background values of Cr in ultramafic rocks range from 1100 to 3400 ppm, dropping to ~ 200 ppm in gabbros and basalts and <10 ppm in granites. As a result, most chromite deposits are closely associated with peridotites and pyroxenites or their retrogressed equivalents such as serpentinites (Worst, 1960; Ahrens, 1965).

### 1.3.4 Origin of Chromite-Rich Rocks

Chromite-rich layers occur as regular horizons in mafic-ultramafic sequences, and form as fractionates in cooling ultramafic magma chambers. The chromitite layers are envisaged to have formed as cumulates due to gravitational settling of denser chromite crystals at the base of the magma chamber (Irvine, 1967). Alternatively, chromite layers could have formed by a process of episodic *in situ* growth, triggered by changes in the magma composition (Wilson, 1982). Such changes could have been in response to magma mixing, or contamination due to assimilation of wall rock material. Minerals closely associated with chromite, either as phenocrysts or as matrix phases, include olivine, orthopyroxene, clinopyroxene, plagioclase, magnetite, rutile and sulphides. As a result of retrograde metamorphic re-equilibration and weathering, these original igneous minerals may be replaced by hornblende, biotite, chlorite, serpentinite, talc, quartz, chalcedony, dolomite, goethite, illite and saponite (Irvine, 1967; Worst, 1960; Wilson, 1982). The chromite spinel varies widely in composition within the limits of the crystal formula $(Mg, Fe^{2+})O{\cdot}(Cr,Al,Fe^{3+})_2O_3$. Chromite compositions are controlled by original parent magma chemistry and equilibration with silicate phases during magma cooling. Further re-equilibration of the composition may occur during subsequent metamorphism, especially at granulite grade, which may result in Cr and Fe enrichment (Rollinson et al, 2002; Stowe, 1987). Within a layered ultramafic sequence, chromite content and composition, in sequentially fractionated layers varies from an ultramafic base to the more mafic top. In general, chromites near the base (i.e. early fractionates) are enriched in Cr and Mg while layers higher in the sequence (i.e. later fractionates) are enriched in Fe and Al. As fractionation progresses Cr may also be substituted by V and Ti. Hence in an ultramafic fractionation sequence, high-Cr chromites occur in early Mg-rich differentiates and Fe-rich chromites occur in later differentiates (Irvine, 1967; Worst, 1960; Wilson, 1982).

### 1.3.5 Eluvial Chromite

Apart from the concentrations of chromite in layers within ultramafic complexes, chromite also occurs as interstitial grains throughout the olivine-bearing rock types. These olivine-bearing rocks include norites, gabbros, dunites and pyroxenites. Chromite composition in these rocks varies from 0.48 to 3.09 per cent of the rock (Ahrens, 1965; Worst, 1960). A small portion of this chromite settled to form chromitite seams whilst the remainder is retained within the rock mass as finely disseminated chromite and chromite interstitial to olivine. This retained chromite is much finer grained than seam chromite and is the primary source of eluvial chromite (Cotterill, 1981). During weathering of the serpentinite rock and transportation by rainwater, the heavier chromite and magnetite grains are re-deposited along watercourses and vleis or valleys as the speed of the water is retarded sufficiently for the heavier particles to settle. The lighter serpentinite material is removed and the chromite concentration in the soil is increased, thus resulting in eluvial chromite (Keech et al, 1961; Worst, 1960; Prendergast, 1987).

**Fig. 1.1** Location of Chrome Operations in Zimbabwe

*(Map of Zimbabwe showing location of ferrochrome smelters, chrome mines, mafic and ultramafic zones with chrome prospects).*

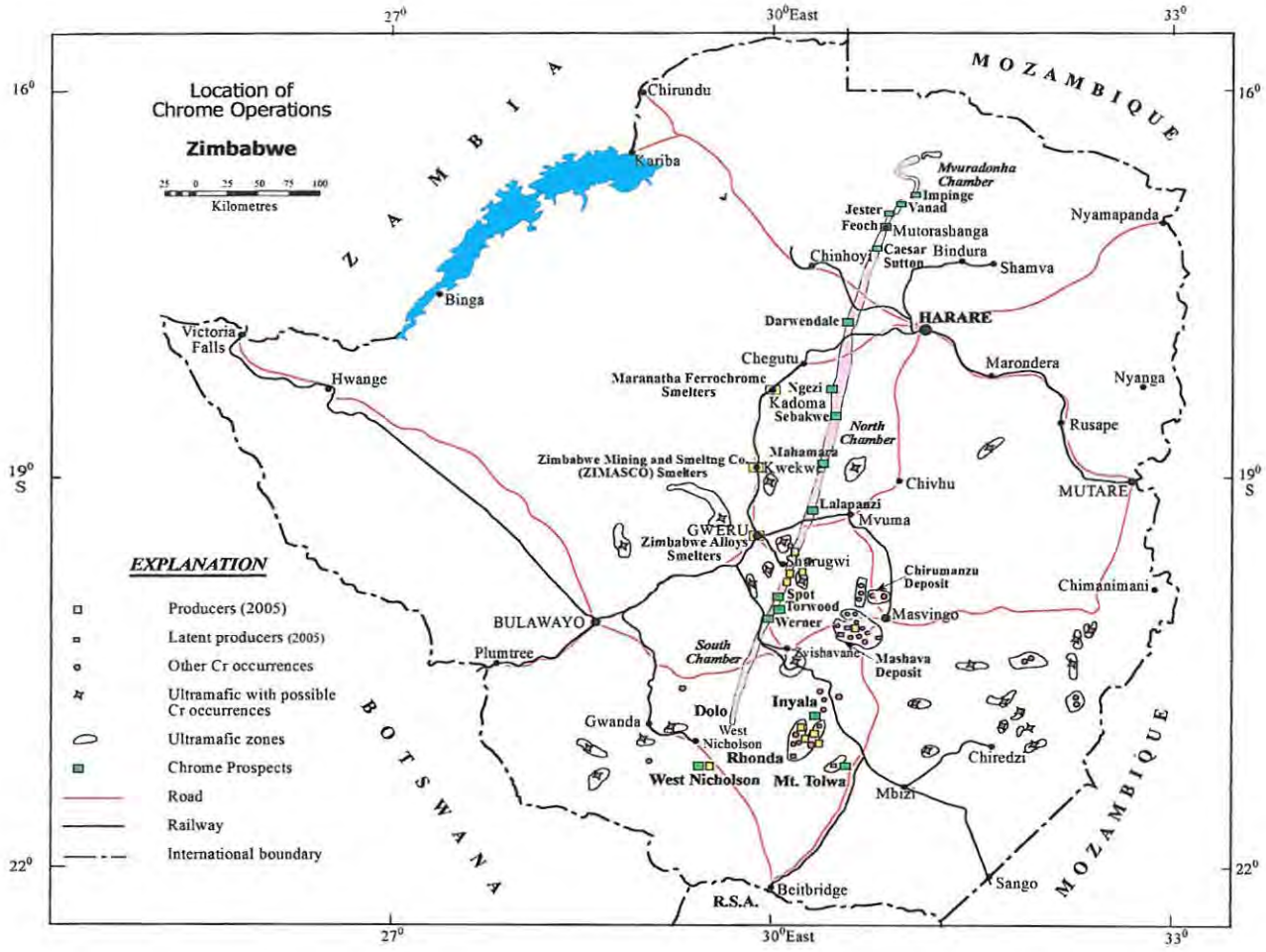


## 1.4 Background to the Zimbabwean Chromium Industry

The nearly century-old Zimbabwean Chromium Industry (Fig 1.1), has undergone a series of phased changes, having evolved from a primarily chromite ore mining and exporting industry, to a prominent producer of the world's high quality ferrochromium alloys.

### 1.4.1 Chromite Mining History on the Great Dyke

Prior to the 1940s chromite was mined by excavation along the margins of the Great Dyke where the seams were exposed at the surface (Fig. 1.2). By the late 1940s outcropping chromitite seams were largely depleted forcing mining activities to shift to underground operations. Incline shafts

and adits[1] were developed, first at Mutorashanga (Fig. 1.3). These underground operations were made profitable by the introduction of electric powered drills and box scrapers, the development of the resue mining methods and the extension of the railway line and electricity grid northwards to Mutorashanga (Cotterill, 1981).

**Fig. 1.2** Outcrop Excavation, the Main Method of Mining Chromite Prior 1940s

*[Photograph showing trenching down to between 2 to 4 metres vertical depth. Note the brown dumped waste material is from near surface, oxidized serpentinite rock excavation, whilst the grey is relatively fresh rock from deeper excavation].*

**Fig. 1.3** Adit Portal, Underground Access to Great Dyke Chromite Seams

*[Photograph showing a typical underground operation at the North Dyke, designed to produce 500 tonnes per month. Access to the seam is via a horizontal shaft system. Two 1-tonne cocopans, (see one at the shaft entrance) are drawn by a 2.5 tonne, battery-powered electric, locomotive, partly obscured by the men standing in front of the battery charging bay].*

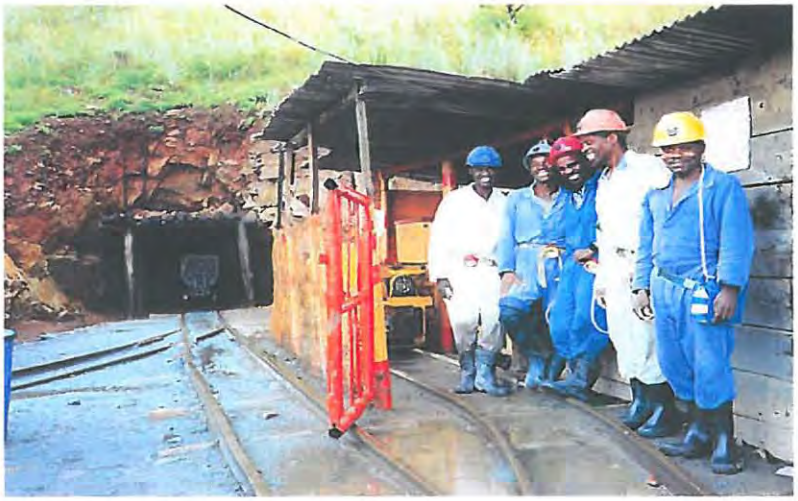

[1] A horizontal shaft system (Zimbabwe Mines Mineral Act, 1996)

### 1.4.2 Chromite Ore Production in Zimbabwe

After the shift to underground mining, which commenced in the Mutorashanga area, mining activities on the Great Dyke proliferated to cover virtually the Great Dyke's entire length. By the late 1960s, Zimbabwe had become the world's third largest producer of metallurgical-grade chromite, after South Africa and the former USSR[2], with Zimbabwean production coming also from Archean ultramafic podiform deposits particularly those at Shurugwi (Fig.1.1). Increased demand of chromium in the 1970s resulted in an all-time record production of 876 000 tonnes of chromite in 1975 (Fig.1.4). During this period underground mining in the Mutorashanga area reached its climax with ore being hauled out of decline shafts from incline depths greater than 700 metres (Prendergast, 1987).

**Fig. 1.4** Chromite Ore Production in Zimbabwe (Central Statistics Data, 2005)

*[Ore production data showing increasing chrome mining activities in Zimbabwe since 1905].*

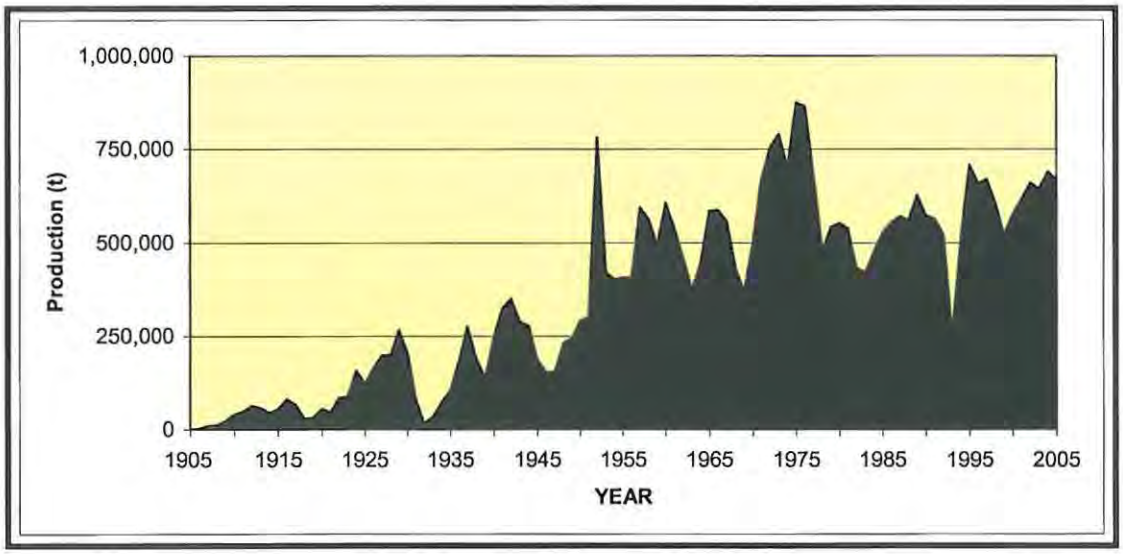


## 1.5 Diversity of Chromite Ore Sources in Zimbabwe

Chromite production has previously been dominated by podiform deposits particularly those associated with the Archaean granite greenstone terrain (e.g. Shurugwi deposits, Mashava deposits, and Inyala Rhonda deposits (Fig.1.1). However as these resources have been progressively depleted, production has tended to be replaced by the stratiform Great Dyke ores, which now accounts for about 60% of the ore supply to the three major ferrochrome smelting companies in Zimbabwe. Other secondary chromite sources such as dumps and eluvials soils have continued to get prominence as companies seek mining cost advantages.

[2] Union of Soviet Socialist Republic (USSR) a federation of countries under Russia, now split into several independent states.

### 1.5.1 Great Dyke Chromitite Layers

The Great Dyke of Zimbabwe is a layered ultramafic complex derived from three magma chambers namely the Mavuradonha, North and South chambers. The stratigraphy of the different chambers is similar at the top, consisting of mafic norites and gabbros, some of which is still preserved in localized centres along the Great Dyke's length. Below the mafic top, an ultramafic sequence, which consist of a top Pyroxenite Succession of alternating pyroxenite and dunites and a Dunite Succession, which consist of dunite layers only. The bases of all the dunite units are marked by chromitite layers which are 10 to 35 cm thick in the Pyroxenite Succession and ±10 cm within the Dunite Succession. The stratigraphy of the lower ultramafic sequence varies between the different chambers and contains as much as 11 chromitite layers in the North chamber. These chromitite layers of the Great Dyke contain the bulk of Zimbabwe's known chromite resources (Worst, 1960; Wilson, 1982; Wilson and Prendergast, 1989).

### 1.5.2 Archean Podiform Deposits

Apart from the Great Dyke Chromite seams, contribution to the overall chrome ore production was made from the Archean podiform deposits. By far the largest contribution has been from Shurugwi, an Archaean ultramafic belt. These deposits contained exceptionally good quality lumpy ores and could be mined at extremely low cost by virtue of their large size. The size of these deposits enabled the application of cheap opencast mining methods at surface and cost-effective sublevel caving underground mining methods at depth. Other similar Archaean greenstone-hosted chromite deposits occur as remnants within the granite-gneissic terrain as well as within the Limpopo belt. The most notable of these are the Inyala and Rhonda deposits in southern Zimbabwe and numerous other smaller deposits in the Nhema, Chirumanzu and Mashava communal lands (Cotterill, 1981; Stowe, 1968; Worst, 1964).

### 1.5.3 Heavy Mineral Deposits and Eluvial Deposits

The occurrence of heavy mineral deposits and their exploitation throughout the world is widespread and a precursor to the eluvial chromite mining. The recognition of such a class of ore deposits, an important source of zirconium, titanium, thorium, rare elements, a range of industrial minerals, diamonds, sapphire, garnets and occasionally precious metals and gemstones have led to development of significant heavy minerals mining operations world wide. These mineral deposits range from those resulting from wave action along coastal areas in beach environments such as the alluvial diamond deposits that occur along the west coast of South Africa and in Namibia. Located along some ancient rivers are fluvial diamonds such as along the Buffels, Orange and Vaal rivers of South Africa. Similarly most rivers over granite greenstone terrains are important

sources of alluvial gold. Granite greenstone terrains are also important host to tin placer deposits. Associated with coastal dunes of Australia, South America and South Africa are heavy mineral sands hosting major titanium feedstock, zircon sands among other minerals. World class heavy sands mines are located at Richards Bay and Namaqua sands in South Africa. In Brazil and the Philippines laterites above ultramafic complexes, consisting of both autochthonous and semi-autochthonous horizons, contain high concentrations of nickel, cobalt and chromite. Some of these important deposits are the Las Buenas and Olympic in the Philippines and Jucupiranga in Brazil (Marker et al., 1990). The importance of nickel laterite deposits is very significant and accounts for 40 % of annual global ferronickel production (Brand et al., 1998; Elias, 2002). The Cerro Montoso S.A in Columbia is another example of an important lateritic ferronickel producer (Gleeson et al., 2004).

In the late 1950s eluvial chromite mining commenced near Mutorashanga, on the Great Dyke, principally as feed for Low Carbon Ferrochrome (LCFeCr) production. A chromite concentrate (52-55 % $Cr_2O_3$) was produced by a combination of gravity and wet magnetic separation methods. The fine-grained nature of these concentrates rendered them less suitable for arc furnace smelting and as new stainless steel technology reduced the demand of this type of alloy, local smelters switched increasingly to High Carbon Ferrochrome (HCFeCr) production and eluvial mining ceased by 1975 (Keech et al, 1961; Kimble, 1976).

## 1.6 Ferrochrome Production in Zimbabwe

During the 1950s important changes in the World Chromium Industry took place as industrialized nations became steadily less competitive as ferrochrome producers, resulting in the smelting business migrating to developing countries in Africa, Asia and Latin America. This back integration was prompted by the perceived advantages in setting up smelters at the source of raw materials (De Wit, 2002) In particular, the savings on freight charges, the prospects of inexpensive energy and relatively low labour costs were notable advantages often cited. Reports of the vast chromite resources of the Great Dyke and at Shurugwi, as well as reliable coke source from Wankie Colliery and the promise of cheap electricity from Kariba's hydro-electric power led to the establishment of Zimbabwe Alloys Limited (formerly Rhodesian Alloys Limited) in 1953 as the first ferrochrome operation in Africa (http//zal02/company history).

In 1953 the first alloy was tapped at Zimbabwe Alloys heralding a new and second phase of Zimbabwean and African ferrochrome production. The expansion of the steel industries of the world which had began during the 1930s and their attendant benefits of research directed towards the development of refractories greatly increased the world consumption of chromite (Mills, 2002). Since then there has been a trend in Zimbabwe towards increasing domestic production of

chromium alloys and by 1979 virtually all ore exports had been replaced by Ferrochrome production and export.

### 1.6.1 Current Challenges Facing Zimbabwean Chromium Industry

Since the early 1980s, increasing labour charges, power costs, and fluctuating world market chromium prices forced a progressive shift from large company production and deep level mining operations towards small-scale low-cost production by co-operatives and tributors[3] (Fig. 1.4) from shallow winzes[4] and adits (Fig. 1.5).

**Fig. 1.5** Portal, Adit Section, Caesar Mine Mutorashanga

*[Photograph showing a typical shaft portal set-up at a 400t per month underground section. Note the ore and waste handling arrangement. This mining section has fully mechanized tramming and ore storage facilities, able to discharge directly into an ore haulage truck].*

Amid the fast dwindling supply of Zimbabwe's Archaean podiform ores such as those mined at Shurugwi, it was recognized that the future of the chromite industry lies in the Great Dyke and that systems must be established to mine these ores economically or to seek alternatives. On the larger-scale operations at Mutorashanga, experiments were conducted to investigate the effectiveness of employing large-scale underground mechanized units such as the *Road Header* and *Diamond wire cutting* methods, all of which were found to be largely inappropriate (Zimbabwe Alloys Road Header Project Report, 1989). In the short term the smelting companies have been encouraging reliable mining contractors to develop mechanized surface mining operations on the thicker, upper group chromites where the geology and topography permit low ore-to-waste stripping ratios (Fig. 1.6). These operations produce chromite at a lower cost than underground mining, but resources amenable to this sort of mining are limited and such operations only offer a

[3] Chromite producers under a lease agreement with actual mineral titleholder (Zimbabwe Mines Mineral Act, 1996)
[4] A winze is a decline shaft system (Zimbabwe Mines Minerals Act, 1996)

short-term to medium-term bridging period (10 years) before underground mining has to continue supplying ore.

**Fig. 1.6** Open-strip Mechanized Mining Operations, Great Dyke Upper Seams

*[Picture showing open-strip mining in progress. Earth moving equipment remove top soil and serpentinite overburden to expose the chromite seam, the chromite seam is then broken up by mechanical pavement breakers and lifted by hand. This operation at South Dyke is depleting the thicker seam 2 (0.25 – 0.30m), and produce up to 6000 tonnes of chromite per month, after stripping and removing 150 000 tonnes of soil and serpentinite overburden waste. The serpentinite overburden is drilled and blasted prior to excavation and mining is expected to achieve a 15 metre vertical depth. Note the brown top soil, the grey serpentinite rock and the unbroken seam under the water and the clean and unfrozen pyroxenite hanging wall under the seam].*

### 1.6.2 Mining Strategies, Zimbabwean Chromium Industry

New methods designed to reduce underground mining costs and beneficiation costs are continually being tested in large company-supported operations (a beneficiation plant is shown in Fig 1.7 and an eluvial plant in Fig 1.8). Advances reported include, limited mechanization of development using trackless mini-loaders and stoping operations using scrapers (Zimbabwe Alloys Limited Mines Report, 2001). Cost reduction in the order of 25-50% are anticipated, as well as increased productivity by as much as 50-58% to 10-12 tonnes per man month from the current 5 tonnes per man month.

**Fig. 1.7** Beneficiation Plant, Upgrades Low-Grade Chromite Ores

*[Picture showing a modern chrome processing plant capable of recovering chrome from low grade waste dumps and eluvial soils].*

**Fig. 1.8** Eluvial Concentrator Plant

*[Picture showing part of the feed preparation process at an eluvial concentrator plant. Soils are mixed with water then stirred to liberate chromite grains, the resultant slurry is then fed into a dense media separation process to recover the chromite grains and lighter material and clay slime carried away to waste with the water].*

These challenges have led Zimbabwe Alloys Limited as well as other chromium producing companies to look for alternative sources of ore in order to stay competitive on the world market. The success of beneficiation technology in upgrading low-grades and waste dumps, the improved technology in fines handling by smelters and the advent of briquette and sintering technology have renewed interest in the chromite-rich soils, placer and low-grade resources. These chromite-rich

soils of the Great Dyke have attracted attention as possible sources of cheap ore, as a result of their anticipated ease of mining and relative abundance. Beneficiation test work at Zimbabwe Alloys limited demonstrated that these soils could concentrate eluvial chromite soils up to a product of 48% $Cr_2O_3$ and 2.4 Cr: Fe ratio or better.

## 1.7 Objectives of this Investigation

This study aims to explore the occurrences and potential for economic chromite concentrations in Great Dyke soils. The possibility of incorporating these chromites as alternative ore sources, which could be utilized by Zimbabwe's chromium industry and elsewhere for other uses, is evaluated. The study summaries data collected over the years by different stakeholders and examines data collected during a regional investigation, by Zimbabwe Alloys Limited (2002) in order to establish distribution patterns and relative resource abundance along the Great Dyke's entire length. The study also focuses on specific areas were detailed investigations were done by the author and on geochemical characterisation of the various chromites from the dominant eluvial deposit environments sampled by the author.

This report gives a brief review of developments of the Zimbabwean Chromium Industry, appraises current knowledge of the Great Dyke, including the persistent seams' resources and ultimately examines the variations and distribution of eluvial deposits throughout the Great Dyke. In addition to exploring the feasibility of incorporating these eluvials into future ore sources that could be economically exploited by the Zimbabwean Chromium Industry the overall purpose of this study includes:

1 Investigating the provenance and depositional environments for the soil chromite concentrations.
2 Assessing the effects of various factors in the distribution and resultant quality of eluvial chromite concentration in Great Dyke soils.
3 Investigating possible variations in quality, distribution patterns and any of the factors likely to influence economic exploitation viability of these eluvial chromites.
4 A reconnaissance assessment of the abundance and regional distribution of eluvial soils of the Great Dyke.
5 Investigating the geochemical characters of eluvial concentrates from different regions of the Great Dyke.

## CHAPTER 2

# 2.0 An Overview: Geology of the Great Dyke of Zimbabwe

## 2.1 Introduction

Understanding of the Great Dyke geology and its regional setting has attracted the attention of many since its recognition as a geological entity by Carl Mauch during an expedition into interior southern Africa during the late 1860s (Harger, 1934). Zealley (1912) described the Great Dyke and quotes Mennell's description of the Great Dyke during 1910 as "the great mass of coarsely crystalline picrite extending for nearly the whole distance across Rhodesia[1] from north to south". Notable early geological investigations of the Great Dyke were carried out by Lightfoot (1927) and by Hess (1950). However a fully comprehensive account of the Great Dyke was only published after Worst mapped almost the entire length of the Great Dyke, (1958, 1960). Subsequent to Worst's publications a number of researchers have investigated various aspects of the Great Dyke geology. Notable milestones were recorded in the works of Hughes (1970, 1976), Bichan (1969, 1970), Hamilton (1977), Wilson (1976, 1982), Podmore and Wilson (1987), Prendergast (1988a), Wilson and Prendergast, (1989), Wilson and Chaumba (1997), Mukasa et al. (1998) and Obertür et al. (2002). The development and subsequent exploitation of the Great Dyke platinum resources resulted in a surge in platinum-related publications on the platiniferrous horizons of the Great Dyke. Notable among many others are publications by Prendergast (1988b), Prendergast and Keays (1989), Wilson et al. (1989), Wilson and Tredoux (1990), Prendergast (1991) Wilson (2001), Oberthür et al. (2000, 2002) and Wilson et al. (2000). The following is an overview of the Great Dyke geology, its structure, setting, stratigraphy and mineralization.

## 2.2 The Great Dyke of Zimbabwe General Information

The Great Dyke of Zimbabwe is an intrusive igneous complex similar in some respects to the Stillwater Complex of Montana, USA, and the Bushveld Complex of the Republic of South Africa as well as the Munni-Munni Complex in Australia. This late Archaean igneous intrusion consists of mafic and ultramafic rocks and extends for 550 km from Mavuradonha in the north of Zimbabwe to the North Marginal Zone of the Limpopo belt in southern Zimbabwe. Its width varies between about 4 km and 11 km. The Great Dyke of Zimbabwe's northern end assumes a horseshoe configuration and has been locally termed the Snake's Head. This Snake's Head part of the Great Dyke of Zimbabwe has been affected by the Pan African orogeny of 500 Ma (Wiles, 1968). Hamilton (1977) previously reported a Rb-Sr age of 2461±16 Ma for the Great Dyke of Zimbabwe. More recent determination on the age of the Great Dyke by Mukasa et al. (1998) yielded an age of 2570 Ma. Armstrong and Wilson (2000), Wingate (2000) and Oberthür et al. (2002), confirm the latter dating at 2575 ±0.7. The later dating is almost 100 million years older than the Rb-Sr dates reported by Hamilton, (1977) and

[1] Rhodesia was renamed Zimbabwe (1980)

implies that the emplacement of the Great Dyke of Zimbabwe was contemporaneous with the youngest trondhjemite-tonalite-granodiorite-granitoid suite in the Zimbabwe craton (Oberthür et al. 2002). This thus contradicts the view that the Great Dyke of Zimbabwe was the first major event after the stabilization of the Zimbabwe craton and the revised emplacement age of the Great Dyke links it with the emplacement of Late Archaean granitoids (Chilimanzi and Razi suites) of the Zimbabwe craton. The Great Dyke's revised age falls within the ranges of ages recorded for the tectonic events in the Limpopo belt, including granitoid magmatism, metamorphic events and the Northern Marginal Zone (NMZ) thrusting. The age of the thrusting of the western part of the NMZ is the same age as the Great Dyke whilst the same thrusting in the east deformed grantoids younger than the Great Dyke. These observations led to the conclusion that the thrusting, magmatism and cratonization may have been diachronous from west to east (Oberthür et al. 2002).

## 2.3 Subdivisions of the Great Dyke of Zimbabwe

The Great Dyke of Zimbabwe is longitudinally subdivided into a series of narrow contiguous layered chambers and sub-chambers. Worst (1960) envisaged the Great Dyke of Zimbabwe to comprise four contiguous boat-like layered complexes, which he called from north to south, the Musengezi, Hartley, Selukwe, and Wedza complexes. He distinguished these complexes mainly on their stratigraphic variations and regarded them as fault-bound remnants of four lopoliths whose feeder zones were thought to overly the mafic centres (Fig. 2.1). More recently gravity surveys by Podmore and Wilson (1987) have revealed the existence of extensive dyke-like feeders, which led them to subdivide the Hartley complex into the Darwendale sub-chamber to the north and the Sebakwe sub-chamber to the south. Further research by Wilson and Prendergast (1989) led them to divide the Great Dyke of Zimbabwe into two major chambers and a third smaller chamber at the extreme northern end of the Great Dyke of Zimbabwe. Wilson and Prendergast (1989) based their argument partly on the basis of Prendergast's earlier observations (1988) that "for the entire length of the Great Dyke the only unequivocal structural and stratigraphic break occurs at Lalapanzi between the Selukwe and the Hartley Complex". Thus from Wilson and Prendergast's (1989) observations the three chambers comprising the Great Dyke of Zimbabwe are the Mavuradonha, the North Chamber and the South Chamber (Fig. 2.1). Whilst no subdivisions are yet recognized for the Mavuradonha Chamber, the North Chamber is subdivided into three sub-chambers comprising, the Musengezi, Darwendale, and Sebakwe sub-chambers. The South Chamber comprises of two sub-chambers namely the northerly Selukwe and at the southerly the Wedza. Overall the North Chamber has the greatest volume and stratigraphic thickness up to 3350 metres as illustrated in Table 2.1 (Wilson, 1996).

**Fig. 2.1** The Great Dyke, Chambers, Sub Chambers, and Associated Satellite Dykes and Fractures

*(Modified after Wilson and Prendergast 1989)*

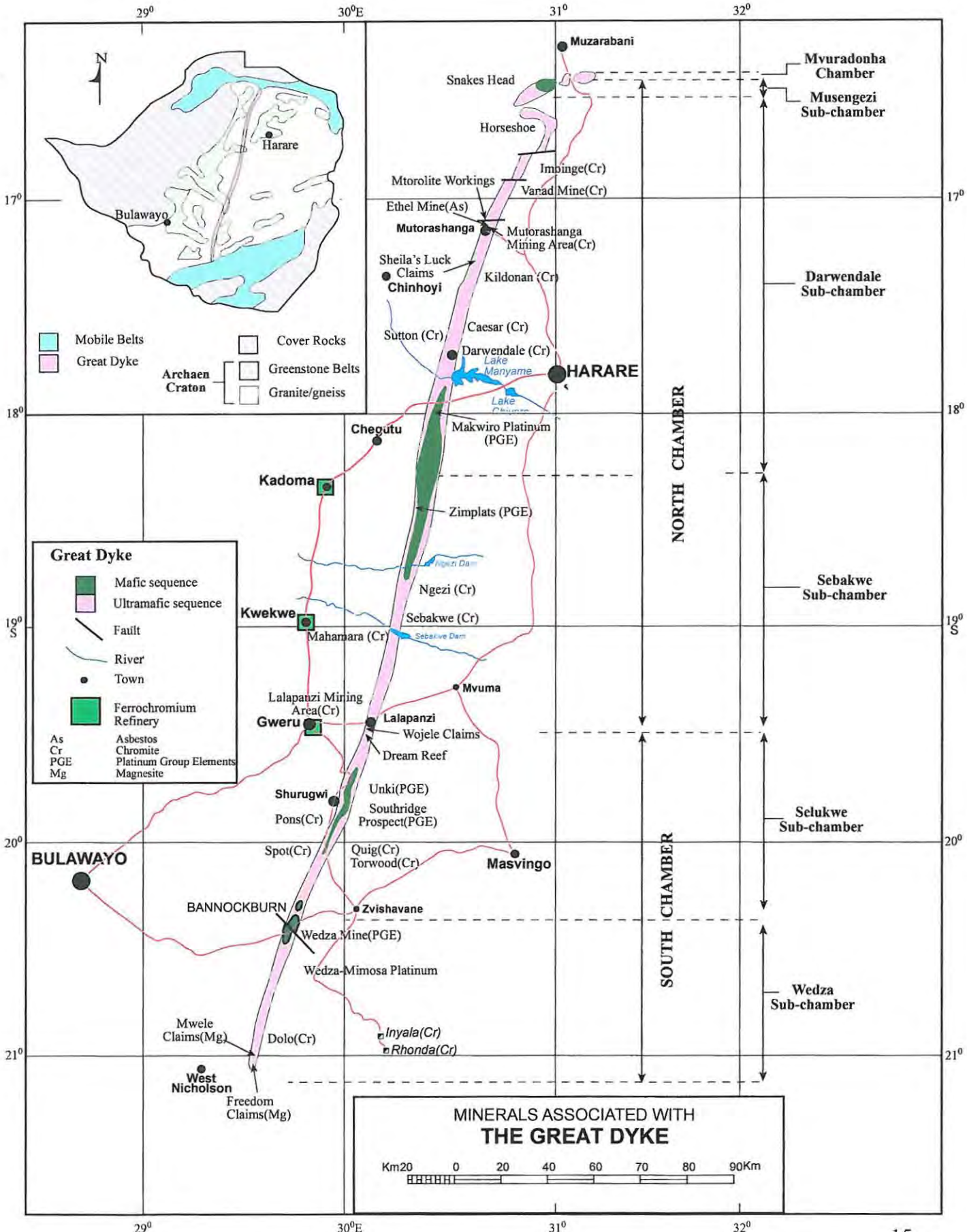

**Table 2.1** Main Subdivisions, Lengths and Stratigraphic Thicknesses of Sub-Chambers (Wilson, 1996)

| Chamber | North | | | South | | Mavuradonha |
|---|---|---|---|---|---|---|
| Sub-Chamber | Musengezi | Darwendale | Sebakwe | Selukwe | Wedza | Not Applicable |
| Length (km) | 25 | 210 | 120 | 96 | 80 | Not Applicable |
| Thickness (m) | 2450 | 3350 | 3350 | 1900 | 1900 | Not Applicable |

## 2.4 Geographic Regions of the Great Dyke

The subdivisions according to Wilson and Prendergast (1989) have not, however, been fully adopted within the local and mining circles. Thus for this reason and for the purposes of clarity the alternative geographic subdivisions or their variations are briefly described. The geographic subdivisions are illustrated in Fig. 2.2 and are explained below.

(a) North Dyke (also Northern Great Dyke)

This is the area from the northern banks of Lake Chivero, northward up to the Snake's Head. This area consists of the northern portion of the Darwendale sub-chamber as well as the entire Musengezi sub-chamber and the Mavuradonha Chamber.

(b) Middle Dyke (also Middle Great Dyke)

This is the area from the southern banks of Lake Chivero, southwards including the southern remainder of the Darwendale sub-chamber as well as the entire Sebakwe sub-chamber to Lalapanzi and further south including the entire Selukwe sub-chamber.

(c) South Dyke (also Southern Great Dyke)

The area coincides with the Wedza sub-chamber or the southern part of the South Chamber and includes the Bannockburn area southwards to the Doro Range where the Great Dyke terminates.

**Fig. 2.2:** Geographic Regions of the Great Dyke

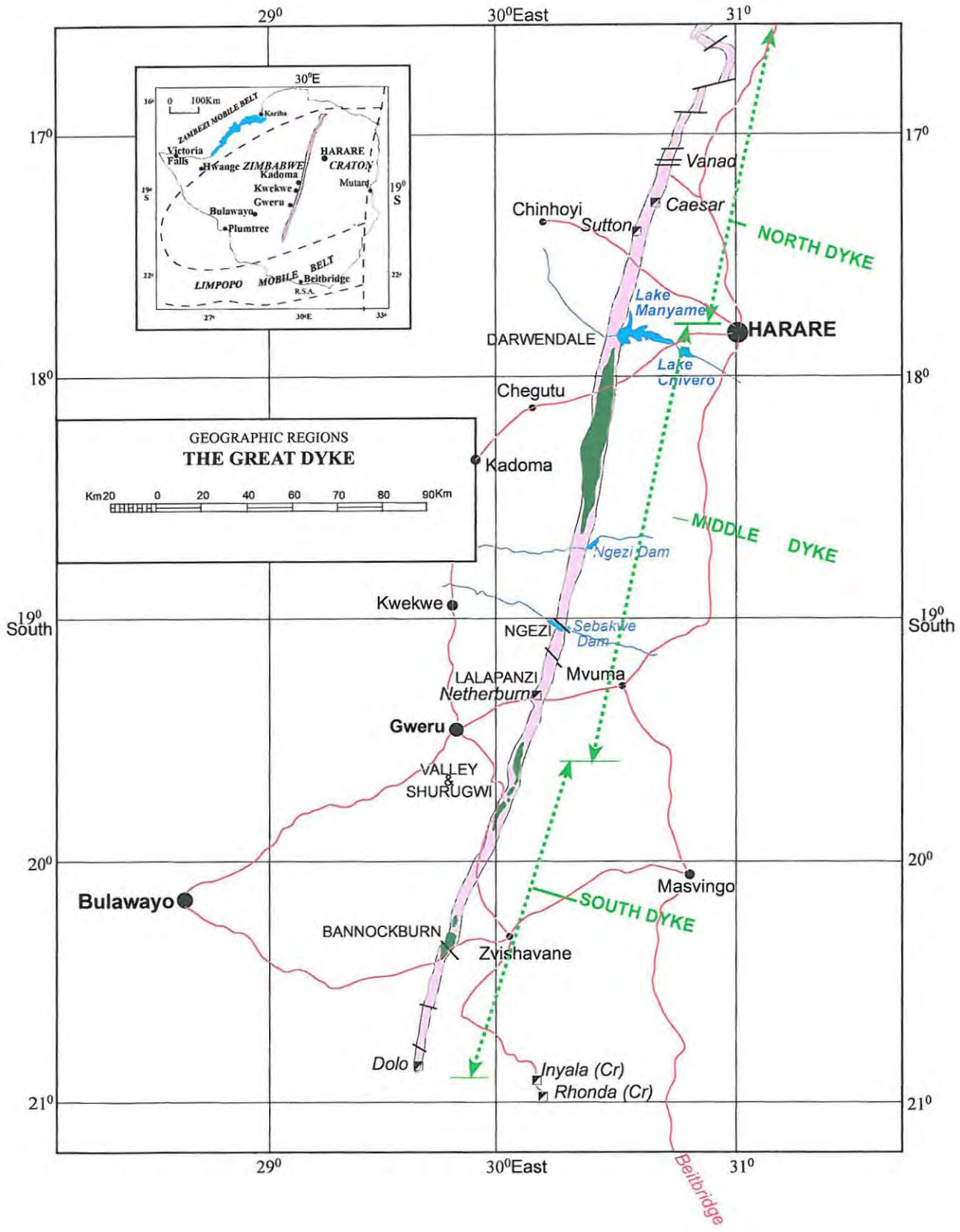

## 2.5 Structure of the Great Dyke

Podmore and Wilson (1987) interpreted the overall shape, of the Great Dyke, using 18 gravity profiles measured across its width, along its entire length. These cross-profiles were measured at 25 km intervals from Doro Range at the extreme south of the Wedza sub-chamber to Mutorashanga on the northern half of the Darwendale sub-chamber.

**Fig. 2.3** Relative Cross-Sectional Area for 18 Gravity Traverses

*[Cross- section showing sampling position identified by vertical lines (Podmore & Wilson, 1987)].*

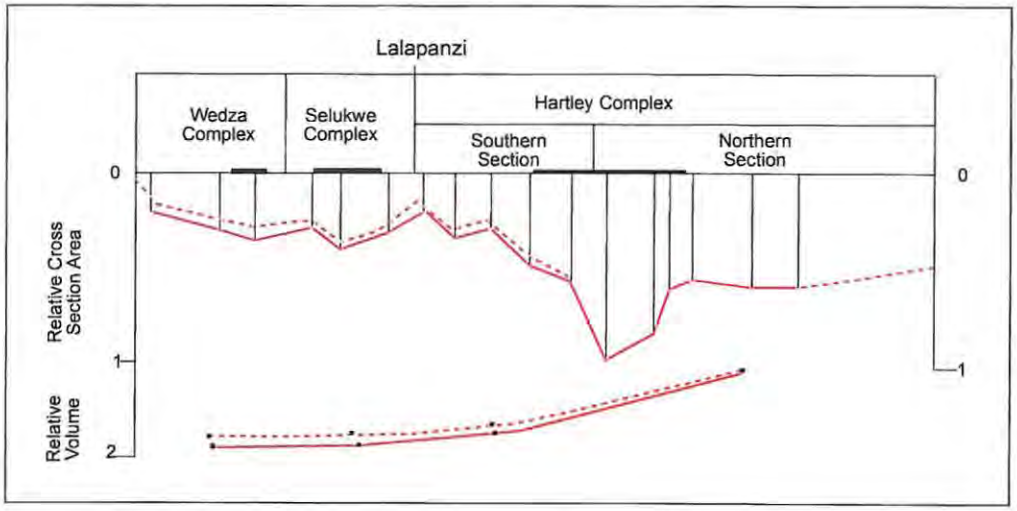


These gravity profiles show a bell shaped Bouger anomaly, which was compiled into a geological model of densities and thicknesses of layers using an interactive computer model by Podmore and Wilson, (1987). Murahwi (1995) summarized the most important facts of their interpretation in the following six points.

"*(1)* A clearly dyke-like deep structure averaging about 1km in width exists at depths of between 4 km and 10km along almost the entire length of the Great Dyke. The deep structure is less evident at Lalapanzi than elsewhere and this is taken as supporting evidence for the boundary between the North and South Chambers. (Fig. 2.3)

(2) The Great Dyke magma chamber has a Y-shaped cross-section in contrast to Worst's (1960) conjecture of shallow boat-like complexes with feeders at the centres. Nonetheless, the original structural concept is incorporated to the extent that the axial feeder dyke may have been broader and discharged larger volumes of magma in the centres of the Selukwe and Wedza sub-chambers. Discrete central feeders are not recognized.

(3) Overall, the magnitude of the Great Dyke structure increases steadily from south to north with the largest anomalies occurring near the gabbroic remnants in each sub chamber (Figure 2.3)." The coincidence of mafic (gabbroic) remnants with greenstone belts in the adjacent host rocks is taken to imply competency contrasts culminating in greater volume development of the Great Dyke at these points" (Wilson and Prendergast, 1989).

(4) The noticeable asymmetry of certain gravity profiles is attributable to either local tilting of the Great Dyke or the irregular development of the deep structure. The inferred tilt to the east is consistent with the proposed uplift of the craton in the east relative to the west (Podmore and Wilson, 1987). This, however, does not explain the asymmetry of the synclinal structure in some areas (Prendergast, 1988b)

(5) A number of profiles indicate the existence of a substantial lower magma chamber at about 5 km depth parallel to the length of the Great Dyke with an approximate width of 2.5km (Podmore and Wilson, 1987).

(6) The form of each sub-chamber is a doubly plunging syncline with layers dipping gently inwards (Figure 2.4). The layers attain maximum thickness in the axial zone."

**Fig. 2.4** Transverse Section, Darwendale Sub-chamber

*[Generalized cross-section showing the structure of the Great Dyke, Darwendale sub-chamber. (after Wilson and Prendergast, 1989)].*

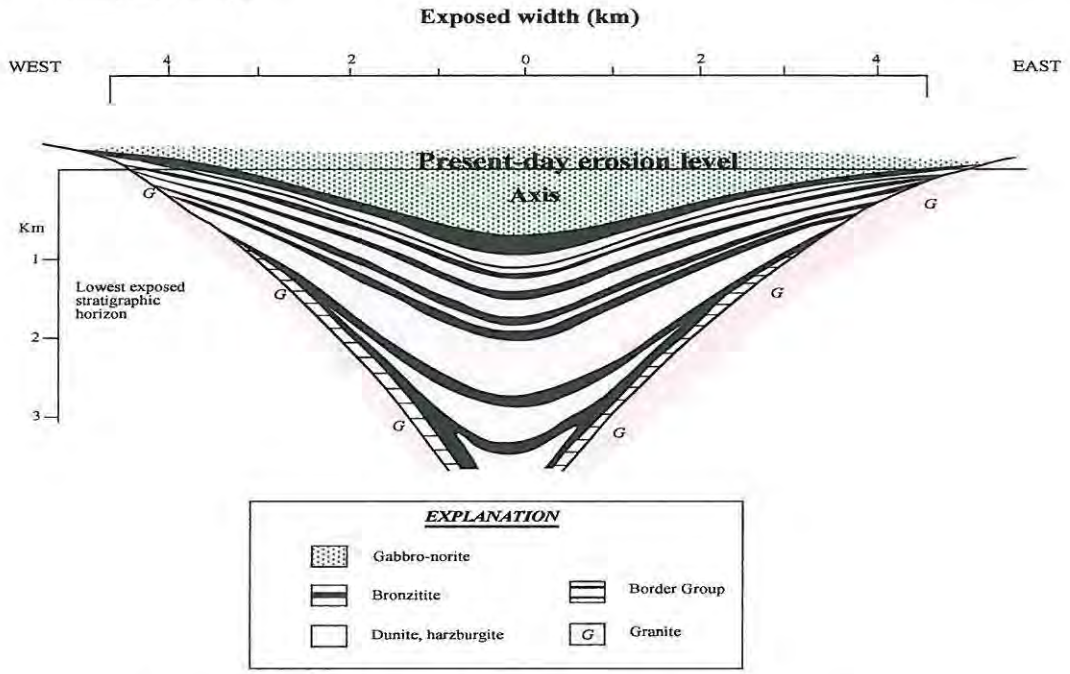


## 2.6 Stratigraphy, Lithology and Cyclic Units of the Great Dyke

Each of the Great Dyke sub-chambers is divided into two major stratigraphic portions: a lower Ultramafic Sequence and an upper Mafic Sequence (Wilson and Prendergast, 1989) (Fig. 2.5). The stratigraphic succession in the Ultramafic Sequence is characterized by varied developments in the North and South major chambers (Wilson and Prendergast, 1989). The North Chamber has relatively fewer but thick cyclic units averaging 100m in thickness with well developed pyroxenite layers at the top. In contrast, the South Chamber has a greater number of thinner cyclic units up to 30m thick with olivine pyroxenites predominating over pyroxenites in the upper parts. The Mafic Sequence is similar throughout the entire length of the Great Dyke.

### 2.6.1 The Ultramafic Sequence

The Ultramafic sequence is subdivided into two zones; the lower dunite succession which is overlain by the pyroxenite (bronzitite) succession (Fig. 2.5). Both successions are composed of cyclic units. Cyclic units in the lower dunite succession comprise olivine cumulates with a basal chromitite layer (Wilson, 1982). The upper pyroxenite cyclic units consist of a thin basal chromitite layer overlain by a dunite layer which grades upwards through harzburgite and olivine pyroxenite into pyroxenite at the top of each unit (Prendergast, 1987). Dunite layers comprise interlocking olivine grains with typical planar boundaries and triple point junctions. In an entire sub-chamber the dunite layers grade laterally into harzburgite towards the margins (Wilson, 1982). A significant proportion of chromitite occurs in the dunite layer, where it can form up to 4 % by volume. Where the poikilitic harzburgites are present, they are mostly transitional between dunites and olivine pyroxenites. Poikilitic harzburgite comprises a mosaic of interlocking crystals of orthopyroxenite with olivine crystals contained in the orthopyroxenite crystals. The relative extent of the poikilitic harzburgite varies in the different sub-chambers. The poikilitic harzburgite grades into granular olivine orthopyroxenite where olivine occurs as discrete grains. As the proportion of olivine gradually decreases upwards, the rock eventually grades into olivine pyroxenites. This transition is marked by a change in texture of olivine from granular discrete grains to irregular interstitial crystals (Wilson and Prendergast, 1989). Wilson (1992) noted that the grain size of the pyroxenites correlates directly with the size of the magma chamber, with the largest and smallest average grain sizes occurring in the Darwendale and Wedza sub-chambers respectively. Layering on a scale of a few centimetres is observed in the olivine bronzitite or harzburgite and this, according to Wilson (1982), represents a rhythmic fluctuation in the proportions of olivine and orthopyroxenite. The cumulus and post-cumulus mineral phases in the Ultramafic Sequence are summarized in Table 2.2. In all these sub-chambers a websterite layer acts as a marker horizon at the top of the Ultramafic Sequence (Wilson, 1982).

**Table 2.2** Stratigraphy of a Cyclic Unit, Ultramafic Sequence, North Chamber

*[A summary of relative mineral abundances in different Great Dyke lithologies (Wilson 1982)].*

| Rock type & Sub-unit | | Cumulus Minerals (%) | | | Post Cumulus Minerals (%) | | |
|---|---|---|---|---|---|---|---|
| | | Olivine | Orthopyroxene | Chromite | Clinopyroxene. | Plagioclase. | Opx. |
| Top | Bronzitite | - | 95- 100 | - | 0-5 | 0-2 | - |
| | Olivine bronzitite | 0-50 | 50-100 | - | 0-1 | 0-1 | - |
| | Harzburgite | 70-90 | - | 0-5 | 2-15 | 0-5 | 2-15 |
| | Dunite | 94-100 | 2-5 | - | 0-5 | 0-2 | 0-5 |
| Base | Chromitite | 0-10 | - | 90-100 | - | - | 0-20 |

- Numbers refer to modal proportions of individual minerals.

**Fig. 2.5:** The Major Stratigraphic Subdivisions of the Great Dyke

*[Stratigraphic column showing Great Dyke lithologies and variation of magnesium ratio within the upper stratigraphy (Wilson and Prendergast, 1989)].*

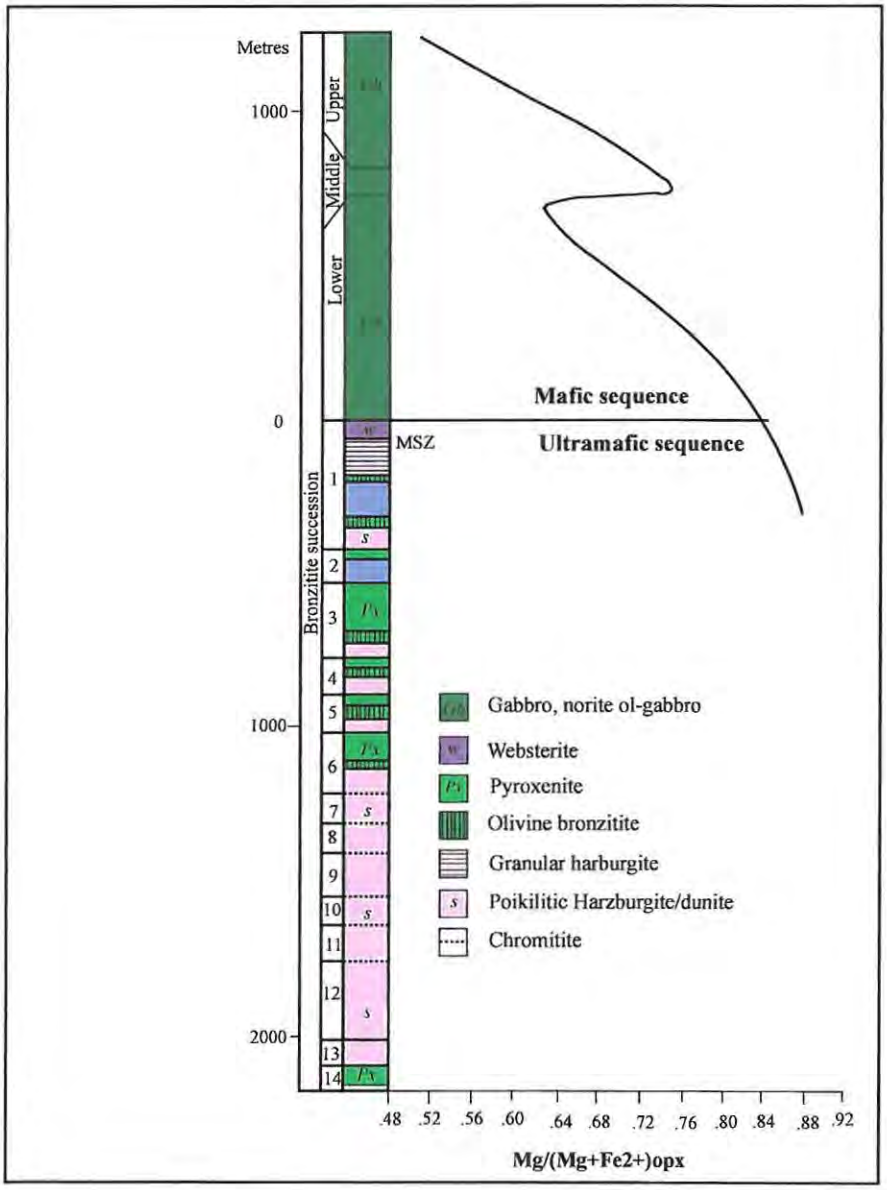


## 2.6.2 The Mafic Sequence

The Mafic Sequence of the Great Dyke is marked by the first appearance of cumulus plagioclase. The Mafic Sequence exhibits some striking similarities in terms of stratigraphic succession throughout the entire length of the Great Dyke and its distribution along this length somehow coincides with zones flanked by greenstone belts (Wilson, 1982; Murahwi, 1995). The sequence attains its maximum thickness in the Darwendale sub-chamber, a feature that prompted Wilson and Prendergast (1989) to suggest that the magma chambers coalesced during this stage of crystallization (Wilson, 1996; Wilson and Prendergast, 1989). The Mafic Sequence has been subdivided into the Lower, Middle and Upper Mafic Units with respect to notable textural variations (Fig. 2.5.).

Wilson and Prendergast, 1989). The Mafic Sequence has been subdivided into the Lower, Middle and Upper Mafic Units with respect to notable textural variations (Fig. 2.5.).

### 2.6.3 The Lower Mafic Unit

This unit at the base of the Mafic Sequence is ± 700metres thick and consists of medium to coarse-grained gabbro, norite and gabbronorite containing primary orthopyroxene. Olivine is generally absent except in the olivine gabbro layer at the base of the succession. An upward-increasing abundance of orthopyroxene and transition from cumulus orthopyroxene at the base to post-cumulus orthopyroxene at the top has been observed (Wilson and Prendergast, 1989).

### 2.6.4 The Middle Mafic Unit

Overlying the Lower Mafic Unit is the Middle Mafic Unit, which is ± 100 metres in thickness, characterised by the re-appearance of olivine as a cumulus phase and has fine-grained to medium-grained gabbro and feldspathic orthopyroxenite as dominant rock types in the succession. This unit bears some textural similarities with the topmost pyroxenite layer of the Ultramafic Sequence (Wilson and Prendergast, 1989).

### 2.6.5 The Upper Mafic Unit

This unit marks the final phase of magmatic activity of the Great Dyke and caps the Mafic Sequence. The package is ± 300 metres thick. The unit is characterised by a cumulus iron oxide phase (e.g. magnetite) which appears together with norite and hypersthene derived from the inversion of cumulus pigeonite (Wilson and Prendergast, 1989). On the basis of inferred mineral trends and composition and comparison with other similar intrusions, Wilson and Prendergast (1989) estimated about a third of this package to have been eroded away.

### 2.6.6 Border Group

In several places, the magma chambers that constitute the Great Dyke are characterised by a Border Group abutting the country rock. This Border Group comprises a steeply dipping package of massive to complexly layered rocks of diverse types (Wilson, 1982; Wilson and Prendergast, 1989). Commonly the group is composed of acicular cumulus pyroxenes, which are oriented perpendicular to the wall rocks. The ultramafic layering approaches the Border Group asymptotically and then gradually merges with it at the margins, as indicated in Figure 4 (Wilson, 1998).

### 2.6.7 Satellite Dykes

Associated with the Great Dyke is a suite of quartz gabbro and gabbronorite satellite dykes that, like the Great Dyke of Zimbabwe, trend NNE. These satellite dykes are closely related to major fracture patterns postulated to be the result of the craton–wide tectonic control that rise to the form and alignment of the Great Dyke (Wilson, 1996). These satellite dykes fall into two groups: the Southern

Main Satellite dykes and the Outer Satellite Dykes (East Dyke and Umvimeela dykes) (Jones et al. 1975; Hamilton, 1977).

### 2.6.8 The Southern Satellite Dykes

These comprise a series of elongate and aligned mafic bodies to the south of the Wedza sub-chamber covering a distance of 80 kilometres, and are intrusive into the Limpopo Belt. These dykes range in width from 150 metres to 600 metres and consist of olivine-bearing feldspathic pyroxenites. These dykes have been dated at 2545 ±120 Ma (Robertson and van Breemen, 1970) and are thought to have a contemporaneous emplacement with the Great Dyke. These southern satellite complexes exhibit evidence of the 1950 Ma tectonothermal Limpopo Metamorphic event (Jones et al., 1975).

### 2.6.9 The Outer Satellite Dykes

The outer Satellite Dykes flank the Great Dyke with the Umvimeela dyke 1-18 kilometres to the west of the Great Dyke and the East dyke 10-24 kilometres east. These dykes run parallel to the Great Dyke over its entire length, although the East dyke tends to be more continuous. Both dykes, however, are revealed by aeromagnetic survey and satellite imagery to be persistent features with thicknesses of 200 metres and 100 metres respectively (Mushayandebvu, 1995; Wilson, 1996). The dykes are essentially quartz gabbroic and gabbronorite in composition.

## 2.7 The Tectonic Setting of the Great Dyke

The gravity data along the length of the Great Dyke referred to in section 2.4 are consistent with a broad Y or a funnel-shaped basin with gently inward-dipping margins (Podmore, 1970; Podmore and Wilson, 1987). The transverse shape of the layered sequence is synclinal, with flat layers in the axis (Fig. 2.4). The layering is characterised by steep margins as well as at depth due to down warping in the axial zone. The layers are usually continuous and attain a maximum thickness along the axial zone.

The linearity of the Great Dyke for a distance of up to 550 km is an intriguing feature. It has come to be accepted that the Great Dyke and its satellites were intruded during a period of crustal extension, which resulted in incipient continental rifting (Worst, 1956, 1960; Bichan, 1970; Wilson, 1987, 1990). Wilson and Prendergast (1989) developed and made popular a four-stage development model for the emplacement of the Great Dyke. The sequential emplacement of the Great Dyke of Zimbabwe and fracture pattern associated with the emplacement events as envisaged by Wilson and Prendergast (1989) are summarized in Fig. 2.6.

**Fig. 2.6** Emplacement of the Great Dyke

*[Sequence of events leading to the development of the Great Dyke fracture pattern and subsequent emplacement (after Wilson and Prendergast, 1989)].*

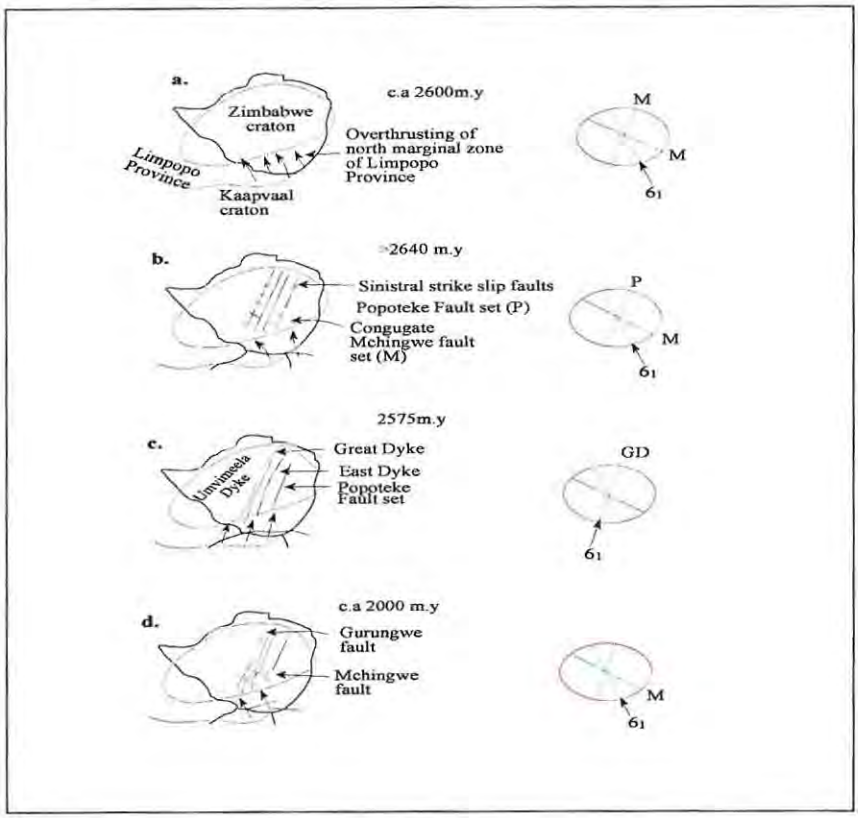


(a) In the initial phase, continental collision and overthrusting of the North Marginal Zone of the Limpopo belt on the southern margin of the Zimbabwe craton led to NNW-directed maximum compressive stress.

(b) The second phase involved the development of craton-wide NNE- and NNW-trending sinistral strike-slip fractures belonging to the Popoteke and Mchingwe fault sets respectively.

(c) The third stage saw the rotation of the compressive stress from NNW to NNE leading to the emplacement of the Great Dyke and its satellites.

(d) The fourth and final stage was characterized by rotation of the maximum compressive stress, back to a NNW direction resulting in dextral movements along the Mchingwe fault (Fig. 2.6)

## 2.8 Mineralisation and Mineral Deposits of the Great Dyke

Prominent mineral deposits of the Great Dyke of Zimbabwe are chromitite, asbestos and platinum group elements (PGEs) together with the associated base metal by-products of nickel, copper and cobalt as well as precious metals by–products of gold and silver (Fig 2.7). Sporadic mining of magnesite deposits associated with fracture zones occurs from time to time. All the known economic mineralisation on the Great Dyke of Zimbabwe is confined to the Ultramafic Sequence.

**Fig. 2.7** Location of Chromite Deposits, Great Dyke and Adjoining Areas

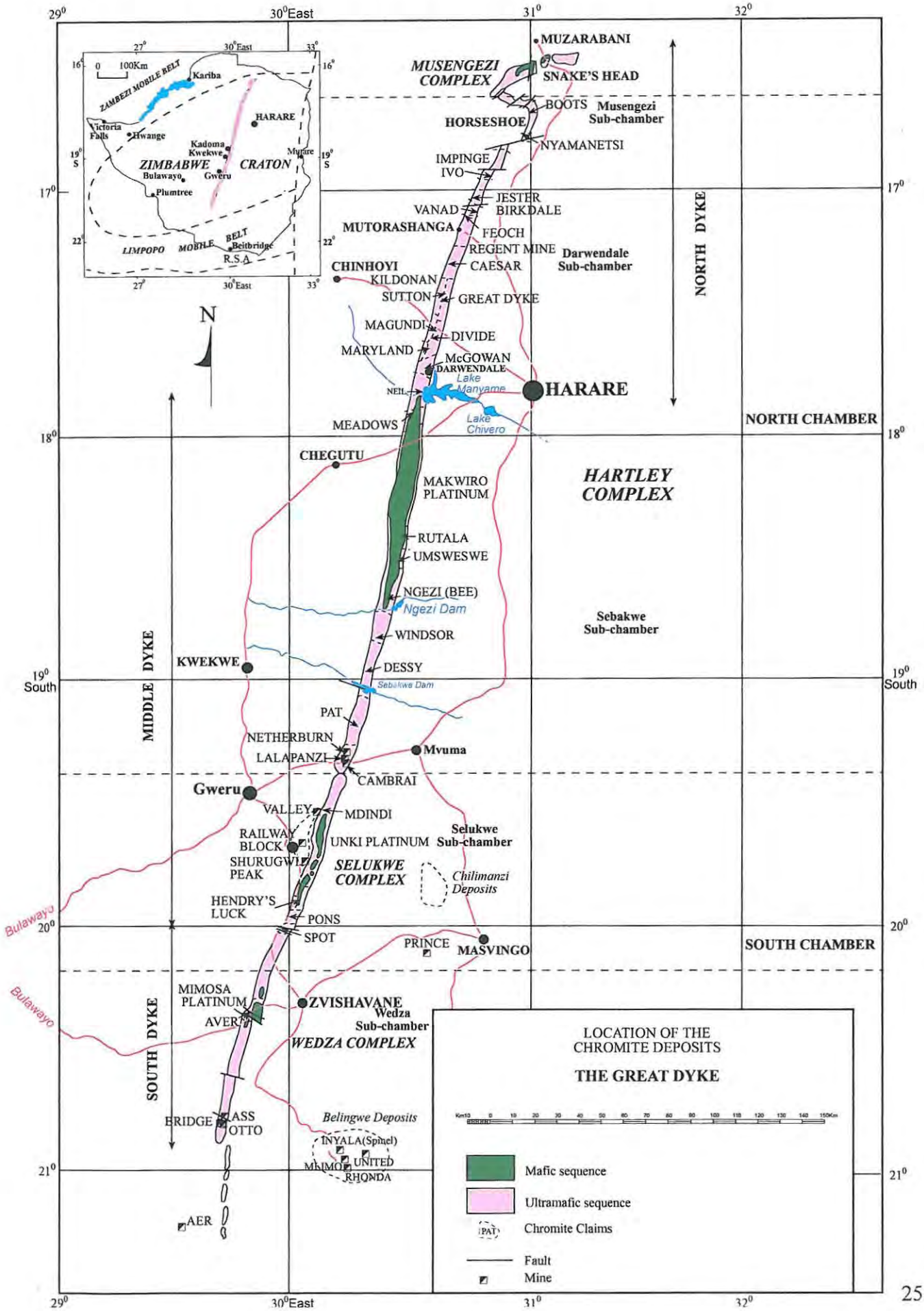

### 2.8.1 Chromitite Layers

The chromitite occurs as narrow layers within the ultramafic sequence and has been numbered sequentially from the top of the sequence downwards with respect to their associated cyclic unit (Prendergast, 1987; Prendergast and Wilson, 1989; Wilson, 1982; Worst, 1960, 1964). In addition to the main seams, numerous minor, thin chromitite layers have been identified as a result of mining activities especially in the Mutorashanga area. Differences exist between Worst's (1960) nomenclature and that of Wilson and Prendergast (1989) (Fig. 2.8). Previously the seams were numbered from top to bottom as number 1, number 2, etc., but the numbering was changed to C1 (chromitite layer 1), C2 (chromitite layer 2), etc. (Wilson and Prendergast, 1989; Wilson, 1996). The C1 chromitite layer has been further subdivided into C1c, C1d, C1e and C1f. The new nomenclature, among other advantages, relates chromitite layers to cyclic units, which are in turn based on observed mappable features and allows further subdivisions and can accommodate new layers and cyclic units which might in future be recognized base on sound petrological criteria. The chromitite layers have been subdivided into the lower group and upper group chromitite seams. The lower group chromitite (C4 –C12) differ from the upper group chromitite (C1c, C1d, C2, and C3) in that they are high-grade (Table 2.3) and thinner (±10 centimetres). The lower group chromitites are located within the dunite succession and basal units of the bronzitite succession whilst the upper group chromitites are restricted to the upper parts of the bronzitite succession. Each chromitite layer has a sharp basal contact and a rather poorly defined and gradational hanging-wall contact. Overall an upward decrease in modal chromitite abundance and grain size is observed in the units. The massive chromitites are made up of interlocking polygonal chromitite crystals.

### 2.8.2 The Lower Group Chromitite Layers

The chromitite seams belonging to the lower group of chromitites exhibit strong vertical and lateral variations in chromite content, grain sizes and the proportion of interstitial phases. The units usually exhibit fine rhythmic layering over a considerable thickness, up to 150 cm, in the hanging-wall (Worst, 1960). At Mutorashanga, individual chromitite seams vary in thickness attaining a maximum thickness of 10-15 cm at the axial zone (Prendergast, 1985; Wilson, 1982). Chromite grain size decreases outward from the axial zone. In contrast, the proportion of interstitial phases increases towards the margin of the transverse sections (Wilson, 1998).

Seam C4 is well developed in the Darwendale sub-chamber. It averages 10 cm in thickness (range 4-20 cm) and is normally coarse-grained and hard (Table 4.0). It has four special features that differentiate it from the other lower group chromitites:

(i) It has the lowest friability making it the most desirable source for metallurgical ore,

(ii) The footwall comprises a thick pyroxenite layer in contrast to the other lower group seams which have dunite as their footwall,

(iii) The seam is directly overlain by a 1 m thick zone of olivine-chromitite cumulate, with the olivine now replaced by post-cumulus orthopyroxene,

(iv) Overall, the seam has a coarse mean grain size (5-10 mm).

In the Darwendale Sub chamber, seam C5 is up to 10 cm thick of more-or-less solid, usually friable to semi-friable ore overlain by up to 3 m of disseminated chrome spinel (Prendergast, 1984). The $Cr_2O_3$ %( content weight) and Cr:Fe ratio vary from 36 to 50 % $Cr_2O_3$ and 2.3 to 3.3 Cr:Fe ratios respectively. The Cr: Fe drops to 2.0 at the top of the layer.

**Fig. 2.8** Stratigraphy of the Ultramafic Sequence and Chromitite Layers in Sub-Chambers

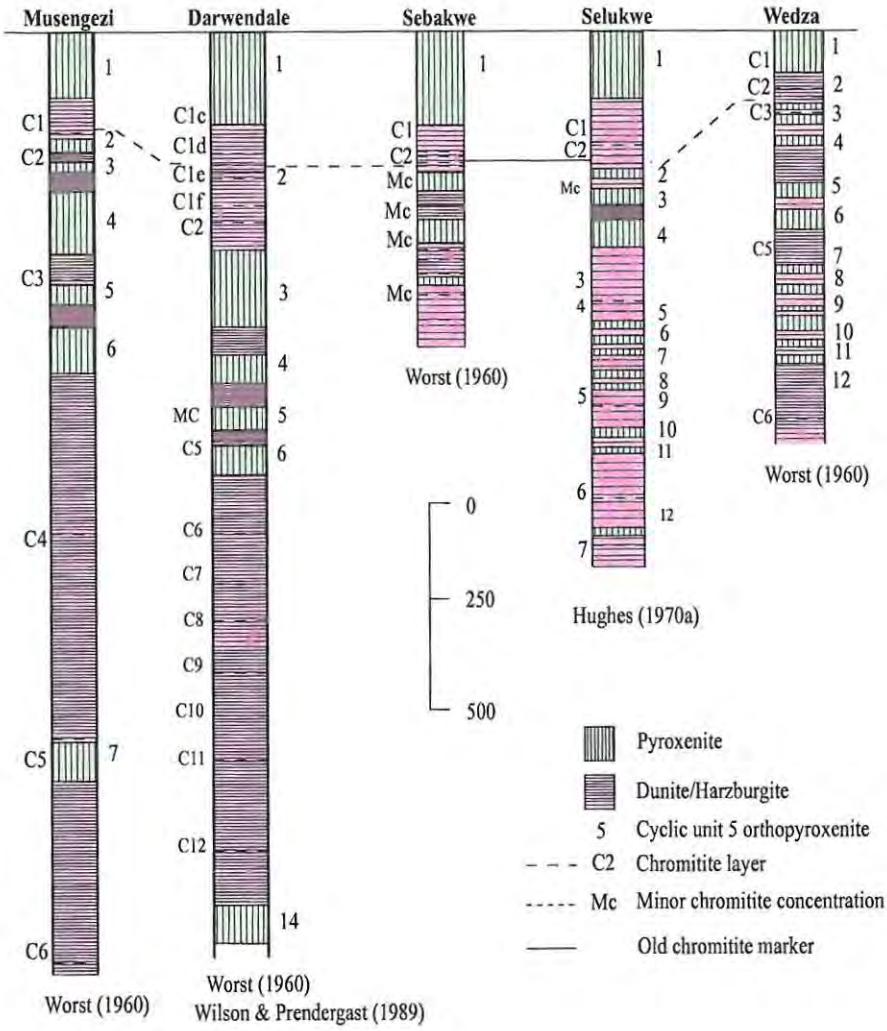


Seams C6 and C7 have been exploited extensively in the Mutorashanga area. These seams are largely friable and average 9-10 cm in thickness. The average $Cr_2O_3$% content and the Cr:Fe ratio are > 48 and 2.8 respectively. In the Mutorashanga area, seams C6 and C7 are severely affected by transverse faulting, resulting in the duplication of the seams. Local thinning and thickening of seams

is attributed to thrusting. In general, ore associated with thrust zones tends to be indurated. The C7 chromitite seam, north of Darwendale, consists of massive, monomineralic, interlocking, and coarse grains of chromitite up to 10 mm in size at the axial zone. These gradually pass into fine-grained chromitite grains intergrown with olivine at the margins (Wilson, 1998). The MgO content and Cr:Fe ratio of chromitite seams C6 and C7 decrease laterally from 14.2 % and 3.3: 1 in the axial zone to 12.9 % and 2.8: 1 near the margin of the transverse section respectively. Average thickness of seam C8 is less than 10 cm and its grades are comparable with those of C6 and C7. Seams C9 and C10 are similar to seams C6 and C7 and are exposed in the low ground along the margins of the Great Dyke of Zimbabwe (Wilson and Prendergast, 1989).

### 2.8.3 Upper Group Chromitite Layers

Contrary to the lower group chromitites, the upper group chromitites bear close resemblance to each other and can be correlated stratigraphically throughout the entire length of the Great Dyke (Fig.2.7). Significant longitudinal and transverse variations in internal stratigraphic, olivine/chromite modal ratios, and chromitite compositions are important features of the upper group chromitites. Individual units show an upward gradation from massive chromitites through semi-massive chromitites to strongly disseminated olivine-chromitites at the top (Prendergast, 1987). Locally, nodules are present in each of the Upper Group chromitite seams (Hughes, 1970; Prendergast, 1979). Seams are highly irregular, with single layers varying in thickness from 5 to 100 cm. In composite seams, the total thickness of massive to disseminated olivine chromitites may be up to 4 m (Prendergast, 1987). They are frequently hard and lumpy in outcrop, but tend to become less compact and friable down dip towards the axis of the basin. Rapid lateral variation in olivine/chromite ratios and the number and thickness of the component layers has been recognized. In the Darwendale sub-chamber, the olivine/chromite ratio and thicknesses of the layers all decrease outward from the axial zone in C1 (C1c-C1e) and C2a. In general, Cr: Fe ratios vary between 1.2 and 2.7 in the C1 and C2a seams of the Darwendale and Sebakwe sub-chambers (Cotterill, 1981; Wilson and Prendergast, 1989). The general $Cr_2O_3$% content in C1 and C2a seams is between 45-47 (Wilson, 1998). Although Seam C3 is present in all complexes, it has a poor Cr:Fe ratio, and has not been developed. Its thickness is less than 10 cm.

A greater proportion of the upper group chromitite seams have been mined along outcrop to a depth of 4 m. Lower seams are accessed by sinking inclined shafts and sub-inclines (Worst, 1960). North of the Mutorashanga Pass the chrome workings extend beyond the axis of the Great Dyke of Zimbabwe.

Mining problems arise from the low mechanical strength of the serpentinites such that considerable maintenance of the underground workings is required. In addition high stripping ratios (20-30 tonnes of waste to 1 tonne of ore) together with the lateral variations in thickness of seams, and faulting result in high input costs to maintain underground workings. Apart from this, about 10 % of the ore is lost during handling and transportation due to its friability (Cotterill, 1981).

**Table 2.3** Characteristics of the Chromitite Seams of the North Chamber

*[Revised after Cotterill, 1981; Wilson and Prendergast, 1989].*

| Chromitite Layer | $\%Cr_2O_3$ Range (Mean) | Cr/Fe Ratio Range (Mean) | Width (mm) Range (Mean) | Depth Below No.1 Seam (metres) | Distance between Seams | Remarks |
|---|---|---|---|---|---|---|
| C1 (C1c-C1e) | 38-46 (42) | 1.6-2.3 (1.9) | 10-400 (160) | 0 | 0 | Mainly hard lumpy in outcrop |
| C2a | 32-46 (39) | 1.4-2.3 (1.8) | 0-600 (180) | 30 | 30 | Mainly hard lumpy in outcrop |
| C3 | 25-40 | 1.4-2.0 | 0-500 (30) | 170 | 140 | Mainly disseminated |
| C4 | 44-52 (±48) | 2.5-3.0 (±2.8) | 40-200 | 700 | 530 | Mainly Hard lumpy (outcrop and at Depth) |
| C5 | 36-52 (±45) | 2.3-3.5 (±2.6) | 0-400 (100) | 900 | 200 | Grade variable.Gradational into hangingwall. Cr/Fe ratio decreases upwards. |
| C6 | 49-50 | 3.1 | 0-400 (100) | 1018 | 118 | 50% hard lumpy (outcrop), friable (at depth). Grade consistent. |
| C7 | 48-49 | 3.1 | 0-400 (90) | 1112 | 94 | 30% hard lumpy (outcrop), friable (at depth). $\%Cr_2O_3$ increases to 52.5% at Depth on axis of Dyke |
| C8 | 49-51 | 2.9 (2.8-3.1) | 0-400 (75) | 1246 | 134 | 20 % hard lumpy in outcrop, friable at depth |
| C9 | 43-47 (46) | 2.9 (2.8-3.3) | 0-200 (100) | 1362 | 116 | Limited Data |
| C10 | (49) | 3.2 | 0-190 (100) | 1490 | 128 | Limited Data |

### 2.8.4 Eluvial Chromite

A significant amount of chromite can be recovered from soils along the Great Dyke of Zimbabwe. Chromite-bearing eluvial soils have been exploited in the hilly northern part of the Great Dyke of Zimbabwe around the Mutorashanga. The soils contain from 3 to 40 % chromite grains being derived from the serpentinites (Cotterill, 1981). Soils at Mutorashanga have yielded 10 to 25 % chromite. Chromite grains have been recovered by treating over spiral concentrators followed by cleaning on electromagnets (Slatter, 1979). Final products have a $Cr_2O_3$ content and Cr:Fe ratio varying between 48-55 % and 2.0 – 2.50 respectively (Peacocke, Simpson & Associates, 2000; Slatter, 1979). The grain sizes of chromite crystals in soils are generally smaller than those in seams, averaging 0.2-0.4 mm in diameter (Cotterill, 1981).

### 2.8.5 Nickel

Nickel laterite deposits associated with the serpentinites are found around the Impinge area, north of Mutorashanga on the Great Dyke (Cotterill, 1981; Slatter, 1979). The nickeliferous laterites in the vicinity of Impinge contain up to 0.8 – 2.5 % Ni (Cotterill, 1981; Prendergast and Wilson, 1989). A significant proportion of Ni occurs in eluvial soils having concentrations up to 0.6 to 1.2 % nickel (Cotterill, 1981). According to Cotterill (1981), the inferred reserves of Ni from the laterites and eluvial soils amount to several tens of millions of tonnes. The serpentinite bedrock beneath the eluvial chromitite-bearing soils is lateritised to depths of up to 2 m (Wilson and Prendergast, 1989). The weathering of ultramafic rocks gives rise to nickeliferous laterites. The highest nickel contents are linked to the distribution of secondary phyllosilicates that are generated by the breakdown of olivine, pyroxene and serpentine.

### 2.8.6 Platinum Group Elements

The association of the sulphide-rich zones with the pyroxenites in the Ultramafic Succession, and its association with major cyclic units is unique to the Great Dyke of Zimbabwe. Elsewhere, in layered magmatic intrusions, the sulphide rich zones are known to occur in association with the Mafic Succession (Wilson et al., 1989; Wilson, 1996; 1998). Concentrations of platinum group elements (PGE) are found in the P1 layer pyroxenites. The sulphide mineralisation is hosted by medium-grained poikilitic feldspathic orthopyroxenite comprising 85 % cumulus orthopyroxene and 15 % post-cumulus phases of mainly plagioclase and augite (Brown, 1988).

Two major zones of concentrations of sulphides have been identified: the Main Sulphide Zone (MSZ) and the Lower Sulphide Zone (LSZ). The MSZ and LSZ respectively are 3 metres and 6.5 metres respectively below the websterite layer at the top of the Ultramafic Sequence (Fig. 2.8). Significant concentrations of platinum group elements occur in the MSZ. Despite its great thickness, the LSZ is barely economic. At Hartley Mine, the MSZ comprises a lower PGE sub-zone rich in Pt, Pd and other precious metals and an upper sub-zone enriched in base metals with low PGE content. In the Darwendale sub-chamber, the MSZ is 2-3 m thick with the PGE sub-zone having a thickness of 10-30 cm (Brown, 1998). Pronounced variations in sulphide contents, which correlate with the Cu/Ni and Pd/Pt ratios occur across transverse sections. The average Pt/Pd ratio is 1.3 whereas that of Cu/Ni ratio is 0.6. Axial zones of the Darwendale and Musengezi sub-chambers comprise low-grade mineralisation. The extreme marginal zones are rich in sulphide mineralisation comprising finely disseminated pyrrhotite, chalcopyrite, pentlandite, and minor pyrite. High degrees of alteration have mainly affected the high-grade ore zones in which the primary mineral phases have been replaced by tremolite, talc, magnetite, biotite, chlorite, quartz, carbonate and chromite all intergrown with the sulphides. Such alteration is insignificant in the axial zone (Wilson, 1998).

tremolite, talc, magnetite, biotite, chlorite, quartz, carbonate and chromite all intergrown with the sulphides. Such alteration is insignificant in the axial zone (Wilson, 1998).

Main platinum group mineral phases identified in the MSZ include braggite ([Pt, Pd] S), cooperite, (PtS), laurite ($RuS_2$), moncheite ($PtTe_2$), merenskyite ($PdTe_2$), maslovite (PtBiTe), michenerite (PdBiTe), kotulskite (PdTe), polarite (PdBi), sperrylite ($PtAs_2$) and hollingworthite (RhAsS) (Wilson, 1998).

## 2.9 Compositional Variation of Mineral Phases in Ultramafic Sequence

The mineral chemistry of Great Dyke lithologies has profound influence on the weathering and alteration processes. Compositional trends indicate an average decrease in Mg contents through the Ultramafic sequence from cyclic Unit 10 upwards (Fig. 2.7).

**Fig. 2.9** Compositional Variation of Mineral Phases in Ultramafic Sequence, Hartley Complex, Darwendale

*(Modified After Wilson and Prendergast, 1989).*

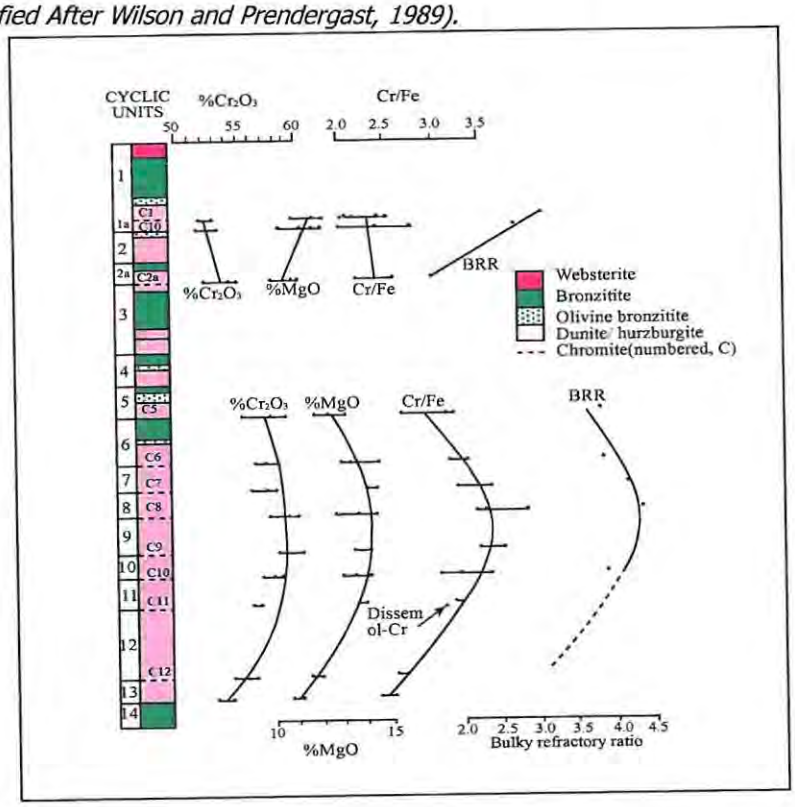


Chromites in the Great Dyke occur as a cumulate phase in the layers at the base of each cyclic unit. Dissemination of chromite occurs throughout the cyclic units of the Ultramafic Sequence. In the chromitite layer, the chromite compositional parameter $Fe^{2+}/(Fe^{2+} + Mg)$ increases from a minimum (0.32) in cyclic unit 10 to a maximum (0.646) in chromitite layer C1c of cyclic unit 1 (Wilson and

**Fig. 2.10** Chromite Chain Textures

*[Photomicrograph showing chromite (black) chain textures enclosing olivine (serpentinised) crystals brownish in plane* polarized *light].*

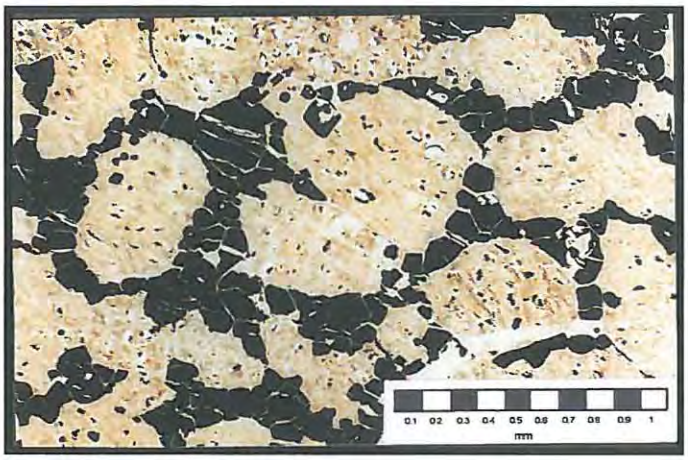


Interstitial chromites in dunites have higher $Fe^{2+}/ (Fe^{2+} + Mg)$ ratios than that in chromitite layers, whilst chromites enclosed in olivines are also more Fe-rich that enclosed in orthopyroxene (Wilson and Prendergast, 1989). The compositional parameter $Fe^{3+}/ (Cr+Al+Fe^{3+})$ increases upwards from about cyclic unit 9 in both chromitite layers and disseminated chromite. The chromitite layers however have higher $Fe^{3+}/ (Cr+Al+Fe^{3+})$ ratios than disseminated chromite in the dunite layers.

**Fig. 2.11** Euhedral Chromite Grains

*[Photomicrograph of chromite (dark) disseminated in serpentinite showing euhedral forms (plane polarized light)].*


**Fig. 2.12** Skeletal Chromite Grains

*[Photomicrograph (plane polarized light) showing chromite grains (black) enclosing sepentinised olivine].*


## 2.10 Alteration Processes in the Great Dyke

Rocks in the Great Dyke are variably altered as a result of post-emplacement processes. Rocks especially rich in olivine such as dunite and harzburgites tend to be affected. Pyroxenites and gabbros contain little or no olivine and are generally unaltered (Worst, 1960). Alteration of olivine-rich rocks is generally a result of hydration and carbonation processes driven by meteoric fluids that penetrate the rocks from the earth surface downwards. Fractures and faults cutting the dunite and harzburgite will accommodate a more effective penetration of the fluids, and alteration will be centered along such structures. Serpentinisation, however, does extend to greater depths along faults. Serpentine is not the only mineral that forms during alteration. Others include magnetite, brucite, talc, magnesite, opaline silica and various hydrated Ni-Mg-silicates such as garnierite have all been observed on the Great Dyke of Zimbabwe. As a result of alteration the bulk composition, of the original rock changes resulting in associated changes in density and volume). Systematic changes occur with alteration intensity. As a result of fluid-driven alteration, olivine is commonly replaced by serpentine (generally lizardite) a process called serpentinisation. From deep mining and drilling it appears that the intensity of serpentinisation decreases with depth. This means that with depth, an increasingly larger proportion of the original olivine crystals remain unaltered. In general, surface and near-surface rocks contain no fresh olivine, whereas no serpentinisation occurs in un-fractured rocks beneath depth of ~300m (Worst, 1960).

**Table 2.4** Bulk Compositions of North Dyke Serpentinites at Various Depths

*[The compositions are compared to the composition of an unaltered dunite, (Worst, 1960)].*

| | **Dunite** | **Serpentinite1** | **Serpentinite2** | **Serpentinite3** |
|---|---|---|---|---|
| Sample Id | **P568** | **P469** | **G32** | **G112** |
| Depth location | Fresh | 55m depth | 30m depth | 3m depth |
| SiO2 | 38.06 | 32.44 | 39.32 | 34.86 |
| Al2O3 | 1.57 | 2.01 | 1.21 | 3.57 |
| Fe2O3 | 1.56 | 5.41 | 2.18 | 5.72 |
| FeO | 8.29 | 4.19 | 2.36 | 3.42 |
| MgO | 47.18 | 44.06 | 39.27 | 34.27 |
| CaO | 0.60 | 0.00 | 0.00 | 3.00 |
| Na2O | 0.07 | 0.00 | 0.06 | 0.22 |
| K2O | 0.16 | 0.08 | 0.05 | 0.21 |
| H2O | 0.15 | 8.91 | 12.11 | 12.02 |
| CO2 | 0.00 | 0.49 | 0.31 | |
| TiO2 | 0.00 | 0.02 | | 0.35 |
| P2O5 | 0.00 | | | |
| Cr2O3 | 2.31 | 2.36 | 3.09 | 2.19 |
| MnO | 0.13 | 0.03 | 0.04 | 0.14 |
| NiO | | | 0.12 | |
| **Total** | **100.08** | **100.00** | **100.12** | **99.97** |

Serpentine is not the only mineral that forms during alteration. Others include magnetite, brucite, talc, magnesite, opaline silica and various hydrated Ni-Mg-silicates such as garnierite have all been observed on the Great Dyke of Zimbabwe. As a result of alteration the bulk composition (and specific density and volume) of the original rock changes. Systematic changes occur with alteration intensity. Since alteration is largely driven by the availability of meteoric water (plus any compounds dissolved within it), in combination with oxidation in the atmosphere and the potential to accommodate rock volume increases, the most strongly altered rocks will be found at surface. These rocks have chemical compositions that deviate most from their original composition. Changes in chemical composition with depth as a result of decreasing amounts of alteration can be illustrated with bulk chemical compositions of serpentinite from the North Dyke as reported by Worst (1960).
With increased alteration, the following trends can be:

MgO: MgO content gradually decreases from ~47wt% to <35wt%.
$H_2O$: $H_2O$ content increases dramatically from <0.2wt% to >12wt%
$CO_2$: $CO_2$ content may increase dramatically

$SiO_2$: $SiO_2$ content generally decreases slightly, but it could increase again near surface with deposition of opaline silica

$Fe_2O_3$: $Fe_2O_3$ content increases sharply within the surface oxidation zones

These trends are mostly due to serpentinisation of original olivine in combination with continued alteration of the serpentinite closer to surface. Chemically the following reactions occurred during alteration of the original dunite (Deer et al., 1992). Serpentinisation was driven by the addition of water to olivine without significant changes in rock volume:

$$\mathbf{5Mg_2SiO_4 + 4H_2O = 2Mg_3[Si_2O_5](OH)_4 + 4\ MgO + SiO_2} \quad \textbf{(1)}$$

*olivine* *serpentine*

For this reaction to proceed, significant amounts of MgO and $SiO_2$ must be removed in solution. This will result in a significant increase in the pH and $Mg^{2+}$ content of the fluid. Any iron contained in the olivine will be transformed into magnetite, which may also incorporate excess Ni. The above serpentinisation reaction will occur at depth, where the overburden pressure of overlying rocks confines volume increases. Mg and Si will move with the fluids closer to surface.

A different reaction that may occur is:

$$\mathbf{2\ Mg_2SiO_4 + 3H_2O = 2Mg_3[Si_2O_5](OH)_4 + Mg(OH)_2} \quad \textbf{(2)}$$

*olivine* *serpentine* *brucite*

This reaction is accompanied by a significant volume increase and can only proceed if such an increase can be accommodated (e.g. in fracture openings along faults, or near surface). The chrysotile asbestos fibres intergrown with fibrous brucite found in Ethel Mine may have formed by this reaction. Serpentine may alter in the presence of $CO_2$-rich or silica-rich fluids. This process will result in the formation of talc and magnesite:

$$\mathbf{2Mg_3[Si_2O_5](OH)_4 + 3CO_2 = Mg_3[Si_4O_{10}](OH)_2 + 3MgCO_3 + 3H_2O} \quad \textbf{(3)}$$

*serpentine* *talc* *magnesite*

or

$$\mathbf{4Mg_3[Si_2O_5](OH)_4 + 4SiO_2 = 3Mg_3[Si_4O_{10}](OH)_2 + 3MgO + 5H_2O} \quad \textbf{(4)}$$

*serpentine* *talc*

Reaction (3) will proceed if $CO_2$-rich fluids can penetrate the rock. Such fluids are likely to be acidic and will react with the alkaline fluids resulting from the serpentinisation process at depth (reaction (1)). Therefore, it is expected that the formation of talc and magnesite will more effectively occur closer to surface and possibly in dilatant sites, e.g. along fracture openings.

Reaction (4) requires a high Si activity in the fluids. Fluids generated at depth during reaction (1) may transport Si closer to surface where volume increases can be more readily accommodated so that reaction (4) can proceed. MgO liberated during this reaction will result in highly alkaline fluids enriched in Mg. This reaction also suggests that the formation of talc will preferentially occur closer to surface. These altered rocks when eventually exposed through erosion and denudation processes will easily weather resulting in soil formation and release of chromite, magnetite and other less easily weathered minerals. Apart from the above alteration phases, several other secondary alteration products may form near surface. This includes opaline silica ($SiO_2.nH_2O$), which accumulates in open spaces by evaporation from solution. A semi-precious variety of this type of opaline quartz is mutorolite. Ni released during serpentinisation from the crystal lattice of olivine may be incorporated in serpentine to form the Ni-serpentine garnierite, $(NiMg)_3[SiO_5](OH)_4$. Garnierite can be found as a bright green, soft coating along fracture planes in weathered serpentinite rock (Worst, 1960).

### 2.10.1 Implication of Weathering Processes on the Geology of the Great Dyke

Alteration in the Great Dyke mainly affects dunite. Original olivine crystals are strongly altered to a depth of ~300m with alteration products progressing according to the sequence:

**Olivine ⇒ serpentine ⇒ talc ± magnesite ± brucite.**

This alteration sequence result in the gradual decrease in MgO content and an increase in the $H_2O$ content of the rock, whilst quartz is redistributed. The most completely altered rocks can be found near surface. MgO liberated during the alteration process will react with available meteoric water to result in highly alkaline and Mg-rich fluids. These fluids are flushed out of the system by groundwater flow (Nyamapfene, 1991).

### 2.10.2 Great Dyke Soil Formation

The strongly altered near surface serpentinite rocks act as a shield for less weathered dunite at depths, protecting them from corrosive atmospheric conditions. Exposed serpentinite rock is rapidly weathered to give soils, and in the process liberating chromite disseminated or interstial to the serpentine. Fig. 2.10 to Fig. 2.12 shows chromite dissemination in serpentinite.

## CHAPTER 3

# 3.0 Geomorphology of the Great Dyke

## 3.1 Introduction

The geomorphology and present landscape of the Great Dyke reflects its erosion history since exposure to surface. The chromite-rich soils of the Great Dyke are a result of weathering of its exposed geology due to the influence of climate, topography and landscape changes over time. The geomorphological history of the Great Dyke is linked to the geomorphic events affecting the Zimbabwe basement complex and the entire southern Africa.

This chapter reviews historical developments in landform and landscape classification and their application to southern Africa, Zimbabwe and the Great Dyke. The significance of geomorphic processes in the distribution and occurrence of soils and eluvial chromite deposits of the Great Dyke is also reviewed. The present day knowledge of southern African geomorphic history has benefited largely from information gathered through fairly recent coastal and offshore oil exploration drilling, which brought to light essential stratigraphic data along much of the continent's margins. Such data has been key, to providing essential chronological controls as well as providing important dating evidence from terrestrial sequences and kimberlites from the continental interior. Analysis of marine sediments plays a major role in deducing the rates of weathering on the continental surface of Southern Africa (Partridge and Maud, 1987).

The effects of continent-wide tectonic and eustatic events and climatic changes associated with continental drift are evident in the present day stratigraphic, geomorphic and pedological features of the Great Dyke and its environs. This report follows the classification and analysis of Partridge and Maud (1987) with adaptation of appropriate aspects of Zimbabwean geomorphology from Lister (1987).

## 3.2 Landform and Landscape Evolution: A brief Overview

The concept of base level, the lowest level to which a river can erode its bed, dictates that over long geological periods the rate of landscape lowering may be balanced by isostatic uplift, but if no uplift occurs then theoretically the land surface could be worn down to the sea level. The sea level being the base–level, below which erosion cannot normally take place (Pritchard, 1986). Davis (1899) using this concept of base level explained the development of landscapes and suggested for the first time that erosion progressed in cycles.

### 3.2.1 Erosion Cycles

The development of landscapes was envisaged by Davis (1899) to consist of an initial youth stage, followed by a maturity stage and finally an old age stage. The initial stage of youth, he suggested, begins after uplift, with a landmass above sea level, leading to erosion by rivers. The rivers drain directly into the sea in an attempt to wear down the landscape to sea level. The inception of the second stage of maturity would then follow with the consequent streams being joined by subsequent streams developing along lines of weakness and generally flowing at an angle to the consequent streams. Subsequent streams would in turn be joined by obsequent streams, which would flow generally opposite the consequent stream thereby achieving a major lowering of the plane. The third and final old age phase would thus be characterised by a flat plane interrupted occasionally by remnant inselbergs (Pritchard, 1986).

Davis's (1899) suggested mode of development of planes which is governed by erosion and removal of material from the entire watershed surface, resulting in widespread low-level peneplains without vestigial remnants of older surfaces at higher level, was soon to come under criticism, inherently due to recognition of a series of erosional surfaces. Penck (1924), after making the observation that slopes neither decreased in angle nor did they become gentle with age, argued that slopes eroded and retreated laterally whilst maintaining their original angle (i.e. "they retreated parallel to themselves" (Pritchard, 1986)). Penck's (1924) ideas became the basis of the theory of pediplanation

### 3.2.2 Pediplanation and Parallel Retreat of Scarp

King (1949) adopted and modified Penck's (1924) ideas and applied them to the landscape of Africa. King (1949) studied closely four important aspects of hill slopes, which included examining the nature of the slope, the erosion and the process of parallel retreat. The four elements of his study are listed below and illustrated in Fig. 3.1

- Waxing slope or crest is subject to chemical or mechanical weathering, exfoliation and surface wash.

- Free-face or scarp is subject to pressure release, gulleying, basal sapping, and rock fall.

- Constant debris or talus slope is subject to intense chemical weathering, leaching and gulleying weathering. Weathering material will be in transit.

- Waning slope or pediment is subject to sheet wash, gulleying and deposition.

**Fig. 3.1** Four Elements of Study in Retreat of Scarps

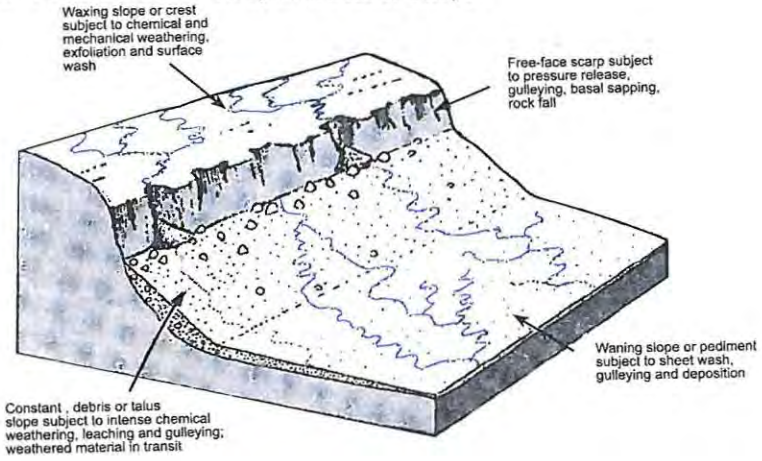


Weathering causes the scarp to retreat slowly parallel to itself by losing material to the talus slope. As weathering progresses rock waste accumulate on the debris or talus slope and the crest becomes progressively smaller resulting in development of extensive pediments and until finally adjacent pediments merge to form extensive areas of gently sloping surfaces (Fig. 3.2). Using this model, King (1949) suggested that the preservation in the African landscape of ancient land surfaces, separated by prominent escarpment, is possible only if landscape development is dominated by the more or less parallel recession of the intervening scarps.

**Fig. 3.2** Landscape Development According to Penck (1924) and King (1949)

*Diagrams illustrating lateral retreat, considered to be the main process involved in landscape lowering. This process rather than vertical lowering is now widely accepted as the dominant mechanism of landscape lowering.*

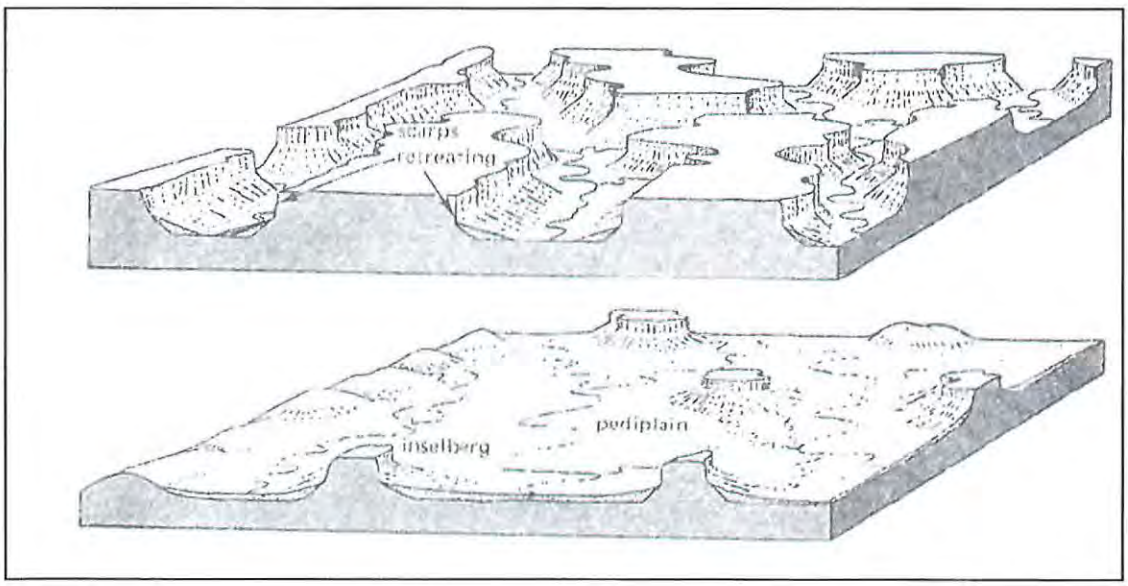

Despite scarp-parallel recession gaining widespread acceptance, Moon and Selby (1983) challenged the idea of a strictly parallel retreat, citing evidence for the constant readjustment of slopes to equilibrium, which in turn is dependent on local rock mass strength. This predominance of back-wearing over down-wearing, particularly in the evolution of the interior plateau of southern Africa, had earlier been questioned by Wellington (1955).

### 3.2.3 Identification and Correlation of Land Surfaces

Following pioneering studies in East Africa by Wayland (1931), the emphasis on identifying and correlating of African land surfaces at a regional and continental scale began in earnest. It was suggested that these surfaces could have been produced by successive cycles of erosion, initiated by intermittent uplift since the Triassic. The recognition of the Great Escarpment as an erosional feature and its role in separating the marginal areas of the southern African sub-continent from the interior plateau was soon to become central to surface correlation. The importance of the Great Escarpment, which "forms an enormous horseshoe-shaped step at distances ranging from 50 to more than 500 km from the present coastline" has attracted the attention of many geomorphologists. Furthermore the observation and correlation between land-surfaces with tectonic events "culminated in the model of isostatic compensation, linking onshore erosion and offshore sedimentation to mechanical properties of the lithosphere and mantle" (Partridge and Maud, 1987). Other models have been proposed as possible alternatives for marginal uplift among them the "phase-change model" of Smith (1982). In this model Smith (1982), proposes that the movement of the African plate over pre-existing oceanic ridges during the course of continental drift provided a heat source necessary for continental uplift. The creation of a new base level as a result of lowering of the sea level as is envisaged during the Cenozoic and attributed by Vail et al. (1977) to be the basis of an alternative origin for onshore erosion.

Summerfield (1985), in an examination of eustatic fluctuations and onshore denudation cycles, showed that the effects of such fluctuations to be critically dependent on both the rate of concurrent tectonic adjustments along the coastal margin and geometry of this margins. He thus argued that this "does not necessarily result in landscape rejuvenation". The dominance of continental uplift in shaping the gross morphology of the African continent is supported by the work of Cogley (1985).

### 3.2.4 Landform Development Sequence and Classification

The sequences of cyclic erosion of land surfaces are landmarks of major geomorphic events. The geomorphic history recognized in Zimbabwe, like the rest of Africa, can thus be traced through a series of major evolutionary stages commencing prior to Gondwana break-up during the late Jurassic (Lister, 1987). The Gondwana configuration prior to its separation into various southern continents had Africa

in a central and inland position and was thus at a considerable elevation. Pre-rifting elevations are estimated to have been about 2400 metres above sea level in the east and 1500 metres above sea level in the west of the continent (Rust and Summerfield, 1990). The margins of the continent, after rifting and Gondwana break-up, were at a higher elevation and were thus rapidly eroded to a gently sloping plain close to oceanic base level. At the same time erosion proceeded in the plateau area inland of the escarpment edge with the interior network of river systems providing the erosion base level. The result of this was an unusual situation of two land surfaces of the same age being cut at different levels above and below the Great Escarpment (Partridge and Maud, 2000). The resultant vast erosional surfaces form the present day African surface. Above this surface a number of mountain massifs were preserved behind the Great Escarpment.

In Zimbabwe these are classified as Gondwana and Post Gondwana surfaces and are typified by the Zimbabwe Eastern Highlands. Field investigations by Partridge and Maud (1987) suggest that pre-rifting Gondwana surface, as suggested by King and King (1959), is not preserved in southern Africa as a sub-aerial planation feature, even in relic form. The break up of Gondwana as a result of rift faulting resulted in the initiation of the Great Escarpment (Fig. 3.4). The Great Escarpment was characterised by short rivers draining seaward and long inland drainage, which was characterised by river capture. The dawning of Cenozoic saw southern Africa transacted by the widespread African surface interrupted only by occasional high standing mountain massifs. The warm and humid climate during most of the Cretaceous is thought to have greatly facilitated rapid erosion through the well-developed drainage network. This permitted deep weathering mantles to develop over susceptible lithologies (Partridge and Maud, 2000). The advance of planation and the decline in erosion rates during the later part of the Cretaceous resulted in extensive deep weathering and development of the African surface with its deep saprolite occupying much of the landscape.

The catastrophic events that brought the Cretaceous to a close were accompanied by major global change in climates. Desiccation during this period resulted in widespread development of duricrust, which had an effect of armoring the deep weathered profiles from further erosion (Fig. 3.3). Associated with these deep-weathered laterites are silcrete profiles usually underlain by thick kaolinitic saprolite as well as the development of the Kalahari basin which was largely in response to specific topographic and changing moisture regime. The African landscape inherited from the Cretaceous underwent negligible changes due to the general absence of regional tectonics.

**Fig. 3.3** Development of Duricrust

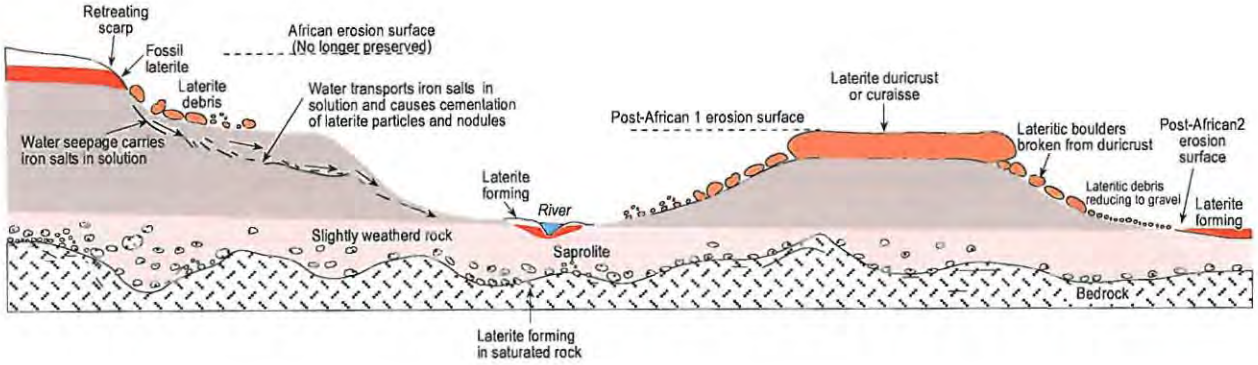


**Fig. 3.4** Great Escarpment and Events during Miocene and Pliocene in Southern Africa

*(Modified after Partridge and Maud, 1987)*

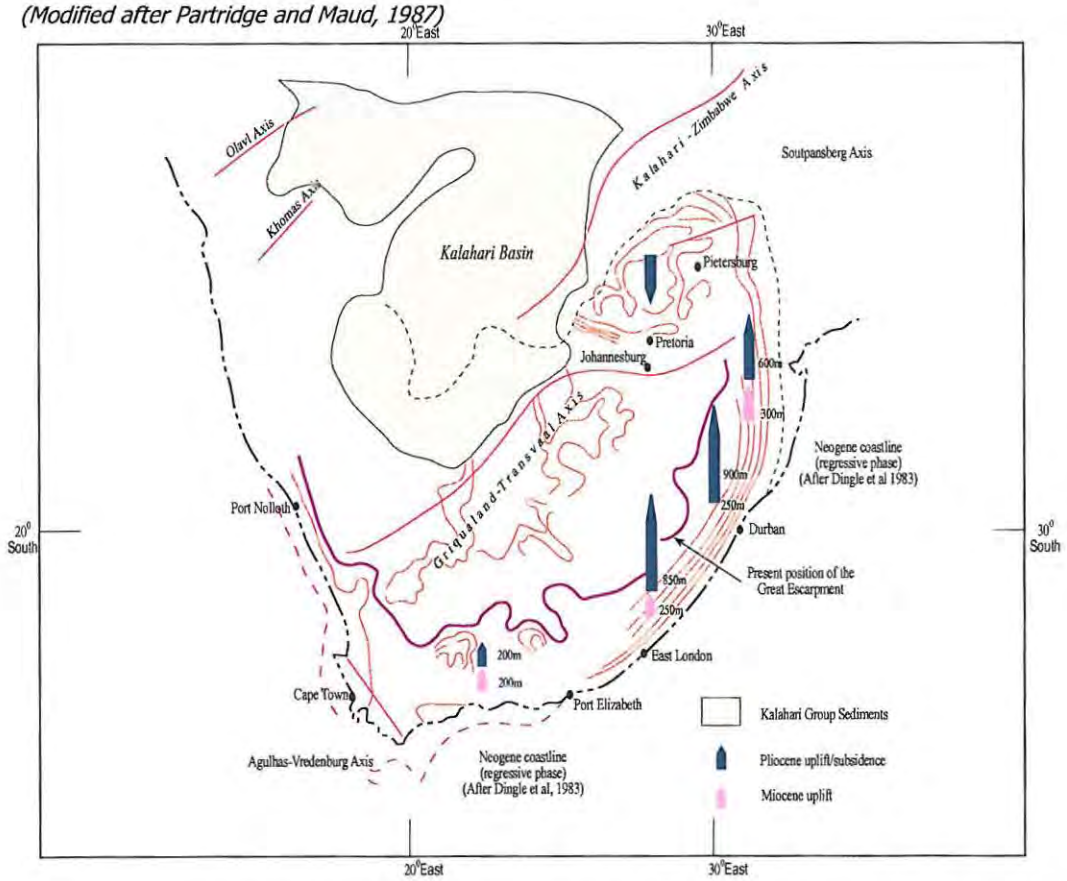


During the Miocene, moderate uplift of between 150 to 300 metres occurred with a slight tilting of the African surface to the west and "limited coastal monoclinal warping" (Partridge and Maud, 1987). This was followed by the inception of the Post-African 1 erosion cycle formed in response to this uplift. This cycle was characterised by imperfectly planed surfaces and major deposition in the Kalahari Basin as well as slight steeping of the westward flowing river courses. River incisions during Neogene resulted

in drainage patterns largely controlled by the pre-Karoo topography exposed by Cretaceous stripping. The interior of the sub-continent was subjected to modest and localised movements along the Griqualand-Transvaal and the Kalahari-Rhodesia Axes, which in addition to accentuating the southern rim of the Kalahari rim, resulted in reorganized drainage pattern due to cutting-off of southwards flowing drainage systems (Partridge and Maud, 2000). After the Post African 1 cycle of erosion, another major asymmetrical uplift (up to 900 metres on the eastern margin) of the subcontinent resulted in major westward tilting of the previous landscape. The second uplift and subsequent further tilting resulted in considerable increase in offshore sedimentation. The effect of this tilting and subsequent erosion of lithological units is evident on the Great Dyke where the northern part of the Great Dyke has the mafic and ultramafic successions largely eroded and the dunite-succession rocks exposed, whilst the southern part has the upper lithologies largely preserved. This uplift resulted in the initiation of yet another erosion cycle of major valley incision. The incision of coastal gorges, down-cutting and formation of higher terraces along interior rivers resulted in the formation of the Post African II erosion surface (Partridge and Maud, 2000).

## 3.3. Erosion Surfaces of Zimbabwe.

The cyclic sequences of the erosion surfaces of Zimbabwe were first noted by King (1967) and later confirmed and adopted by Lister (1987) Comparison is drawn between these cycles and those of Partridge and Maud's (1987) ( See Table 3.1).

**Table 3.1** Landscape Evolution

<table>
<tr><th colspan="3">Partridge and Maud (1987)</th><th colspan="2">King (1967) Lister (1987)</th></tr>
<tr><td>Post African II</td><td colspan="2">Late Pliocene to Present</td><td>Late Pliocene to Present</td><td>Quaternary</td></tr>
<tr><td>Pliocene Uplift</td><td>Pliocene</td><td>2.5 Ma</td><td>Pliocene</td><td>Pliocene</td></tr>
<tr><td>Post African I</td><td colspan="2">Mid-Miocene to Late Pliocene</td><td rowspan="2">Miocene</td><td rowspan="2">Post African</td></tr>
<tr><td>Miocene Uplift</td><td colspan="2">18Ma</td></tr>
<tr><td rowspan="2">African</td><td colspan="2" rowspan="2">Late Jurassic to mid Tertiary</td><td>Mid-Cretaceous to end-Oligocene</td><td>African</td></tr>
<tr><td>Early Cretaceous</td><td>Post Gondwana</td></tr>
<tr><td>Gondwana Break up</td><td colspan="2">120Ma</td><td>Mid to late Jurassic</td><td>Gondwana</td></tr>
</table>

## 3.3 The Geomorphic Provinces of Zimbabwe

According to Lister (1987) "Zimbabwe can broadly be divided into four major geomorphic provinces, each exhibiting its own distinctive geomorphology." These distinctive geomorphic provinces are largely controlled by relief (Fig. 3.5). Altitudes in Zimbabwe, range from below 250 metres above sea level at the confluence of Save and Runde rivers in the south-east of the country to nearly 2600 metres above sea level, at Nyanga, in the eastern highlands. About 66% of the area of Zimbabwe stands above 1000 metres above sea level and hence the average elevation of the country is high and accordant with topography in most parts of the country (Lister, 1987). The topography exhibits a broad southwest to northeast trend parallel to the central belt of highland forming the Zambezi-Limpopo divide. The eastern highlands region however, follows a north to south trend, which is parallel to the Great Escarpment. In most localities the geomorphology reflects the underlying geology. The most obvious and dominant terrains, are the "granite topography", which exhibits kopjes and balancing rocks. Other resistant lithologies such as the Great Dyke pyroxenites and greenstone-belts' banded-ironstones, result in characteristic hill-types and hill-slope profiles. The six major erosion cycles recognised in southern Africa are observed in Zimbabwe.

**Fig. 3.5** Geomorphic Provinces of Zimbabwe

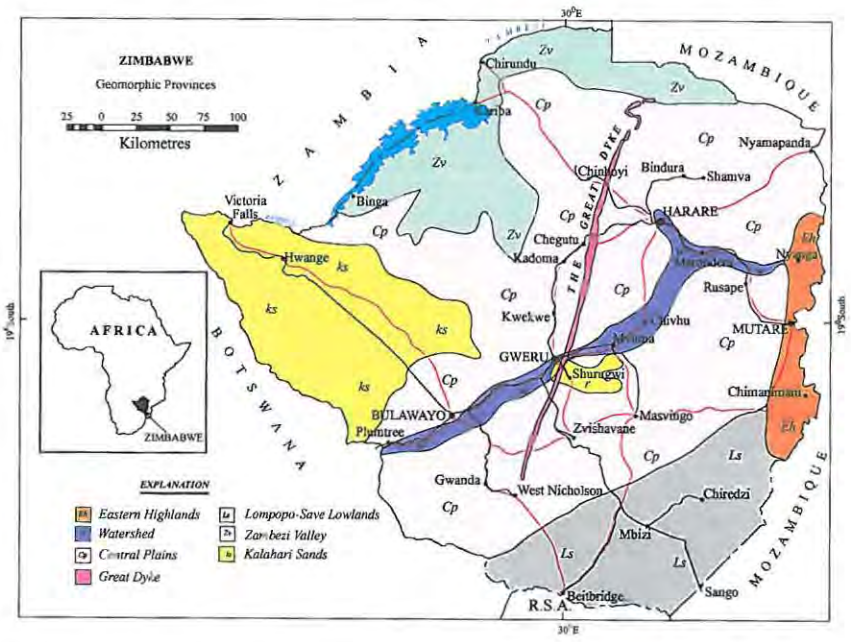


*The four major geomorphic provinces of Zimbabwe are:*

- *Eastern Highlands*
- *Limpopo-Save Lowlands*
- *Zambezi Valley*
- *Central Region*

### 3.3.1 Eastern Highlands

The Eastern Highlands is a 250 km northerly trending mountainous belt. The belt is characterised by high relief and areas above the African erosion surface elevation of Partridge and Maud (2000). The drainage, within the Eastern Highlands, is either westwards to the Nyan'ombe, Odzi and Save rivers or eastwards to the Gairedzi, Pungwe and Honde rivers. The belt conforming to the eastern Highlands forms part of the Great Escarpment and has been the locus of repeated uplift particularly during movements that initiated the African and post African erosion cycles (Lister, 1987)

### 3.3.2 The Limpopo-Save Lowlands

The Limpopo-Save lowland consists of Post-African II surface which is extensive over a wide area, northwards from the Limpopo River (Lister, 1987). The excessive erosion that occurred since the Pliocene uplift is attributed to constant and repeated sheet wash. After the Pliocene uplift major rivers of Mwenezi, Runde and Umzingwane incised the land surface initiating the Post-African II erosion cycle (Lister 1978).

### 3.3.3 The Zambezi Valley

This is a trough, considered essentially to be a graben structure (Lister, 1987). These down faulted valleys namely the Mid-Zambezi and Lower-Zambezi basins are occupied by the Karoo sequences. Governing the landscapes within the Zambezi valley geomorphic province is the Post-African II erosion cycle.

### 3.3.4 The Central Region

The Central Region covers more than half the entire country and includes the Central Watershed, the Great Dyke and the Kalahari sand cover. The Central Watershed is at an angle to the Great Dyke (Fig. 3.5). Where the two intersect African surfaces are preserved on some peaks as at Lalapanzi. Flanking these areas are zones of Post-African I erosion surfaces and occasional Post African II incision within the large rivers.

## 3.4 The Great Dyke Geomorphic Features.

The Great Dyke generally stands above its surroundings and carries an older summit planation (Lister, 1987). It stands out as a ridge where the more resistant pyroxenite and gabbroic rocks are exposed or less commonly as plains where the fast weathering serpentinites are exposed near surface. The Great Dyke exhibits the African, the Post-African I and Post-African II surfaces along its length. The types of exposed surface have important pedological influences and hence are important for the ultimate eluvial chromite concentration in the soil.

### 3.4.1 Geomorphic Features of the North Dyke

The northern tip of the Great Dyke was dislocated by faulting into an ENE- trending Mavuradonha Mountains, which peaks at 1628 metres above sea level at Banirembizi, (Plain of Zebras), and the Nyaruswiswi hills and carry the African surface (Lister, 1987). The altitude is generally above 1300 metres above sea level and topography consists of extremely hilly and broken-up terrain with deeply incised river valleys. This type of terrain occurs as far south as the Suguru gap where the Gurungwe fault breaks the Great Dyke (Fig.3.6). Along the entire Great Dyke, only in the Musengezi complex do gabbroic rocks occupy low-lying terrain as opposed to complexes where the same rocks invariably form high relief. Southwards between Suguru gap and Darwendale the Great Dyke shows its typical form being approximately 3 to 4 kilometres wide and less than 1600 metres above sea level. In this section the Great Dyke forms a topographic step separating a Post African I surface of relatively higher granite plateau (1500 metres above sea level ) on the east from lower ground (1200 metres above sea level) to the west

**Fig. 3.6** North Dyke Region Location of Important Geomorphic Features

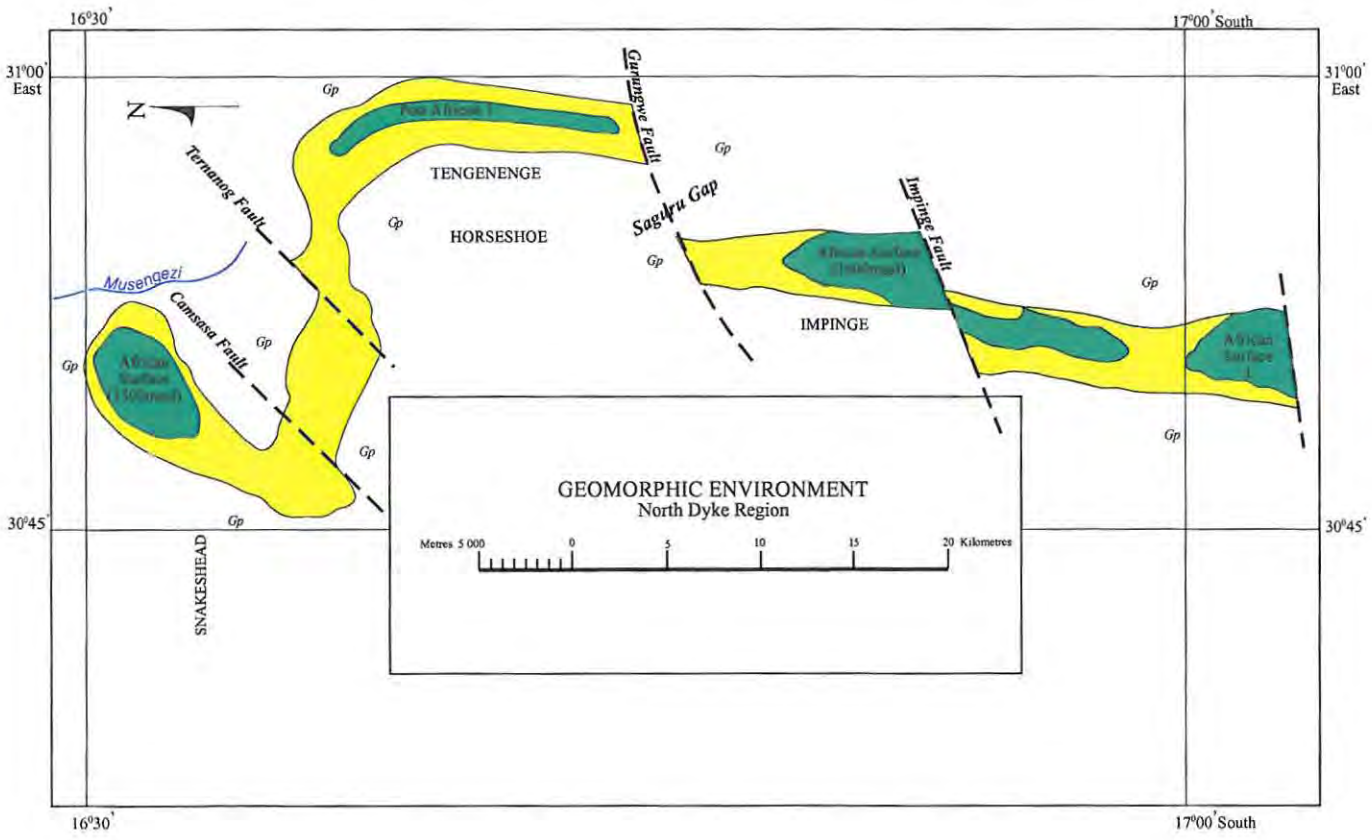

**Fig. 3.7** Longitudinal Section of the Mavuradonha Sub Chamber

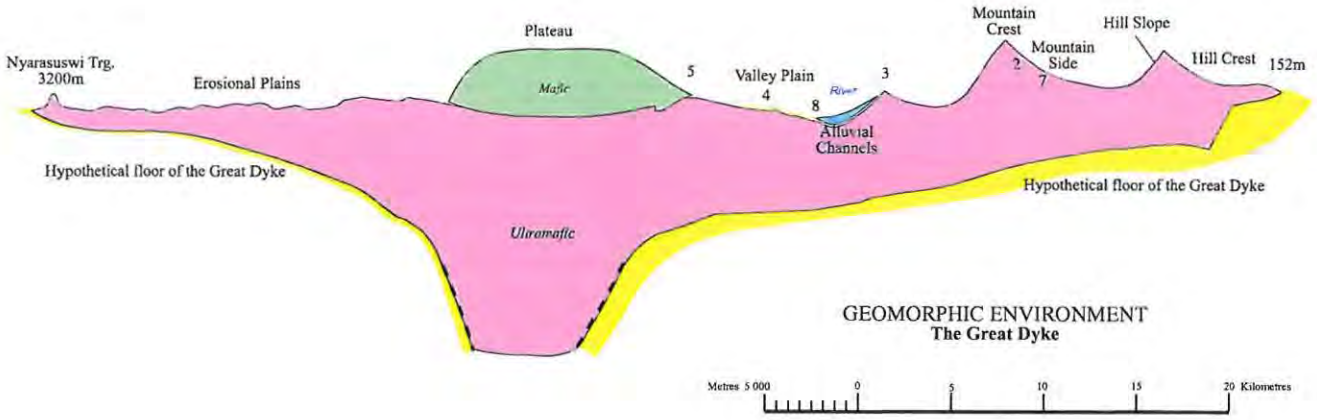


The Mvurwi range summit planation is at 1550 metres above sea level. Although the Great Dyke is a synclinal structure, at Mvurwi Range it forms numerous spectacular hills and ridges some of which rise to altitudes of approximately 1700 metres above sea level. Examples are the Mvurwi Peak (1746 metres above sea level), to the immediate south of Mutorashanga Pass, the Chikonyora and Smoky Peaks west of Centenary.

### 3.4.2 North Dyke Mutorashanga Viewpoint.[1]

Mutorashanga Viewpoint offers a spectacular view of the northern section of the Darwendale sub-chamber of the lower party of the Ultramafic Sequence (Fig. 3.8). The location of the viewpoint is just west of the axis on the dunite succession. The view to the north along the axis shows progressively lower horizons in the sequence by virtue of the southerly plunge of layering. Conversely the view to the south is up the sequence and the lower cyclic units of the brozitite succession.

[1] Geological Society of Zimbabwe Great Dyke Excursion (1997)

**Fig. 3.8** Sketch Showing the Ultramafic Sequence of the Hartley Complex at Mutorashanga Viewpoint – View to the North

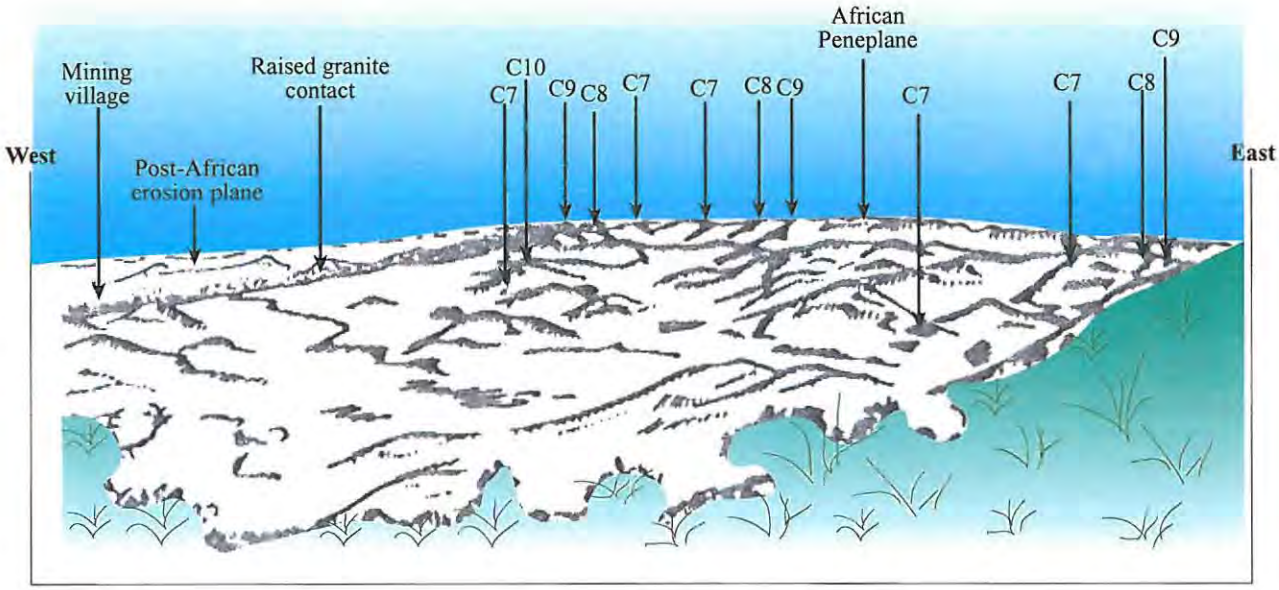


Deep valleys and high standing hills characterize the landscape produced by weathering of the serpentinite under sub-tropical conditions (Fig. 3.8). The North Dyke has an annual rainfall of 1000mm and average annual maximum temperature of 20°. From the viewpoint the inward-dipping attitudes of the chromitite layers are obvious though the southerly plunge of the Great Dyke combined with the steep topography results in complex outcrop patterns. Towards the northwest, close to the Mining village of Mutorashanga, the granitic contact can be seen as a low ridge parallel to the Great Dyke margin. Contact metamorphism from the emplacement of the Great Dyke has resulted in local hardening of the granitic rocks, rendering them slightly resistant to weathering and erosion.[2] An important feature of the landscape on either side of the Great Dyke in this area is the difference in general elevation, the west side being 250m lower than the east side (Wilson, 1982). The Darwendale sub-chamber lies to the west of the central watershed and it would appear that it has acted as a resistant mass, in places surmounting to the Post–African I erosion surface, with the west side reflecting a more juvenile erosion character. Remnants of the mature African erosion surface are observed in high-standing platforms on the axis of the Great Dyke. The subsequent weathering characteristic appears to have been a major influence on the physical nature of both eluvial chromite concentrations and the layer chromitites. A further important weathering effect has been the development of laterite formation of silicate nickel in some areas on the east side (Prendergast et al., 1997).

[2] Geological Society of Zimbabwe Great Dyke excursion notes 1997(Wilson and Prendergast).

**Fig. 3.9** Sketch Showing the Ultramafic Sequence of the Hartley Complex at Mutorashanga View Point – View to the South

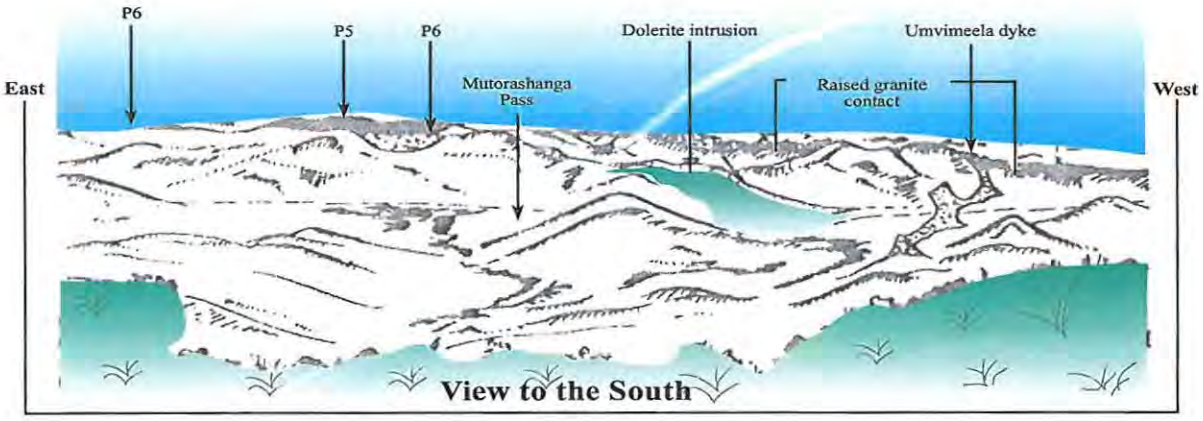


The western granitic contact is marked by low hills close to the Great Dyke - granite contact (Fig. 3.9). The serpentinite hills are barren of trees but of significance are the notable vegetation anomalies. Dolerite intrusions in the middle ground are well wooded and so are the pyroxenite layers higher in the sequence. In the North Dyke area the African surface has been eroded on both flanks of the Great Dyke by the Post-African I erosion cycle and sometimes to such an extent that at certain localities, valleys from east and west have coalesced thereby forming passes through the range. Examples are the Airey's Pass, Birkdale Pass and Mpinge Pass. The Mutorashanga Pass and the Caesar Pass are however on the higher African surface. In the northern portion of the Mvurwi Range and southwards to about 2 kilometres south of the Mutorashanga Pass only the dunite succession is preserved and therefore serpentinite is the only outcropping lithology of the Great Dyke. From Mvurwi Peak southwards the lithologies are progressively overlain by pyroxenite. Southwards from Darwendale into the Middle Dyke the Great Dyke does not forms a pronounced topographic feature.

### 3.4.3 Geomorphic Features of the Middle Dyke

South of Darwendale to Ngezi Dam the Great Dyke exhibits mild topographic expression and is virtually incorporated within the surrounding Post African I erosion surface of the region. The Great Dyke can however still be traced by soil colour and vegetation patterns (Worst, 1960; Lister, 1987). Small and sporadic hills (e.g. Rutala Hills, Majuja, Seigneury, Dawn and Lone Kopje) form residuals of the African surface at altitude of between 1243 to 1356 metres above sea level in the Middle Dyke. These hills are generally made up of silicified serpentinite. The Great Dyke is thought to have been a topographic feature during Mesozoic times remnants of which are seen from the central Mashava Mountains whose relief rarely exceeds 100 metres. There is a distinctive African planation level at approximately 1420 metres above sea level, which exhibits less irregular topography than the Mvurwi Range in the North Dyke region. All the major rivers flow through the Mashava Mountains, (e.g. Muzvezve, Ngezi,

Munyati and the Sebakwe) eroded through the Great Dyke Post-African I surface to form valleys linking up Post-Africa II plains on both sides of the Great Dyke (Lister 1987).

The southern part of the Middle Dyke extends from Ngezi dam to Lalapanzi. The Middle Dyke has a very regular appearance with the topography consisting of a prominent Great Dyke dominated by serpentinites. At Lalapanzi the Great Dyke crosses the central watershed and the Zambezi-Limpopo divide. At this locality deposits of the Karoo Kalahari sands have been preserved. A characteristic lateritic duricust profile of the African surface is also preserved seen at Lalapanzi (Fig.3.10). The area east of the Limpopo–Zambezi divide extending to Shurugwi, defines the most southerly part of the Middle Dyke. The African surface extends southwards from Lalapanzi on the serpentines with several pyroxenite layers, which form conspicuous scarps and ledges (Lister, 1987). Near the mafic unit of the Unki Platinum Deposit, the Selundi Range forms a steep, flat-topped ridge of African land surface along its crest. Further south the Chironde Range has an irregular summit line with only the highest peaks reaching the African surface. South of Chironde Range, the relatively less resistant serpentinites of the Great Dyke, enabled the Post-African I surface to develop equally across the Great Dyke and the surrounding granites (Lister, 1987)

**Fig. 3.10** Duricast Characteristic of African Surface, Lalapanzi.

3.4.4 Geomorphic Features of the South Dyke.

The South Dyke extends from Shurugwi through the mafic lithologies around Mimosa Mine to Doro Range and the Great Dyke termination. At Torwood and southwards granites terrace above the Great Dyke as domes due to stripping of the old African surface and exposure of the etched surface. The Great Dyke rocks are more deeply incised to Post-African I erosion cycle while the surrounding granite stand out higher. The resistance of the southern-most end of the Great Dyke pyroxenites shown by the Doro Range, which forms a dominant central ridge, and drains on either sides. At the southern tip of the Great Dyke the granites stand out in a spectacular "amphitheatre" formed by the harder

younger granite adjacent to the Great Dyke. The granite hills sometimes go up to African surfaces (Fig. 3.11).

**Fig. 3.11** Section of the Resistant Pyroxenite Ridge in Granite Surroundings, South Dyke

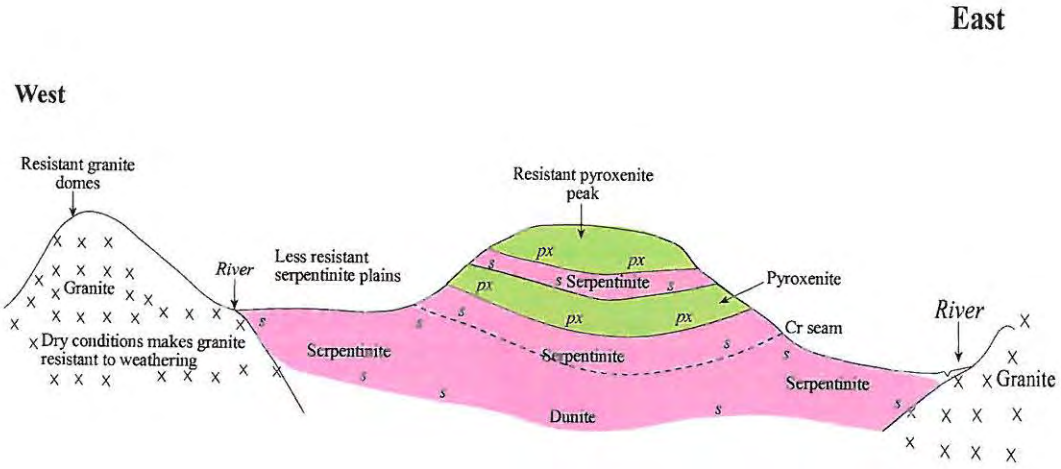


**Fig. 3.12** Pyroxenite Ridge at Doro Range

*(Picture showing the Doro Range, a pyroxenite ridge resistant to weathering. Picture taken from a granite dome and facing west from about 4km east of the Great Dyke).*

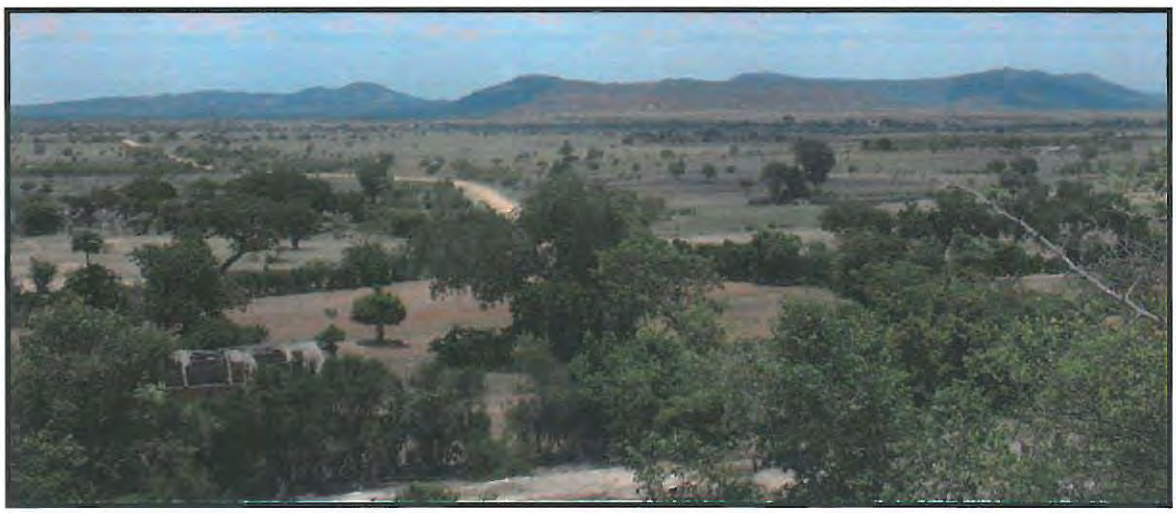

## 3.5 Summary on Land Surfaces Influence on Great Dyke

### 3.5.4 African Surface Influence

The African surfaces, on the Great Dyke, are confined to mountain peaks such as the Mvurwi Range, the Mavuradonha range at the North Dyke and the Mashava and Chironde ranges in the Middle Dyke where it has been preserved as the resistant pyroxenite and gabbroic rocks. Elsewhere it occurs at Lalapanzi where it has survived erosion at the intersection of the Great Dyke with the Zambezi-Limpopo divide due to low rates of denudation. The pyroxenite and gabbroic ridges are zones of weathering and erosion and may not preserve any accumulation mineral from weathering breakdown. These lithologies are however host to minerals such as PGEs, chromite, several base metals, gold and silver which can be released during weathering and deposited elsewhere.

### 3.5.5 Post-African I Surface Influence

The Post-African I surface is by far the most dominant surface on the Great Dyke. It is largely confined to the Great Dyke areas flanking the pyroxenite and gabbroic ridges and the areas where the Great Dyke does not form prominent ridges. The Post-African I surfaces on the Dyke are predominantly underlain by serpentinites which provide ideal sites for the development of colluvial and eluvial soils. Where the Post African I surface overlies gabbroic and pyroxenite sequences, thick agriculturally important soils often develop. The Post-African I surface extend further than the Great Dyke width giving extensive flat plans conducive to heavy mineral deposition.

### 3.5.6 Post-African II Surface Influence

The Post-African II surface is associated largely with incision valleys across the Great Dyke were major rivers have cut through to link areas of Post-African II erosion on either side of the Dyke. These areas are usually associated with removal of previous deposition and where active deposition is taking place black clayey soils develop. These are also referred to locally as black cotton soils.

### 3.5.4 The Influence of the Zambezi-Limpopo Divide on the Great Dyke

The incision of the Zambezi River in the north and the Limpopo River incision in the south gave rise to the Kalahari-Zimbabwe up-warp axis of Du Toit (1933). The resultant uplift in central Zimbabwe is largely responsible for the present day drainage pattern observed in Zimbabwe and the rest of southern Africa. This drainage pattern has existed since the union of the proto-Middle and proto-upper Zambezi Rivers during Pliocene to early Pleistocene. The incision of the Zambezi under relatively wetter condition and the incision of the Limpopo under drier condition have resulted in different effects on the landscape which can be seen on the Great Dyke and its environs from the central watershed. The effects of weathering and erosion are greater in the wetter northerly draining plains which are

rugged and more deeply incised by swift flowing rivers. Contrary, the southerly draining plains are flatter and characterised by more gentle plains, with fewer large rivers which typically drain by sheet-wash erosion.

### 3.5.5 The Effects of Climate on Geomorphology

Geomorphology has an indirect effect on soil distribution pattern in Zimbabwe (Fig 3.13). The geomorphic provinces of Zimbabwe thus largely coincide with the six agro–climatic regions observed in the country. The high rainfall, high altitude regions form prime agricultural regions of the country. The interplay between high relief and high rainfall and hence high weathering rates promote good soil development. The resultant soils tend to be deep and rich due to high bioactivity. These soils support greater vegetation, which in turn result in abundant organic matter responsible for acidic conditions which promote rapid breakdown of organic matter.

The Great Dyke however traverses almost all of the country's natural regions, the influence of which is only notable at local levels. Apart from the region I, in the Eastern Highland and region VI, of the Lowveld, the Great Dyke has local expression of all these natural regions.

**Fig. 3.13** Agro - Climatic Regions of Zimbabwe

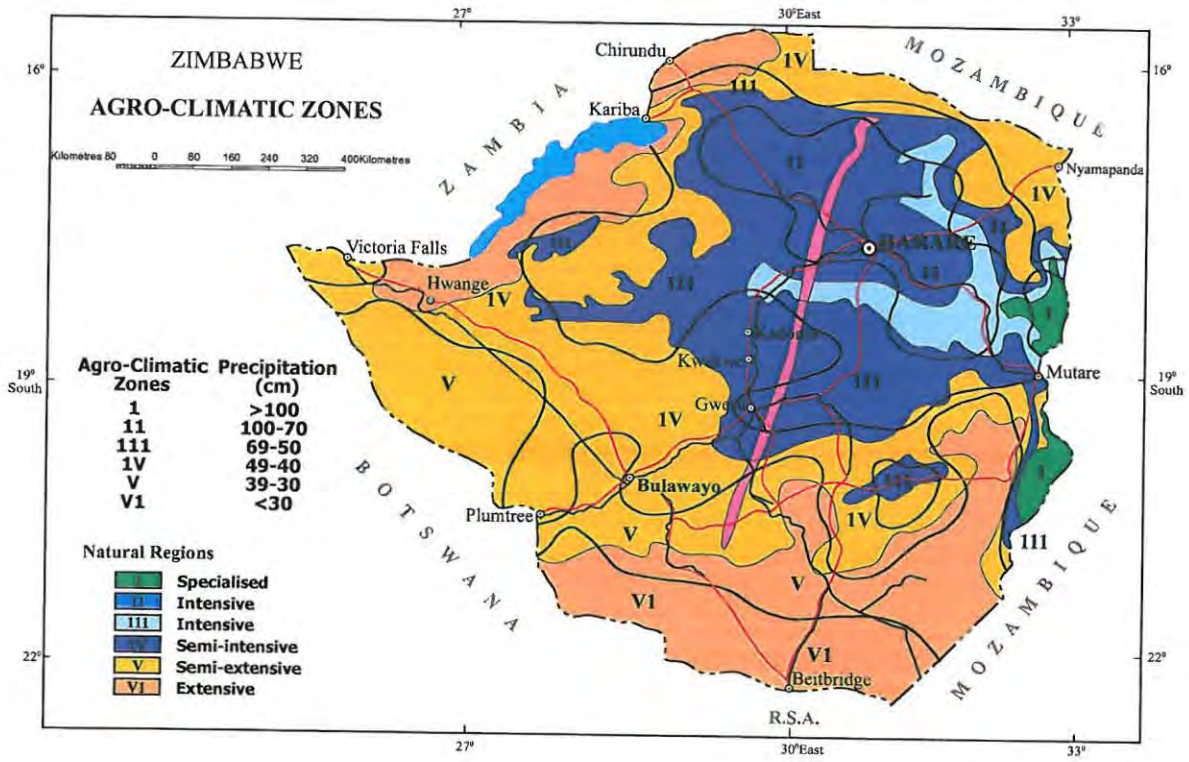

## Chapter 4

# 4.0 Role of Surfaces Processes in Great Dyke Soil Profile Formation

## 4.1 Introduction

Regolith and landform study is a prerequisite to understanding the distribution and occurrence of placer and residual mineral deposits. The importance of soils as a sampling media and often as the host to economic concentration of minerals is due their widespread distribution with 75% of all exposed land surfaces covered by soil (Levinson, 1974). The soil usually overlies bedrock from which it is derived due to chemical and physical breakdown process on exposure to carbon dioxide ($CO_{2)}$, water ($H_2O$) and other elements of nature. The concentration of minerals in the soils is a result of climatic influence and depositional setting. Both these factors have a profound implication on resultant soils cover type. Mineral types have different degrees of resistance to weathering. Oxide minerals tend to be most stable and hence are most resistant to weathering, silicates are of intermediate resistance whilst carbonates and sulphates are least resistant. Atmospheric factors affecting soil minerals are oxygen, water and carbon dioxide. These affect the soil minerals through the process of ionization, hydration and carbonation, hydrolysis and oxidation (Mann, 1982). Regolith study and landscape analysis permits the characterization of mineral environments and enable understanding of the process of soil profiles formation. Regolith study is important in elucidating soil deposition and erosion history and any historical changes in climate which could have led to different chemical weathering regimes. Such climatic changes are often encrypted in the soil profile. The recognition and understanding of soil profiles enables the formulation of complex soil surveys, and dictates the appropriateness of any sampling domain (Bradshaw and Thomson, 1979; Levinson, 1974).

## 4.2 Soils Formation

Soil is a product of both chemical and physical weathering. The process of soil formation involves soluble compounds, which move down with meteoric water. This downward percolation of water is influenced by water table elevation changes. In an open system soluble compounds are flushed out of the system as a result of leaching (Fig. 4.1). This process results in the formation of acidic soils such as podzols and also forms laterites. Closed systems result in precipitation of insoluble new substances above the water table (Fig.4.2). The closed system results in alkali soils and calcretes. These insoluble minerals or their replacement and alteration products become preserved in the soil profiles as residual minerals. These residual minerals are usually oxides and include minerals such as iron II oxide ($FeCr_2O_3$), tin oxide ($SnO_2$), iron III oxide ($Fe_3O_4$) and titanium oxide ($TiO_2$). Where the oxides have accumulated they can breakdown as a result of physical weathering and may be re-deposited as placer deposits.

The development of soil is an integral part of weathering (Fig. 4.3). Soil can thus be defined as a product of weathered rock more or less in-situ above the bedrock.

**Fig.4.1** Soil Profile Open System

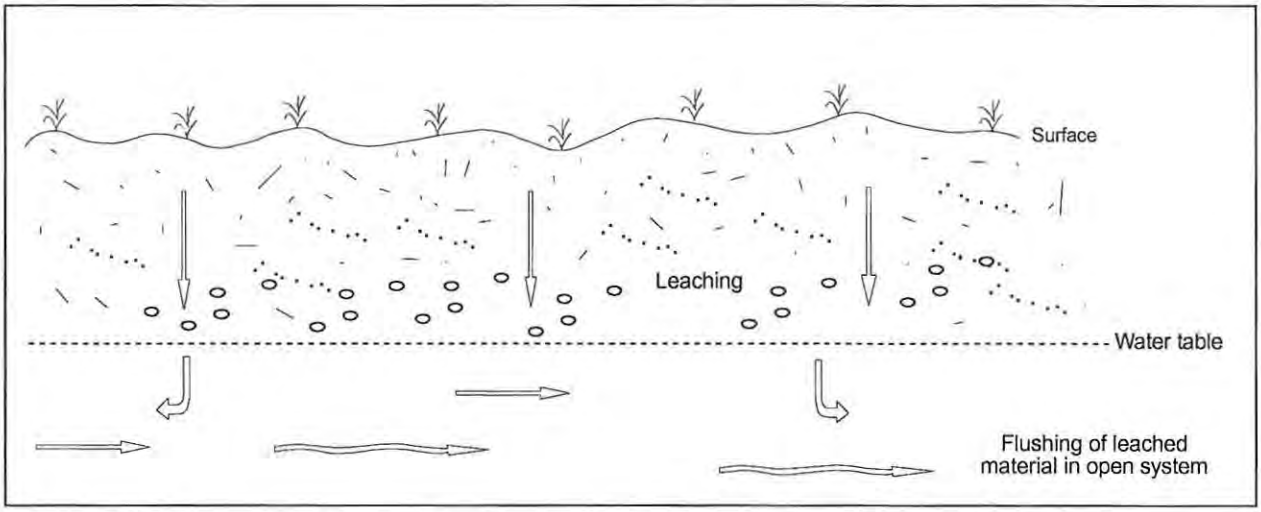


**Fig. 4.2** Soil Profile Closed System

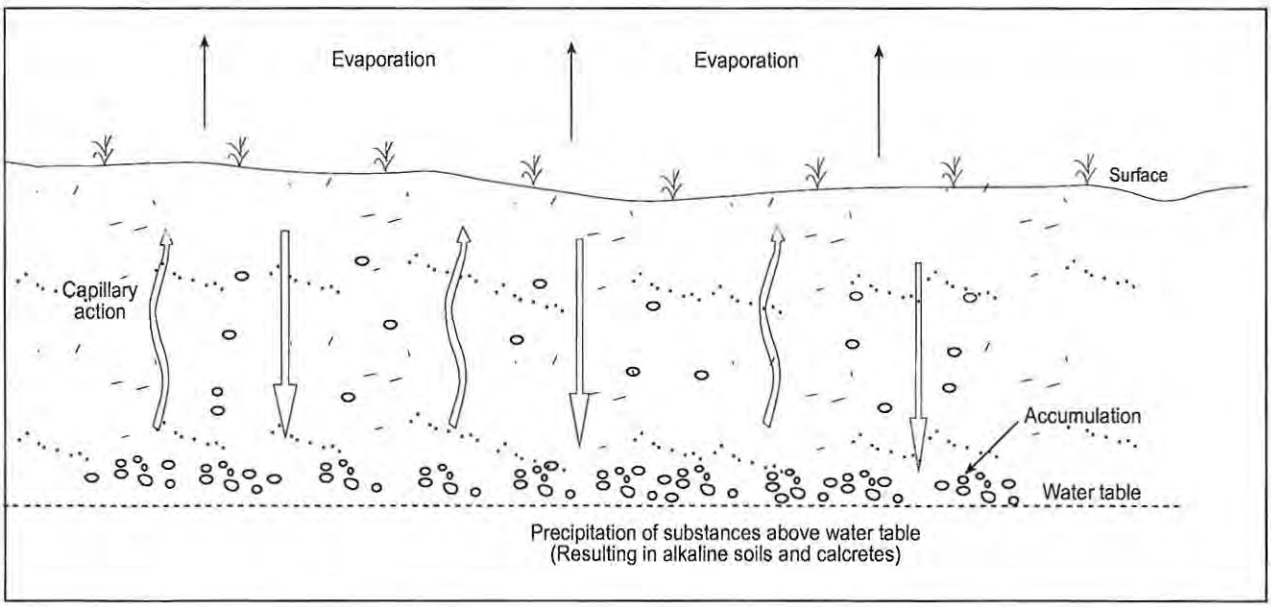

**Fig.4.3** Soil Regolith

*(A soil regolith showing the entire weathered material above bedrock)*

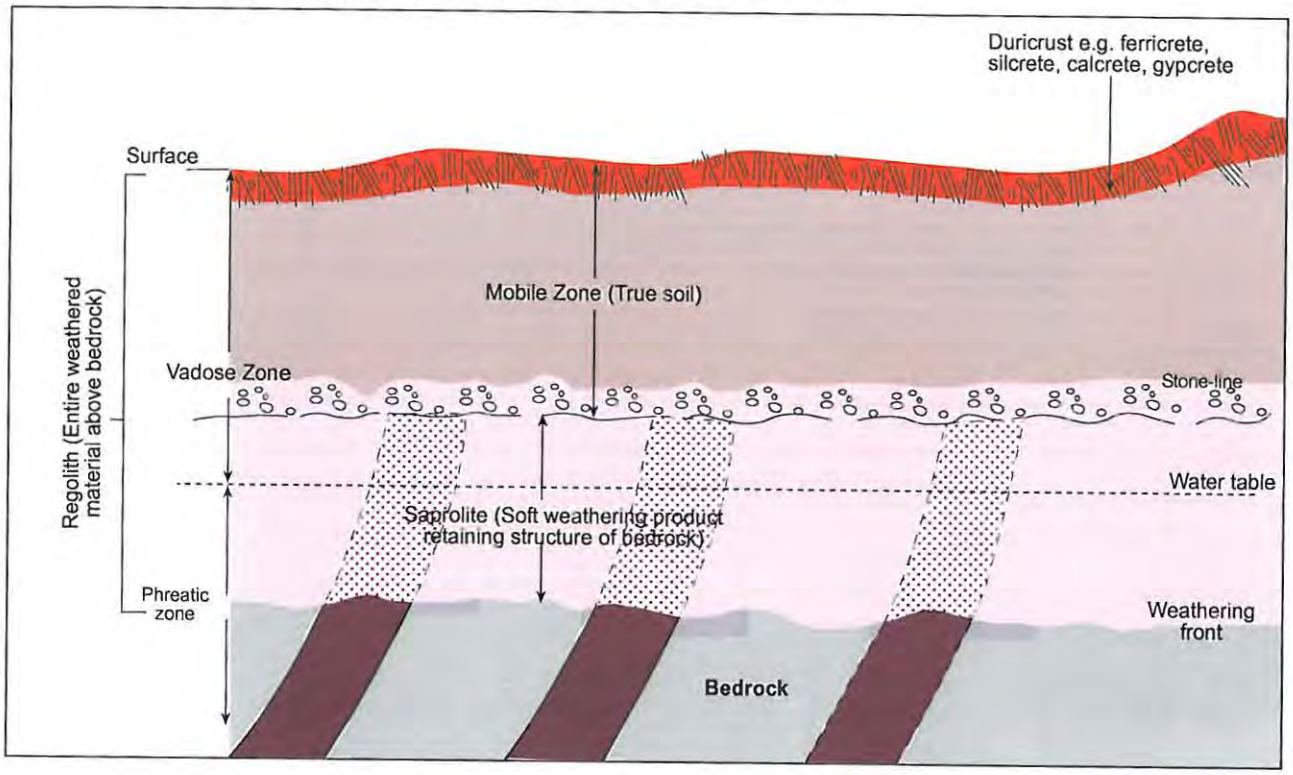


4.2.1 Chemical Weathering Processes

Minerals show different degrees of resistance to weathering. Minerals readily react with oxygen to produce stable oxides and silicates. Carbonates, sulphides and sulphates are however more susceptible to alteration due to the effect of oxygen ($O_2$), carbon dioxide ($CO_2$) and water ($H_2O$). These effects could be ionization, hydration or hydrolysis, carbonation and oxidation (Mann, 1982). These reactions tend to occur as a combination in nature. At a neutral pH of 7, water breaks into ionic components of $H^+$ $OH^-$ resulting in slow reaction where minerals interact with water through hydrolysis. However due to the dissolution of atmospheric $CO_2$ in water ($H_20$) carbonic acid is formed and creates an acidic environment. Acidic environment promote faster rates of reaction.

**Fig 4.4** Oxidation Process Involving Fe

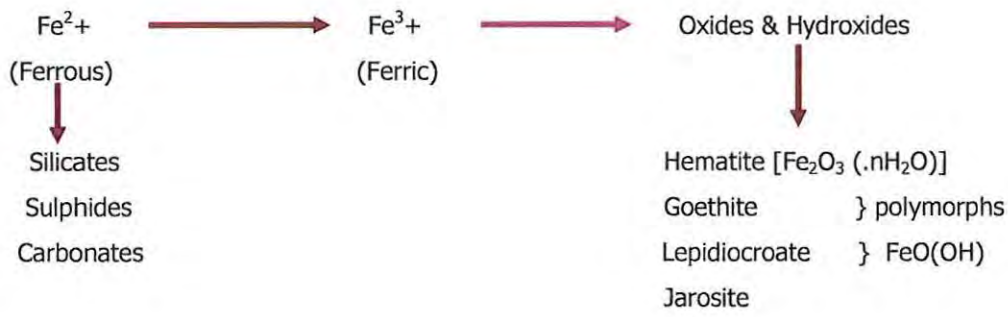

The presence of carbon dioxide in the environment is promoted by the numerous bioactivities associated with most essential life supporting systems. Some elements such as Fe and Al have low solubility and tend to rely on bioprocesses for mobilization. Of these chemical processes, oxidation is most dominant. Important elements prone to oxidation include Fe, S and Mn and these generally oxidize as illustrated in Fig. 4.4.

### 4.2.2 Role of Biological Activities in Soil Formation

Living organisms play a significant role in soil formation. Their role is both in physical and chemical breakdown of materials during soil formation. The activities of termites for example result in breakdown and mobility of soil particles. Termites and other organisms loosen soil through barrowing which both allows aeration and greater water circulation. Termites are able to pick up soil particles with their mandibles from lower horizons and bring them closer to surface where weathering effects are greater (De Dapper, 1989). Other possible effects of soil fauna include the up-working of fine particles closer to surface with the subsequent collapse of small cavities and galleries created by removal of particles soil thickness. The whole process results in concentration of coarse elements at the base of the profile. Some micro-organisms in soils are able to enzymatically attack compounds such as sulphides. The processes of acidolysis, hydrolysis and oxidation of minerals result in redistribution of elements within the soil. Thiobacillus and thiooxidants oxidizes sulphide and ferro-oxides oxidizing them and are as a result often referred to as biological miners (Eckhardt, 1985).

### 4.2.3 Soil Profile A, B and C Horizons

A soil profile is the vertical display of soil horizons. Such a soil profile is illustrated in Fig. 4.5 showing generic descriptions of the different horizons. Soil horizons are distinguished through texture, colour and structure of the soil. Soil formation is process characterised by loss of most mobile material, with stages of development being from saprolite to B-horizon at the base to A-horizon at the top. Soil development also involves landscape lowering (Twindale, 1990; Butt, 1982).

#### $A_0$ Horizon

At the top of the horizon is the $A_0$ horizon. The $A_0$ horizon is primarily composed of organic matter. Fresh litter is found at the surface, while at depth all signs of vegetation structure have been destroyed by decomposition. The decomposition is largely due to biological activity.

#### $A_1$ Horizon

Beneath the $A_0$ horizon is the $A_1$ horizon. The $A_1$ horizon marks the beginning of the true mineral soil. In this horizon organic material mixes with inorganic products of weathering. The horizon typically is a dark coloured horizon due to the presence of organic matter. Eluviation, the removal of inorganic and

organic substances from the soil by leaching occurs in this $A_1$ horizon. The downward movement of water drives the process of eluviation.

**Fig. 4.5** Description of Selected Horizons in Hypothetical Soil Profile (Young, 1976)

| *General Geological Usage* | | Description |
|---|---|---|
| $A_0$ | $A_{00}$ | Loose leaves and organic debris, largely un decomposed. Area of maximum organic activity. |
| | $A_0$ | Organic debris partially decomposed or matted. |
| | $A_0$ | Organic debris fully destroyed. |
| $A_1$ | $A_1$ | A dark-coloured horizon with a high content of organic matter mixed with mineral matter. |
| $A_2$ | $A_2$ | A light coloured horizon of maximum eluviation of clay, iron oxide and/or organic matter. Prominent in podzolic soils; faintly developed or absent in chernozems |
| B | $B_1$ | Transitional from $A_3$ |
| | $B_2$ | Maximum accumulation of silicate clay minerals, or of iron and organic matter; maximum development of blocky or prismatic structure, or both. |
| | $B_3$ | Transitional to C |
| C | $C_{ca}$<br>$C_{cs}$<br>$C_{sa}$ | Horizons $C_{ca}$, $C_{cs}$ and $C_{sa}$ are layers of accumulation of calcium carbonate, calcium sulfate, and soluble salts found in some soils. C horizon is comparatively unaffected by soil-forming processes. |
| D | | Bedrock |

$A_2$ Horizon

Eluviation is a dominant process in the $A_2$ horizon. Leaching or the removal of soluble materials is active in this horizon. The $A_2$ horizon often has a high concentration of resistant and insoluble quartz, which renders the horizon ashy-grey in appearance. Like $A_1$ the $A_2$ horizon is usually poor in metal content due to the process of leaching. Eluviation is significant in relatively humid climates, where ample precipitation occurs resulting in a surplus in the water balance. Eluviation is thus a more dominant process in tropical and humid areas than in arid and semi arid area.

B-Horizon

Beneath the $A_2$-horizon is the B-horizon. The B-horizon is a zone of illuviation where downward moving, particularly fine material, is accumulated. The accumulation of fine material leads to the creation of a denser layer in the soil. The illuviation process involves precipitation of less soluble compounds as oxides, silicates and clays together with some metals. In closed systems the B-horizon is enriched with calcium carbonate in the form of nodules or as a layer. This occurs when carbonate precipitates out of downward moving water or from capillary action. Where precipitation is high and environments characterised by surplus water balance the illuvial layer is found relatively deeper within the soil profile. In semi-arid and arid climates, where precipitation is scarce, illuvial zones are found

relatively closer to the surface. Capillary action may bring up cations such as calcium and sodium dissolved in soil water upward, where they can precipitate into a layer (Riffer, 2004).

C Horizon

The C-horizon is derived from the soil parent material, which is either in situ or transported and deposited into its present location by sedimentary processes. The C-horizon consists of saprolite, which is the soft weathering product of bedrock (D horizon). The saprolite is distinguished by relict bedrock structures. The C-horizon can be up to 100 metres thick in deeply weathered terrains.

### 4.2.4 Profile Formation and Landscape Reduction Etching Mechanisms

Landscape lowering and weathering activities are closely associated (Fig 4.6). At the etch surface some Iron oxides may form due to the process of accumulation.

**Fig. 4.6** Profile Formation and Etching Mechanisms

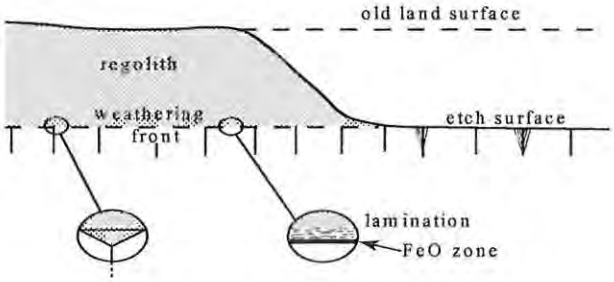


### 4.2.5 Soil Classification

Soil classification systems have a bearing on landform situations and models. Fig. 4.7 summarises a hierarchical system of classification of landforms situations and models (Young, 1976). In considering landform regimes soil classification takes into account paleo conditions and the effects of plate tectonics on continental landmass. Most influential of all, are the climatic conditions of temperature and precipitation. Temperature and precipitation also influences the type of vegetation. Temperature affects the rate of decomposition and generation of acidic enviroment, which in turn enhance the rate of weathering. Climate influences the type of organism and their abundance in the soil. Latitude has an indirect influence on soils as it influences climate. Topography and altitude influence temperature and rate of weathering (Köppen, 1936).

### 4.2.6 Soil Composition

Mineral soil is composed of about 95 % inorganic materials and 5% organic material by volume. In the inorganic fraction of the soil, a large number of minerals occur as a mixture. Minerals in soils occur in three different size fractions, the diameters of which are as follows:

- Sandy fraction (2.0 - 0.02mm)
- Silt fraction (0.02 – 0.002mm)
- Clay fraction (<0.002mm)

The minerals that occur in the sand and silt fractions are mostly primary minerals formed at high temperature and are inherited from the igneous, metamorphic or from sedimentary protolith. The minerals that occur in the clay fraction are considered to be secondary minerals formed by low temperature reactions and are inherited by soils from sedimentary rocks or formed in soils during weathering or pedogenesis. Minerals in soils are classified into crystalline and amorphous (or non crystalline). Most of the minerals are crystalline. There are however, some amorphous minerals in a few soils. These minerals can further be divided into two kinds namely light minerals and heavy mineral, which in turn may be subdivided into essential, accessory and secondary minerals

**Fig. 4.7** Hierarchical Classification of Landform Situations and Models (Young, 1976)

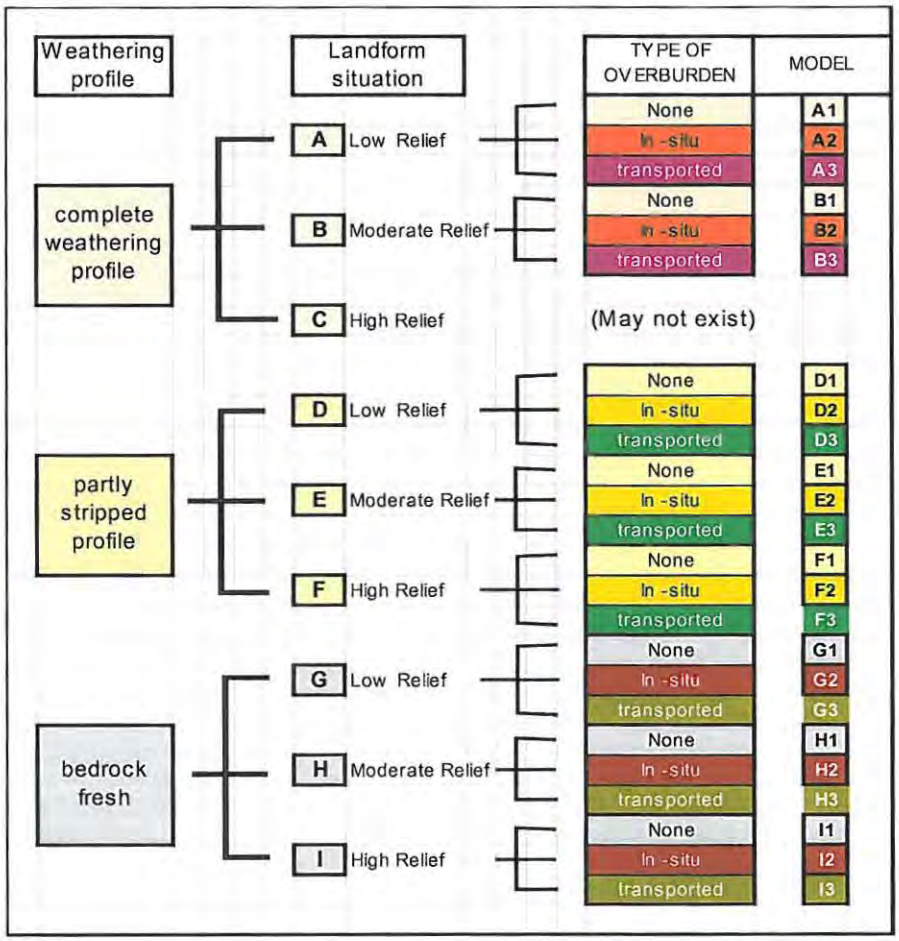

## 4.3 Zimbabwean Soils

Zimbabwe is located in the sub-tropics and at least six climatic regions of pedological significance can be recognised. The climatic regions of Young (1976) recognized in Zimbabwe are as detailed in the following Table 4.1 and summarized in Fig. 4.7. The classical view that the five major soil-forming factors are interdependent and the recognition of the situation where one factor is dominant over others can be seen in Zimbabwe and its soil distribution pattern. There is a close relationship between rainfall and soil distribution patterns. Some very important soil-vegetation relationships are also known to occur in Zimbabwe (Nyamapfene, 1991). There is also a close relation between rainfall and vegetation. The existence of these close relationships between rainfall, vegetation and soils was the basis on which the country was divided into natural regions. These natural regions are basically agro-climatic, but also take into account relations between vegetation and soils as well as physical features (Nyamapfene, 1991; Vincent and Thomas, 1960). Fig. 4.8 shows the country's natural regions.

**Table 4.1** Climatic Regions Pedogenic Significance in the Tropic and Sub-Tropics
*(Adapted from Young 1976)*

| Climatic region | Mean annual rainfall (mm) | Dry season months | Köppen equivalent | Natural vegetation | Zonal soils |
|---|---|---|---|---|---|
| Moist savanna | 900-1200 | 3-5 | Aw, Cwa | Forest and grassland | Ferruginous and ferrallitic soils,( pH 5-6) kaolinitic + smectitite. Base saturation 40-60%. Leached in wet season, dry to 1m in dry season. |
| Dry savanna | 600-900 | 6-8 | Aw, Cwa | Grassland with 5-50% tree cover | Ferruginous and ferrallitic soils, (pH 6-7). Base saturation 60-90%. Less intense leaching. Dry to 2m in dry season. |
| Semi-arid (semi-desert, steppes) | 250-600 | 8-10 | Bsh | Xerophytes, perennial grasses | Brown calcimorphic soils,sierozems, arenosols and lithosols. Carbonate accumulating in profiles. Dry most of the year. |
| Tropical, high altitude (>1600m) | >600 | 0-6 | Cwb, Cwa | Evergreen forests, merging to grasslands and alpine at high altitudes | Humic latsoils; podzolic at high altitudes |
| Sub-tropical humid | >900 | 0-3 | Cfa | Deciduous woodlands | Leached ferruginous soils |

Parent rock material is the most dominant factor in the development of soils. Igneous and metamorphic rocks dominate the Zimbabwean land surface, and constitute 65% of the country's land area (Nyamapfene, 1991). Granites[1] *senso latto*, the most extensive lithology on the Zimbabwean craton, account for 46 % of the land surface covered by these igneous and metamorphic terrains. The granites in Zimbabwe are divided into the older gneissic complex (circa early Precambrian) and younger granites (Proterozoic and later) although neither subdivision is homogenous (Stagman, 1978). Thus whilst granites generally give rise to sandy soils the geological complexity of these granites naturally result in more complex soils types (Nyamapfene, 1991). Associated with these granitic terrains are the greenstone belts, which constitute metamorphosed basaltic and andesitic lavas together with various sedimentary packages. Although less extensive in area than the granites these formations are an important feature of the Zimbabwean geology. Apart from their importance as host to valuable minerals such as gold, they also give rise to the agriculturally important red soils (Nyamapfene, 1991). Basalts extruded during the Jurassic period occur extensively to the south of the country in the Mwenezi district and at Tuli, Sengwe and Chisumbanje areas and to the north in the Batoka gorge and at Jocholo area (Swift, 1961). These Jurassic basalts are different from the basalts of basaltic greenstones, which give raise to red soils referred to earlier. These basalts occur in parts of the country, which are relatively flat and receive relatively low rainfall, with a rainfall mean of about 550 mm but very often less than 450 mm (Nyamapfene, 1991).

Unconsolidated and aeolian Kalahari sands of Tertiary age cover large parts of northwest Zimbabwe. Extensive work by Bond (1952, 1962, and 1967) sheds a great deal of light on the past climatic conditions of deposition as well details of the provenance. These Kalahari sands consist of well-rounded quartz grains with frosted surfaces (Stagman, 1978). The sand is fine to medium grained. The thickness varies from area to area but can be as much as 75 metres in places. They also vary in colour from a pale yellowish colour to reddish brown.

The Great Dyke that consists of mafic and ultramafic rocks contains high-grade ores of chromite, nickel and platinum group elements (PGEs). The mafic rocks give rise to formations rich in ferromagnesian minerals and thereby giving rise to red and yellowish red clays in well-drained positions. The ultramafic rocks give rise to soils characterised by dominance of magnesian over calcium and often contain toxic levels of the heavy metals such as chrome and nickel (Nyamapfene, 1991; Cooper, 1978).

[1] True granites (granite *senso stricto*) i.e. those containing at least 65% alkali feldspar are rare in Zimbabwe. The term granites here refer to such rocks as tonalites, adamellites and granodiorites.

**Fig. 4.8** Distribution of Zimbabwean Soils (Nyamapfene, 1991)

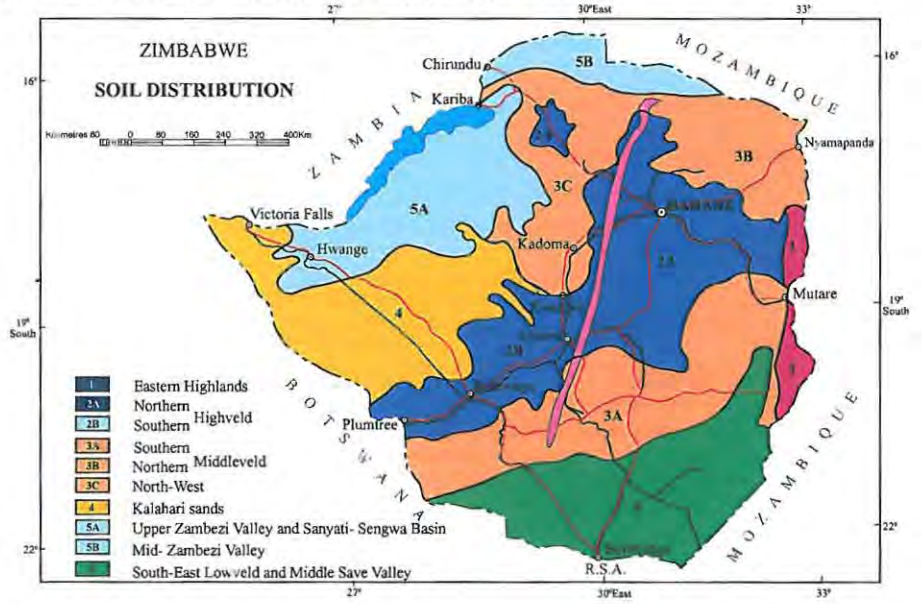


### 4.3.1 Great Dyke Soils

The soils of the Great Dyke of Zimbabwe closely follow the geology, with some overlying eluvial and alluvial deposits. The mafic and ultramafic (serpentine) rocks of the dyke are rich in ferromagnesian minerals and weather easily to clays. Generally the soils in well-drained locations are clayey, reddish and rich in iron oxides. In poorly drained positions, soils consist of dark montmorillonitic clays, which have a large swell and shrink capacity expressed by cracks at the surface during the dry season. Soils on mafic and ultramafic rocks are very similar in most of their properties.

### 4.3.2 North Dyke Soils and Soil Profiles

Landscape analysis identified various soil types along the Great Dyke's at North Dyke. Typical soil types include, mature soil profiles, immature soil profiles, and black cotton soils. Soils in these profiles are derived from residual those from *in situ* or transported material from either proximal or distal source. The mature profiles have predominantly residual to proximal soils, while the immature profiles and black cotton soils have predominantly transport proximal to distal soils. Also identified at North Dyke were laterites and stone line profiles. The North Dyke is characterised by pronounced topography with many steep slopes resulting in predominantly shallow soils. These profiles have inadequate time for thick soils formation since they are located on slopes susceptible to constant erosion. Their shallowness and high lithic fragments content result in a low water-holding capacity, which restricts plant growth. These soils are invariably immature. Along drainage channels and in valley bottoms the soils are generally deeper, extensive and chromite enriched. Serpentinite outcrops over a large part of the North Dyke (60%) and the soils overlying these rocks are only capable of supporting sparse grassland vegetation (Fig. 4.9). Erosion of some North Dyke soils is more rapid due to well-pronounced topography and poor vegetation cover (Fig. 4.11).

**Fig. 4.9** Soil Distribution on the North Dyke

*(Forestry Commission data provided by the Surveyor General Office, Harare)*

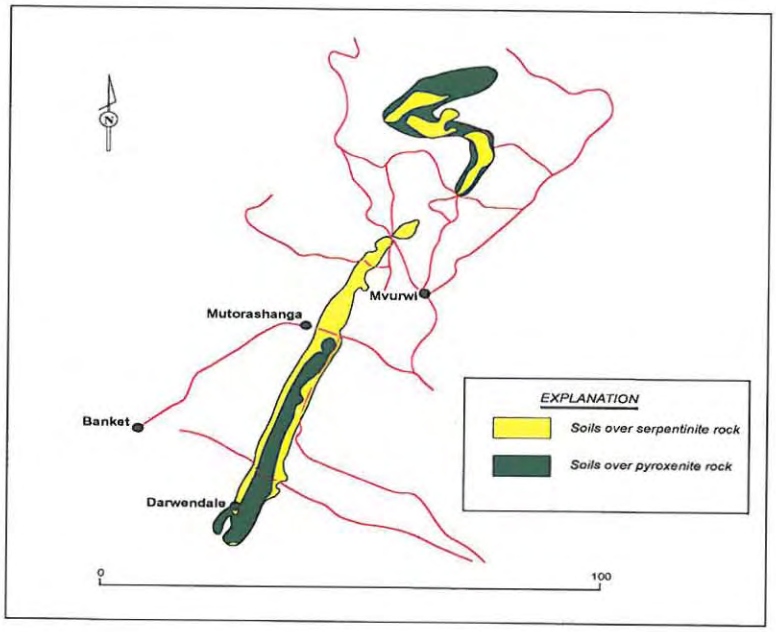


**Fig. 4.10** Jester Valley Showing Chromite-rich Soils

*(Picture showing part of the Jester Valley Eluvial Deposit. Note the Hilly terrain characteristic of the North Dyke. Also note the scrubby and stunted bush vegetation typical of the serpentinite bedrock areas.)*

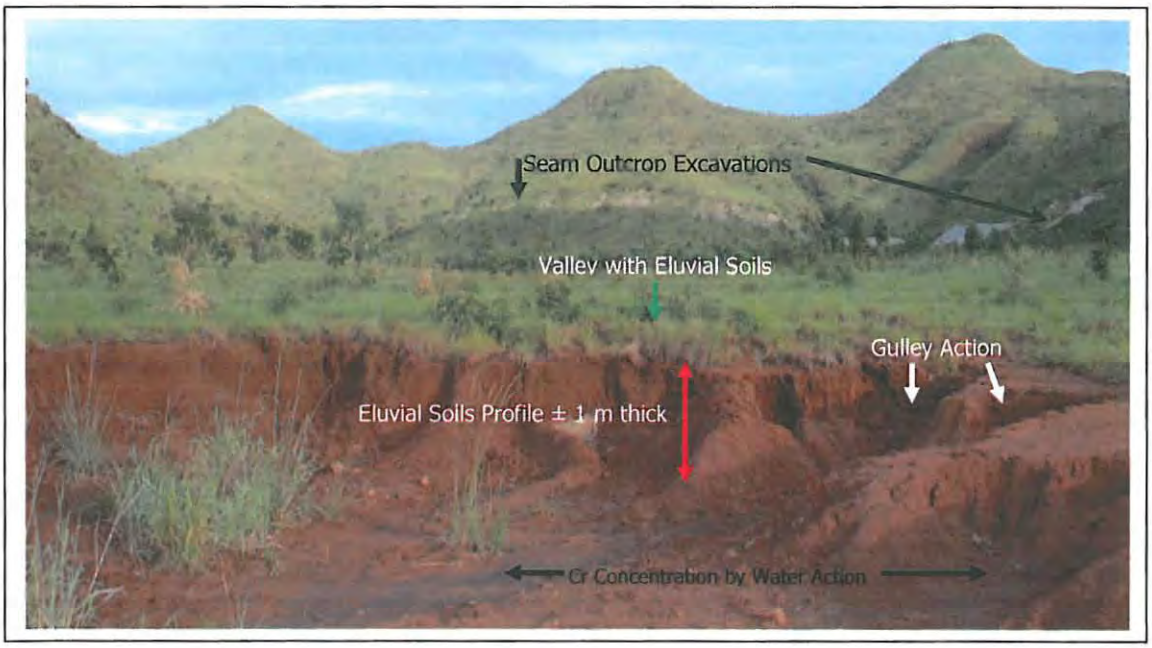

**Fig. 4.11** Deposition Characteristics, Jester, North Dyke

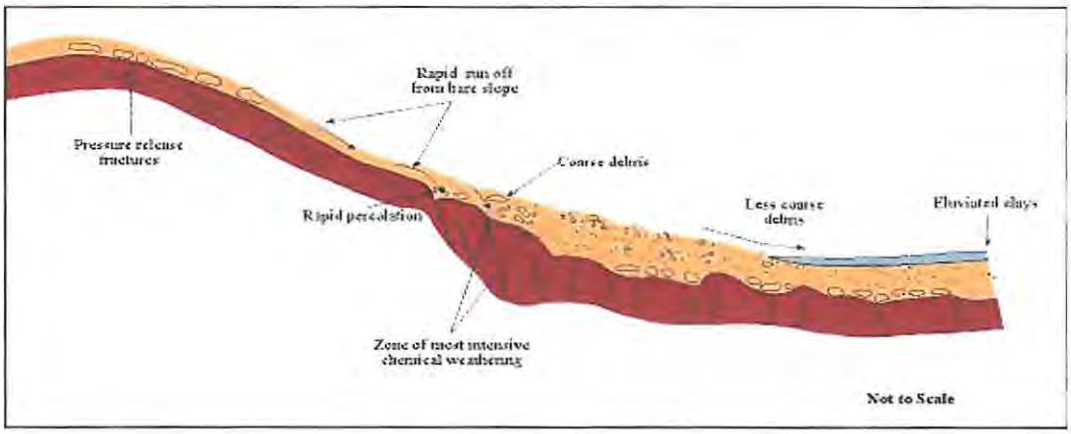


4.3.3 Immature Soil Profiles

The immature soil profiles are associated with hill slopes and have typically very thin soils of less than 10 centimetres. Immature soils usually contain large rock fragments of serpentinite or sometimes other Great Dyke lithologies. The profile show no proper distinction between the different soil horizons apart from a surface veneer of heavy mineral concentrates resulting from surface water run-off preferentially carrying away in suspension the lighter weathered serpentinite material. The thickness of these immature profiles is very inconsistent along strike and tends to improve where gradient is gentle (Fig. 4.11). These profiles have no prospects of getting thicker as they are rapidly eroded and the loose soils washed down as some form of gravity flow during the rainy season. These profiles feed the lower valleys with soil material, which forms the colluvium component of the mature profiles.

4.3.5 Graded Soil Sediments Profiles

At the foot of the talus slope of the hills are soil profiles with characteristic graded bedding. A typical profile is made up of a series of layers whose particle sizes fine upwards. This gradual decrease in the average grain size up through the beds is due to both distribution-grading[2] and also coarse–tail grading [3](Birkland, 1984). This graded bedding of soil sediments and soil particles carried downhill by running water is deposited as the flow begins to slow down due to loss of gradient. The deposition at Jester valley is stratified with each strata-representing deposition over one season and the bedding formation is partly during heavy downpours while the fine material is due to reworking of sediments and deposition resulting from waning storm currents. Reverse or inverse graded bedding was also noted on a few places. This inverse grading is attributed largely to seasonal variation in flow and reworking of the sediments deposit. These stratified soils are of very restricted distribution and contain

[2] Preferential deposition of large particles first and then finer particles.
[3] Preferential off-loading of larger particles due to loss of gradient.

layers of variable thickness and chromite enrichment. These characteristics present problems in quantifying and evaluation of resources associated with this depositional environment.

### 4.3.6 Mature Soil Profile

Notable in this soil profile are four distinct horizons. At the top is a dark brown soil horizon of about 5 centimetres thickness. This zone contains decomposing organic debris and typically contains numerous animal borrows. The top half of this horizon equates to the $A_0$ horizon whilst its base could be an equivalent of the $A_1$-horizon. Below this layer and grading from it is a pale brown horizon. This layer is usually not more than 20cm thick with an abundance of grass roots as a main distinguishing feature. Apart from supporting grass roots, it also has evidence of animal burrowing. This is the zone of leaching and equates to the $A_2$ horizon. Below $A_2$ horizon is the B-horizon, which is marked by a reddish brown loamy top and dark brown base. Heavy minerals occur in appreciable amounts within the B-horizon. Roots sometimes persist into this zone. At certain localities, a stone-line appears at mid way through the B-horizon. Texture is dominantly loam with high chromite content and with frequent occurrence of pisolites. Where a stone-line exists, a reddish loamy soil forms the bottom half of the B-Horizon below the stone line. This zone can be a mixture of a loamy texture with rare exotic fragments, pisolites, and small-unweathered serpentinite particles. The C-horizon consists of decomposing serpentinite material, which progressively contains weathered core-stones and eventually consolidates into fresh bedrock with depth.

### 4.3.7 Stone-line Profiles

Stone-line profiles at North Dyke are mainly associated with in situ and proximal soils. The thick transported soils are often devoid of stone-lines (Fig. 4.13). Where present at North Dyke the stone lines are weakly developed and may consist of single or double stone layer. The stone-lines are predominantly of serpentinites fragments with occasional chromitite, pyroxenite and opaline silica fragment. The origins of these stone-lines remain a bit of an enigma. It is possible that these develop on transported horizons where selective removal of light material during *in situ* pedological process concentrates stones in a particular horizon. In a few isolated places the stone-lines are predominantly made up of chromitite fragments, which are occasional worked by artisanal miners for the chromite cobbles when they have a chance encounter with them.

### 4.3.8 Lateritic Profiles

The deep red to bright orange-red soil, typical of some North Dyke (and also Middle Dyke) areas, is a product of lateritisation. Lateritisation occurs in predominantly hot and rainy areas, where chemical weathering proceeds at a rapid rate. Soils subject to lateritisation tend to be acidic and are devoid of preserved organic matter as decomposition and leaching are extreme. Exposure of the soil to the hot tropical sun, e.g. by deforestation, bakes the soil dry, reducing infiltration, increasing runoff. These

zones of laterite in the North Dyke and Middle Dyke areas are reported to contain significant nickel content although they contain negligible amounts of heavy minerals largely due to the reduced infiltration and hence slow rate of soil development (Wilson and Prendergast, 1989).

### 4.3.9 Black Cotton Soil Profiles

Black cotton soils are confined to low-lying zones with poor drainage. The soils are largely transported and result from inward drainage mainly of very fine particles, which accounts for their high clay content, consisting mainly of expansive clays. These clay soils have well-developed surface mulch (loose surface horizon), and display seasonal cracking. Bacterial activity, in these poorly drained areas, is slowed down during the prolonged wet periods thus inhibiting the decomposition of dead vegetation allowing it to accumulate in thick layers. Decaying plant matter releases organic acids that react with iron in the soil. The iron is reduced rather than oxidized giving the soil a black to bluish - grey colour (Nyamapfene, 1991).

### 4.3.10 Synthesis: North Dyke Soils and Profiles

At North Dyke, interplay of transported colluvial and alluvial processes and chemical (soil forming) processes resulted in different soil profiles ranging from the thin hilltop to hill slope immature soil profiles to the relatively thicker mature profiles in valley bottoms. This variation in soil profile thicknesses was demonstrated by systematic logging of profiles on a straight line from hill top to valley bottom.

## 4.4 Middle Dyke Soils Profiles

Serpentinite, which outcrops over a large part of the Middle Dyke, controls the soil distribution patterns. Soils overlying the serpentinite rocks are only capable of supporting sparse grassland vegetation and hence are largely devoid of trees. However these soils also consist of largely mafic soils derived from norites, gabbros and pyroxenites (Worst, 1960). Since the Middle Dyke areas have a much lower relief than the North Dyke, erosion is not such an issue, and the soils are rather deeper than those found on the North Dyke. Landscape analysis shows the Middle Dyke to consist of a central and discontinuous pyroxenite and predominantly serpentinite flanks. These flanks receive annual deposition of material eroded from the prominent ridges. Most of the deposition is flat laying Great Dyke flanks where they form Black cotton soils similar to those describe for the North Dyke. Also at the flanks are mature soils of transported and *in situ* chromite rich soils. These soils are invariably associated with stone-lines and pisolites layers (Fig. 4.12). At Lalapanzi the deposition of Kalahari sands have fossilized the African surface. These Kalahari sands form thick reddish brown soils consisting of coarse quartz grains. The red coloration being iron staining. The characteristic lateritic profile of the African surface caps the central ridges and consists of lithified fragments of silica, ferricrete and serpentinites (Fig. 4.14). The mature soils

of Great Dyke flanks contain fragments from all the higher lithologies such as the ferricrete and pyroxenites and serpentinite. They are also characterized with pisolites in some areas.

### 4.4.1 Black Cotton Soils

The Black cotton soils at Middle Dyke are similar to those in the North Dyke and are confined to areas of poor drainage. Where a stone line is present chromitite may accumulate into economic deposits usually exploitation by small workers on the Great Dyke. The soils are rich in clays and apart from possible non-chromite chromium content and chromitite fragments associated with its stone-lines, these soils are not known for economic concentration of chromite.

### 4.4.2 Mature Soil Profiles

These profiles are typically 1 to 2 metres thick and have no distinct $A_1$-horizon. At the top of the profile is an $A_2$-horizon, which is chocolate brown and grades into B-horizon. The A-horizon is limonitic brown in places and sometimes lithified due to the cementing effect of the rock Fe content. The B- horizon hosts a ±1 metre thick pisolitic layer below, which is 30 to 60 cm polymictic stone-line layer. At the base of the B- horizon are serpentinite fragments, which are intimately associated with soils (Fig. 4.13) The C- horizon consists of weathered unconsolidated serpentinite at the top. Beneath the weathered serpentinite is consolidated serpentinite rock.

**Fig. 4.12** Stone- line Profile at Lalapanzi

(*Photograph showing a stone-line profile at Lalapanzi, Middle Dyke. Note: the soil lithic content which renders such deposits a less attactive source of eluvial soils)*

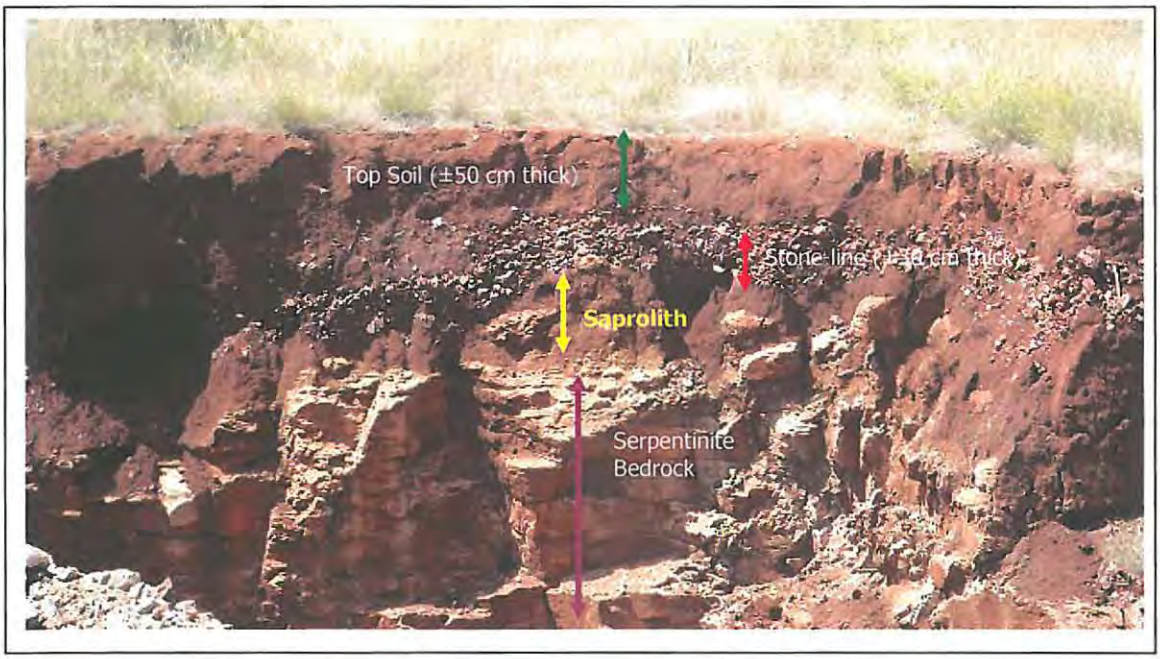

**Fig. 4.13** Pisolites and Quartz Stone-line at a Soil Profile at Lalapanzi, Middle Dyke

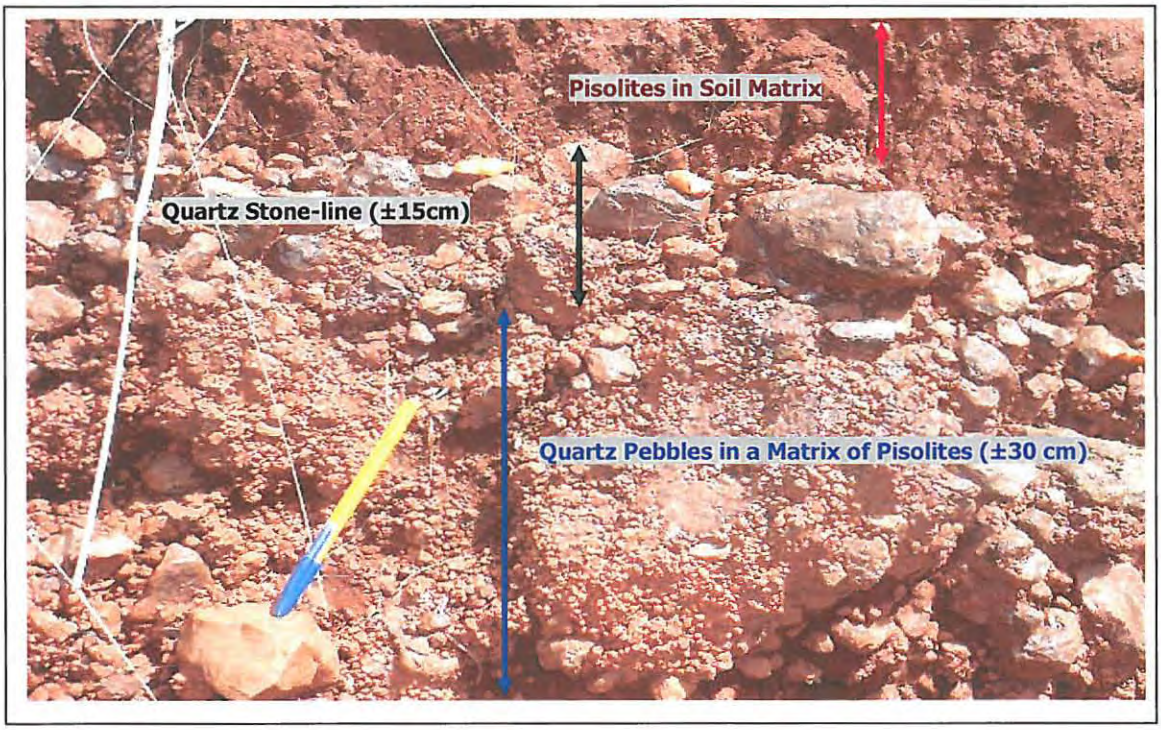


**Fig. 4.14** Lateritic Duricrast at Lalapanzi, Middle Dyke

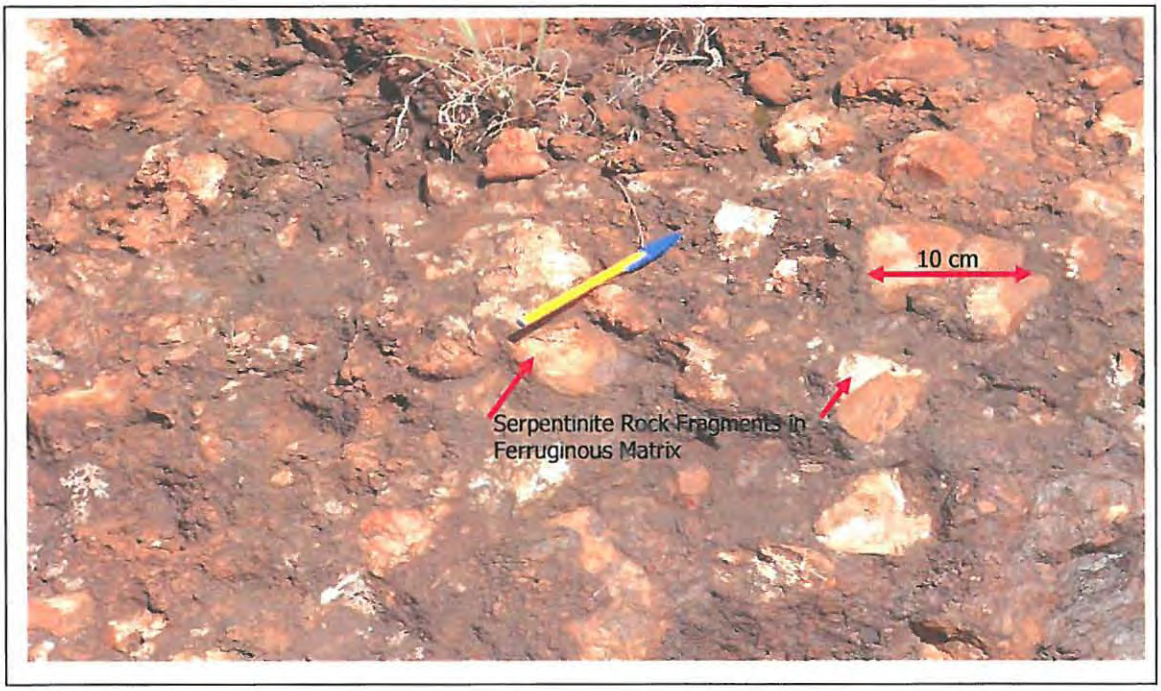

## 4.5 South Dyke Soil Profiles

The South Dyke has a semi-arid climate and a relatively higher relief than the Middle Dyke both along the Great Dyke central axis and on the surrounding country (Figs. 4.15 & 4.16). The surrounding country consists of prominent granite domes whilst the Great Dyke has a central pyroxenite ridge. Serpentinite, which outcrops on the Great Dyke flanks, controls the soil distribution patterns. Soils overlying these serpentinite rocks are however, derived also from the norites, gabbros and pyroxenites ridges that formed the Great Dyke central axis (Worst, 1960). Through erosion, material from the ridges was brought down and splayed into the flat plains on the Great Dyke flanks where depositional alluvial fans form at the immediate foot of the ridges. Within these flat lying flanks sheet-wash erosion redistributes the soils through a braided stream environment.

**Fig. 4.15** Section of the Great Dyke at Dolo, South Dyke

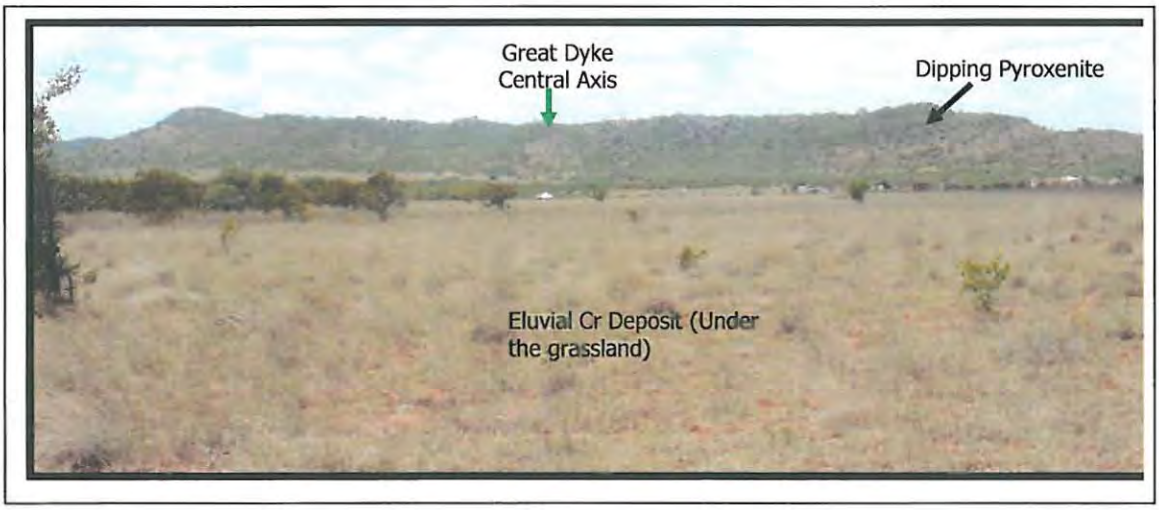


**Fig. 4.16** Alluvial Fan Depositional Environment

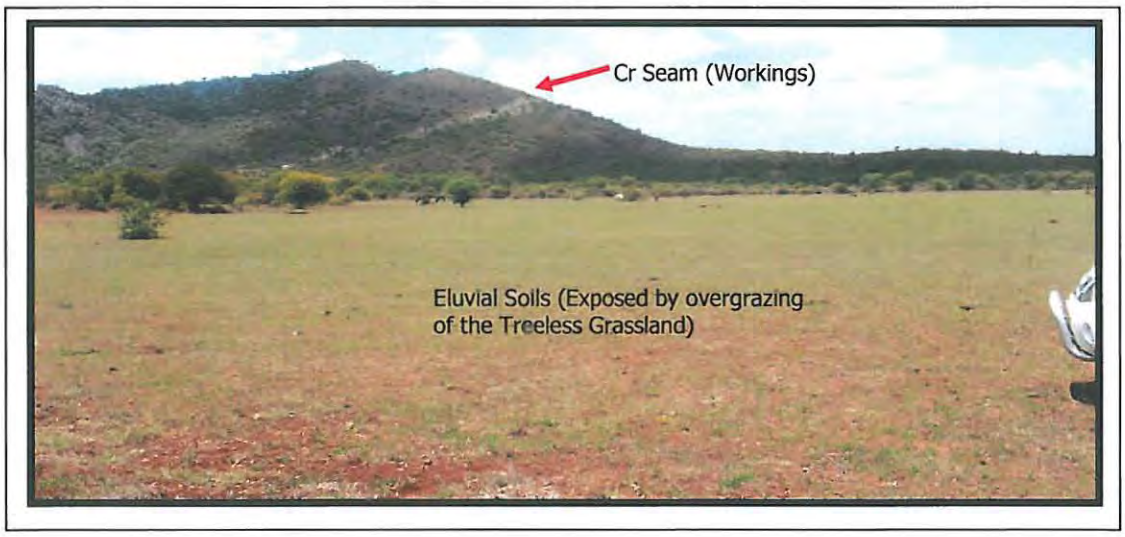

The soils of the semi-arid South Dyke are derived mainly from the erosion of the mountain ridges due to weathering, a combination physical and some chemical processes. The debris of fallen rocks and finer particles accumulates at the base of the mountains and is sorted naturally as rainwater carries the smaller particles downwards into the valley floors, creating the gravels, sands and silts of the lowland plains, and leaving the larger fragments further up the incised valleys near the mountain base (Fig. 4.17).

**Fig. 4.17** Sketch of a Simplified Single Source, Alluvial Fan

*(Contours are convex down slope and closer together near the apex. The dashed lines represent channels that have not recently been invaded by water or debris flows. The solid, sinuous lines emanating from the apex indicate channels that have conveyed flows recently).*

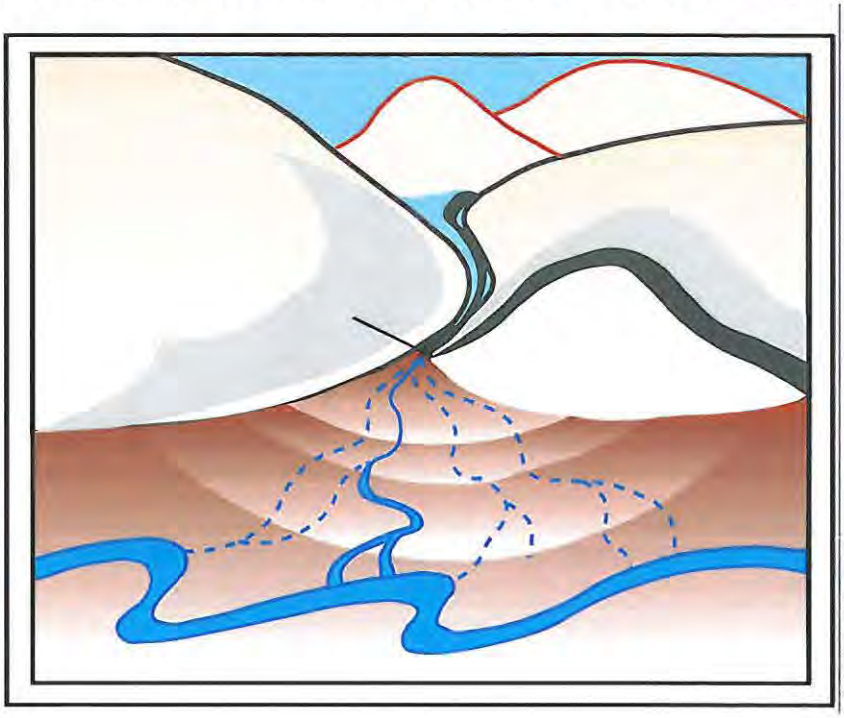

These alluvial fan deposition processes result in very thick profiles near the mountain base of about 4 metres, which progressively gets thinner to less than a metre in the distal parts of the resultant alluvial fan. The differently sized particles created by this process are however initially not strictly soils. They are simply mineral particles, similar to sand grains, which need to be stabilized and bound together by some form of structure[1]. The resultant fan shaped deposit of water-transported material typically form at the base of topographic features where there is a marked break in slope. Consequently, alluvial fans tend to be coarse grained at the mouth and relatively fine grained at the edges. In some places two or more fans growing together may coalesce to form a general accumulation of overlapping fans along a mountain front. In the simplest form of widely spaced valley sources fan geometry tend to be a simple cone emanating from a single well defined drainage stream which breaks into more or less radial

channels down the cone. Where the sedimentary accumulations from several sources encroach on one another,or where the deposition is forced by gradual widening or slope reduction along a valley, the simple conical fans along a mountain becomes obliterated. At their downstream margins these fans merge with the smoother depositional topography of valley floors and the sheet wash erosion redistributes these depositions through braided stream environments (Fig. 4.18).

### 4.5.1 Sheet wash/ Braided Stream Plain Profiles

**Fig. 4.18** Braided Stream Environments, South Dyke

*[Photograph showing a braided stream environment, where soils are redistributed and reworked by successive seasonal water flows, resulting in the upgrade of the eluvial resource. Soil profiles in this deposit can be up to 2metres thick. Note the pyroxenite ridge in the background. The deposit is up to 2 km wide and runs along the Great Dyke length, here, for 7 km].*

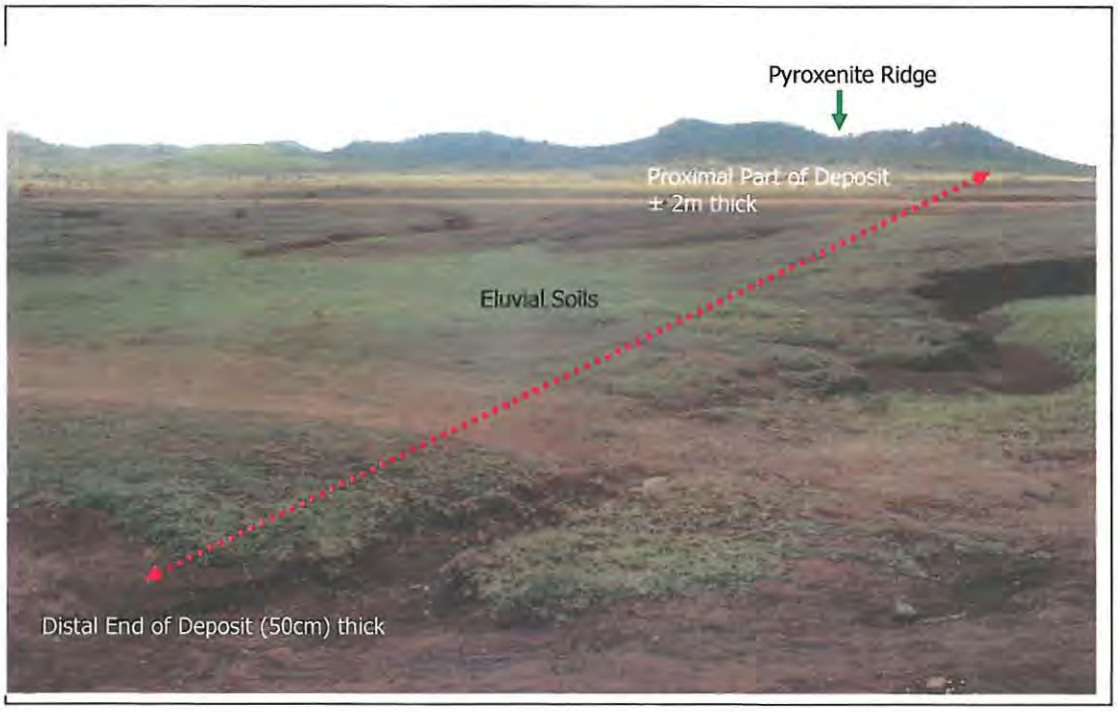


In the lower reaches the streams meander broadly over the flood plain before they link up with the trunk stream draining parallel to the plain strike. Braided streams are created when the discharge of water cannot transport its load and there is a decrease in stream velocity resulting in sediments deposition on the floor of the channel creating bars. The bars in turn separate the channels into several smaller channels creating a braided appearance. A section of a braided stream profile is shown in Fig. 4.19).

**Fig. 4.19** Braided Stream Soil Profiles, South Dyke

*[Note: the top eluvial soil from deposition and the bottom soil derived from **in situ** soil development from bedrock].*

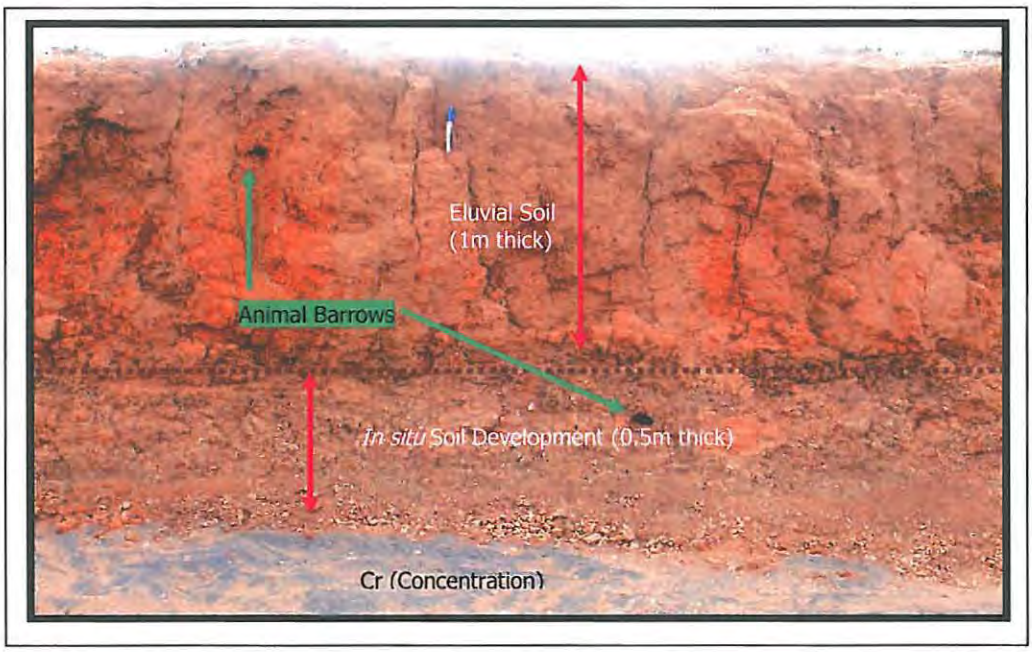


## 4.6 Synthesis

### 4.6.1 Factors Affecting Soil Development

Soil research has shown that soil profiles are influenced by five separate, yet interacting, factors namely parent material, climate, topography, organisms, and time. These factors give soil profiles their distinctive character (Marsh, 1987) and this in turn has a direct influence on the liberation and enrichment of heavy mineral in the soils.

### 4.6.2 Parent Material

Soil parent material is the material that soil develops from and may be rock that has weathered in place (bedrock), or material that has been deposited by wind, water, or ice. The physical and chemical composition of the parent material plays an important role in the determination of soil properties, especially during the early stages of development (Marsh, 1987). Soils developed on parent material that is coarse grained and composed of minerals resistant to weathering are likely to exhibit coarse grain texture (Marsh, 1987). Typically soils from the Great Dyke pyroxenites, that are resistant to weathering are coarse-grained. These coarse grained soils will retain chromitite locked as interstitial

aggregates of the coarse grains, which in turn inhibit optimum levels of chromite concentration (Marsh, 1987). Soils that develop from fine-grained rock or rock that easily weather like the dunite/serpentinites parent material not only develop thicker profiles but result in heavier minerals being liberated into the soil fraction (Marsh, 1987). The dunites, which flake off on exposure to air, weather rapidly to give fine-grained soil horizon that characterise the Great Dyke flanks (Wilson 1982). Parent material composition also has a direct impact on soil chemistry and their draining properties. Serpentines and their unaltered equivalents dunites both have a high content of soluble bases and produce clayey soil less susceptible to leaching. In poorly drained areas weathering of serpentinites produce clayey black cotton soils. Parent rock materials with low soluble ions and water moving through the soil removes the bases and substitutes them with hydrogen ions making the soil not only soil acidic but promoting alteration to poor draining clayey soils. Soils developed over coarse-grained pyroxenite are low in soluble bases and coarse in texture, which facilitates leaching. Parent material influence on soil properties tends to decrease with time as the soil is further altered and climate becomes more important.

### 4.6.3 Climate

Distribution of Great Dyke soils tends to show a strong geographical correlation with climate, especially pronounced at regional scale. Temperature and precipitation strongly influence physical and chemical reactions on parent material. Climate also determines vegetation cover, which in turn influences soil development. Precipitation also affects horizon development factors like the translocation of dissolved ions through the soil. As time passes, climate tends to be a prime influence on soil properties while the influence of parent material is less (Marsh, 1987).

### 4.6.4 Climate, Vegetation and Weathering

Climate affects both vegetative production and the activity of organisms. Hot, dry semi-arid South Dyke regions of the Great Dyke have sparse vegetation and hence relatively less incorporated organic material in the soil. A lack of precipitation inhibits chemical weathering leading to coarse textured soils in this semi-arid region. Bacterial activity in the colder regions of the Great Dyke also slows or inhibits the breakdown of vegetative matter causing it to build up particularly in areas where the broad leaved miombo woodland are extensive. In the warm and wet areas, bacterial activity proceeds at a rapid rate, thoroughly decomposing leaf litter. The high annual precipitation characteristic of the North Dyke and Middle Dyke areas also flushes some organic material from the soil. These factors combine to create soils lacking much organic matter in their upper horizons.

### 4.6.5 Topography (Relief)

Topography, or the relief of the land, can have a significant impact on soil formation. Topography influences the runoff of water; its orientation affects microclimate, which in turn affects vegetation.

### 4.6.6 Effect of Topography on Soil Erosion

The slope of the Great Dyke flanks, in the high relief areas like the North Dyke, affects the degree of runoff that is generated when it rains on the surface. The diagram below (Fig. 4.20) adopted from Riffer, (2004) shows a relationship between hill slope position, runoff and erosion.

**Fig. 4.20** Hill Slope Position, Runoff & Erosion (Riffer, 2004)

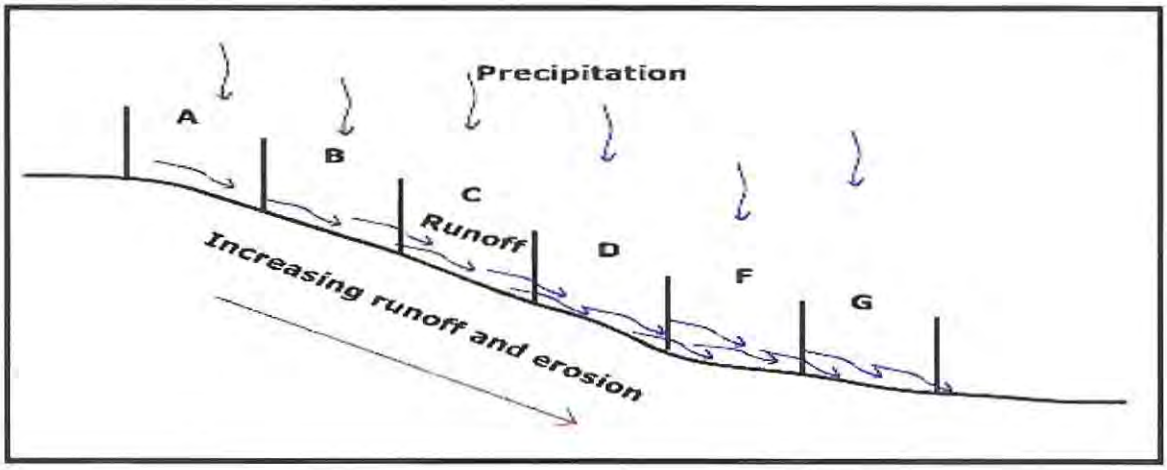


The hill slope in the diagram above shows several segments with the amount of precipitation falling on each segment being the same. As the water starts to flow downwards, the water that has accumulated in upper segment A runs off adding to what falls into segment B by precipitation. The water in B runs into to C and C into D and so on. Consequently the water in each segment increases with distance down the slope. This is due to fact that the amount in any one segment is dependent on what falls from precipitation and what flows into it from an upslope hill slope segment. Additionally, as the water runs down slope its velocity is increasing. As a result, the rate of erosion increases towards the base of the slope and thus rather than infiltrating into the soil to promote weathering and soil development, water runs off. Erosion causes stripping of the soil thus preventing parent material remain in place to develop into a soil. Hence soils on slopes, especially at the mid-slope and near the bottom of the slope tend to be weakly developed (Marsh, 1984).

### 4.6.7 Effect of Relief on Deposition and Soil Texture

Water velocity not only determines the rate of erosion but the rate of deposition of material in suspension. The diagram below shows the relationship between location relative to relief position and texture. Three positions A, B, and C are progressively located further from the base of a slope. A soil texture triangle can be used to illustrate the variation in soil textures at the three sites (Refer to Figs. 4.21 & 4.22).

**Fig. 4.21** Location, Deposition and Soil Texture (After Marsh, 1984)

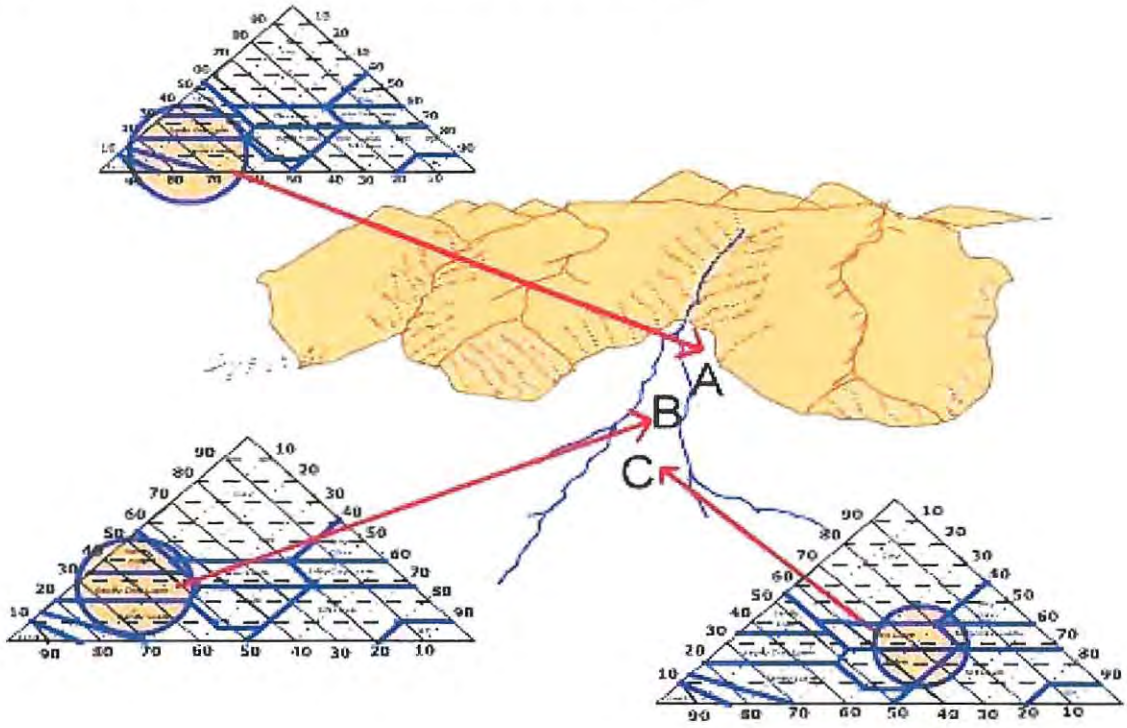


**Fig 4.22** A Soil Texture Triangle (After Marsh, 1984)

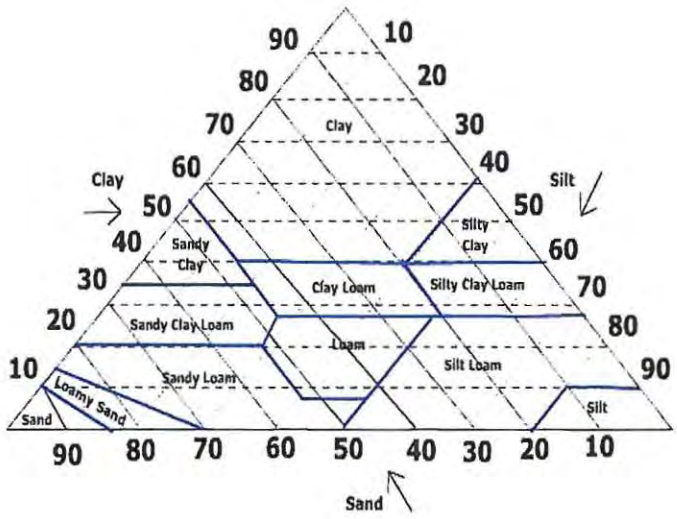


*A soil texture triangle used to classify the texture class of a soil into sand, silt, and clay.*

As water empties from a mountain stream, its velocity starts to decrease, the largest size particles, like pyroxenite grains, are the first to drop out of suspension (Site A). Fine, clay size particles can be

carried further away from the base of the slope before they are deposited. As a result, coarse textured soils tend to be found near the base of the mountain and fine textured soils are located further away (Site C).

### 4.6.8 Effects of Microclimate due to Relief

Hill slope orientation affects the microclimate of a locality. As the inclination of the surface increases, so does the local sun angle. As the local sun angle increases, the intensity of heating increases causing warmer surface temperatures and increased evaporation. Orientation of the hill slope is certainly important too. Those slopes, which face into the sun, receive more insolation than those facing away. Thus inclined surfaces facing into the sun tend to be warmer and drier, than flatter surfaces facing way from the sun. The eastern flank of the Great Dyke will thus have different soil development characteristic than the western flank. The microclimate also impact vegetation type which in turn influences soil profile development.

### 4.6.9 Presence of Older Land Surface

Older land surfaces sometimes preserve soils derived from earlier weathering regimes. These older layers not only mask soil development but can introduce material which does not weather easily thus influencing soil development. The ferricretes of Middle Dyke and silcretes associated with African planation on the North Dyke are more resistant to weathering and thus restrict weathering effects on underlying lithologies. Older surfaces on high relief may also introduce materials into the newer and lower elevation profile soils from previously existing profiles thus greatly increasing the thicknesses of the profile. The Kalahari sand cover over the Lalapanzi area of the Great Dyke shielded this part of the Great Dyke from erosion, weathering and soil development.

## 4.7 Discussion (Effects of) Soil Forming Processes

### 4.7.1 Eluviation Processes

Eluviation is the process of leaching out the weathered material in a soil profile. The leached out material is either dissolved into solution, which drains away or down to deposit the soluble material further down the profile within the zone of accumulation. Within the Great Dyke soils this process is responsible for the ultimate concentration of heavy minerals as the decomposing ultramafic rocks are washed away usually by sheet erosion, which carries away lighter weathered material. The heavy minerals largely chromite and magnetite remain behind due to density grading. These processes of sifting away lighter weathered material also benefit from wind erosion within the Great Dyke serpentinite flat plains. The process together with other processes is responsible for the surface concentration of heavy minerals.

### 4.7.2 Alluviation Processes

In the semi arid South Dyke and the hilly terrain of the North Dyke erosion on the hills causes generation of large quantities of rock debris which is then carried down the hills during storms. These form turbidity currents which result in alluvial fans which in addition to spreading out soil particles over the flat lying extensive plains where further weathering and eluviation can readily effect heavy mineral concentration. The turbidity currents also aid release of heavy minerals from the weathered material through attrition and collision of the particles. The suspension of the particles is also effective in grading the particles in suspension and separation of lighter and heavy particles.

## Chapter 5

# 5.0 Distribution Patterns and Relative Chromite Content of Great Dyke Soils

## 5.1 Introduction

The distribution of chromite and other heavy minerals content and size of eluvial deposit, is a function of the intensity of weathering processes, landscape regimes and depositional environment. On the Great Dyke, intense weathering is responsible for thorough break down of lithic material in soils, resulting in the release of chromite. Chromite interstitial to mineral grains and chromites enclosed within mineral grains are liberated as a result of weathering. In order to determine modal proportions of the resultant free chromites in different soil environments, samples were taken, screened into different size fraction and processed as illustrated in Fig. 5.1. Different sieve sizes were selected in order to screen samples soil particle sizes into clay, silt and sandy fractions within the range <63 μm up to >1000 μm.

## 5.2 Sampling and Sample Preparation

Soil samples were collected from North Dyke, Middle Dyke and South Dyke regions of the Great Dyke and analyzed for size range distribution and mineral content. Sampling was directed at different eluvial depositional environments. Each of the samples was dry-sieved into seven different size fractions, using metallic sieves ranging from <63 μm up to >1000 μm. The sieved sample fractions were weighed and each sample processed through a bench scale Mosley concentrator for the recovery of heavy mineral concentrates. The heavy mineral separates were further washed by wet screening, dried and then weighed. The washed and dried mineral separates were examined under binocular microscope. Polished sections of the same separates were examined under reflected light microscope. The fine fraction of <63 μm largely derived from dry sieving and from Mosley separation and underflow from subsequent wet screening were combined and analyzed for major elements using an X-Ray fluorescent technique( See Appendix 1- X-Ray Florescence Analytical Technique). This analysis was aimed at determining the presence of ultra fine chromite, too light to concentrate. Also levels of non-chromite chromium minerals, which could invariably influence metallurgical balances between recoverable and non recoverable chromite would be determined. The sampling, sample preparation and analytical procedures done are summarized in the process flow chart in (Fig. 5.1.) The results of these investigations were used to characterize the eluvial chromite deposits and establish regional distribution of the various grades of eluvial chromite. The fine fractions (clay-size and silt-size fractions) represent unrecoverable chromium in the eluvial soils. The analyses from the fine fraction represent ultra fine chromite and non-chromite chromium currently considered unrecoverable and hence of limited interest to this study.

**Fig. 5.1** Sampling and Sample Processing Flow Chart

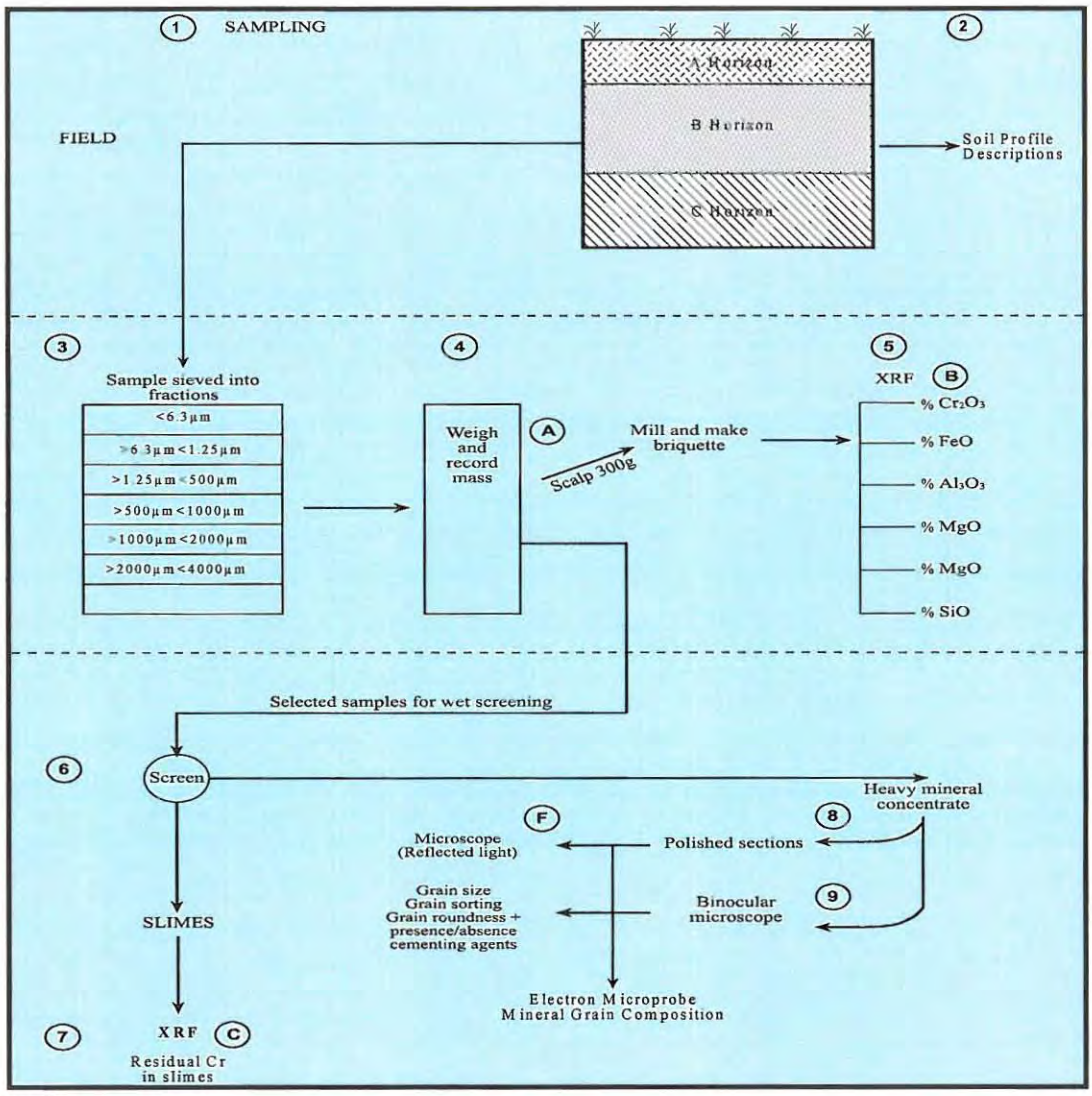


Explanation

| | | | |
|---|---|---|---|
| 1 | Field Sampling | A | Record of Fraction Mass |
| 2 | Pit Logging | B | Record of XRF Analyses |
| 3 | Sample Sieving | C | Record of Slimes Analyses |
| 4 | Weighing | F | Record of Microprobe Analyses |
| 5 | XRF- Analysis Bulk Samples | | |
| 6 | Wet Screening | | |
| 7 | XRF Analysis Slimes | | |
| 8 | Polished Sections | | |
| 9 | Heavy Mineral Grains | | |

## 5.3 North Dyke, Middle Dyke and South Dyke Soil Sampling

Samples (±5 kilograms) were collected from three different regions of the Great Dyke (Fig 5.2) Analyses of the different *in situ* samples confirmed the presence of chromite in all sampling sites. Results of the bulk assay of the different samples are results shown in Table 5.1.

**Fig. 5.2** Selected Soil Profiles for Sampling

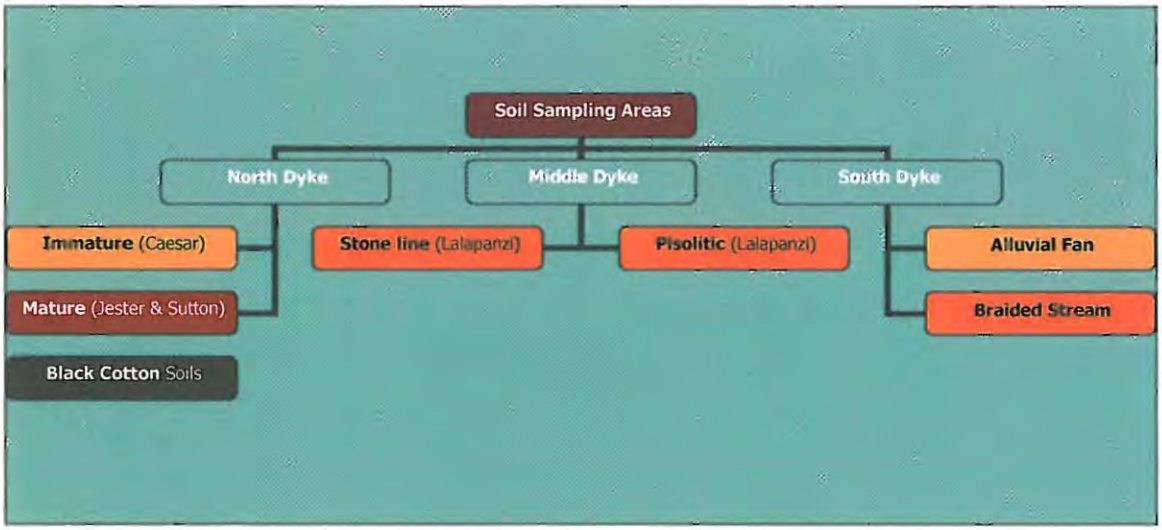


**Table 5.1** Bulk Analyses of Great Dyke Soils

| Sample Location | %$Cr_2O_3$ | %FeO | %$SiO_2$ | %MgO | %CaO | %$Al_2O_3$ | $TiO_2$ | Total |
|---|---|---|---|---|---|---|---|---|
| Immature Profile (Caesar) | 14.39 | 29.64 | 29.14 | 11.71 | 0.13 | 8.84 | 0.14 | 93.99 |
| Mature Profile (Jester) | 28.95 | 28.36 | 17.56 | 10.05 | 0.10 | 9.11 | 0.15 | 94.28 |
| Mature Profile (Sutton) | 21.50 | 32.20 | 16.11 | 9.98 | 0.10 | 10.96 | 0.18 | 91.03 |
| Black Cotton Soils (Sutton) | 0.86 | 34.01 | 29.84 | 9.72 | 0.57 | 18.01 | 0.18 | 93.19 |
| Stone line Profile (Middle Dyke) | 16.88 | 32.20 | 20.88 | 10.26 | 0.15 | 10.85 | 0.16 | 91.38 |
| Pisolitic Profile (Middle Dyke) | 12.91 | 40.50 | 14.56 | 8.83 | 0.04 | 8.70 | 0.15 | 85.69 |
| Alluvial Fan Profile (South Dyke) | 16.13 | 34.48 | 18.20 | 9.62 | 0.11 | 9.20 | 0.15 | 87.89 |
| Braided Stream Profile (South Dyke) | 17.11 | 30.19 | 20.88 | 10.11 | 0.15 | 11.70 | 0.15 | 90.29 |

Chromite concentration in the Great Dyke soils is predominantly confined to the soil solum. Chromite also concentrates at surface as a result of wind action or rainwater action. In order to minimize biased sampling, detailed soil logging was done prior to sampling. In most cases sampling was from the B-horizon, which is easily distinguished by its colour, its general lack of organic material, paucity of lithic fragment and is devoid of relict bedrock structures. All pits were carefully logged (Appendix 2- Typical log sheet), and the B-horizon identified and sampled. In addition to sampling, the landscape regime was carefully evaluated. Selection of sampling areas in each region of the Great Dyke was confined to dominant and widespread depositional environments.

### 5.3.1 North Dyke Sampling

Samples were collected at North Dyke from 4 different locations. Mature soil profile samples were collected from the Jester area, an eluvial deposit with soil thicknesses exceeding 1 metre. Sampling pits were excavated on a very flat part of the deposit, within a valley plain whose saprolith sometimes exceed 4 metres thickness. The area is a treeless-grassland characterised by very poor soils supporting only scrubby grass. The landscape regime is clearly a valley of residual soils with virtually no outcrop and lack lithic fragments. Mature soils samples were also collected from the Sutton area. This area differed from Jester in that the soils are thinner (less than 1metre) and is located, in an area characterised by intermittent tree occurrence, within a grassland. There are frequent outcrop exposures, and the soils are thin and have abundant lithic particles. This site is a gentle, concave sloping erosional plain. The site constitutes a pediplain with either residual or proximal to source colluvial soils. The extensive hill slope environment at Caesar consists of an upper miombo[1] woodland zone associated with pyroxenites and lower treeless grassland. The soils at Caesar are generally thin (more so under the miombo woodland) and usually about 0.3 metres thick. The landscape regime is erosional with frequent outcrop exposures, thin soils and dominant lithic fragment soil composition. The soils, however, are residual or proximal to source.

Other notable environments at North Dyke include mountain slope or hillcrest or plateau, that are purely erosional environment with no distinct soil development. The fourth sampling site at North Dyke was within the black cotton soil vleis at Sutton. These soils are associated with poor drainage and occur adjacent to densely wooded watercourses. The North Dyke is relatively wet and receives annual precipitation of ±1000 mm.

[1] Miombo a woodland dominated almost exclusively by *Brachystagia sp., Jilbernada sp, and Uapaca sp.*.

### 5.3.2 Middle Dyke Sampling

Sampling at Middle Dyke was confined to two areas all at Lalapanzi, (Fig. 5.4). The two dominant types of eluvial profiles on the Middle Dyke are the pisolites profile and the stone line profile. The prevalence of these profile types in the Middle Dyke region is due to the generally flat physiography and the relatively high levels of precipitation (annual rainfall 800 mm) of the Great Dyke in this region. This environment promotes development of residual deposits with extremely deep saprolith (in excess of 2 metres in places). Transported material is virtually absent although soils contain abundant lithic fragments of upper lithologies now eroded away. The extensive grasslands and sparse to dense woodlands hinder development of any significant aeolian deposits. The pisolitic profile is located on the central part of the Great Dyke, 15 kilometres north of Lalapanzi. The profile consists of iron-coated nodules of mainly serpentinite particles. The coatings have a protective effect on these particles against weathering. The B-horizon is almost entirely made up of these pisolites set in a fine soil matrix. The stone line profile at Lalapanzi is similar and contains a stone-line of predominantly ferricrete. The stone line profiles are however relatively shallower (±0.50 metres) and contain extremely thick saprolith containing large lithic fragments (±10 cm diameter). Their lithic fragment content reduces the attractiveness of these prospects as eluvial chromite deposits. The edges of the Great Dyke at Lalapanzi are predominantly of black cotton soils. These black cotton soils offer no prospect of hosting economic concentration of chromite and may possibly present complexity in extraction processes.

### 5.3.3 South Dyke Sampling

South Dyke is a semi-arid region with poor scrubby grass and sporadic dry scrub and acacias. The eluvial depositional environment of South Dyke is a braided stream environment with abundant surface chromite. The landscape is a depositional regime where some of the prospective lithologies are however masked by transported material such as colluvium, alluvium and aeolian deposition. The geomorphic environment of the sampling site is set in a pediplain with *in situ* residual and proximal to distal colluvial soils. At South Dyke and upslope from the braided stream environment sampling was also done on an alluvial channel located in an area covered by alluvial sheet-wash and flood plains. Areas of black cotton soil, identified, within areas of interest, were not sampled as they may well be devoid of chromite.

## 5.4 Field Sampling and Sample Preparation

### 5.4.1 Pitting Procedure

Pits were dug to a maximum diameter sufficient to allow for excavation down to bedrock rock. Pits were dug with at least one good clean vertical face from which sampling and logging was done.

The sidewall of the pit, on which sampling was undertaken was logged in a similar manner to drill hole core. Depths were measured with a measuring tape from surface down. A bulk sample was collected from one side of the pit equivalent to the width of a 'standard' spade (±15 cm). The sampling depth averaged a minimum of ± 20 cm to maximum of ±100 cm and the sampling intervals were controlled by the soil profile. Both topsoil and saprolite horizons were excluded. As much as 5-10 cm of 'top soil' present in some areas was excluded. This sampling procedure produced a sample of ± 10 kg for a 20 cm depth of sample interval and up to 50 kg for a 100 cm depth of sample interval. Samples were collected into suitable bags and appropriately tagged to avoid contamination and mixing.

### 5.4.2 Sample Preparation

The samples were brought in from the field into the sample preparation shed for processing. Each bulk sample was carefully and completely emptied from the sample bag onto a clean (or cleaned) plastic sheet, spreading it out as much as possible to allow the sample to dry in the sun. The entire sample was tipped on to a sheet without any loss of fines. The sample was disaggregated during drying by crushing any coarse clods of soil, with a rubber mallet taking care not to break up any rock fragments or laterite blocks. During drying the sample was adequately protected from wind and possible cross contamination. Following drying the sample was weighed. A 6-chute Jones riffle splitter was then used to split the sample to generate a sieving sample and a duplicate. Both portions were weighed. During splitting it was ensured that the complete sample went through the splitter and that any heavy mineral separates formed are evenly distributed in the splitter. All material with diameter greater than 1cm was screened off prior to splitting. This screened 'coarse reject' was weighed, split by hand and half of it was recombined with the duplicate sample. Half the total weight of the screened coarse reject was recorded against the sieving sample to allow for subsequent correction in mass balances. The duplicate sample was bagged and stored away. A riffle splitter was used to split the sieving sample to give a sample of ±5 kg for sieving. Each of the samples was dry sieved into seven different size fractions, using metallic sieves ranging from <63 µm up to >1000 µm.

## 5.5 Relative Chromite Content in Various Great Dyke Soils by Source and Size Fraction

The chromite concentrates from various eluvial chromite samples collected from North Dyke, Middle Dyke and South Dyke were estimated by weighing. The effective separation of concentrates plus heavy minerals was checked by binocular microscope and standard visual estimation charts and weights adjusted accordingly. The silt-size and clay size fraction (<63 µm) and the coarse rejects fraction (>1000 µm) were weighed and weights incorporated into the results for mass balancing purposes. The coarse rejects were visually inspected for the presence of chromitite fragments whilst X-Ray Fluorescence analysis was used for the clay-size and silt-size fraction.

5.5.1 North Dyke Soil Chromite Distribution

**Fig. 5.3** Particles Size Distribution of Selected North Dyke Soils

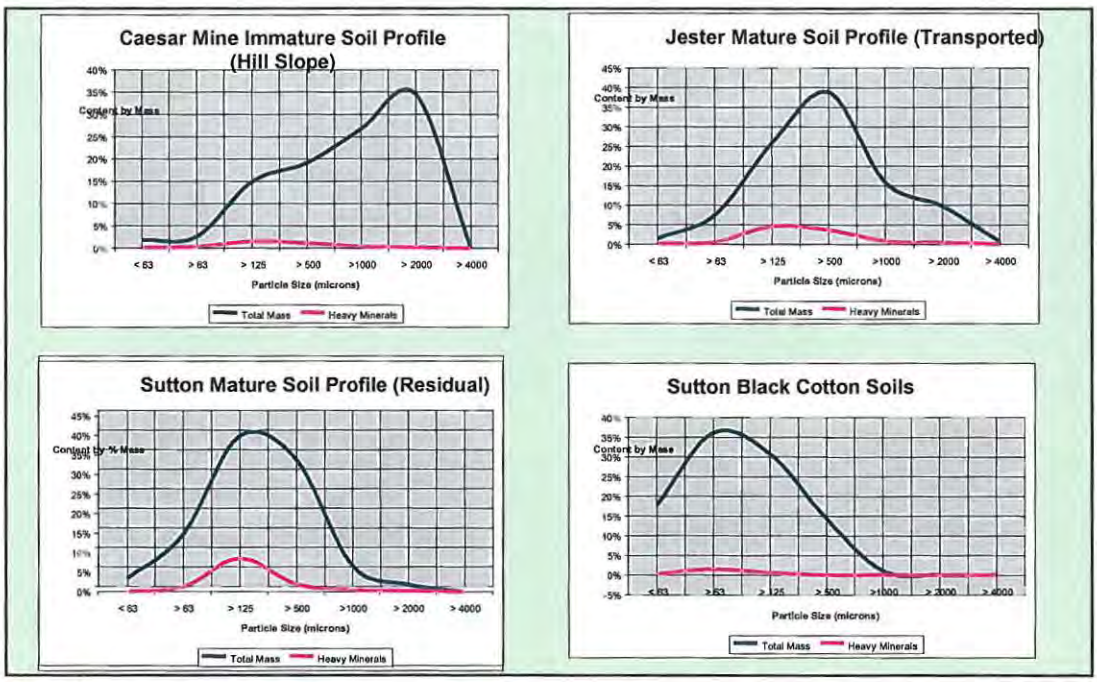


The soil particle size distribution patterns of each landscape type are characteristic and different. At North Dyke, Caesar Mine area, soils sampled represented a hill slope landscape type regime of immature, largely transported to partly residual soils. These soils show a binomial distribution of particles sizes with a higher proportion of larger lithic fragments set in less finer materials. The observed particle size distribution is indicative of an immature soil profile and incomplete weathering process. The heavy minerals content is greatest within the fine particle sizes range where disseminated and interstitial heavy minerals were liberated by weathering processes. Where weathering process have effectively broken down the residual lithic fragments and soils are mature, as typified by the Sutton and Jester mature soils, the soil particle and heavy mineral content is normally distributed with highest modal abundances for Jester soils peaking at around 500 microns. However unlike the Jester soils, Sutton soils, which are exclusively residual and mature, the modal peak is just above 125 microns particle sizes. In the Sutton black cotton soils, which are clays, the particles were extremely fine and predominantly of the 63-micron size range. The heavy mineral content of the soils was greatest in the Sutton mature soils (12 .3 % mass) and the Jester mature soils at (10.4% mass). Both the hill slope immature soils and the Black Cotton soils of Sutton contain very low levels of heavy mineral content at (3.9% mass) and 2.5 % mass) respectively. See distribution graphs in Fig.5.3.

**Fig. 5.4** Comparison of Selected North Dyke Soil Types

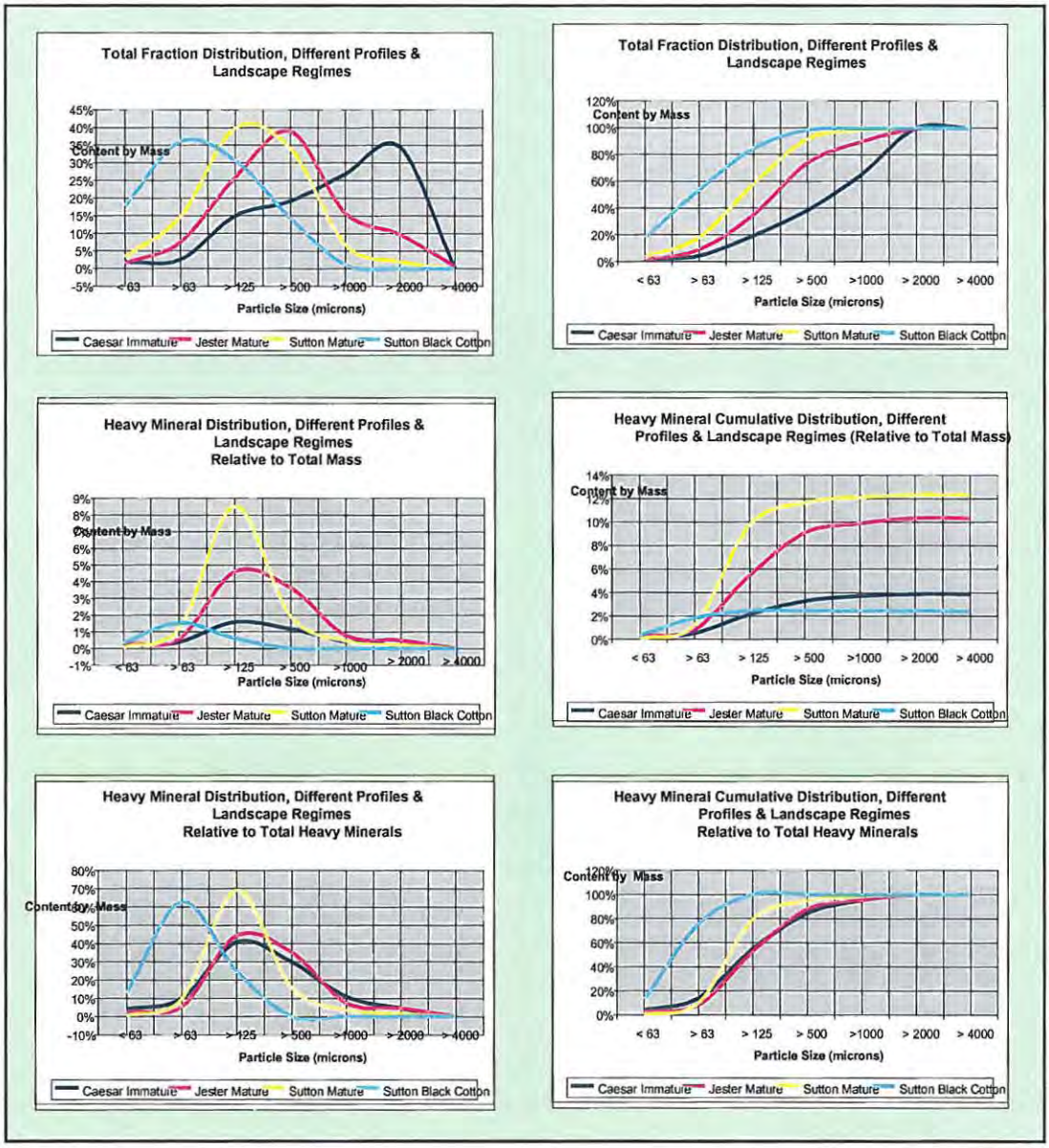


The Sutton black cotton soils, as expected, are finer grained and normally distributed just around 63-micron particle size and typically clayey. The mature soil profiles of Jester and Sutton are similarly normally distributed with modal soil particle size of just over 125 µm for Sutton and 500 µm for Jester. This difference is attributed to the longer residence period that mature soils have undergone to attain near uniform soil particle sizes (Fig.5.4). Immature profile at Caesar however has a large spread of soil particle sizes with the bulk of the particles greater than 1000 microns. This profile is not only poorly developed but also retains most of the chromites un-liberated within

the larger lithic particles. This immature profile and the black cotton soil profile contain relatively lower concentration of chromites.

### 5.5.2 Middle Dyke Soil Chromite Distribution

In the Middle Dyke area two sampling sites were selected, one with significant layer of pisolites and another, which hoist a prominent stone-line, profile. The soil particle size distribution pattern showed remarkable similarity (Fig.5.5).

**Fig. 5.5** Particle Size Distribution of Selected Middle Dyke Soils

*(Graphs showing similar distribution patterns between two different Middle Dyke profiles).*

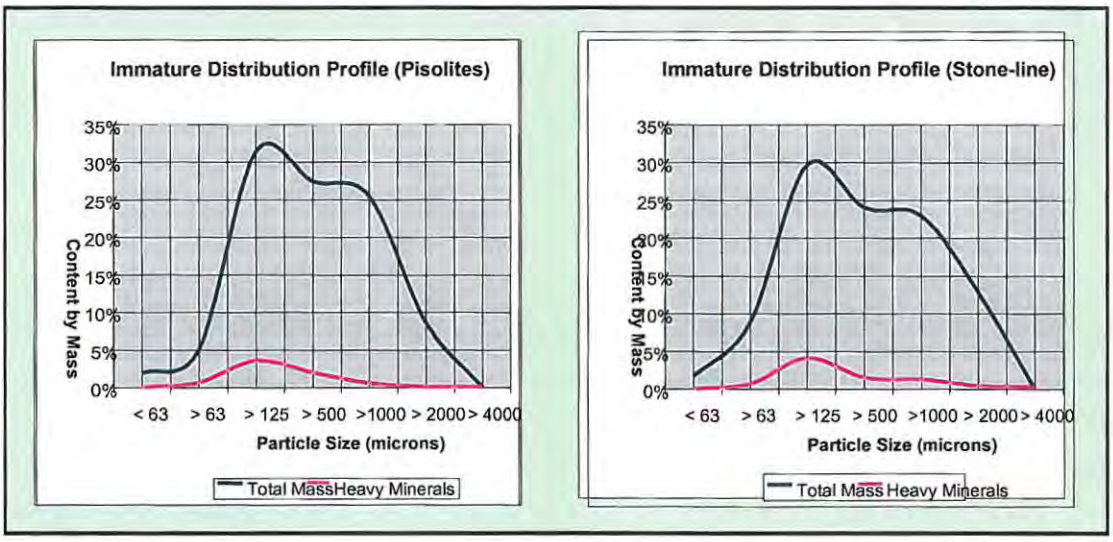


Soil profiles selected in the Middle Dyke have particle size distribution is that showed similar bimodal distribution. This bimodal distribution is largely due to the resistant stone line particles of the pisolites population. Lithic fragments of the stone-line and pisolites contain no chromite and tend to be very resistant to weathering. The pisolites are resistant to weathering due to the iron coating and the stone line profiles are composed largely of resistant silica and cherty (Fig 5.6).

**Fig 5.6** Comparison of Selected Middle Dyke Soil Types

*[Graphs showing compositional and grain size distribution in prominent Middle Dyke soil profiles. Note the striking similarities between the two profiles, the pisolith and stone-line profiles]*

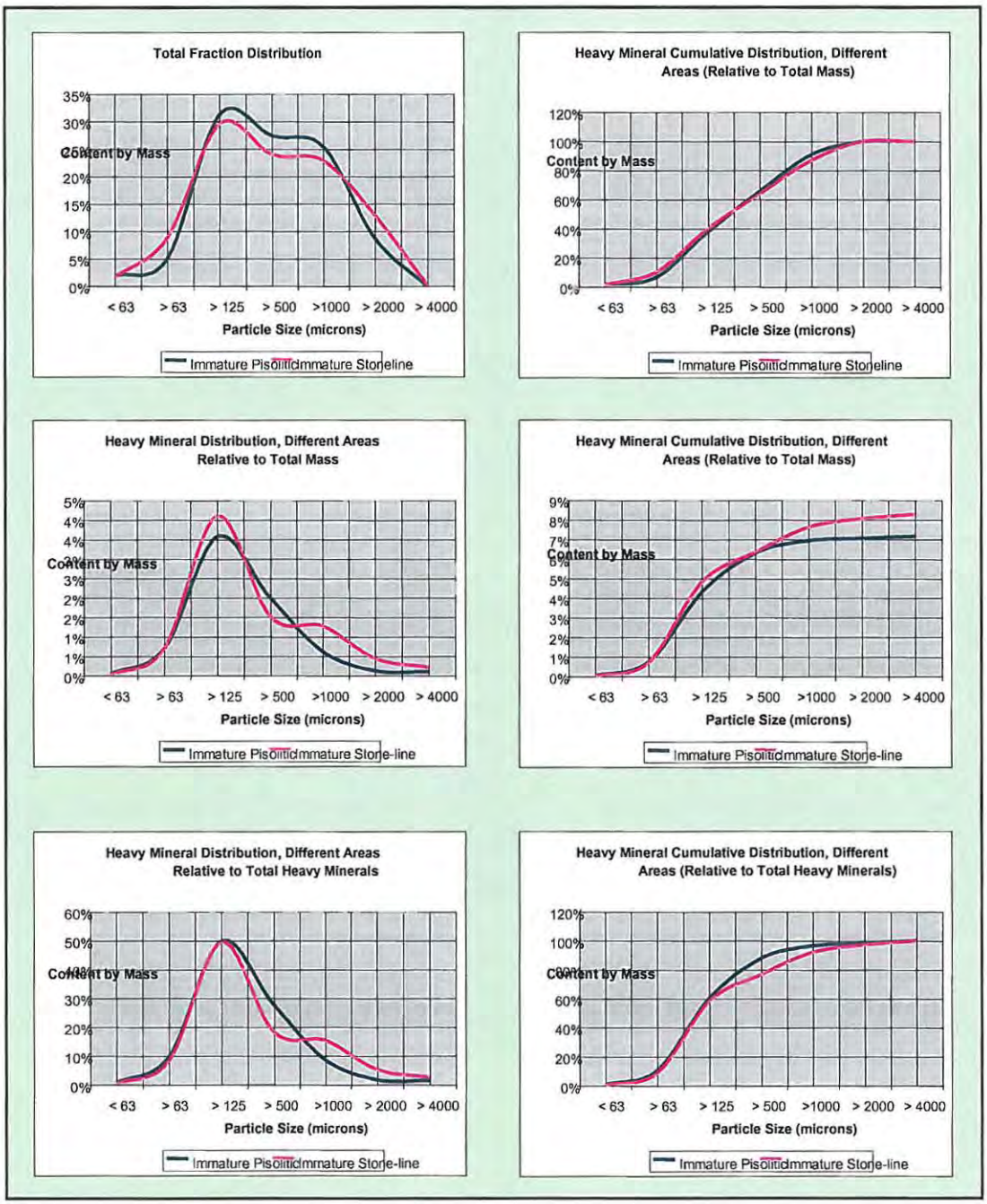

5.5.3 South Dyke Soil Chromite Distribution

**Fig. 5.7** Particles Size Distribution of Selected South Dyke Soils

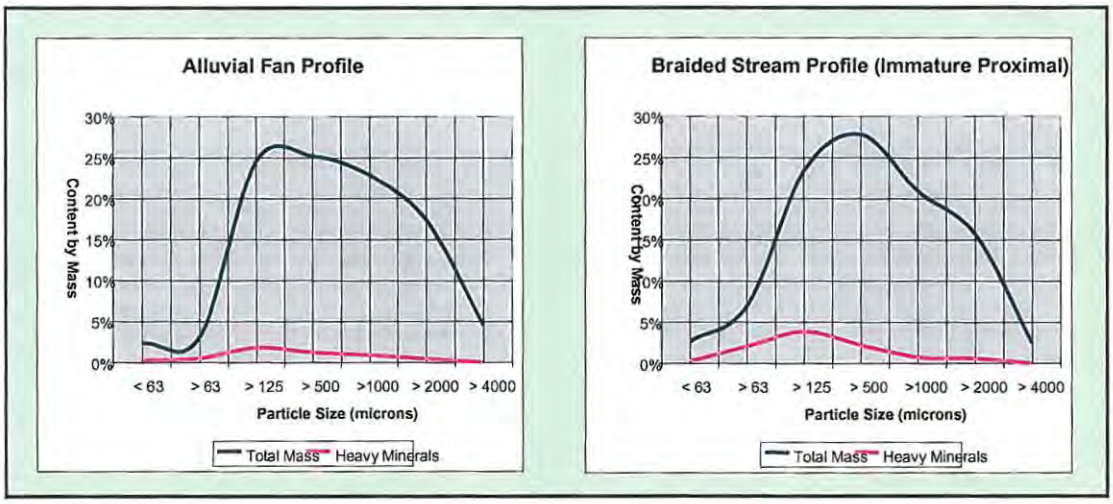


Two dominant South Dyke soil profiles types were selected, one a predominantly distal alluvial fan type profile and another, a proximal immature braided stream profile. These profiles are neither exclusive to the South Dyke area nor are they the only profile types that exist in the South Dyke region of the Great Dyke. Despite the different depositional environments for these two soil profile types, the size particle distribution pattern is very similar (Fig.5.7). The similarity is probably a result of periodic pulses of sediment deposition, which tend to be seasonal. Whilst the distribution of heavy minerals within the two different soil profiles is similar, the braided stream profile contains a significantly higher average total heavy mineral content of about 10 % compared to the Alluvial fan profile which contains just over 5 % average total heavy mineral content (Fig 5.8). The greater heavy mineral content of the braided stream soil profile is attributed partly to relatively longer residence time and hence prolonged pedological processes and upgrading due to sediment re-working within the braided stream depositional environment.

**Fig. 5.8** Comparison of Selected South Dyke Soils Samples

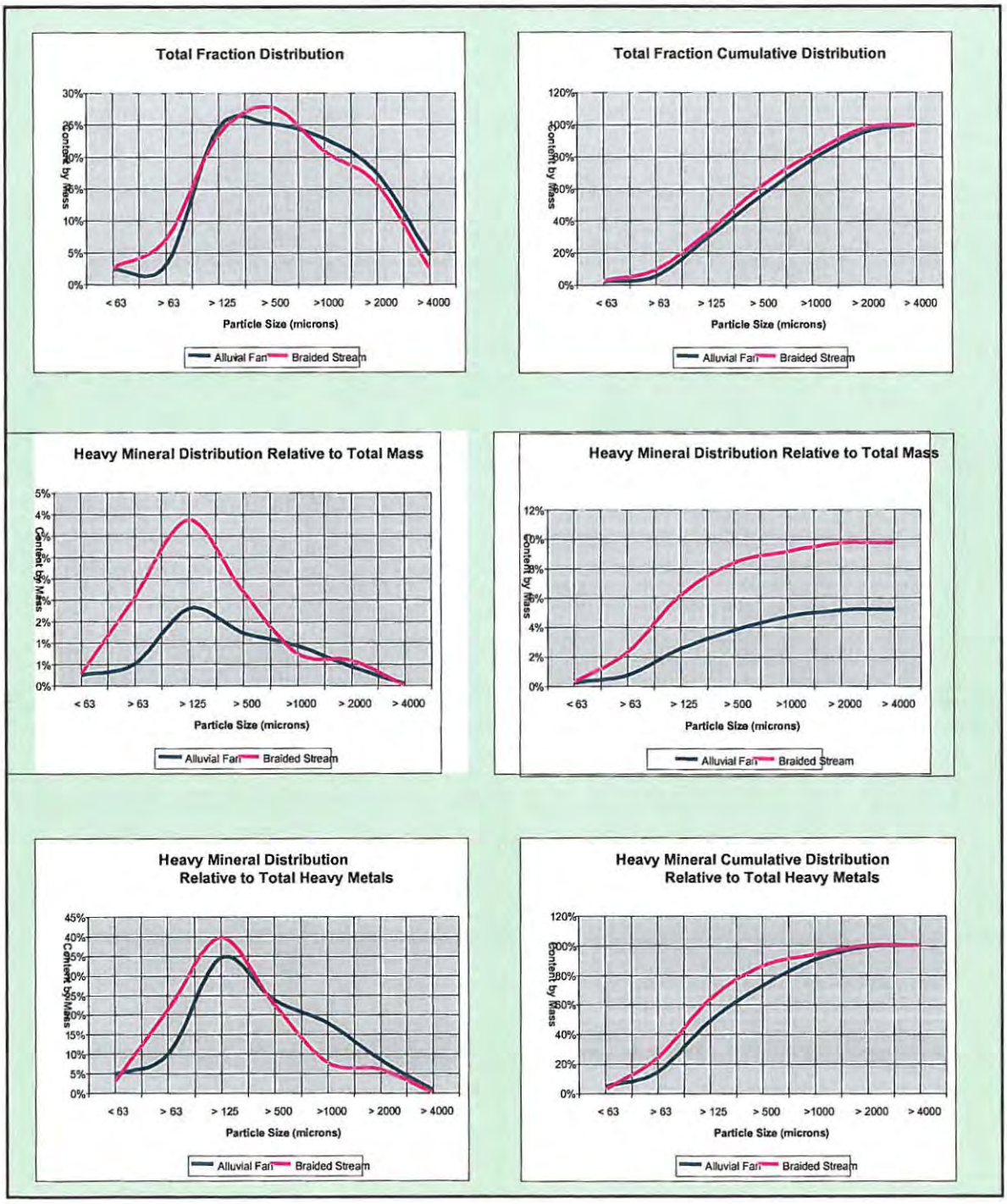

## 5.5 Coarse Fraction Chromite Content

The coarse fractions are diverse for each region of the Great Dyke and for each depositional environment. The bedrock geology generally controls the local soil encountered. However, in certain areas, foreign material introduced through deposition also controls the soil type. The Jester samples contained no fragments and occur above Dunite Succession rocks, where the serpentinite easily weather. The Caesar and Sutton soils contain lithic fragments, which are mostly serpentinite. The Caesar soil samples occasionally contain transported pyroxenite material from upper lithologies. The black cotton soils of the Sutton vleis contain transported material which is well rounded and include fragments of pyroxenite, serpentinite and chromitite. The chromitite fragments could well be responsible for the chromium contained in the bulk sample (Table 5.1).

The sampled areas in the Middle Dyke have large and dominant coarse fraction, which constitutes 30% of the rock fragments. This significantly dilutes the grades. The fragments are predominantly of chalcedony, ferricrete and serpentinite. Where pisolites occur in the >1000 µm fraction they are coated with iron oxides which is thought to inhibit further particle degradation and release of interstitial chromium in serpentinite.

The South Dyke contains predominantly pyroxenite and magnesite fragments. The coarse fraction constitutes only 10 % of the total mass. The greatest grade contaminant in the South Dyke are loose pyroxene grains occurring as individual crystals in the >1000 µm range.

## 5.6 Fine Fraction Chromite Content

Non-chromite chromium and ultra fine chromite in clay-sized and silt-sized fraction is generally low and sometimes below XRF detection limits. Some of the clay-size and silt-size fractions were analyzed and results are summarized in Table 5.2 below.

**Table 5.2** XRF Analyses of Great Dyke Eluvial Soils Slimes

| Sample Location | %$Cr_2O_3$ | %FeO | %$SiO_2$ | %MgO | %CaO | %$Al_2O_3$ | $TiO_2$ | Total |
|---|---|---|---|---|---|---|---|---|
| Immature Profile (Caesar) | 3.76 | 36.00 | 29.30 | 9.72 | 0.56 | 18.34 | 0.19 | 97.87 |
| Mature Profile (Jester) | 3.45 | 42.80 | 27.56 | 8.84 | 0.26 | 16.11 | 0.15 | 99.17 |
| Mature Profile (Sutton) | 3.12 | 37.20 | 28.11 | 9.98 | 0.30 | 16.96 | 0.18 | 95.85 |
| Pisolite Profile (Middle Dyke) | 0.00 | 38.32 | 30.12 | 9.12 | 0.23 | 17.54 | 0.18 | 96.37 |
| Stone line Profile (Middle Dyke) | 0.00 | 36.20 | 29.88 | 10.26 | 0.15 | 18.00 | 0.16 | 95.53 |
| Alluvial Fan Profile (South Dyke) | 1.43 | 34.02 | 29.84 | 12.72 | 0.57 | 18.01 | 0.18 | 96.77 |
| Braided Stream Profile (South Dyke) | 1.60 | 32.86 | 30.16 | 11.71 | 0.55 | 17.75 | 0.17 | 94.80 |

## 5.7 Distribution of Chromite-Rich Soils in the various Regions of the Great Dyke

A total of 1314 intersections from pits dug over the entire strike of the Great Dyke of Zimbabwe and sample collected for a Zimbabwe Alloys Limited regional survey were analyzed and used to characterize the various eluvial depositional environments. The evaluation entailed pitting and sampling of the eluvial areas in ground accessible to Zimbabwe Alloys Limited. The survey covered the entire Great Dyke from South Dyke to North Dyke but excluded the whole of the more northerly Mavuradonha sub-chamber, whose eluvial resource together with those covering the Impinge area belong to, Zimbabwe Mining and Smelting Company (ZIMASCO), another ferrochrome producer with chrome interests on the Great Dyke. Maps of eluvial soil distribution together with details of grades and tonnages were however made available courtesy of ZIMASCO Mutorashanga operations management. The regional work conducted by Zimbabwe Alloys Limited involved the analysis of satellite imagery Landsat 7 and Spot data, the compilation of a supervised classification system, and finally delineation of areas with eluvial soil deposits. Prospective areas were identified at North Dyke, Middle Dyke and South Dyke. Pits were excavated over these areas at an initial grid of 1000 metres along strike of the Great Dyke and 200 metres across. Summarized in Table 5.3 is the data collected during the Zimbabwe Alloys Limited sampling campaign. The samples collected were screened into <1 mm and >1 mm fractions. Only the <1mm fraction was analyzed for chromite content and used in the data analyses and geostatistical evaluation. The geostatistical analysis was done to give an indication of data quality and as a precursor to resource tonnage estimation of the various regions of the Great Dyke.

**Table 5.3** Summary of available Data at Arbitrary Cut-Offs

*[Data obtained courtesy of Zimbabwe Alloys Limited Sampling Campaign, 2002].*

| | >8%$Cr_2O_3$ Sample Cut-Off | | | >10%$Cr_2O_3$ Sample Cut-Off | | |
|---|---|---|---|---|---|---|
| | North | Middle | South | North | Middle | South |
| Number of Pits | 392 | 393 | 254 | 392 | 393 | 254 |
| Assayed Pits | 214 | 211 | 164 | 214 | 211 | 164 |
| Pits satisfying cut-off | 78% | 31% | 44% | 67% | 24% | 33% |
| -1mm fraction by weight | 79% | 71% | 75% | 80% | 72% | 76% |
| %$Cr_2O_3$ | 16.1 | 12.5 | 12.0 | 17.6 | 14.0 | 13.4 |
| %FeO | 26.9 | 24.7 | 17.1 | 27.6 | 25.4 | 17.4 |
| Nominal area (assayed) $km^2$ | 33 | 13 | 14 | 29 | 10 | 11 |
| Extrapolated area $km^2$ | 61 | 24 | 22 | 52 | 19 | 17 |

The nominal area assumes a perfect grid of pits dug at intervals of 1km along the Dyke and 200 m across. Therefore each pit represents an area equal to 0.2 $km^2$. Multiplying this area by the number of assayed pits and proportion of pits satisfying a cut-off gives the nominal area. Similarly, multiplying 0.2 $km^2$ by the total number of pits and proportion of pits satisfying a cut-off gives the extrapolated area.

## 5.8 Geostatistical Analysis of the Zimbabwe Alloys Limited, 2002, Sampling Data

The Middle Dyke was excluded from the exercise at this stage due to the excessive amount of pebbles and therefore ranked lower as a prospective area. (Datamine software was used in geostatistical modelling). One of the major drawbacks in analysing the data was that it lacked proper selection criteria for the data because

- The pits were not elevated resulting in the terrain being assumed perfectly flat.
- Data lacked geological information, for the delineation of areas of geological homogeneity.
- There were no physical and topographic features in the database to act, as controls, therefore the 0.2 $km^2$ area coverage per pit could be an overestimation.

Correlation analysis results showed, either poor or no correlation between most of the variables within the <1 mm size fraction. The depth of sample or thickness of the horizon were very poorly correlated with grades and did not exceed a correlation coefficient of 0.3. The fraction size (in weight percent) was also poorly correlated with grades and does not exceed a correlation coefficient of 0.4. The highest correlation coefficient was between the chromite grades in the -1mm size fraction, being 0.76 and 0.71 for the South and North Dyke, respectively. A relatively high correlation coefficient of 0.77 between the South Dyke iron oxide grade was unmatched by the low North Dyke correlation coefficient of 0.46. On the basis of the statistical analysis the following procedure for geostatistical analysis was employed.

1. Multiplying the grade (%$Cr_2O_3$, %FeO) by proportion (sample fraction weight), model the result and carry out estimates (kriging) whose result will be in percent-proportion

2. Modeling the proportion and carry out proportion estimates on the same block size as in 1

3. Dividing the result 1 by result 2 to get the grade

4. Modelling depth and estimate average thickness of each block to get total volume

5. Multiplying total volume by specific gravity and proportion to get the tonnage of *in situ* sample weight.

For the purpose of calculating semi-variograms the east and west zones of the Great Dyke in each region were combined since the statistics were very similar. This approach had its drawbacks in that it tended to give very long ranges across the Great Dyke zones when characteristics on both sides were similar. This could be seen in the long ranges of 4700 m for the thickness and 5000 m

for the chromite grade. Where there was both a short-range and a long-range structure, the shot range was indicative of the optimum sampling grid for each zone. The initial sampling pit grid was approximately 1000 metres along strike and 200 metres across. In order to determine the optimum grid for infill sampling, the range at eighty percent of the variance was taken as the maximum sample spacing. This was derived from a rule of thumb for setting the search radius when estimating block grades. Since there were different variables to consider, the shortest range in each direction would be accepted even though the shortest range along strike could have been from a different variable compared to shortest range across strike. The parameters of the modelled semi-variograms are shown in Tables 5.4 and 5.5.

**Table 5.4** Model Semi-Variograms for North Dyke Sampling

| | | | Range (m) | | Range at 80% of Sill (m) | |
|---|---|---|---|---|---|---|
| Variable | Nugget | Spatial Variance | Along Strike | Across Strike | Along Strike | Across Strike |
| $\%Cr_2O_3$ x Proportion | 15.2 | 16.5 | 2600 | 550 | 1586 | 336 |
| $\%FeO_x$ Proportion | 9.5 | 14.5 | 1520 | 350 | 927 | 214 |
| Proportion | 0.0056 | 0.0059 | 1800 | 500 | 1098 | 305 |
| Thickness | 0.063 | 0.132 | 4300 | 750 | 2623 | 458 |
| $\%Cr_2O_3$ | 16 | 22 | 2150 | 600 | 1312 | 366 |
| | | | Sampling Grid Size | | 927 | 214 |

**Table 5.5** Model Semi-Variograms for South Dyke Sampling

| | | | Range (m) | | Range at 80% of Sill (m) | |
|---|---|---|---|---|---|---|
| Variable | Nugget | Spatial Variance | Along Strike | Across Strike | Along Strike | Across Strike |
| $\%Cr_2O_3$ x Proportion | 1.0 | 6.0<br>8.0 | 1200<br>6000 | 400<br>1100 | 732<br>3660 | 244<br>671 |
| %FeO x Proportion | 3.0 | 6.25 | 2100 | 1250 | 1281 | 763 |
| Proportion | 0.0001 | 0.0086<br>0.01 | 1500<br>1800 | 350<br>1300 | 915<br>1098 | 214<br>793 |
| Thickness | 0.066 | 0.062 | 1250 | 4700 | 763 | 2867 |
| $\%Cr_2O_3$ | 8.0 | 2.00<br>11.13 | 3000<br>10000 | 300<br>5000 | 1830<br>6100 | 183<br>3050 |
| | | | Sampling Grid Size | | 732 | 183 |

*[Where there are two rows, the top row is for the short-range and the bottom is for the long range. These semi-variograms were used to estimate tonnages within geological, physical, infrastructural and topographic constraints. In situ bulk densities measurements for each area were also determined and incorporated into the database].*

## 5.9 Conclusions from the Geostatistical Analysis.

The ideal sampling grid for the North Dyke should not exceed 925 m along strike and 210 m across strike while the corresponding figures for the South Dyke are 730 m and 180 m.
In reality however this may only be an artifact of the sampling grid. The sampling grid cannot yield information for variability shorter than the 200 m employed in the sampling campaign range due to data limitation. This needs to be further investigated for the tonnages calculated and presented in this report to be more confidently categorized in terms of the resource definitions and requirements of the JORC Code (Joint Australasian Resources Committee, 2004). The sampling data collected by Zimbabwe Alloys Limited need to be improved with respect to size fraction information in order to increase confidence in grade distribution. The grade distribution information collected during the current evaluation is too small a sample to enable upgrading the resource to any class better than the inferred category of JORC code (2004).

## 5.10 Distribution and Summary of Eluvial Resources

The data collected by Zimbabwe Alloys Limited during the 2001 to 2002 sampling campaign, information received from Zimbabwe Mining and Smelting Company (Zimasco) on the tonnage grades and distribution of eluvial chromite north of Impinge as well as reconnaissance surveys by the author were used to compile and calculate inferred resource maps. The distribution of eluvials is summarized in the following tonnages summaries in Table 5.6. Surface maps compiled to assist in resource tonnage estimation are exemplified by Fig. 5.9.

**Table 5.6** Great Dyke Eluvial Chromite Resources

| **Great Dyke Regions** | Resource (tonnes) | Estimated *in situ* grade (%$Cr_2O_3$) | Confidence levels (grade & thickness) | Assumed product grade (%Cr2O3) | Assumed product Cr:Fe ratio | Resource estimate (tonnes) | Reserve equivalent (tonnes) |
|---|---|---|---|---|---|---|---|
| North Dyke (Zimasco) | 50,000,000 | 20.00 | 98% | 48.00 | 2.40 | 49,000,000 | 41,650,000 |
| North Dyke (Zim Alloys) | 70,000,000 | 18.00 | 98% | 48.00 | 2.40 | 68,600,000 | 58,310,000 |
| Middle Dyke (Zim Alloys) | 20,000,000 | 15.00 | 75% | 48.00 | 2.40 | 15,000,000 | 12,750,000 |
| Middle Dyke (Others) | 45,000,000 | 15.00 | 66% | 48.00 | 2.40 | 29,700,000 | 25,245,000 |
| South Dyke (Zim Alloys) | 40,000,000 | 16.00 | 90% | 48.00 | 2.40 | 36,000,000 | 30,600,000 |
| South Dyke (Others) | 25,000,000 | 16.00 | 66% | 48.00 | 2.40 | 16,500,000 | 14,025,000 |
| | 50,000,000 | 12.00 | 66% | 48.00 | 2.40 | 33,000,000 | 28,050,000 |
| | 300,000,000 | 16.25 | 83% | 48.00 | 2.40 | 247,800,000 | 210,630,000 |

**Fig. 5.9** Distribution of Eluvial Soils, South Dyke

*(Typical eluvial Resource distribution map showing South Dyke eluvial soils).*

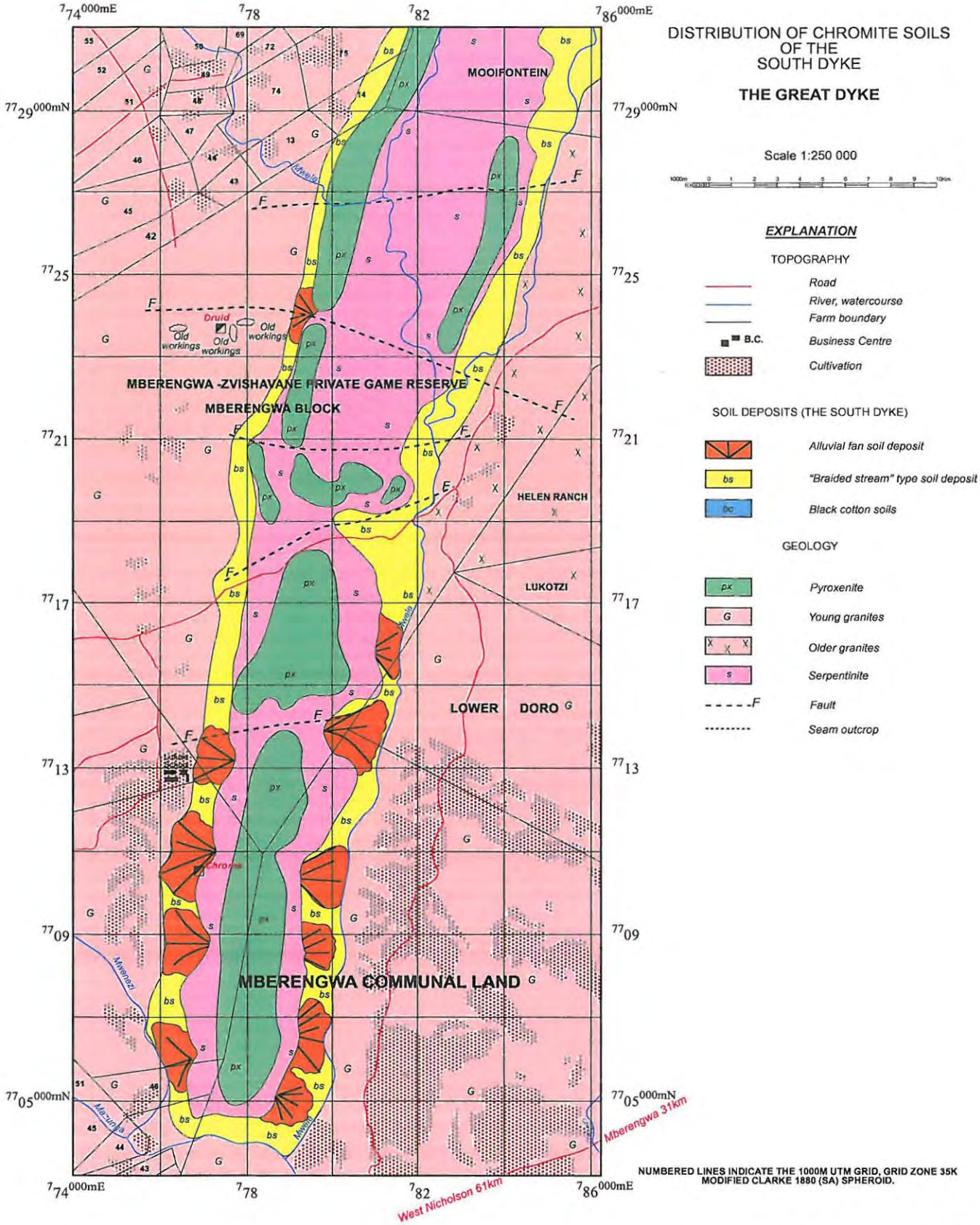

## Chapter 6

# 6.0 Mineralogy and Composition of Eluvial Chromite

## 6.1 Introduction

Samples from mature, residual and high-grade (± 20% $Cr_2O3$) soils were obtained from Jester and Sutton areas in North Dyke. Samples from a distally transported "braided stream" depositional environment and of relatively lower-grade (± 12% $Cr_2O3$) were obtained from South Dyke. Also obtained were samples from a proximally transported "alluvial fan" depositional environment from, South Dyke. These areas were selected, for mineralogical analysis mainly, on the basis of their characteristic soil chromite content and relative abundance in terms of geographic distribution and average soil thicknesses and on the basis of their bulk composition characteristics. The soil bulk composition in terms of relative heavy mineral content and paucity of lithic or un-weathered fragments was used as a sampling environment selection criterion. Partly for these reasons, areas on the Great Dyke with black cotton soils, those with high lithic fragments and those soils on steep slopes particularly in the North Dyke were excluded. Separates obtained from Mosley table concentration of these samples were screened, sieved, washed and examined under binocular microscope. Using a binocular microscope grains were examined for grain sizes variation, roundness and sorting. These parameters are important indicators of particle transport history. Alluvial materials particles are expected to generally progress from an angular condition at their source area to a greater degrees of rounding downstream (Powers, 1953). With the aid of a binocular microscope the presence or absence of grain cementing was also were investigated. The presence of these cementing agents may result in composite granules. Other important features which were investigated using a binocular microscope included determination of grain morphology and grain surface features. The process of transportation results in damage to the grain surfaces. This usually results in a dull grain surface and sometimes percussion marks, striations, impression marks, frosting and polishing (Bates and Jackson, 1980). The binocular microscope was also used to estimate the amount of residual silicate minerals contained in the separates. Polished sections of some of the chromite grains were then examined by reflected light microscopy. An Olympus polarizing microscope was used for mineral identification and petrographic description. As the composition of the mineral separates was predominantly chromite, the petrography was confined to reflected light microscopy. This technique enabled examination of crystal morphology (form and habit), zoning, cleavage, parting, twinning, inclusions and intergrowths (Ineson, 1989, Craig and Vaughan, 1994). Reflected light microscopy also enabled examination of textures that were considered peculiar to each of the different grain suites. Photomicrographs and petrographic descriptions of the different suites of mineral suites of separates, examined under reflected light microscope, are detailed in the following sections.

## 6.2 Petrography of the Eluvial Chromite Grains.

The petrography focused mainly on the chromite petrology, textures and other features that might be peculiar to each of the heavy mineral-grain suites. Properties of the chromites examined under reflected light microscopy included shape and size of the grains. Chromite grains are known to be affected by late alteration which may result in inclusions or development of irregular grain boundaries particularly where chromite is intergrown with gangue minerals (Power et al., 2000; Irvine, 1975) Grains affected by such alteration tend to exhibit a trellis pattern of gangue mineral alteration, in which the gangue mineral develops along chromite-grain cleavage planes (Rollinson et al, 2002). The grain boundaries and shapes of the chromite grains are important parameters in distinguishing chromite grains derived from interstitial spaces within dunites and those derived from olivine crystals inclusions (Prendergast, 1985). As observed by Wilson (1982), grains exhibiting the chromite octahedral form are usually those derived from within olivine crystals inclusions and grains derived from interstitial spaces within dunites are often irregular, as they tend to fill interstitial gaps available between adjacent olivine crystals. Chromite grain-size is also an essential distinguishing feature between chromite grains derived from dunites and pyroxenites and those derived from chromite seams. The average grain-size for those chromites derived from olivine inclusions range between 0.05 to 0.2mm in diameter. This size range is considerably finer-grained than seam chromites grains, which are generally between 1mm to 3mm in diameter (Wilson, 1982). The type and nature of inclusions observed in these chromite grains can only be examined superficially by means of reflected light microscopy as some of the suspected inclusions such as olivine, phlogopite, and other minor mineral constituents (which may possibly include sulphides) can only express themselves as round inclusion inside the chromites of up to 10μm in diameter (Appel et al., 2002). Another limitation to textural examination of the chromite grains is due to the small variations in reflectivity and colour of the chromite grain, which is limited to dark and light shades of grey. The compositions associated with the different shades, however, were subjected to further analysis by electron microprobe.

## 6.3 Mature Residual Soil Chromite

Samples collected from Jester and Sutton areas of the North Dyke were prepared into 10 polished sections for examination under a reflected light microscope. The sample identity and details of fraction size are summarized in the Table 6.1 below. Mineral grains from these same samples were also examined under binocular microscope. These samples were collected from an area with mature profiles consisting of residual soils. The soils that overlie the Dunite Succession of the Great Dyke occur within flat plains and are considered to have resulted from *in situ* pedological processes. The soil samples were noted to be chocolate brown in colour (2,5YR 3/6 – Munsell Chart) and contained virtually no lithic fragments.

**Table 6.1** Mature Residual Soil Samples

| Fraction size | | | | | |
|---|---|---|---|---|---|
| Sample Identity Number | <63µm | >63µm <125µm (a) | >125µm <500µm (b ) | >500µm <1000µm (c) | >1000µm <2000µm (d) |
| | 8 | 9 | 10 | 11 | 12 |
| | 14 | 15 | 16 | 17 | 18 |

## 6.4 Mature Residual Soil Chromite Ore Petrography

**Fig. 6.1** Photomicrograph of Selected Samples from Sample (8 –12, Jester & 14-18, Sutton)

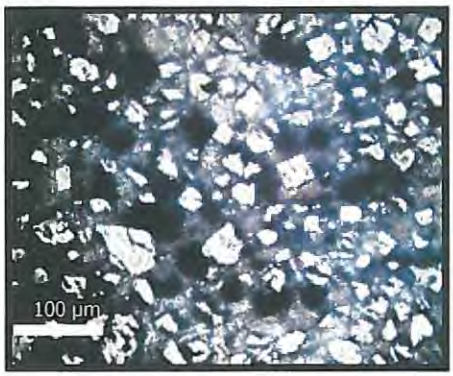


(a) Chromite grains (x 10 magnification)

Grain mounts contains ±10 % residual gangue minerals (dark). The individual chromite grains (light) range in form from euhedral through sub-hedral to anhedral with both angular and rounded grain varieties. The grains are variable in size from the largest ± 60µm to grains below 10µm. Overall the grains are whole but are sometimes fractured and corroded. When observed under the binocular microscope the grain surfaces are pitted and corroded.

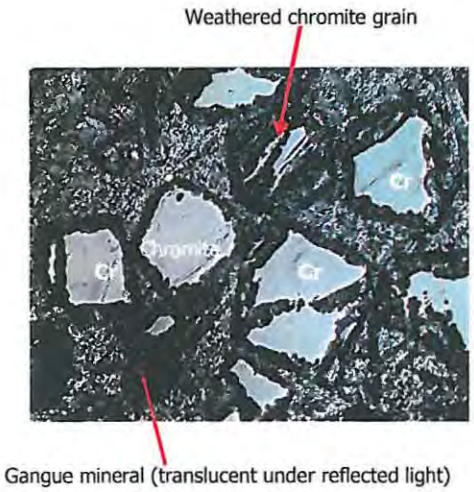


(b) Chromite grains (x 20 magnification)

Grain mounts consist of silicate-free individual chromite grains. The individual chromite grains (grey) have corroded rims and are weathered along fractures. Average grain size is ± 150µm. The grains generally exhibit a relict chromite octahedral shape now slightly obscured by weathering. There are residual gangue minerals, which under reflected light are elongate translucent subhedral grains. The gangue minerals are largely serpentine and occasionally pyroxenes.

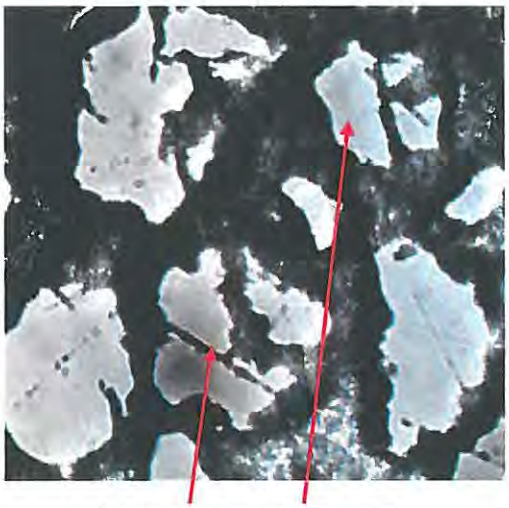

Fractured and corroded chromites

(c) Chromite grains (x 100 magnification)

Some grains were noted to have zones of distinctive brighter grey colour. Such zones were identified and marked for further microprobe analysis for possible compositional variation. The individual chromite grains are either fractured or corroded resulting in angular and rounded varieties of anhedral chromite grains. The corrosion along the chromite grain rims may imply differences in original composition between the grain core and its rim. This feature was further investigated by aid of electron microprobe.

Average grain size is ± 300µm

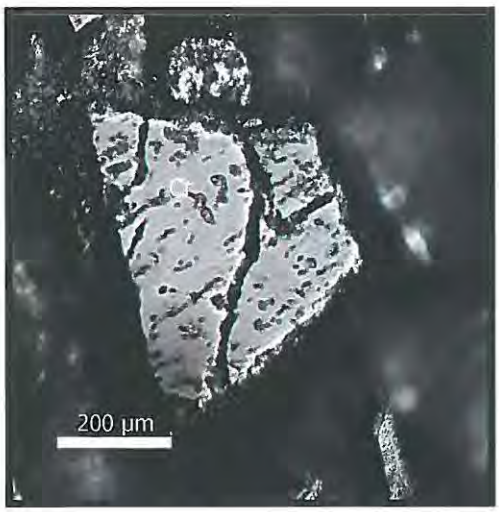


(d) Chromite grains (x 50 magnification)

A relatively un-weathered chromite grain with the characteristic fractures of the chromite grains. The grain is euhedral and contains no inclusions. The grain sides are straight and relatively un-corroded indicating a possible original straight grain boundary typical of silicate free massive poly-crystalline crystals. The small grain size (200 µm) and polygonal shape however could suggest that the grain was derived from an interstitial phase where the grain could have been located along grain boundaries of coarse grains of chromite or olivine. The grain boundary could also be due to co-precipitated with a number of other minerals with typical straight grain boundary relationship (Reynolds, 1985; Fisk and Bence, 1980).

*Note: Samples from Jester and Sutton area were observed to be similar in characteristics and were thus treated as same sample.*

## 6.5 Proximal Alluvial Fan Soil Chromite

Samples collected and classified as proximal transported soils, from the South Dyke, alluvial fan environment were prepared into 5 polished sections for petrography and examination under reflected light microscopy. The sample identity and details of size fraction are summarized in Table 6.2 below. Reflected light microscope petrographic study, on these samples, was complimented by study of the grains of these same mineral suites under binocular microscope.

**Table 6.2** Proximal Soil Profile Sampling

*[Sample 1, 2, 3, 4 & 5 were derived from sieved fraction of a proximal soil profile take at the base of a hill on an alluvial fan. The soils are from a proximal transported deposit].*

| Fraction size | | | | | |
|---|---|---|---|---|---|
| **Sample** | **<63µm** | **>63µm** | **>125µm** | **<500µm** | **<1000µm** |
| **Identity Number** | **1** | **2** | **3** | **4** | **5** |

6.5.1 Proximal Soil Chromites Petrographic Descriptions

**Fig. 6.2** Photomicrograph of Sample 1 (<63µm)


Magnification X 20

Samples 1 consist of angular grains, which are subhendral to euhendral. An examination of these grains under binocular microscope reveals the grain surfaces to be rough and percussion marked. The sample contains residual silicate grains of up to 15% and of the same grain size as the chromites. The uniform grain size is largely a result of sample screening. Some of the chromites have silicate grains enclosed within their structure.

**Fig. 6.3** Photomicrograph of Sample 2(>63µm)

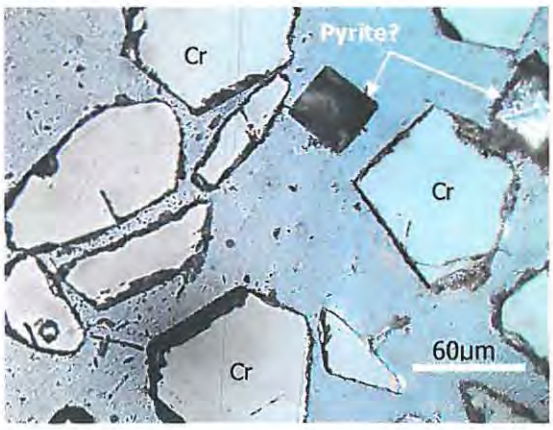


Sample 2 consists of angular grains. The grains exhibit both polygonal form and octahedral crystal forms. Some grains have sharp un-weathered sides as well corroded edges. The fracturing is along crystal plains. Most of the grains show tendencies to fracturing with grains split into two or more fragment. In this section, opaque minerals (probably pyrite) are present together with the chromite grains (X 50).

**Fig. 6.4** Photomicrographs of Sample 3(>125μm)

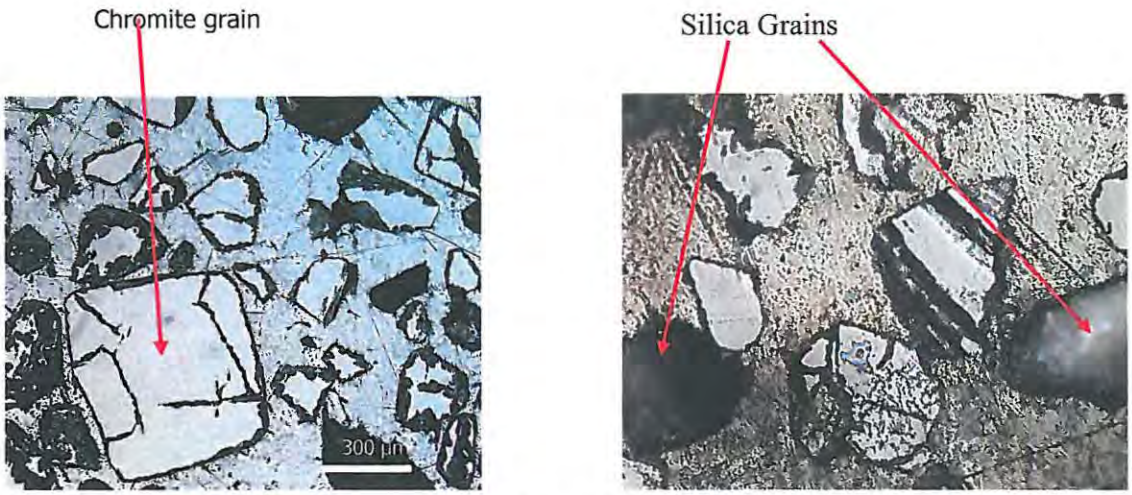


Magnification X 50

Sample 3 contains the occasional relatively large crystal (200μm). The large grains are fractured to varying degree of intensity. Fragmentation is probably a result of polishing during sample preparation The large grains are euhedral and well formed. The small grains have concoidal fracturing more noticeable along the edges and are associated with corrosion, particularly on the edges of the grains (Fisk and Bence, 1980).

**Fig. 6.5** Photomicrographs of Sample 4 (>500μm)

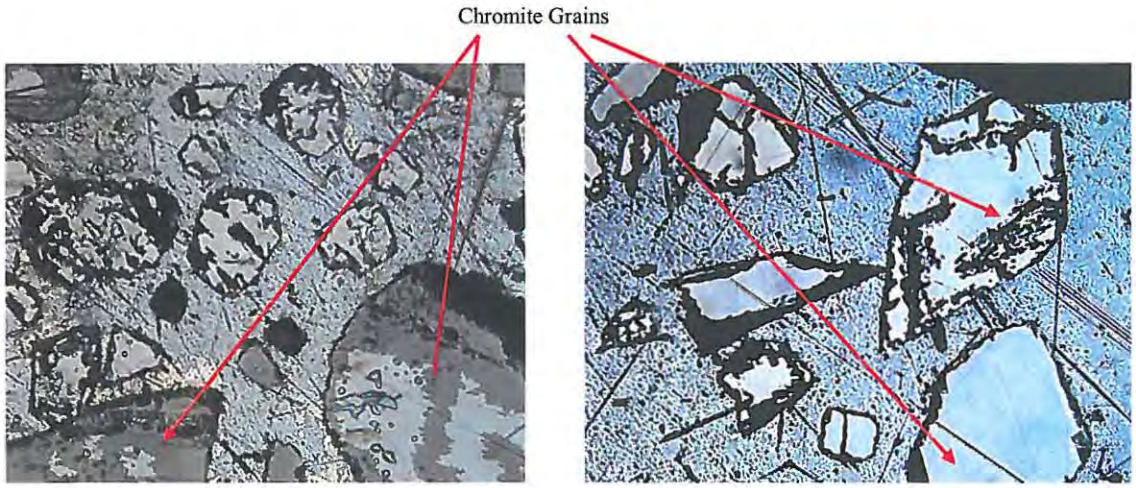


Magnification X 20

Sample 4 contains large amounts of pyroxene (magnesium silicate) grains (Fernandes, 1982). These are distinguished from the chromites by their greenish-grey appearance. The chromites are distinguished by their characteristic fractures and a grey-brownish tint (Onyeagocha, 1974). The chromite grains are polygonal and have serrated edges. They are relatively un-fractured and the

grains are generally an assortment of small and large grains. The smaller grains have concoidal-fractured edges and weathered around the edges. Overall the samples contain very few chromite crystals and are dominated by the silicates.

**Fig. 6.6** Photomicrographs of Sample 5(>1000µm)

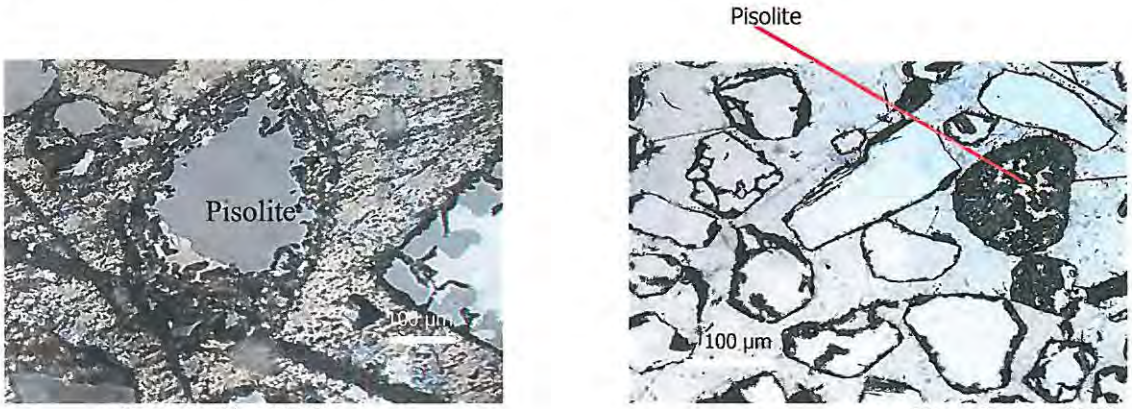


Magnification X 50 Magnification X 20

In Sample 5 the large and dominant chromite, grains are absent. The chromite grains are an assortment of fractured and angular weathered small grains. A pisolite enclosing a chromite partially exposed by sample preparation can be seen in the picture. The mineral separates contain about 40% silicate grains, which appear greenish grey under reflected light. These silicate grains are probably orthopyroxenes and dominate the sample.

## 6.6 Distally Transported Soil Chromite

A sample collected from a braided stream distally transported soil environment was sieved and prepared into 5 polished sections for examination under reflected light microscopy. The sample identity and details of size fraction are summarized in Table 6.3 below. Reflected light microscopy on these samples, was complimented by binocular microscopy.

**Table 6.3** Transported Soil Sampling

*[Sample 19, 20, 21, 22, & 23 are sieved fraction of a distally transported soil profile taken from a braided stream environment].*

| | Fraction size | | | | |
|---|---|---|---|---|---|
| **Sample Identity Number** | **<63µm** | **>63µm** | **>125µm** | **<500µm** | **<1000µm** |
| | **19** | **20** | **21** | **22** | **23** |

6.6.1 Distally Transported Soil Chromite Petrography

**Fig. 6.7** Photomicrograph of Sample 19 (<63µm)

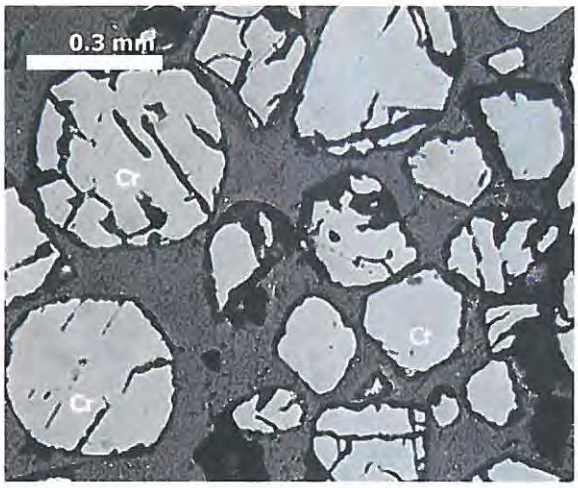


Magnification X 50

Sample 21 consist of well-rounded grains. An examination of these grains under binocular microscope reveals the grain surfaces to be smooth but frosted. The sample contains no residual silicate grains.

**Fig. 6.8** Photomicrograph of Sample 20 (> 63µm)

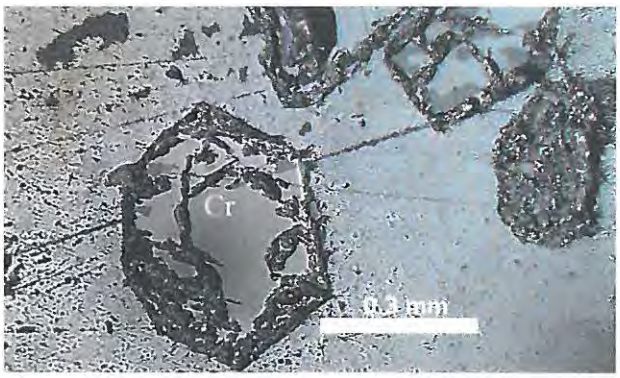


Magnification X 50

Sample 20 consists of more angular grains than sample 19. The grains exhibit both polygonal form and octahedral crystal forms. Some grains have sharp un-weathered sides but most grains are characterised by corroded edges. The fracturing is along crystal plains. Most of the grains show tendencies to fracturing with grains split into two or more fragment.

**Fig. 6.9** Photomicrograph of Sample 21 (>125µm)

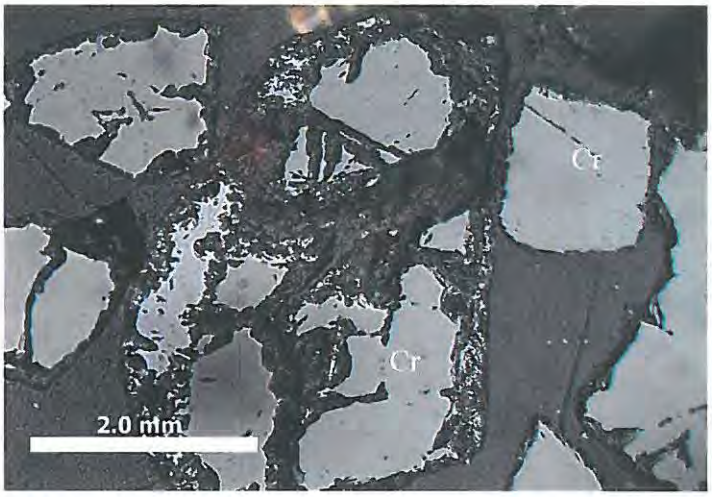


Sample 21 (X 100) contains the occasional relatively large crystal (+300μm). The large grains are fractured to varying extents. The fracturing along lines of weakness may be a result of polishing, during sample preparation. The large grains are euhedral and well formed and sometimes enclose silicate material. The smaller grains are more angular with corroded edges.

**Fig. 6.10** Photomicrograph of Sample 22

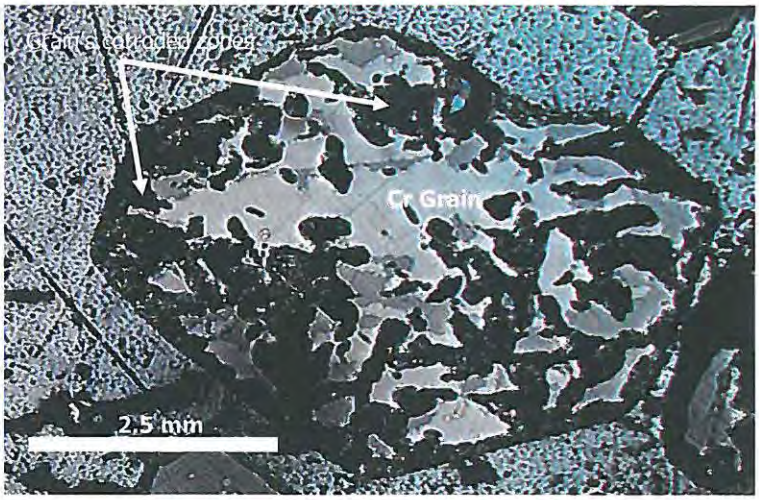


Sample 22 has large chromite grains characterised by polygonal shapes but with corroded surfaces. They are relatively un-fractured and grains are generally an assortment of small and large grains dominated by the size of the occasional large grain. The smaller grains are rounded and sometimes weathered around the edges. The sample contains very few gangue minerals grains and is dominated by the chromite.

**Fig. 6.11** Photomicrograph of Sample 23 (X 150)

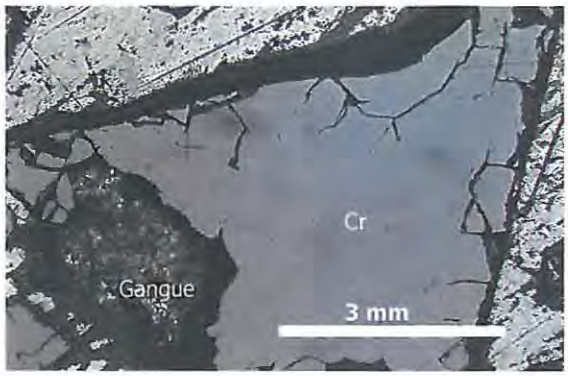


In Sample 23 the large and dominant chromite grains are rare. However, where these occur, they are fractured due to weathering processes. Above is a typical large grain seen here with an enclosed gangue mineral.

## 6.7 Pisolite Petrography

Occurring in most samples examined were pisolite, Fe-oxide concretion which typically develop around chromite or silica grain (Fig 6.12) In polished section microscopy pisolite grains appear as ochre coloured grains, which in section clearly display discontinuous successions of concentric rings (Leblanc, 1980). In plane-polarized light, the rings are observed to be characterised by reddish to black areas, irregularly distributed in each ring suggesting a distinct compositional variation between the rings. An electron microscope image of such concretion from the eluvial chromite suite is shown in Fig 6.13.

**Fig. 6.12** Photomicrographs of Pisolites (X 100)

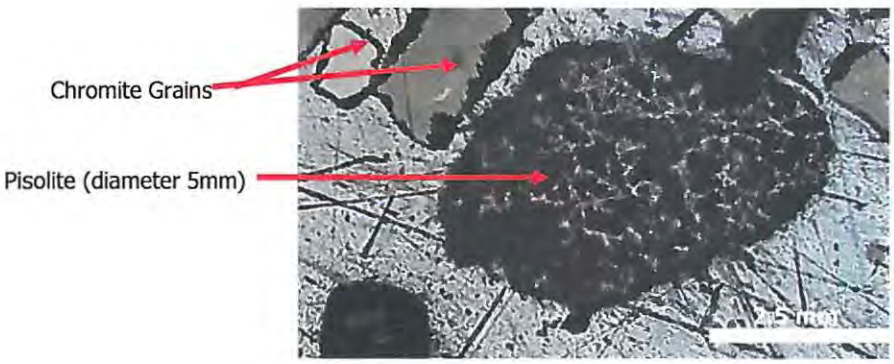


*Top:* *A pisolite grain (Note: that this pisolite grain has not been polished and exhibits the ferruginous coating to the grain)*

**Fig. 6.13** Polished Pisolite Grain (X 100)

*[A polished pisolite showing ferruginous coating developed around a chromite grain core]*

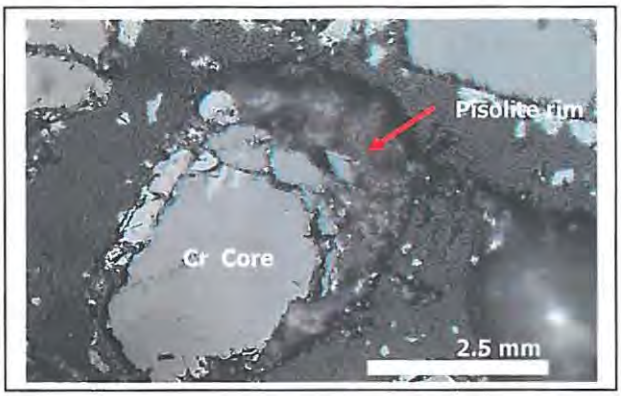


**Fig. 6.14** Scanning Electron Microscope (Microphotographs of Pisolites and Chromite Grains)

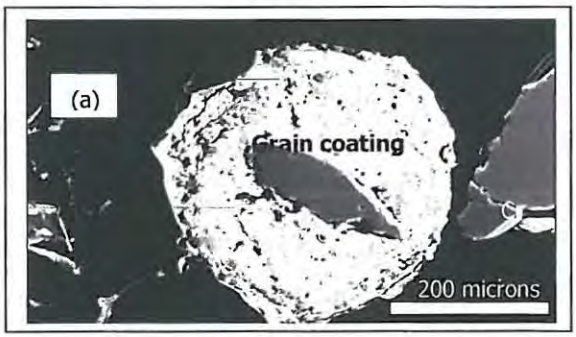


*(a) Pisolite developed around a chromite grain core*

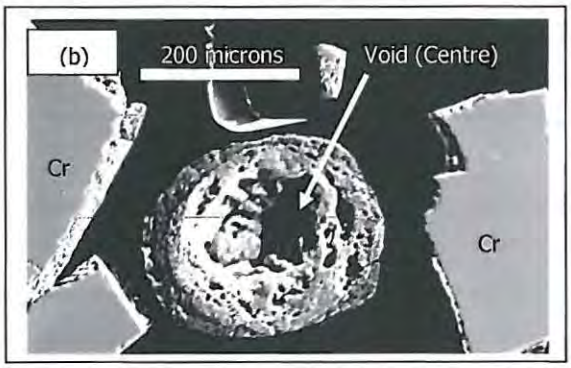


*(b) A pisolites showing outer concentric rings and a central void once occupied by grain core*

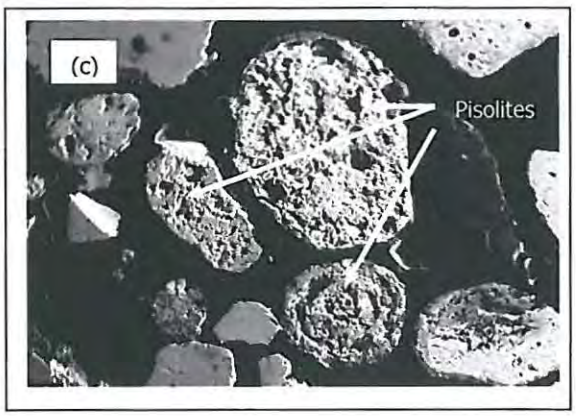


*(c) An assortment of pisolites*

## 6.8 Discussion

Petrography shows that chromite grains from the residual and mature depositional environments, such as the Sutton and Jester areas and proximal profiles such as the alluvial fan deposits of the South Dyke, are mainly angular to sub-rounded. There is however relatively more rounding in smaller grains of these same suites compared to larger ones, confirming effects of some degree of attrition weathering. There are also variations in extent of corrosions on the grains. This corrosion is not restricted to any particular particle size and could be a result of localized climatic conditions.

In general the fine fractions have less silicate gangue than the coarse fractions. In the South Dyke samples, the dominant silicate gangue is pyroxene grains whose abundance increases dramatically in the 500μm and coarser fractions. Other observations noted included some cubic opaque isotropic mineral. The presences of such cubic mineral may suggest soils derived from weathering of upper stratigraphy and host of the Great Dyke PGEs.
The Great Dyke eluvial chromites are probably derived from interstitial chromite originally locked up within dunites (serpentinites). Pyroxenites typically contain less interstitial chromite than the dunites and are therefore a less important source of eluvial chromite soils.

## 6.9 Synthesis and Conclusion

The chromite grains from the South Dyke area are typically lower grade than those from the North Dyke. This is attributed to the semi-arid conditions of the South Dyke, which hinder chemical weathering processes and hence the rapid breakdown and release of chromite into the soil. Notable other differences between the North Dyke and South Dyke include the more polygonal nature of the South Dyke grains as opposed to the North Dyke corroded and angular grains. Similarities include the small grain size of all the eluvial chromite, which are all within the average range of between 70μm and 500μm. The observation generally supports the view that the entire eluvial depositional environment is largely residual or proximal to source. Chromite grains from North Dyke are derived from both interstitial and from inclusion in olivine crystals. The chromite grains from South Dyke could be predominantly from dunite interstices. There is greater rounding of grains due to attrition on samples from South Dyke deposits. The North Dyke chromites are more corroded than those from other areas due to wetter climatic conditions. The results of the petrography indicate that the South Dyke eluvials are likely to be of lower grade. Lower rates of chemical breakdown of lithic fragments result in less chromite being released into the soils. North Dyke chromites are likely to have high Fe content as they are derived largely from grains previously enclosed within olivine crystals. Some eluvials are may preserve other economic minerals associated with the easily weathered Main Sulphide Zone, host to PGMs and gold.

## Chapter 7

# 7.0 Geochemistry of Eluvial Chromite

## 7.1 Introduction

The compositions of different Great Dyke chromite vary and this variation is partly due to their modification during subsolidus cooling (Wilson, 1982). Fine grains of chromite in olivine, from dunite or harzburgite, tend to be more iron-rich than coarse grained chromites interstitial to these minerals. This phenomenon, which is also evident in eluvial chromite, is ascribed to subsolidus re-equilibration exchange of Fe and Mg between these fine-grained chromite and the enclosing olivine or orthopyroxene, and results in alteration that is typically absent from larger-grained seam-type chromites (Prendergast, 1985; Larsen and Pedersen, 2000). Complex textures, which are only, exhibited as light and dark grey chromite patches within some of the eluvial chromite grains under reflected light microscopy, can be revealed in more detail, when examined through a scanning electron microscope. However the scanning electron microscope unlike electron microprobe analyses is incapable of detecting different mineral phases represented by these differently coloured chromite patches (Lehman and Roux, 1986; Appel et al., 2002). Thus the polished sections of the eluvial chromite grains, examined under reflected light microscope, were further analyzed for possible compositional variations using an electron microprobe. The presence of 'ferritchromit' or magnetite rims to these grains was also investigated, by electron microprobe and noted to be absent. These magnetite rims, which can be found in chromites from ultramafic rocks of any paragenesis, are usually characterized by low alumina (Barnes and Roeder, 2001). Polished thin sections were analyzed for Mg, Al, Cr, Fe Mn, Ti, Ni, Cu, Zn and Si by electron microprobe. The results were acquired as oxides. $Fe^{3+}$ in spinel was then calculated in accordance to the charge balance equation of Droop (1987). In addition to the microprobe analyses, results obtained from examining the differing grains under binocular microscope and reflected light petrography were available for characterising these soil-derived chromites, their mineral composition and variations.

## 7.2 Micro-Morphology And Mineralogy

Under the binocular stereoscopic microscope, the heavy mineral extracts from eluvial chromite soils appeared as small black to dark brown ovoid grains. These grains are mainly of the order of microns to millimeters in size. The surfaces of the grains are generally slightly rough with black, bright metallic and sometimes partly ochre coloured. In polished section microscopy, the black to metallic grains were further observed to be octahedral chromite grains, displaying relative optical homogeneity whilst the partly ochre-coloured grains were observed, by optical microscopy, to clearly display discontinuous successions of concentric rings and hence implying chemical

heterogeneity. In plane-polarized light, the rings were observed to be characterised by reddish to black areas, irregularly distributed in each ring suggesting a distinct compositional variation between the rings. An image of such concretions from the eluvial chromite suite is shown in Fig. 7.1. These concretions are pisolites, which are primary mineral grains enveloped by irregular secondary concentric layers.

**Fig. 7.1** Pisolites and Chromite Grains

*[Photomicrograph showing pisolites (mineral concretions) with central void from where chromite primary grain core has been removed and outer concentric rims envelope. Note also the chromite grain on the photomicrograph bottom right with characteristic fractures around the grain margins. The Cr grain has a diameter of 5 mm]*

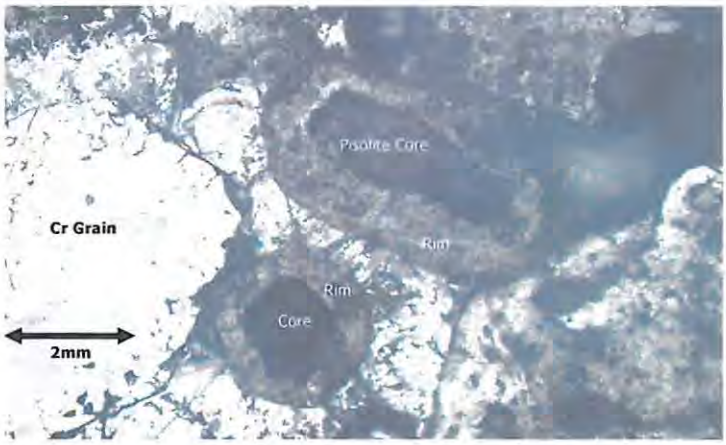


## 7.3 Method of Study

### 7.3.1 Electron Microprobe

The mineral chemistry of chromite suites obtained from the three different types of chromite-rich soil of the Great Dyke, which were described in previous chapters, were determined using the electron microprobe. A total 19 polished sections were examined at selected points on different grains. All the analyses were carried out in the Department of Geology, Rhodes University, South Africa. A Jeol Superprobe 733 instrument was used for all the analyses. The Joel Superprobe 733 settings used are appended to this report (Ref Appendix 3).

### 7.3.2 The Determination of Ferrous and Ferric iron from Microprobe Data

Microprobe analyses determine iron as total oxide $FeO_t$ and in order to estimate ferrous and ferric proportions of iron, the Droop (1987) method for the calculation of $Fe^{3+}$ was used. Prior to computation of the data collected from microprobe analyses results, the data were appraised in

terms of oxide content and all readings with total oxide less than 98% or grater than 102 % were discarded as unsuitable. The computation of accepted oxide readings was done using Barnes and Roeder's version of spinel stoichiometry calculation template (Barnes and Roeder, 2001). The determination involves calculation of cationic proportions from the reported oxides weight percentages normalized to 32 oxygens. In ferric iron determination and when the resultant cation total (S) was found to be greater than the correct (stoichiometric) cation total (T) then $Fe^{3+}$ was estimated by the following equation:

$$Fe^{3+} = 2X(1-T/S)$$

*Where X equals 32, the correct number of oxygens and T, for spinels equals 24.*

If S< T, then all iron is ascribed to $Fe^{2+}$, otherwise negative $Fe^{3+}$ values will be obtained. To check that the calculated $Fe^{3+}$ <$FeO_t$, the formula is normalized to T cations and if $Fe^{3+}$< $FeO_t$ then all iron is set as $Fe^{3+}$ in order to avoid negative calculation of $Fe^{2+}$. To determine the proportions, the formula is then written normalized to T cations, with $Fe^{2+}$ as $FeO_t$ minus calculated $Fe^{3+}$.

## 7.4 Chromite Chemical Compositions

The usefulness of chromite chemical composition in geochemistry lies in its application as an indicator of crystallisation conditions and early magmatic evolution of mafic and ultramafic bodies from various magmas. This emanates from the fact that chromite is one of the first minerals to crystallize from these magmas and that it is very stable under a wide range of geological conditions (Eales and Reynolds, 1983; Roeder, 1994). Chromite crystallizes into spinel structures, which like magnetite ($FeFe_2O_4$) and spinel ($MgAl_2O_4$) can be expressed as a complete solid solution of the oxides of chromium, aluminium, magnesium, ferrous iron, ferric iron and titanium (Roeder, 1994). The spinel-group includes oxide minerals, whose structure consists of 32 oxygen anions and 24 cations, all arranged in a close-packed cubic framework. Eight of the cations occupy the tetrahedral sites (X-sites) and the remaining 16 cations occupy octahedral sites (Y-Sites) giving the general spinel formula:

$$XY_2O_4$$

This generalized formula of spinels, also expressed as $(Mg,Fe^{2+})(Al,Cr,Fe^{3+})_2O_4$, and "its deceptive simplicity give little hint of the complex array of parameters that appear to govern compositional variations within the group" (Eales and Marsh,1983). The chromite series consists of a solid solution series with end members being, chromite ($Fe^{2+}Cr_2O_4$) and magnesiochromite ($Mg\ Cr_2O_4$). Pure end members are, however, rare and unaltered. Great Dyke chromites are ferroan magnesiochromites, with the formula:

$$(Mg,Fe^{2+})Cr_2O_4$$

A number of minor elements can substitute for the dominant cations, and these include Al, Ti, $Fe^{3+}$, Ni, Mn and Zn. There is notable replacement of Cr by Al and to a lesser extent $Cr^+$ by $Fe^{3+}$ in the

Great Dyke altered chromite. Apart from the variations due to minor elements compositional levels, the group exhibits extreme variation in the $Fe^{2+}/(Mg+Fe)$ or Fe-number, Cr/(Cr+Al) or Cr-number. The Cr- and Fe- numbers are based on two common projections of the spinel prism together with the Cr-Al-$Fe^{3+}$ triangular plot representing projection onto the end face of the prism. In addition plots of the commonly occurring minor constituent of chromite, $TiO_2$ content against $Fe^{3+}/(Fe^{3+}+Al+Cr)$ are sometimes used (Barnes and Roeder, 2001).

Solid solution among other spinel-group minerals is also extensive and has sometimes led to confusion in the naming of these minerals particularly with respect to the term spinel, which is sometimes used to include all the spinel-group minerals as well for the $MgAl_2O_4$-rich end member. For this reason and for a clearer understanding of the controls on eluvial chromite composition and the interpretation of eluvial chromite compositional data and the interaction of complex primary and secondary controls on chromite composition, a review of these factors is outlined below (Liang and Elthon, 1990).

### 7.4.1 Primary Controls on Chromite Composition

### 7.4.2 Magma or Host-rock Composition

Chromite occurrence in the mafic and ultramafic rocks of the Great Dyke is almost always associated with olivine, either as inclusions or interstitial aggregates or as chromite disseminations or layers of massive chromite (Wilson 1982). The small size of early chromite crystals and the relatively small amount of chromite enclosed in olivine crystals is largely due to lower solubility of chromium in basaltic magma (Roeder, 1994). The solubility of chromium as well as iron is very sensitive to the oxygen fugacity (Roeder and Hill, 1991). The $Fe^{2+}$ and $Cr^{2+}$ states tend to be more soluble than the $Fe^{3+}$ and $Cr^{3+}$ states.

### 7.4.3 Degree of Fractionation in Primary Layered Sources such as the Great Dyke

According to Cameron (1978) with increasing fractionation, the $Y_{Al}$ and the $Y_{Fe}$ ratios of chromite in chromitites increase whereas the $Y_{Cr}$ ratio decreases. This decrease in $Y_{Cr}$ ratio is as a result of gradual decrease of $Cr^{3+}$ content in the melt with continued spinel crystallisation. Ti, which has a significantly lower distribution coefficient than Cr, tends to become enriched in the melt relative to the solid phase during crystallisation. Since Ti is also virtually free from the influence of $fO_2$, increasing Ti content is taken to indicate increasing degree of magma differentiation. In layered intrusions such as the Great Dyke it has been noted that there is a corresponding relationship between chromite composition and chromite concentration in the rock (Cameron, 1975). Another trend observed was that of increasing $X_{Mg}$ and $Y_{AL}$ with increasing chromite concentration

accompanied by decrease in $Y_{Cr}$ and $Y_{Fe}$ ratios. These trends are a result of differing solubilities of these elements within the crystallizing portion of the melt. Thus a small grain crystallizing from a limited reservoir of liquid would have a higher Cr content than a larger grain from the same volume of liquid, due to low solubility of chromium in the liquid (Hamlyn and Keays, 1979).

### 7.4.4 Role of Oxygen Fugacity in Chromite Chemistry

It has been demonstrated on basaltic melts that $Fe^{2+}/Fe^{3+}$ ratio of chromite tends to be proportional although lower than that of coexisting melt (Roeder and Reynolds, 1991). It has therefore been concluded that increasing $fO_2$ results in increasing $Fe^{2+}/(Fe^{2+}+Fe^{3+})$ ratios of crystallizing spinels. Similarly $X_{Mg}$ ratio of co-precipitating silicates, under isothermal conditions, rises with increasing $fO_2$ (Hamlyn and Keays, 1979; Wilson, 1982; Hulbert and von Gruenewaldt, 1985). The $X_{Mg}$ ratio however, has been noted to decrease with decreasing temperature and this has been attributed to depletion of Mg in the melt as a result of crystallization of Mg-rich silicates. Similarly, with decreasing temperature and constant $fO_2$, both the $Cr_2O_3$ content and the $Cr/(Fe^{2+}+Fe^{3+})$ ratio decrease (Hill and Roeder, 1974; Murch and Campbell, 1986).

### 7.4.5 Crystallization of Co-existing Phases

Melt compositional changes resulting from crystallization of early silicate phases, mainly olivine, pyroxene and plagioclase, are the most significant factors affecting chromite composition at liquidus temperatures. Depletion of olivine in the melt will result in an increase in $X_{Fe}$ of chromite and the residual melt, but will have little effect on the Cr/(Cr+Al) ratios. However the Cr/(Cr+Al) ratio is largely affected by the presence of orthopyroxene. Orthopyroxene can accommodate larger quantities of Al into its lattice than olivine, and therefore chromite crystallizing in the presence of orthopyroxene will have a higher Cr/(Cr+Al) ratio than that with olivine. Resorption or crystallization of plagioclase results in significant variation in $Al_2O_3$ content of the melt, which in turn has a major effect on the Cr/(Cr+Al) ratio of chromite (Roeder and Reynolds, 1991).
The crystallization of clinopyroxene is believed to be the main control on limiting chromite crystallisation during early stages of magmatic evolution leading to decreased Cr/(Cr+Al) ratios in chromite as a result of the effect of a higher Cr/Al ratio in clinopyroxene than the coexisting melt (Irvine, 1967;Eales et al., 1980).

### 7.4.6 Effects of Pressure on Chromites

Published experimental work suggests that changes in pressure have negligible effect on solubility of Cr in basaltic melts or on Cr/(Cr+Al) ratio of coexisting chromite. Minor changes in Cr/(Cr+Al) ratios in chromite with changing pressure are a result of the effect of pressure on liquidus

temperature and hence decreasing temperatures tend to lead to minor decreases in Cr/(Cr+Al) ratios.

### 7.4.7 Post-cumulus Alteration of Chromites

Chromites interstitial to silicates and those wholly enclosed in silicates have been noted to "continue to equilibrate at sub-solidus temperature with interstitial melt that may be present, and with coexisting silicate phases" (Rollinson, 1995). Thus the primary chromite chemistry is typically masked by sub-solidus reaction with associated silicates, and re-equilibration amongst adjacent chromite grains, due to the high cation diffusivity of chromite relative to silicates. On the contrary, chromite compositions from chromitite layers tend to represent liquidus compositions due to the lack of significant alteration by sub-solidus processes unlike chromites from silicate-rich environments. This difference is largely attributed to the large mass/surface area ratio of seam chromite relative to silicate phases (Rollinson, 1995).

### 7.4.8 Sub-solidus Reaction of Chromites with Co-existing Silicates

Major alterations in chromite composition are principally a result of sub-solidus re-equilibration, which are typically restricted to the re-distribution of magnesium and ferrous iron between chromite and the host silicates. The extent of these alterations is influenced by the rapidity of divalent cation diffusion relative to the trivalent cations. It has been noted that trivalent cations are therefore more likely to preserve the original cation ratios of the parental liquid than divalent cation ratios. Sub-solidus re-equilibration between olivine and chromite, where olivine shows an appreciable increase in Mg near the olivine-chromite boundary, has been observed in a number of layered intrusions, including the Great Dyke (Wilson and Chaumba, 1997; Wilson, 1982). The study by Wilson (1982) showed that the Mg content of olivine increases systematically, from a distance of approximately 60 microns outward to the chromite grain boundary (Fig.7.2). Wilson (1982) also observed similar zoning at orthopyroxene-chromite grain boundaries, which was accompanied by lower rates of Mg and Fe exchange than that between chromite and olivine. Rates of reaction during sub-solidus re-equilibration, are thus essentially controlled by diffusion rates, and are not particularly temperature-dependant (O'Neill et al., 1995). Chromites lack compositional zoning, a feature of faster diffusion coefficients of chromite. Chromite has diffusion coefficients 60-100 times faster than olivine (Scowen et al., 1991; Barnes, 1986).

**Fig.7.2** Compositional Profiles of Olivine at Contact with Enclosed Chromite Grains

*[Individual analytical points (error bars indicated) are shown for the three axial directions and curves represent the modeled diffusion profiles. The star indicates that suitable crystals for analysis in the b direction could not be found for SAT 2(sample SAT 2 was from the Main Satellite.) Sample No 19 was from CU8; Nos 62 was from CU2 (after Wilson, 1982)]*

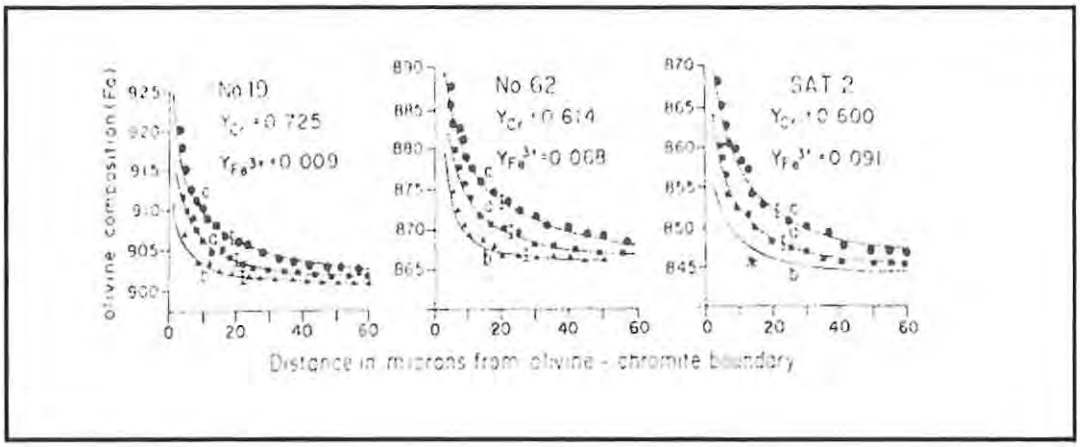


7.4.9 Sub-solidus Reaction of Chromite with Liquid

In distinguishing between chromites in chromitites and disseminated chromite, Cameron (1978) showed that whilst the former chromites are relatively homogeneous, the latter showed extensive variation. This difference of chromite compositions and rock textures in these environments is evidence of the extremely localized conditions within the intercumulus liquid. The resultant complexities of the different chromites can obscure compositional variation related to the cumulus stage. Such reactions are prone to and dependent upon the availability of trapped liquid, and will therefore be highest in strongly orthocumulate rocks. In these assemblages, reaction will continue over a wide range of declining temperatures (Henderson, 1975).

It was observed by Roeder and Campbell (1985) that adcumulates contain chromites with a narrow compositional range and high Cr and Al values, whilst those chromites within orthocumulates are characterised by a wide range of compositions. They further noted that total iron; Ti and $Fe^{3+}/Fe^{2+}$ ratios tend to increase from adcumulate to orthocumulate environments. On the Great Dyke, where development of adcumulates is extensive, Wilson (1982) noted the insignificance of the reaction of chromites with intercumulus liquid; although this was present in some of the more orthocumulate harzburgites, where the chromite compositions are highly variable, as a result of the reaction with liquid. Wilson (1982) established that no compositional trend or grain size dependence exists for chromites enclosed by post cumulus silicates and attributes this lack of

correlation to the reaction of the chromites with intercumulus liquids whose environments vary locally.

The relatively high Ti and Fe values of chromites noted in eluvial chromites and whose provenance is associated with grains enclosed by olivine and had been in contact with intercumulus material, indicate that element exchange between chromite and intercumulus liquid occurred. In cumulates of the Jimberlana Intrusion, Roeder and Campbell (1985) observe that $X_{Mg}$ ratios, and Al and Cr values, were higher in chromite enclosed in orthopyroxene as opposed to those enclosed in olivine. Orthopyroxene therefore appears to inhibit the reaction of chromite with intercumulus liquid. In the exceptional situation where chromites apparently enclosed in orthopyroxene exhibit low Al and Cr values, evidence has been found that proved that the chromite was able to maintain direct contact with the liquid.

It has been proposed that the most likely mechanism for Fe-Mg re-equilibration between chromite enclosed in olivine and the residual melt is via lattice inter-diffusion, as opposed to dislocation-based diffusion where contact is achieved through micro-fractures and discontinuities. The exchange of elements such as Cr, Ti, Al, and $Fe^{3+}$ between chrome and the melt, through olivine, is however, more problematic. Roeder and Campbell (1985) suggest that the low solubility for these elements in the olivine structure makes diffusion an unlikely mechanism, and that the chromite may have been able to maintain direct contact with the melt, through fractures in the olivine developed as a result of decreasing temperature.

### 7.4.10 Post- Cumulus Overgrowth in Chromites

Great Dyke chromitites are characterized by very high $X_{Mg}$ ratios and $Cr_2O_3$ values typical of layered intrusions. Hulbert and von Gruenewaldt (1985) considered these high $X_{Mg}$ ratios, too high to be a product of primary factors alone, and they suggested that this enrichment could be a result of post-cumulus overgrowth by sintering. According to their deduction, the *in situ* crystallization of abundant chromite in a semi-stagnant environment will lead to an increase in the $X_{Mg}$ ratios of the residual melt. Interstitial liquid within the chromitite would therefore be enriched in Mg, as would the intercumulus liquid of the underlying silicate cumulate in order to maintain equilibrium. Re-equilibration of the silicate phases with this interstitial liquid would result in relatively high $X_{Mg}$ ratios (Hulbert and von Gruenewaldt, 1985). The Mg-enriched liquid immediately above the cumulate pile would replenish the loss of Mg from the chromitite to the underlying material, allowing Mg-enrichment to be maintained in the intercumulus liquid for some time. Sintering in the presence of Mg-rich interstitial liquid could therefore persist until the overlying Mg-rich liquid was destroyed by convective overturn or double-diffusive convection.

## 7.5 Composition of Eluvial Chromite Grains

The chromite composition of the different eluvial chromites evaluated vary slightly in terms of $Cr_2O_3$ content and other major and minor constituents (See Appendix 4 – Electron Microprobe Analyses: Results of Individual Eluvial Chromite Grain Analysis). From the electron microprobe analyses of eluvial chromites, major oxide constituent are chromium oxide ($Cr_2O_3$), aluminum oxide ($Al_2O_3$), iron II and iron III oxides (FeO; $Fe_2O_3$) and magnesium oxide (MgO). Important minor constituents analyzed include titanium oxides ($TiO_2$) manganese oxide, (MnO) and nickel oxide (NiO). These results were obtained from microprobe analysis done on chromite grains free of silicates.

Chromium oxide, the dominant constituent in the chromite grains, range in composition from about 47 percent to 60 percent $Cr_2O_3$ (refer to individual electron microprobe analyses in Appendix 4). Analyses show Middle Dyke samples to have the lowest local average chromium oxide content of 52.32 percent $Cr_2O_3$, whilst samples from other regions had considerably higher local averages. South Dyke samples contain average chromium oxide of about 57.63 percent $Cr_2O_3$ content. The Jester (North Dyke A) and Caesar (North Dyke B) had average chrome content of 58.50 and 57.20%$Cr_2O_3$ respectively.

Using Droops (1978) estimation methodology for FeO versus $Fe_2O_3$, determinations show the dominant iron oxide to be FeO. South Dyke samples had the least $Fe_2O_3$ at 0.24 percent. The Middle Dyke has an $Fe_2O_3$ content of 1.08 percent, Jester 0.47 percent and Caesar 0.60 percent. FeO content for all the samples is comparable with South Dyke which reported an average of 20.82 percent FeO, whilst Middle Dyke had 19.59 percent, Jester had 18.14 percent and finally Caesar had 18.26 percent.

Aluminum oxide renders refractory properties to the chromites and is an important constituent in chromite ores. Middle Dyke samples have the highest average percent $Al_2O_3$ content of 16.14, South Dyke samples have an average $Al_2O_3$ content of 12.57 percent. Caesar has an average $Al_2O_3$ content of 13.52 percent and Jester an $Al_2O_3$ content of 12.29 percent.

Apart from South Dyke's average magnesium oxide content of 7.42 percent , the Middle Dyke and North Dyke samples were comparable at 9.43 percent Middle Dyke, 9.13 percent Jester and 9.60% for Caesar. Minor constituent abundances are similar throughout the entire sampled regions of the Great Dyke and apart from titanium oxide ($TiO_2$) which was greatest at Middle Dyke with 0.40 percent, South Dyke and Caesar had 0.34 percent and Jester was lowest at 0.30 percent. Manganese oxide (MnO) average content for all the sampled areas was 0.28 percent and nickel oxide (NiO) content averaged 8.07 percent in all sampled areas.

The chrome number or compositional parameter Cr/(Cr+AL) indicate that eluvial chromites from the Great Dyke are similar irrespective of depositional environment (Fig. 7.3). Apart from minor variation which may be attributed to limited local changes, there is no significant difference in the chromites from these different Great Dyke regions.

**Fig. 7.3** Comparison of the Chromium Number of the Different Eluvials

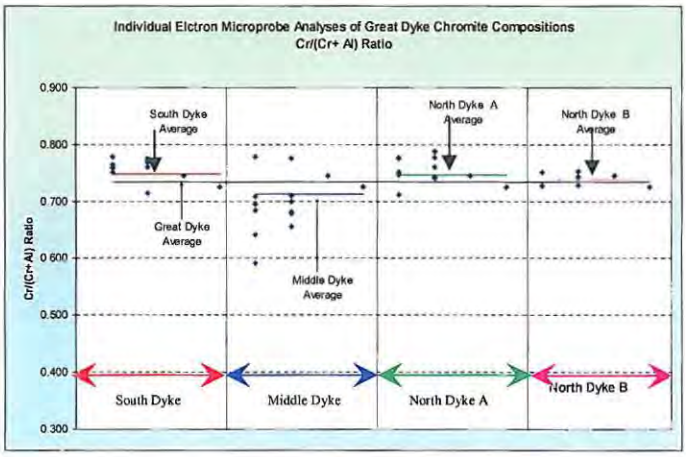


The compositional parameter $Fe^{2+}/(Fe^{2+}+Mg)$ for the Eluvial Chromites ranges from 0,521 to 0,656 and could be considered similar throughout the different Great Dykes depositional environments. However, average analyses show the parameter to be higher for South Dyke at 0,613 and lower for Caesar at 0,523 (Fig. 7.4). These values support earlier observations by (Wilson and Prendergast, 1989) who observed the same parameter to range from 0,320 at the basal cyclic units of the Dyke to 0,646 in the upper units. The observed values imply the eluvial chrome source to have been derived from the upper cyclic units of the Great Dyke.

**Fig. 7.4** Comparison of Fe Numbers from Different Eluvials

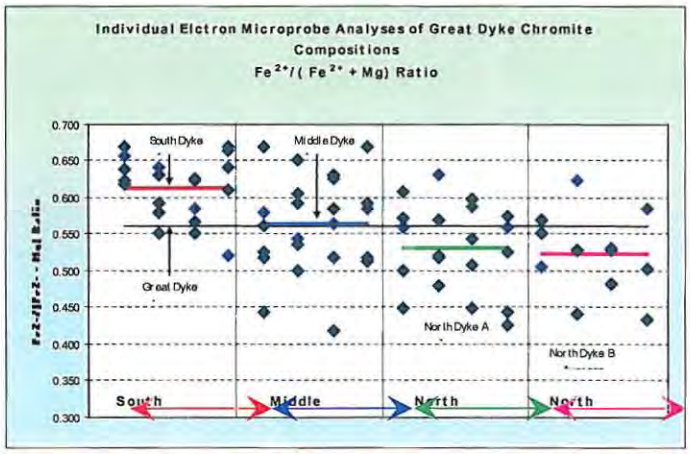

The magnesium ratio Mg ($Mg+Fe^{2+}$) for the eluvial chromites have an inverse relationship with the parameter $Fe^{2+}/(Fe^{2+}+Mg)$ and hence it is higher in the North Dyke and lowest in the South Dyke (Fig. 7.5). The North Dyke eluvials are derived entirely from serpentinites from close to the base of the Dunite Succession whereas the Middle Dyke and South Dyke eluvials are derived from serpentinites of the Bronzitite Succession. The plots of Ti/Cr (Fig. 7.6) indicate lower value of 0,006 for South Dyke chromites and Caesar samples.

**Fig. 7.5** Comparison of Magnesium Ratio

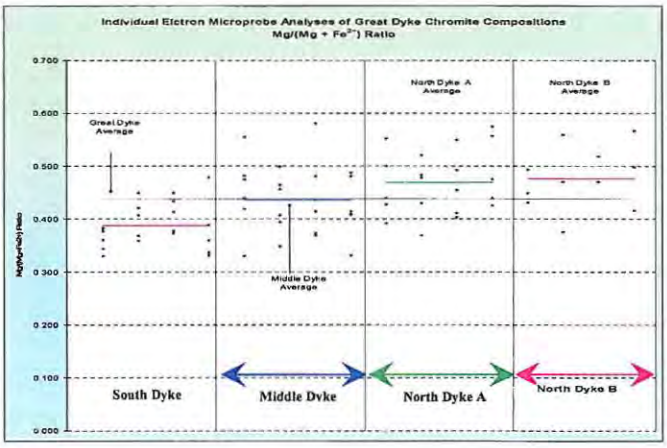


**Fig. 7.6** Ti / Ratios From different Eluvial Chromites

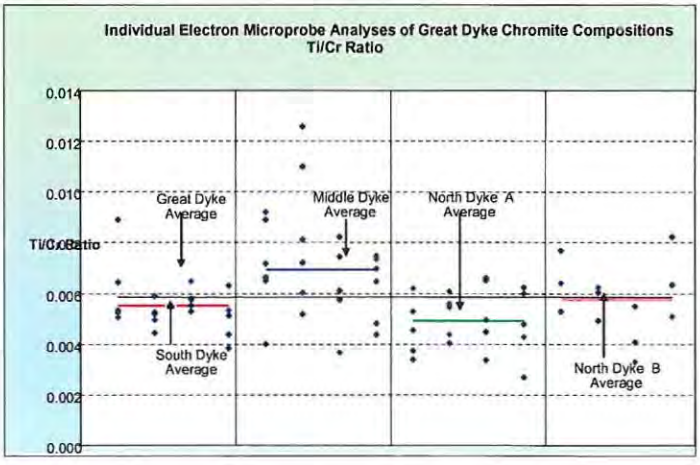

## 7.6 Conclusion, Geochemistry of Eluvial Chromite

Whilst eluvial chromites are predominantly derived from olivines or dunites or their derivatives such as serpentine, the provenance of eluvials is not necessarily limited to these lithologies. It can be demonstrated clearly from a geochemistry point of view that some of the chromites are derived from the Great Dyke chromitites as well as from such other lithologies as the pyroxenites. The different eluvial chromites suites can be correlated to the different Great Dyke regions as well as exhibiting stratigraphic relations with the different successions of the Great Dyke. There are no significant differences between the chromites from the different eluvial suites sampled in terms of major elements composition and hence eluvial product is likely to be similar in terms of chromite and lattice iron content. There are consistent co-relationships between $Fe^{2+}$, Cr, Ti and marked inverse relationship between Al, Cr and $Fe^{2+}$.

## 7.7 Pisolites in Heavy Mineral Separates

Pisolites are concretions that are thought to develop from accretionary growth around separate nuclei in a favorable environment prior to deposition. Pisolites are associated with laterites, that typically cap erosion surfaces (Jones, 1965). Pisolites are also associated with calcium carbonate deposits and usually consist of aggregated globular concretions about the size of a pea within these deposits. In eluvial chromite deposits pisolites range in size from those, less than 1000 μm and enclose chromite or silica grains, to larger concretions that enclose cobbles of serpentinite rock fragments.

## 7.8 Composition of Pisolites

The soils of the Great Dyke like those derived from all ultramafic rocks are exceptionally rich in Fe and in other transitional metals especially Mn, Ni, Cr and Co (Quantin et al., 2001). Eluvial soils are host to Fe- and Mn-oxides, which are major sinks for metals, and play a dominant role in controlling the concentration of these metals. Reduction processes of Fe- and Mn-oxides may increase metal release, possibly with the aid of Fe- and Mn-reducing bacteria. Although goethite is the main constituent of ultramafic soils, minor phases such as Mn- oxides that are more reducible than Fe- oxides could control the trace element availability and their mobility in the soil environment.

By far the most dominant constituent of these pisolites is goethite ($\alpha$FeOOH), a common ferric oxide mineral and after hematite. Goethite typically forms under ordinary temperatures and pressures as a weathering product of ferrous minerals, especially siderite, magnetite, glauconite

and pyrite. Goethite is thus a common mineral of soils and is naturally rarely stoichiometric and usually contains a number of substitutional cations isovalent or heterovalent to $Fe^{3+}$. Owing to the widespread occurrence and abundance of goethite in the environment, the geochemical uptake of trace elements in goethite is important in terms of mass balance and control of the concentration and migration of metals in natural waters, and availability of nutrients and mobility of toxic elements to living organisms. Al can substitute for Fe in goethite with the resulting aluminous goethite having great influence on pedogenic processes (Manceau et al., 2000).

Apart from Fe-Al common occurrences in the pisolites, Mn also occurs as an important mineral constituent. The Mn- oxides known to occur naturally in soils at room temperature and pH of 4.4 (pH 5.2 for hausmannite) include hausmannite, manganite, romanechite, cryptomelane, lithiophorite and pyrolusite. The Mn- oxides that exhibit the greatest and longest-lasting oxidizing ability are the Mn- oxides containing $Mn^{3+}$ and in particular those containing both $Mn^{3+}$ and $Mn^{2+}$. It is also accepted that the combined presence of reducible Mn ion (e.g. $Mn^{3+}$) and a highly soluble $Mn^{2+}$ion facilitates oxidation reactions as a result of fresh $Mn^{3+}$ surface being exposed during the dissolution reaction (Weaver and Hochella Jr., 2003)
Closely associated with manganese is cobalt whose strong enrichment in soils is a result of fixation of cobalt due to oxidation of adsorbed $Co^{2+}$ ion by $Mn^{4+}$ and replacement of the displaced manganese by $Co^{3+}$ ions for $Mn^{4+}$ in the host crystal lattice (Burns, 1975).

Laterite profiles on serpentinite developing during tropical weathering have been shown to alter from serpentinite to montmorillonite, aluminous goethite, and silica. Chromitiferous chloride, a stable component, becomes concentrated in the weathering profile whilst both kaolin and bauxite groups are absent. Alumina occurs chiefly in goethite solid solution. Typically in the upper levels of the profile serpentinite and montmorillonite disappear completely whilst the amount of alumina substitution in goethite increases. The $Fe_2O_3$ and $Al_2O_3$ contents fall with increasing depth whereas $SiO_2$ and MgO increase. As trace elements concentrate as a result of pedological processes, the Ni content of the soils also increases. Observations suggest that Ni is associated with goethite, and possibly is incorporated in the lattice of this mineral (Zeissink, 1969). Nickel together with Co, Mn, Cr and PGE are dominantly hosted by secondary Fe oxides in the regolith, but above the Mg-discontinuity, Ni and Co are locally enriched by co-precipitation with Mn-oxides (Brand and Butt, 2001).
The occurrence and association of nickel with large mafic-ultramafic massifs in climatic regions alternating and contrasting seasons is not unique to the Great Dyke. In Brazil, New Caledonia, Indonesia, Cuba, Canada, former USSR, and in Australia these deposits constitute major nickel resources (De Young Jr. et al., 1985). These deposits like the eluvial deposits of the Great Dyke are a result of weathering profiles developing over fresh serpentinites which progressively, from bottom to top, become altered rock, coarse saprolite, ferruginous saprolite and then the lateritic

overburden. The serpentinites together with neo-formed minerals such as smectites constitute silicate nickel usually confined to un-weathered and partly weathered horizons and are characteristic of the drier ultramafic regions. Where the climate is predominantly humid such as the North Dyke region of the Great Dyke, a ferruginous upper horizon consists of nickel-rich iron oxides-hydroxides where goethite and garnierite are the main Ni-bearing minerals (Barros de Oliveira et al, 1992).

The analyses of the eluvial chromite associated pisolites indicate grades generally above 1.00 %Ni. Such grades warrant further investigation of these nickeliferous laterites of the Great Dyke.

## CHAPTER 8

# 8.0 Summary, Conclusions and Recommendations

## 8.1 General Features of Eluvial Chromite Deposits

The soils of the Great Dyke are derived from mafic and ultramafic rocks. These soils generally exhibit a complex regolith consisting of predominantly transported profiles with isolated occurrences of residual and proximal profiles. The soils are derived mainly from weathering serpentinites. They consist of degraded serpentine, neo-formed hydrated Mg-silicates, carbonates, silica and Fe-oxides. The chromites are concentrated in the soil, through a combination of weathering processes, eluviation and *in situ* pedological processes. Through leaching effect of ground water movements, the soil profile matures into a series of horizons whose characteristics and chemical composition vary with depth. The process results in a Mg-saprolite that overlies an Fe-saprolite. The Fe-saprolite composition is dominated by Fe-oxides and silica. This zone is most important for relatively higher-level chromite concentrations. The eluvial chromite occurs as free grains that can be concentrated by mechanical processes, yielding concentrates of chromite grains that have chromium oxide content values greater than 50 percent. The chromites in the soils are usually fine-grained and are predominantly within the grain-size range of between 125μm to 500μm. This fine-grained nature of these chromites is attributed to their provenance, thought to be from interstitial matrices and from olivine crystal inclusions. The process of weathering and transportation induced attrition play a significant role in grain-size reduction. Concentrating alongside the chromite are manganese oxides and nickel oxides. These oxides are normally associated with pisolites and lateritic duricrast. The pisolites could be developed into important sources of nickel and manganese.

## 8.2 Economic Potential of Great Dyke Eluvial Chromite Deposits

The Great Dyke of Zimbabwe is endowed with extensive eluvial chromite resources estimated at about 12 million tonnes of product at 48% $Cr_2O_3$ and 1.8 Cr: Fe. At 10 % mass recovery, 2.8 ore specific consumption and 80 % chromium unit recovery, this Resource when processed through concentration and subsequent smelting into HCFeCr, could yield about 4 million tonnes of ferrochrome. The eluvial soils of the Great Dyke can be treated with the aid of a Continuous Variable Discharge (CVD) unit to produce chromite concentrates. The CVD treats fresh feed and a circulating load of tails from the spirals after being classified by a hydrocyclone. The gravity circuit consists of a CVD concentrator as the primary unit with a secondary spirals circuit. This combination can achieve recoveries well in excess of 90% chromite. The product grade of 48% $Cr_2O_3$ at a mass recovery of 10 % was surpassed during a Zimbabwe Alloys test work conducted by Peacocke, Simpson and Associates (2000).

## 8.2 Exploration Considerations

The potential economic value of the Great Dyke eluvial chromite deposits dictates that further expenditure be directed at resource evaluation and modeling on a more detailed scale. The evaluation presented in this thesis reveals the complexity of the eluvial as a resource and the variation in quantity and quality of the various eluvial sources. The variability of the eluvial chromite resource, with depth and laterally, dictates that additional work is done at a more detailed scale.

It is recommended that exploration be directed to similar ultramafic deposits in the country for possible occurrence of mineral enrichment in soils. PGEs, usually associated with ultramafic lithologies and chromites, and although found to be in trace amounts or absent in the sampled Great Dyke soils, need to be investigated further and in more detail. It is possible that soil derived from the mafic units of the Great Dyke would contain economic concentrations of PGEs. Pisolites derived from laterites of the Great Dyke contain significant concentration of nickel and manganese, these warrant further investigation.

## 8.4 Conclusions

The eluvial resource of the Great Dyke is a sufficiently large resource and could constitute a self-sustaining industry. Eluvials could be developed into a primary source of chromite for the supply of smelter ore feed and for the supply of chrome sands required by the foundry industry (Prendergast, 1998; Bartholomew, 1990). Together with the briquetting and sintering technology, eluvial concentrates can easily be a cheaper substitute to expensive lumpy ores feed to the smelters. The eluvial chromites are a cleaner product with low silica and high chromium content and could be utilized as chrome sands in foundries (Slatter, 1981).

## 8.5 Recommendations

In order to fully exploit the vast eluvial resource of the Great Dyke it is recommended that further investigation on associated mineral enrichment be done (Naldrett and Lehmann, 1988; Naldrett and Wilson, 1991).

It is recommended that other potential uses of eluvial product concentrate be evaluated and tested to enable expanded use and application. Such investigation could include briquetting and sintering properties of eluvial as well as further use in chemical industry, foundry and building industry.

**References**


Ahrens, L.H., 1965. Distribution of the Elements in our Planet, New York.

Ahrens,T.J.(Ed.), 1995. AGU Reference Shelf 2: Mineral Physics and Crystallography- A Handbook of Physical Constants, Washington D.C.

Appel, C.C., Appel, P.W.U. and Rollinson, H.R., 2002. Complex Chromite Textures Reveal the History of an Early Archean Layered Ultramafic Body in West Greenland. Mineral. Mag. 66(6), p 1029-1041.

Armstrong, R., and Wilson, A.H., 2000. A SHRIMP U-Pb Study of Zircons from Layered Sequence of the Great Dyke, Zimbabwe, and a Granitoid Anatectic Dyke. Earth and Planetary Science Letters, 180, p 1-12.

Barnes S.J., 1986. The Distribution of Chromium among Orthopyroxene, Spinel and Silicate Liquid at Atmospheric Pressure. Geochim.Cosmochim Acta, 50, p 1889-1909.

Barnes S.J., and Roeder P.L., 2001. The Range of Spinel Compositions in Terrestrial Mafic and Ultramafic Rocks. Jour. of Petrol.,. 42(12), p 2279-2302.

Barros de Oliveira, S.M., Trescases, J.J., Jose Melfi, A., 1992.Lateritic Nickel Deposits of Brazil. Mineral. Deposita Vol. 27, p 137-146.

Bates, R.L. and Jackson, J.A., 1980. Glossary of Geology. 2nd Edition. Falls Church, Virginia, American Geological Institute, p 751.

Batholomew, D.S., 1990. Base Metal and Industrial Mineral Deposits of Zimbabwe. Zim. Geol. Surv, Mineral Resource Series No. 22, p 33-36.

Bichan, H.R., 1969. Origin of Chromite Seams in the Hartley Complex of the Great Dyke. In Magmatic Ore Deposits, Wilson H.D.B. (Ed)., Econ. Geolo. Monogr., 4, p 95 –113.

Bichan, H.R., 1970. The Evolution and Structural Setting of the Great Dyke, Rhodesia.In: Clifford, T.N., Gass, I.G. (Eds), African Magmatism and Tectonics. Edinburgh: Oliver and Boyd, p 51-71.

Birkland, P.W., 1984. Soils and Geomorphology, Oxford University Press, New York, p 372.

Bond, G., 1952. The Karoo System in Southern Rhodesia. Proceedings of the Gondwana Symposium. XIX International Geol. Congress, Algiers, p 209-223.

Bond, G., 1962. Past Climates of Central Africa. Inaugural Lecture Given at the University College of Rhodesia and Nyasaland, Oxford University Press, p 34.

Bond, G., 1967. A Review of Karoo Sedimentation and Lithology in Southern Rhodesia. I.U.G.S. Proceedings 1st Symposium on Gondwana Stratigraphy, p 173-195, Angentina.

Bradshaw, P.M.D., and Thomson, I, 1979. The Application of Soil Sampling to Geochemical Exploration in Non-glaciated Regions of the World. In: Geological Survey of Canada Economic Geol. Report 31, p 327 – 338.

Brand, N.W., Butt, C.R.M, and Elias, M., 1998. Nickel Laterites: Classification and Features: AGSO, Journal of Australian Geology and Geophysics, 17, p 81-88.

Brand, N.W., and Butt, C.R.M., 2001. Weathering, Element Distribution and Geochemical Dispersion at Mt Kieth Western Australia. Geochemistry; Exploration and Environment Analysis. Vol. 1, Issue 4, p 391-467.

Brown, R.T., 1998. Hartley Platinum Mine-Geology and Grade Control. In: The Great Dyke of Zimbabwe. Guidebook for the Pre-Symposium Excursion. 8th International Platinum Symposium, June 1998, p16-18.

Burns, R.G., 1975. The Uptake of Cobalt into Ferromanganese Nodules, Soils and Synthetic Manganese (IV) Oxides. Geochimica et Cosmoschimica Acta, Vol. 40, p 95-102.

Butt, C.R.M., 1982. Weathering and the Australian Landscape: History and characteristics of weathering in Australia. In Geochemical Exploration in deeply weathered Terrain e.d. Binith, RECSIRO Inst. Energy Earth Resources 9-12

Cameron, E. N. 1978. The Lower Zone of the Eastern Bushveld Complex, in the Olifants River Trough. J. Petrol., 19, p 437-62.

Cameron, E. N., 1975. Postcumulus and Subsolidus Equilibriation of Chromite and Co-existing Silicates in the Eastern Bushveld Complex. Geochim. Cosmochim. Acta, 39, p 1021-33.

Coghill, B. M. and Wilson, A. H., 1993. Platinum-group minerals in the Selukwe Subchamber, Great Dyke, Zimbabwe: implications for PGE collection mechanisms and post-formational redistribution. Mineral. Mag., 57, p 613-633.

Cogley J.G., 1985. In Partridge, T.C. and Moud, R.R. (1987). Geomorphic Evolution of Southern Africa since Mesozoic. S. Afric J. Geol. 90(2), p 179-208.

Cooper, G.R., 1978. Greenhouse Experiments with Maize Grown in Ultramafic Soils. Technical Communication No. 165, Dept. of Agric. and Tech. Services, South Africa. Proceedings of 8th National Congress of the Soil Science Soc. of Southern Africa, p152-157.

Cotterill, P., 1981. Chromite in Zimbabwe. Chamber of Mines Journal, 23(3), p 45-58.

Cox, P.A., 1989. The Elements: Their Origin, Abundance and Distribution, Oxford.

Craig, J.R. and Vaughan, D.J., 1994. Ore Microscopy and Ore Petrology. 2nd Edition. John Whiley, New York.

CRU - International, 2002. Ferrochrome Market Services,. Ref No. "832/47, July 2002. CRU International Limited, London.

Cunat, P-J., 2004. Alloying Elements in Stainless Steel and Other Chromium–Containing Alloys, International Chromium Development Association (ICDA), and Paris.

Davies, R. D., Allsopp, H. L., Erlank, A.J., and Manton, W. I., 1970. St Isotope Studies on Various Layered Mafic Intrusions in Southern Africa. In: Visser, D. J. L. & Gruenewaldt, G. von (eds), Geol. Soc. S. Afr., Spec. Pub. No. 1, p 576-93.

Davis 1899. In Pritchard, J.M. 1986. Landform and Landscape in Africa. Edward Arnold Limited, London.

De Dapper, 1989. In Pritchard, J.M. 1986. Landform and Landscape in Africa. Edward Arnold Limited, London.

De Linde, J., 2002. The Position of South Africa in World Ferro – Alloy markets, Metal Bulletin, Southern African Ferro- Alloy Conference.

De Wit, J., 2002. Importance of Value in the Chrome Industry, Metal Bulletin, Southern African Ferro- Alloy Conference.

De Young Jr, J.H., Sutphin, D.M., Werner, A.B.T., Foose, M.P, 1885. International Strategic Minerals Inventory- Summary Report- Nickel, U.S.G.S. Circ. 930-D, p 62.

Deer, W.A., Howie, R.A., and Zussman, J., 1992. An Introduction to Rock Forming Minerals. 2nd Edition. Longman Scientific and Technical, Essex, England.

Droop, G.T.T., 1987. A General Equation for Estimating Fe3+ Concentrations Ferromagnesian Silicates and Oxides from Microprobe Analyses, Using Stoichiometric Criteria. Mineralogical Magazine , 51, p 431-435.

Du Toit, A.L., 1933. Crustal Warping as a Factor in the Geographical Evolution of South Africa. S. Afr. Geogr. Jour., 16, p 3-20.

Eales, H.V., Reynolds, I.M.,and Gouws, D.A., 1980. The Spinel Group Minerals of the Central Karoo Thoilites Province: Geol. Soc. South Africa Trans., v83, p243-253

Eales, H.V. and Marsh, J.S., 1983. Al/Cr Ratio of Co-existing Pyroxenites and Spinels in Some Ultramafic Rocks. Chem. Geology, 38, p 57-74.

Eales, H.V. and Reynolds, I.M., 1983. Factors Influencing the Composition of Chromite and Magnetite in Some Southern African Rocks. Geol. Soc. South Africa Special Publication, 7, p 5-20.

Eckhardt, F.E.W., 1985. Solubilization, Transport and Deposition of Mineral Cations by Micro-organisms: Efficient Rock Weathering Agents. In Chemistry of Weathering [(ed) Drever, J.I.], Reidel, D, Publ. Co. p 161 – 173

Elias, M., 2002. Nickel Laterites Deposits- Geological overview, Resources and exploitation, in Cooke,D.,and Pontgratz,J.,(eds)., Giant Ore Deposits: Characteristics, Genesis and Exploration: CODES Special Publication 4, Hobart , University of Tasmania, p 205-220.

Eluvial Project, (2002), Zimbabwe Alloys Limited, Unpublished Internal Camp any Report Gweru

Fenandes ,T.R.C., 1982. Mineralogical Studies of Chromites in Zimbabwe, University of Zimbabwe, Institute of Mining Research, Report C269, p 33.

Fisk, M.R., and Bence, A.E., 1980. Experimental Crystalisation of Chrome Spinel in Famous Basalts 527. Earth Planet Science Letters, 48, p 111-112.

Folk, R.L., 1974. Pretrology of Sedimentary Rocks. Austin, Texas, Hemphill Publishing Company, p 182.

Gleeson, S.A., Herrington, R.J., Durango, J., Velasquez C.A. and Koll,G., 2004, The Mineralogy and Geochemistry of Cerro Matosa S.A. Nickel Laterite Deposit, Montelibano Colombia. Econ. Geol, 99, p 1197-1213.

Hamilton, J., 1977. Strontium Isotope and Trace Element Studies on the Great Dyke and Bushveld Mafic Phase and their Relation to Early Proterozoic Magma Genesis in Southern Africa. J. Petrol., 18, p 24-52.

Hamlyn, P.R., and Keays, R.R., 1979, Origin of Chromite Compositional Variation in the Panton Sill, Western Australia. Contrib. Mineral Petrol., 69, p 75 – 82.

Hamlyn, P.R., and Keays, R.R., 1979. Origin of Chromite Compositional Variation in Panto Sill, Western Australia. Contribution Mineral. Petrol., 69, p 75-82.

Harger, H.S, 1934. An Early Transvaal Geological Map by Carl Mauch, Trans. Geol. Society, South Africa, 37, p 1-4.

Henderson, P., 1975. Reaction Trends Shown by Chrome-Spinels of Rhum Layered Intrusion. Geochim.Cosmochim. Acta, 39, p 1035-1044.

Hess, H.H., 1950. Vertical Mineral Variation in the Great Dyke of Southern Rhodesia Trans. Geol. Soc. Afr., 53, p159-168.

Hill, R., and Roeder, P., 1974. The Crystallization of Spinel from Basaltic Liquid as a Function of Oxygen Fugacity: Jour. Geology, 82, p 709-729.

Hughes, C. J., 1970. Major Rhythmic Layering in Ultramafic Rocks of the Great Dyke of Rhodesia, with Particular Reference to the Sebakwe Area. Geol. Soc. S. Afr. Spec. Publ. 1, p 594-609.

Hulbert, L.J., and Von Gruenewaldt, G., 1985. Textural and Compositional features of Chromite in the Lower and Critical Zones of the Bushveld Complex South of Potgietersrus. Economic Geology, 80, p 872-895.

Ineson, P.R., 1989. Introduction to Practical Ore Microscopy. Longman Earth Science Series. Longman Scientific & Technical, England, UK.

Irvine, T. N., 1965. Chromian Spinel as a Petrogenetic Indicator, Part 1. Theory, Canadian Journal of Earth Sciences, 2(1965), p 649- 672.

Irvine, T. N., 1967. Chromian Spinel as a Petrogenetic Indicator, Part 2. Petrological Applications, Canadian Journal of Earth Sciences, 4(1967), p 71-103.

Irvine, T. N., 1975. Crystallisation Sequence in the Muskox Intrusion and other layered intrusions, II. Origin of Chromite Layers and Similar Deposits of other Magmatic Ores. Geochim.

Cosmochim. Acta, 39, p 991-1020. In Other Layered Intrusions: A New Interpretation. Geology, 5, p 273-7.

Irvine, T. N., 1977. Chromite Crystallisation on the Joint $Mg_2SiO_4$-$CaMgSi_2O_6$-$CaAl_2Si_2O_8$- $MgCr_2O4$-$SiO_2$. Carnegie Institution of Washington Year Book, 76, p 465-472.

Jones, D. L., Robertson, I. D. M., and MacFadden, P. L., 1975. A Palaeomagnetic Study of Precambrian Dyke Swarms Associated with the Great Dyke of Rhodesia. Trans. Geol. Soc. of S. Afr., 77, p 339-345.

Jones, H.A., 1965. Ferruginous Oolites and Pisolites. Journal of Sed. Research, Dec 1965. Vol.35, 4, p 838-845.

Keech, M.A., and Wark, J.M., 1961. A Preliminary Study of the Effects of Eluvial Chrome Mining on the Great Dyke with Reference to Water, Soil and Plant Relationships on Disturbed and Undisturbed Areas. Rhodesia Agric. Journal, 58, p 315-9.

Kimble, L.G., 1976. Mining Practice at African Chrome Mines Limited, Rhodesia, Presentations to the Rhodesian local Section of the Institute of Mining and Metallurgy and Geological Society Summer School.

King, L.C., 1949. In Lister, L.A., 1987. The Erosional Surfaces of Zimbabwe. Bulletin 90, Zimbabwe Geological Survey.

King L.C., and King, L.A., 1959. A reappraisal of the Natal Monocline. S. Afr. Geog. Jour., 41, p 15-30.

Köppen.W.P (1936) In Allaby, M, 2002.Encyclopedia of weathering and climate, NewYork. Facts on File Inc.

Larsen, L.M., and Pendersen, A.K., 2000. Processes in High-Mg, High-T Magmas: Evidence from Olivine, Chromite and Glass in Palaeogene Picrites from West Greenland. Jour. Petrology, 41(7), p 1071-1098.

Leblanc, M., 1980. Chromite Growth Dissolution and Deformation from a Morphological Viewpoint: SEM Investigations. Mineralium Deposita, 15, p 201-210.

Lehman, J. and Roux, J. 1986. Experimental and Theoretical Study of $(Fe^{2+}, Mg)(Al, Fe^{3+})_2O_4$ Spinels: Activity- Composition Relationships, Miscibility Gaps, Vacancy Contents. Geochim.cosmochim.Acta , 50, p 1765-1783.

Levinson, A.A., 1974. Introduction to Exploration Geochemistry Applied Publishing Ltd, Wilmette, Illinois, USA pp 924.

Levinson, A.A., 1980. Introduction to Exploration Geochemistry. 2nd Edition. Applied Publishing Ltd, Calgary.

Li,J.P.,O'Neill, H.St.C and Seifert,F,1995. Subsolidus Phase Relations in the System MgO-SiO2-Cr-O in Equilibrium with Metallic Cr, and their Significance for the Pretrochemistry of Chromium. Journal of Petrology, 36, p 107-132.

Liang, Y and Elthon, D, 1990. Evidence from Chromium Abundance in Mantle Rocks for Extraction of Picrite and Komitite Melts, Nature, 343, p 551-553.

Lightfoot B., 1927. Traverses along the Great Dyke of Southern Rhodesia. Southern Rhodesia Geol. Survey. Short Report, 21

Lister, L.A., 1987. The Erosional Surfaces of Zimbabwe. Bulletin 90, Zimbabwe Geological Survey.

Manceau, A., Schlegel, M.L., Musso, M., Sole, V.A., Gaunter, C., Petit, P.E., and Trolard,F., 2000. Crystal Chemistry of Trace elements in Natural and Synthetic Goethite. Geochimica et Cosmochimica Acta, 64(21), p 3643-3661.

Marker,A., Friedrich,G.,Carvalho,A.and Melfi,A.,1990. Control of the Distribution of Mn, Co, Zn, Ti and REEs during the Evolution of Laterite Covers above Ultramafic Complexes. Jour. of Geochem. Expl.,40, p 361-383.

Mann, 1982.Geochemical Dispersion: Mobilities of metal ions in: geochemical in deeply weathered terrain (ed Smith R.E), CISIRO Inst. Energy Earth Resources, 97-105

Marsh,1984.In www.uwsp.edu/geo/faculty/ritter/glossary/s_u/soil_texture_triangle.html

Marsh,1987. In www.uwsp.edu/geo/faculty/ritter/glossary/s_u/soil_texture_triangle.html

Mills S (2002), An Analysis of the Carbon and Stainless Steel industry and implication for Ferrochrome suppliers, Metal Bulletin Southern African Ferro- Alloy Conference.

Mines and Minerals Act Chapter 20.05, Revised Edition (1996). Zimbabwe Government Printers, Harare.

Moon, B.P. and Selby, M.J., 1983. Rock Mass Strength and Scarp Forms in Southern Africa. Geografiska Annaler, 65A, p135-145.

Mukasa, S. B., Wilson, A. H. and Carlson, R. W., 1998. A Multi-Element Geochronologic Study of the Great Dyke, Zimbabwe: Significance of the Robust and Reset Ages. Earth and Planetary Science Lett. 164, 353-369.

Murahwi, C.Z., 1995. The Geology of the Unki Platinum-Base Metal Deposit, Selukwe Subchamber Great Dyke, Zimbabwe. Geology Dept., Rhodes University. Unpublished MSc Thesis.

Murch, B.W. and Campbell, I.H., 1986. The Effects of Temperature, Oxygen Fugacity and Melt Composition on the Behaviour of Chromium in Basic and Ultrabasic Mmelts. Geochim.cosmochim.Acta, 50, p 1871-1887

Mushayandebvu, M.,1995. In Oberthür, T., Davis, D.W., Blenkinsop, T.G., and Hohndorf, A., 2002. Precice U-Pb Mineral Ages, Rb-Sr and Sm- Nd Systematics for the Great Dyke, Zimbabwe - Constraints on Late :Archean Events in Zimbabwe Craton and Limpopo Belt. Elsevier Precambrian Research, 113, p293-305

Naldrett, A. J., and Lehman, J., 1988. Spinel Non-Stoichiometry as the explanation for Ni-Cu-and PGE-Enrichiched Sulphides in Chromitites. In Geo-platinum, 87. Prichard H.M et al eds Barking Essex: Applied Science, 1988, p 93-109.

Naldrett, A. J., and Wilson, A. H., 1990. Horizontal and Vertical Variations in Noble Metals in the Great Dyke of Zimbabwe: A Model for the Origin of PGE Mineralisation by Fractional Segregation. Chem. Geol., 88, p 279-300.

Ngorima ,C.F., 2001. Mineralogical Examination and Size Analysis for Chromite Content of Soil samples from Anglo American Corporation. University of Zimbabwe, Institute of Mining Research, Report C783, p 6.

Nyamapfene, K., 1991. Soils of Zimbabwe. Nehanda, Publishers, Harare.

Oberthür et al. 2000 In Oberthür, T., Davis, D.W., Blenkinsop, T.G., and Hohndorf, A., 2002. Precice U-Pb Mineral Ages, Rb-Sr and Sm- Nd Systematics for the Great Dyke, Zimbabwe - Constraints on Late: Archean Events in Zimbabwe Craton and Limpopo Belt. Elsevier Precambrian Research, 113, p 293-305

Oberthür, T., Davis, D.W., Blenkinsop, T.G., and Hohndorf, A., 2002. Precise U-Pb Mineral Ages, Rb-Sr and Sm- Nd Systematics for the Great Dyke, Zimbabwe - Constraints on Late: Archean Events in Zimbabwe Craton and Limpopo Belt. Elsevier Precambrian Research, 113, p 293-305.

O'Neill et al, 1995. In Barnes S.J., and Roeder P.L.,2001. The Range of Spinel Compositions in Terrestrial Mafic and Ultramafic Rocks. Journal of Petrology, Vol. 42(12), p 2279-2302

Onyeagocha, A.C. 1974. Alteration of Chromite from Twin Sisters Dunites, Washington, American Mineralogist, 59, p 608-612.

Partridge, T.C. and Moud, R.R. (1987). Geomorphic Evolution of Southern Africa since Mesozoic. S. Afric. J. Geol., 90(2), p 179-208

Partridge, T.C., and Maud, R.R., 1990., South African Journal of Science, 85 428.

Partridge, T.C., and Maud, R.R., 2000. Macro-Scale Geomorphic Evolution of Southern Africa. In Partridge, T.C., and Maud, R.R., 2000. (eds), The Cenozoic of Southern Africa, Oxford University Press, Inc. New York.

Peacocke, Simpson and Associates, 2000. Knelson Continous Variable Discharge Concentrator tests on Eluvial Chromite Submitted by Zimbabwe Alloys Limited. Unpublished internal Report No B8aQ/06/00.

Penck ,W., 1924. Morphological Analysis of landforms, English translation by Czeck, H and Boswell, K.C., London, 1953, p 429

Podmore, F., 1970. The Shape of the Great Dyke of Rhodesia as Revealed by Gravity Surveying. Geol. Soc. South Africa, Spec. Publ. 1, p 610-620.

Podmore, F., and Wilson, A. H., 1987. A Re-Appraisal of the Structure, Geology and Emplacement of the Great Dyke, Zimbabwe. In: Halls, H. C. and Fahrig, W. F. (eds), Mafic Dyke Swarms, Geol. Assoc. Can. Spec. Paper, 43, p 317-30.

Power, M.R., Pirrie, D., Andersen, J.C.O. and Wheeler, P.D., 2000. Testing the Validity of Chrome Spinel Chemistry as a Provenance and Petrographic Indicator. Geology, 28, p 1027-1030.

Powers, M.C., 1953. A New Roundness Scale for Sedimentary Particles. Journal of Sedimentary Petrology, 23, p 117-119.

Prendergast, M. D., 1979. Darwendale. Internal Report, Union Carbide Geology Dept., Zimbabwe.

Prendergast, M.D., (1985), The Chromite Ore Fields of the Great Dyke, Zimbabwe, Union Carbide Internal Report, Unpublished.

Prendergast, M. D., 1984. Chromium Deposits of Zimbabwe. Chromium Review, 2, p 5-9.

Prendergast, M. D., 1987. The Chromite Ore Field of the Great Dyke, Zimbabwe. In: Stowe, C. W. (ed), Evolution of Chromite Ore Fields. New York: Van Nostrand Reinhold, p 89-108.

Prendergast, M. D., 1989. The Geology and Stratigraphic Setting of the Wedza-Mimosa Platinum Deposit, Great Dyke, Zimbabwe. In: Prichard, H. M., Potts, P. J., Bowles, J. F. W. and Cribb, S. J., (eds), Geo-Platinum '87. Barking, Essex: Elsevier Applied Science, p 281-302.

Prendergast, M. D., 1991. The Wedza-Mimosa Platinum Deposit, Great Dyke, Zimbabwe: Layering and Stratiform PGE Mineralisation in a Narrow Mafic Magma Chamber. Geol. Mag., 128, p 235-249.

Prendergast, M. D., 1998. The Great Dyke-Mineral Resources and Mining Development. The Great Dyke of Zimbabwe.Guidebook for the Pre-Symposium Excursion. 8th International Platinum Symposium, June 1998, p 10-14.

Prendergast, M. D., and Keays, R. R., 1989. Controls of Platinum-Group Element Mineralisation and the Origin of the PGE-Rich Main Sulphide Zone in the Wedza Subchamber of the Great Dyke, Zimbabwe: Implications for the Genesis of, and Exploration for, Stratiform PGE Mineralisation in Layered Intrusions. In: Prendergast, M. D. and Jones, M. J. (eds), Magmatic Sulphides-the Zimbabwe Volume. The Institute of Mining and Metallurgy, London, p 43-69.

Prendergast, M. D., and Wilson, A. H., 1989. The Great Dyke of Zimbabwe-II: Mineralisation and Mineral Deposits. In: Prendergast, M. D. and Jones, M. J. (eds), Magmatic Sulphides-the Zimbabwe Volume. The Institute of Mining and Metallurgy, London, p 21-42.

Prendergast, M.D., 1988a. The Geology and Economic Potential of the PGE-rich Main Sulphide Zone of the Great Dyke, Zimbabwe. In Geo- Platinum '87. Prichard, H.M., Potts P.J., Bowles, J.F.W., and Cribb, S.J., (Eds), Elsevier Applied Science, Barking, Essex, p 2812-302.

Prendergast, M.D., 1988b, An Investigation of the Stratigraphy and Petrology of the Pyroxenite No.1 Layer in the Wedza Subchamber of the Great Dyke, Zimbabwe, with special reference to the

characteristic features and origin of the platinum- group element- bearing Main Sulphide zone. Unpublished D Phil. Thesis. Department of Geology, University of Zimbabwe.

Pritchard, J.M. 1986. Landform and Landscape in Africa. Edward Arnold Limited, London.

Quantin, C., Becquer, T., Berthelin, J.,2001. Mn-oxide: a Major Source of Easily Mobilized Co and Ni under Reducing Conditions in New Calodonia Ferralsols. Surface Geoscience Pedology, 334, p 273-278

Reynolds, I.M., 1885. The Mineralogy and Ore Petrography of the Bushveld Titineferous Magnetite – Rich Layers, in Maske, S., ed., Geology of Mineral Deposits of Southern Africa: Johannesburg, Geol. Soc. South Africa.

Riffer, 2004 .In www.uwsp.edu/geo/faculty/ritter/glossary/s_u/soil_texture_triangle.html

Robertson, I.D.M. and van Breemen, O., 1970. The Southern Satellites of the Great Dyke, Rhodesia. In: Visser, D. J. L. and von Gruenewaldt, G., (eds), Symposium on the Bushveld Igneous Complex and Other Layered Intrusions, Pretoria, July, 1969, Geol. Soc. S. Afr. Spec.Publ., 1, p 621-644.

Roeder and Hill, 1991. In Barnes S.J., and Roeder P.L.,2001. The Range of Spinel Compositions in Terrestrial Mafic and Ultramafic Rocks. Journal of Petrology, Vol. 42(12), p 2279-2302.

Roeder, P.L., and Campbell, I.H., 1985. The Effects of Postcumulus Reaction on Compositions of Chrome-Spinels from Jemberlana Intrusion. Journal of Petrology, 26,p 763-786.

Roeder, P.L., 1994. Chromite: From the Fiery rain of Condrules to Kilauea Iki lava Lake. Canadian Mineralogist, 32, p 729-746.

Roeder, P.L., and Reynolds, I.,1991. Crystallisation of Chromite and Chromiuium solubilityin Basaltic melts. Journal of Petrology, 32,p 909-934.

Rollinson, H.R., 1983. The Geochemistry of Mafic and Ultramafic Rocks from Archaean Greenstone Belts of Sierra Leone. Mineral Magazine., 47, p 267-280.

Rollinson, H.R.,1995. Composition and tectonic settings of chromite deposits through time. A discussion. Economic Geology, 90, p 2091- 2092.

Rollinson, H.R., Appel, P.W.U., and Frei, R., 2002. A Metamorphosed, Early Archean Chromitite from West Greenland: Implications for the Genesis of Archean Anorthositic Chromitites.

Rust, D.J., and Summerfield, M.A., 1990. In Partridge, T.C., and Maud, R.R., 2000 (eds), The Cenozoic of Southern Africa, Oxford University Press, Inc. New York.

Scowen, P.A.H., Roeder, P.L., and Heltz, R.T.,1991. Re-equilibration of Chromite of Chromite within Kilauea Iki Lava Lake, Hawaii. Contributions to Mineralogy and Petrology,107, p 8-20.

Slatter D. de L., 1981. Chromium Resources of Zimbabwe. Chamber of Mines Journal, Vol. 23, (4), p 43-51.

Slatter, D. de L., 1979. Production of Ferrochromium Nickel Alloys and Stainless Steels by Direct Smelting of Oxide Ores in Zimbabwe-Rhodesia. Trans-Inst Min. Metall. (Sect. C: Mineral process. Extr. Metall.), 88, C209-214.

Smith, A.G., 1982. Late Cenozoic Uplift of stable Continents in a Reference Frame fixed to South America. Nature, 296, p 400-404.

Stagman, J.G., 1978. An Outline of the Geology of Rhodesia. Bulletin 71, Geological Survey of Rhodesia.

Stowe C. W., 1968. The geology of the country south and west of Selukwe, Bulletin, Geological Survey of Rhodesia, 59, p 204

Stowe C.W., 1987, (ed). Evolution Of Chromium Ore Fields. Van Nostrand Reinolds, New York

Stowe, C.W., 1994. Compositions and Tectonic Settings of Chromite Deposits Through Time:Economic Geology , 90, p 528-546.

Summerfield, M. A., 1985. In Partridge, T.C. and Moud, R.R. (1987). Geomorphic Evolution of Southern Africa since Mesozoic. S. Afric J. Geol., 90(2), p 179-208

Swift, W.H.,1961. An Outline of the Geology of Southern Rhodesia, Bulletin 50, Geological Survey of Southern Rhodesia.

Twindale, C.R., 1990. The Origin and Implications of Some Erosional Landforms, Journal of Geology, 1990, Vol.98 p 343-364.

Vail, P.R., Mitchum, R.M. and Thompson, S., 1977. In Partridge, T.C. and Moud, R.R. (1987). Geomorphic Evolution of Southern Africa since Mesozoic. S. Afric J. Geol., 90(2), p 179-208

Viljoen.A. and van der Walt,E., 1973. The Composition of Chromite Grains from Various Witwaterand Reefs. National Institute for Metallurgy, South Africa, Report 1924, p 3-95.

Vincent, V and Thomas, R.G., 1960. An Agricultural Survey of Southern Rhodesia: Part1- Agro-Ecological Survey. Government Printers, Salisbury.

Wayland, E.J., 1931. In Partridge, T.C. and Moud, R.R. 1987. Geomorphic Evolution of Southern Africa since Mesozoic. S. Afric J. Geol., 90(2), p 179-208

Weaver, R.M., and Hochella Jr, M.F., 2003. The Reactivity of Seven Mn-oxides with $Cr_{aq}^{3+}$: A comparitive Analysis of Complex, Environmentally Important Redox Reaction. American Mineralogist, Vol.88 p 2016-2027.

Wellington, J.H., 1955. In Partridge, T.C. and Moud, R.R. (1987). Geomorphic Evolution of Southern Africa since Mesozoic. S. Afric J. Geol., 90(2), p 179-208

Wiles, J. W., 1968. Some Aspects of the Metamorphism of the Basement Complex in the Sipolilo District. Trans. Geol. Soc. S. Afr.,71, p 79-88.

Wilson, A. H. and Prendergast, M. D., 1989. The Great Dyke of Zimbabwe-I; Tectonic Setting, Stratigraphy, Petrology, Structure, Emplacement and Crystallisation. In: Prendergast, M. D.

and Jones, M. J. (eds), Magmatic sulphides-the Zimbabwe volume. The Institute of Mining and Metallurgy, London, p 1-20.

Wilson, A. H., 1976. The Petrology and Structure of the Hartley Complex of the Great Dyke, Rhodesia. Unpublished PhD Thesis, University of Rhodesia.

Wilson, A. H., 1982. The Geology of the Great Dyke, Zimbabwe: The Ultramafic Rocks. Journal of Petrology, 23, p 240-292.

Wilson, A. H., 1992. The Geology of the Great Dyke, Zimbabwe: Crystallisation, Layering and Cumulate Formation in the P1 Pyroxenite of Cyclic Unit 1 of the Darwendale Sub chamber. J. Petrol., 33, p 611-663.

Wilson, A. H., 1996. The Great Dyke of Zimbabwe. In: Cawthorn, R. G. (ed), Layered intrusions. Elsevier Science, p 365-402.

Wilson, A. H., 1998. The Great Dyke of Zimbabwe.Guidebook for the Pre-Symposium Excursion. 8th International Platinum Symposium, June 1998, p 1-10.

Wilson, A. H., Naldrett, A. J., and Tredoux, M., 1989. Distribution and Controls of Platinum-Group Element and Base Metal Mineralisation in the Darwendale Subchamber of the Great Dyke, Zimbabwe. Geology, 17, p 649-652.

Wilson, A.H. and Tredoux. M, 1990. Lateral and Vertical distribution of plastnum- group elements and petrogenetic controls on the sulphide Mineralisation in the P1 layer of the Darwendale Sub chamber of the Great Dyke, Zimbabwe. Geology, 17, p 649-652.

Wilson, A.H., and Chaumba, J.B., 1997. Closed System Fractionation in Large Magma Chamber: Mineral Composition of Websterite Layer and lower Mafic Succession of the Great Dyke, Zimbabwe. Mineralogical Magazine, 61, p 153-173.

Wilson, J. F., 1987. The Tectonic Setting of the Great Dyke of Zimbabwe and the Mashonaland Igneous Event. 14th Colloquium Afr. Geol., CIFEG Occ. Publ., 12, p 140-141.

Wilson, J. F., 1990. Report on the Preliminary Examination of Zimbabwe Geological Survey's Borehole BH6 from the Great Dyke. Ann. Zim. Geol. Surv., XIV, p 62-63.

Wingate, M.T.D., 2000. Ion Microprobe U-Pb Zircon and baddeleyite. Ages for the Great Dyke and Its Statelite Dykes, Zimbabwe. S. Afr. J.Geol., 103, p 74-80.

Worst, B. G., 1956. The Geology of the Country between Belingwe and West Nicholson. Geol. Surv. S.Rhod, Bull. , 43.

Worst, B. G., 1958. The Differentiation and Structure of The Great Dyke Of Southern Rhodesia. Trans. Geol. Soc. S. Afr., 61, p 283-364

Worst, B. G., 1960. The Great Dyke of Southern Rhodesia Geol. Survey Bull., 47, p 234.

Worst, B. G., 1964. Chromite in the Great Dyke of Southern Rhodesia. In: Haughton, S. H. (ed), The Geology of Some Ore Deposits in Southern Africa. Geol. Soc. S. Afr. Spec. Publ., 2, p 209-224.

Young, 1976 In Nyamapfene, K., 1991. Soils of Zimbabwe. Nehanda Publishers, Harare

Zeally, A. E. V., 1912. In Zeally, A.E.V. 1918. The Occurrence of Platinum in Southern Rhodesia. S. Rhod. Geol. Surv. Short Report., 3.

Zeally, A. E. V., 1918. The Occurrence of Platinum in Southern Rhodesia. S. Rhod. Geol. Surv. Short Report., 3.

Zeissink, H.E., 1969. The Mineralogy and Geochemistry of Nickeliferous Laterite Profile (Greenvale, Queensland, Australia). Mineral. Diposita, 4, p 132-152.

Zimbabwe Alloys Limited Mines July 2001 Report, (2001), Zimbabwe Alloys Limited, Gweru.

Zimbabwe Alloys Road Header Project Report, (1989) Unpublished Internal Company Report Zimbabwe Alloys Limited, Mutorashanga.

## X-Ray Fluorescence (XRF) – Sample Analytical Method

X-ray Florescence spectrometry is based upon the excitation of sample by X-rays. A primary X-ray beam excite secondary X-ray florescence with characteristic of the elements present in the sample. The intensity of the secondary X-rays is used to determine the concentrations of the elements present by reference to calibration standards with appropriate corrections being made for instrumental errors and the effects the composition of the sample has on its X-ray emission intensities. The method is versatile and can analyse up to 80 elements over a wide range of sensitivities, detecting concentrations from 100% down to a few parts per million (ppm). The main limitation of XRF is that it elements lighter than Na (atomic number = 11) cannot be analysed by XRF.

## Procedures and Sample Preparation

Upon receipt of the eluvial chromite samples at Zimbabwe Alloys Limited, Laboratory in Gweru the sample is pulverized to pass through a 75 micron sieve. The pulverized sample is then briquetted to a 40 ton press to give a button that is read on the XRF for chemical analysis. The method is sometimes complemented by use of volumetric analyses particularly in the making of standards. Data is obtained in batches in order to control the application of suitable standards.

# Typical Detailed log Sheet

Extract of a typical log sheet showing logging details. (Explanation key and pit number omitted)

| UTM ZONE | Easting | Northing | Pit No | Surface Soil | Surface | Soil | | Geology | | Slope | Landscape | | Veg | Comments |
|---|---|---|---|---|---|---|---|---|---|---|---|---|---|---|
| | | | | Colour | Chromite | Type | Condition | Outcrop | Float | Direction | Reg | Pos | | |
| | | | | Munsell Code | | | | | | | | | | |
| 35K | 794945 | 7754529 | | 2.5YR3/4 | N-L | C | DM | N | N | E | R | EP | AG | No visible chrome |
| 35K | 795140 | 7754551 | | N2/0 | N-L | C | DM | N | N | E | R | EP | AG | Low level chromite values expected |
| 35K | 795344 | 7754562 | | N2/0 | N-L | C | DM | N | N | E | R | EP | AG | Black vlei soil with carbonate nodules |
| 35K | 795547 | 7754591 | | N2/0 | N | C | DM | N | N | E | R | EP | AG | Prevalent carbonate nodules |
| 35K | 795741 | 7754632 | | N2/0 | N | C | DM | N | N | E | R | EP | AG | Poor sample |
| 35K | 792673 | 7755108 | | 10R2/1 | N-L | C | DM | N | N | Flat | R | EP | AG | Poor sample |
| 35K | 792921 | 7755048 | | N2/0 | N-L | C | DM | N | N | Flat | R | EP | AG | Low level chromite values expected |
| 35K | 795588 | 7755204 | | 2.5YR3/6 | L | S-L | DM | Gabbro | N | E | R | EP | AG | Low level chromite values expected |
| 35K | 795724 | 7755187 | | 2.5YR3/4 | L | C | DM | Gabbro | N | E | R | EP | AG | Low level chromite values expected |
| 35K | 795857 | 7755187 | | 2.5YR3/4 | N | T-S | DM | Gabbro | N | E | R | EP | AG | Poor sample |
| 35K | 792776 | 7756076 | | 10R3/3 | N-L | T-C | DM | N | Serp | W | E | EP | AG | Chocolate brown soil |
| 35K | 792772 | 7756051 | | N2/0 | N | C | DM | N | Serp | W | E | EP | AG | Black vlei soil with carbonate nodules |
| 35K | 790488 | 7750004 | | 5YR5/6 | L | P-S | DY | Gabbro | N | W | R | EP | AG | Highly pisolithic soils |
| 35K | 792889 | 7757012 | | N2/0 | N-L | C | DM | N | Serp | W | E | EP | AG | Black turf near chromite seam +/- 10m |
| 35K | 793086 | 7757001 | | 10YR2/2 | N-L | C | DM | N | Serp | W | R | EP | AG | Poor sample |
| 35K | 790807 | 7750830 | | 2.5Yk3/4 | L | S | DY | Gabbro | Gabbro | W | E | EP | MW | Gullies are prevalent in the area |
| 35K | 790628 | 7750852 | | 5YR5/6 | L | S | DY | Gabbro | Gabbro | W | W | EP | MW | Low level chromite values expected |
| 35K | 793145 | 7758056 | | N2/0 | N-L | C | DM | N | Serp | W | R | EP | AG | Black cotton soil |
| 35K | 793335 | 7758035 | | N2/0 | N | C | DM | N | N | W | R | EP | AG | Black turf |
| 35K | 790943 | 7751551 | | 10YR4/1 | L | C | DM | N | Px | W | E | EP | AG | Poorly developed soil profile |
| 35K | 793324 | 7759007 | | 10YR2/1 | N | C | DM | N | Px | W | R | EP | AG | Black turf |
| 35K | 793516 | 7758993 | | 2.5YR3/4 | N-L | T-L | DM | N | N | W | R | EP | AG | Poor soil profile |
| 35K | 793765 | 7760062 | | N2/0 | N | C | DM | N | N | W | R | EP | AG | Black cooton soil |
| 35K | 794263 | 7760949 | | 10YR2/2 | N | C | DM | N | N | W | R | EP | AG | Black turf |
| 35K | 794982 | 7762624 | | 10YR2/2 | N-L | T-S | DY | Px | N | W | E | EP | AG | Sandy-silty redish-brown soil |

# Electron Probe Microanalyzer (EPMA) JEOL Superprobe 733 Settings

Scanning electron microscope (SEM) equipped with both an energy dispersive and wave length X-ray spectrometers. This microscope is used primarily for mineralogy microanalysis.

Imaging with both secondary and backscattering electrons

- PGT energy dispersive X-ray spectrometer (EDS)
- PET, TAP, and LiF crystals in wave length X-ray spectrometer (WDS)

All analyses were performed with a JEOL 733 Superprobe at **20 kV** and **20nA**. The beam diameter was fixed at 2 µm with a take off angle of **40°**.

Standards used with count times on peak and background counting times are listed in the table below.

| Elements | Lines | Crystals | Standard | Count times On Peak (s | Background counting times (s) |
|---|---|---|---|---|---|
| Si | K? | TAP | Orthoclase | 10 | 5 |
| Al | K? | TAP | Plagioclase | 10 | 5 |
| Fe | K? | LIF | Ni-Magnetite | 10 | 5 |
| Mg | K? | TAP | Olivine | 20 | 10 |
| Ca | K? | PET | Wollastonite | 20 | 10 |
| Zn | K? | LIF | Willemite | 20 | 10 |
| Cr | K? | LIF | Chromite | 10 | 5 |
| Mn | K? | LIF | Willemite | 20 | 10 |
| Ti | K? | LIF | Rutile | 20 | 10 |
| Cu | L? | LIF | Strontium titanite | 20 | 10 |
| Ni | K? | LIF | Ni Magnetite | 20 | 10 |

Appendix 4

Electron Microprobe analyses

## Individual Electron Microprobe Analyses of South Dyke Chromite Compositions

| Analysis No. | 1 | 2 | 3 | 4 | 1 | 2 | 3 | 4 | 1 | 2 | 3 | 4 | 1 | 2 | 3 | 4 | 1 | 2 | 3 | 4 |
|---|---|---|---|---|---|---|---|---|---|---|---|---|---|---|---|---|---|---|---|---|
| Sample No. | SD1 | | | | SD2 | | | | SD3 | | | | SD4 | | | | SD5 | | | |
| $SiO_2$ | 0.00 | 0.00 | 0.00 | 0.00 | 0.00 | 0.00 | 0.00 | 0.00 | 0.00 | 0.00 | 0.00 | 0.00 | 0.00 | 0.00 | 0.00 | 0.00 | 0.00 | 0.00 | 0.00 | 0.00 |
| $TiO_2$ | 0.53 | 0.23 | 0.36 | 0.28 | 0.31 | 0.31 | 0.39 | 0.32 | 0.38 | 0.34 | 0.35 | 0.33 | 0.31 | 0.34 | 0.34 | 0.38 | 0.32 | 0.32 | 0.32 | 0.24 |
| $Al_2O_3$ | 11.13 | 12.19 | 12.50 | 11.34 | 12.82 | 15.65 | 14.71 | 12.65 | 11.18 | 11.59 | 14.04 | 13.92 | 12.57 | 11.89 | 12.55 | 13.71 | 12.15 | 11.56 | 10.30 | 12.97 |
| $Cr_2O_3$ | 58.54 | 57.51 | 58.03 | 59.03 | 57.90 | 58.65 | 57.12 | 57.86 | 57.89 | 58.02 | 57.66 | 58.11 | 59.48 | 57.55 | 55.46 | 54.50 | 57.00 | 57.21 | 57.23 | 57.76 |
| $Fe_2O_3$ | 0.00 | 0.00 | 0.00 | 0.00 | 0.00 | 0.00 | 0.00 | 0.00 | 0.00 | 0.00 | 0.00 | 0.00 | 0.00 | 0.00 | 1.64 | 0.72 | 0.02 | 0.00 | 2.42 | 0.00 |
| FeO | 23.01 | 20.35 | 21.07 | 22.17 | 20.64 | 18.91 | 18.79 | 18.79 | 22.21 | 19.67 | 20.20 | 20.75 | 19.47 | 22.11 | 20.45 | 22.04 | 22.01 | 22.37 | 19.57 | 21.77 |
| NiO | 0.08 | 0.06 | 0.07 | 0.09 | 0.01 | 0.04 | 0.00 | 0.05 | 0.10 | 0.14 | 0.12 | 0.12 | 0.11 | 0.10 | 0.05 | 0.12 | 0.06 | 0.00 | 0.17 | 0.09 |
| MnO | 0.25 | 0.22 | 0.27 | 0.33 | 0.34 | 0.26 | 0.30 | 0.27 | 0.30 | 0.24 | 0.27 | 0.31 | 0.31 | 0.24 | 0.27 | 0.21 | 0.31 | 0.30 | 0.27 | 0.36 |
| MgO | 6.39 | 7.86 | 7.06 | 6.17 | 6.09 | 5.95 | 7.45 | 9.67 | 7.04 | 9.02 | 6.87 | 6.55 | 7.95 | 7.51 | 8.77 | 7.88 | 7.88 | 7.35 | 8.97 | 6.20 |
| Total | 99.93 | 98.42 | 99.36 | 99.41 | 98.11 | 99.77 | 98.76 | 99.61 | 99.10 | 99.02 | 99.51 | 100.09 | 100.2 | 99.74 | 99.53 | 99.56 | 99.55 | 99.11 | 99.25 | 99.39 |
| *Cations per 32 oxygens* | | | | | | | | | | | | | | | | | | | | |
| Al | 0.45 | 0.45 | 0.50 | 0.46 | 0.52 | 0.64 | 0.60 | 0.49 | 0.49 | 0.46 | 0.57 | 0.56 | 0.47 | 0.50 | 0.49 | 0.54 | 0.48 | 0.46 | 0.41 | 0.53 |
| Cr | 1.58 | 1.54 | 1.56 | 1.61 | 1.59 | 1.62 | 1.55 | 1.51 | 1.56 | 1.53 | 1.56 | 1.57 | 1.52 | 1.58 | 1.45 | 1.43 | 1.51 | 1.52 | 1.52 | 1.57 |
| $Fe_3^+$ | 0.00 | 0.00 | 0.00 | 0.00 | 0.00 | 0.00 | 0.00 | 0.00 | 0.00 | 0.00 | 0.00 | 0.00 | 0.00 | 0.00 | 0.04 | 0.02 | 0.00 | 0.00 | 0.06 | 0.00 |
| Ti | 0.01 | 0.01 | 0.01 | 0.01 | 0.01 | 0.01 | 0.01 | 0.01 | 0.01 | 0.01 | 0.01 | 0.01 | 0.01 | 0.01 | 0.01 | 0.01 | 0.01 | 0.01 | 0.01 | 0.01 |
| Mg | 0.32 | 0.40 | 0.36 | 0.32 | 0.31 | 0.31 | 0.38 | 0.48 | 0.36 | 0.45 | 0.35 | 0.33 | 0.38 | 0.40 | 0.43 | 0.39 | 0.38 | 0.37 | 0.45 | 0.32 |
| $Fe_2^+$ | 0.66 | 0.58 | 0.60 | 0.64 | 0.60 | 0.55 | 0.54 | 0.52 | 0.63 | 0.55 | 0.58 | 0.59 | 0.62 | 0.55 | 0.57 | 0.61 | 0.62 | 0.63 | 0.55 | 0.62 |
| Ni | 0.00 | 0.00 | 0.00 | 0.00 | 0.00 | 0.00 | 0.00 | 0.00 | 0.00 | 0.00 | 0.00 | 0.00 | 0.00 | 0.00 | 0.00 | 0.00 | 0.00 | 0.00 | 0.01 | 0.00 |
| Mn | 0.01 | 0.01 | 0.01 | 0.01 | 0.01 | 0.01 | 0.01 | 0.01 | 0.01 | 0.01 | 0.01 | 0.01 | 0.01 | 0.01 | 0.01 | 0.01 | 0.01 | 0.01 | 0.01 | 0.01 |
| Totals | 3.03 | 2.98 | 3.04 | 3.04 | 3.04 | 3.14 | 3.08 | 3.01 | 3.06 | 3.00 | 3.07 | 3.07 | 3.00 | 3.05 | 3.00 | 3.00 | 3.00 | 3.00 | 3.00 | 3.05 |
| $Mg/(Mg+Fe^{2+})$ | 0.331 | 0.408 | 0.374 | 0.331 | 0.344 | 0.359 | 0.414 | 0.479 | 0.361 | 0.449 | 0.378 | 0.360 | 0.377 | 0.421 | 0.433 | 0.389 | 0.383 | 0.369 | 0.449 | 0.337 |
| Cr/(Cr + Al) | 0.779 | 0.775 | 0.745 | 0.726 | 0.752 | 0.715 | 0.745 | 0.726 | 0.760 | 0.770 | 0.745 | 0.726 | 0.765 | 0.760 | 0.745 | 0.726 | 0.759 | 0.768 | 0.745 | 0.726 |
| $Fe^{2+}/(Fe_2^+ + Mg)$ | 0.669 | 0.592 | 0.626 | 0.669 | 0.656 | 0.641 | 0.586 | 0.521 | 0.639 | 0.551 | 0.622 | 0.640 | 0.623 | 0.579 | 0.567 | 0.611 | 0.617 | 0.631 | 0.551 | 0.663 |
| Ti/Cr | 0.009 | 0.005 | 0.006 | 0.004 | 0.005 | 0.005 | 0.006 | 0.005 | 0.006 | 0.006 | 0.006 | 0.005 | 0.005 | 0.004 | 0.006 | 0.006 | 0.005 | 0.005 | 0.005 | 0.004 |

## Individual Electron Microprobe Analyses of Middle Dyke Chromite Compositions

| Analysis No. | 1 | 2 | 3 | 4 | 1 | 2 | 3 | 4 | 1 | 2 | 3 | 4 | 1 | 2 | 3 | 4 | 1 | 2 | 3 | 4 | 1 | 2 | 3 | 4 |
|---|---|---|---|---|---|---|---|---|---|---|---|---|---|---|---|---|---|---|---|---|---|---|---|---|
| Sample No. | MD19 | | | | MD20 | | | | MD21 | | | | MD22 | | | | MD23 | | | | MD24 | | | |
| $SiO_2$ | 0.00 | 0.00 | 0.00 | 0.00 | 0.00 | 0.00 | 0.00 | 0.00 | 0.00 | 0.00 | 0.00 | 0.00 | 0.00 | 0.00 | 0.00 | 0.00 | 0.00 | 0.00 | 0.00 | 0.00 | 0.00 | 0.00 | 0.00 | 0.00 |
| $TiO_2$ | 0.33 | 0.36 | 0.46 | 0.27 | 0.44 | 0.32 | 0.20 | 0.39 | 0.37 | 0.61 | 0.34 | 0.61 | 0.42 | 0.42 | 0.44 | 0.39 | 0.37 | 0.45 | 0.42 | 0.43 | 0.20 | 0.66 | 0.34 | 0.37 |
| $Al_2O_3$ | 17.14 | 15.44 | 14.04 | 16.22 | 21.88 | 11.44 | 18.27 | 17.00 | 16.34 | 15.00 | 15.04 | 16.23 | 15.86 | 16.58 | 19.20 | 15.79 | 14.92 | 14.51 | 13.29 | 15.05 | 18.88 | 17.75 | 17.29 | 14.13 |
| $Cr_2O_3$ | 51.26 | 52.01 | 53.66 | 52.47 | 47.28 | 51.76 | 53.01 | 52.26 | 52.84 | 52.15 | 52.87 | 52.22 | 53.96 | 52.84 | 52.21 | 54.88 | 53.91 | 52.91 | 53.02 | 51.94 | 50.63 | 50.45 | 51.57 | 53.48 |
| $Fe_2O_3$ | 1.25 | 2.05 | 2.6 | 2.21 | 0 | 0.96 | 0.00 | 0.00 | 0.00 | 0.00 | 0.26 | 0.00 | 0.00 | 0.00 | 0.00 | 0.00 | 1.19 | 2.74 | 5.43 | 2.72 | 1.51 | 1.18 | 0.40 | 1.48 |
| FeO | 18.99 | 18.2 | 17.81 | 17.63 | 21.26 | 19.99 | 19.56 | 20.81 | 19.01 | 23.55 | 22.64 | 20.57 | 20.18 | 21.16 | 18.15 | 17.87 | 19.38 | 19.79 | 15.58 | 19.12 | 16.86 | 18.84 | 21.68 | 21.43 |
| NiO | 0.07 | 0.07 | 0.15 | 0 | 0.13 | 0.03 | 0.07 | 0.10 | 0.12 | 0.10 | 0.05 | 0.08 | 0.10 | 0.00 | 0.16 | 0.00 | 0.00 | 0.00 | 0.18 | 0.00 | 0.00 | 0.16 | 0.00 | 0.00 |
| MnO | 0.29 | 0.26 | 0.25 | 0.23 | 0.27 | 0.22 | 0.27 | 0.21 | 0.28 | 0.37 | 0.35 | 0.29 | 0.32 | 0.30 | 0.24 | 0.27 | 0.26 | 0.31 | 0.25 | 0.30 | 0.30 | 0.28 | 0.34 | 0.31 |
| MgO | 10.16 | 10.39 | 10.69 | 11.14 | 8.62 | 9.44 | 8.58 | 8.27 | 9.94 | 7.09 | 7.45 | 7.99 | 8.86 | 7.74 | 9.45 | 9.53 | 9.85 | 9.63 | 12.13 | 9.95 | 11.85 | 10.55 | 8.60 | 8.32 |
| Total | 99.49 | 98.78 | 99.66 | 100.17 | 99.88 | 94.16 | 99.96 | 99.04 | 98.90 | 98.87 | 99.00 | 97.99 | 99.70 | 99.04 | 99.85 | 98.73 | 99.88 | 100.34 | 100.30 | 99.51 | 100.23 | 99.87 | 100.22 | 99.52 |
| *Cations per 32 oxygens* | | | | | | | | | | | | | | | | | | | | | | | | |
| Al | 0.447 | 0.448 | 0.502 | 0.460 | 0.825 | 0.63 | 0.706 | 0.661 | 0.626 | 0.586 | 0.589 | 0.619 | 0.612 | 0.65 | 0.736 | 0.616 | 0.57 | 0.555 | 0.503 | 0.577 | 0.699 | 0.668 | 0.658 | 0.55 |
| Cr | 1.576 | 1.544 | 1.562 | 1.606 | 1.195 | 1.331 | 1.375 | 1.362 | 1.357 | 1.366 | 1.388 | 1.458 | 1.396 | 1.389 | 1.341 | 1.437 | 1.383 | 1.357 | 1.346 | 1.336 | 1.256 | 1.272 | 1.316 | 1.395 |
| $Fe_3$+ | 0.000 | 0.000 | 0.000 | 0.000 | 0 | 0.023 | 0 | 0 | 0 | 0.018 | 0.007 | 0 | 0 | 0 | 0 | 0 | 0.029 | 0.067 | 0.131 | 0.066 | 0.036 | 0.028 | 0.01 | 0.037 |
| Ti | 0.014 | 0.008 | 0.009 | 0.007 | 0.011 | 0.008 | 0.005 | 0.01 | 0.009 | 0.015 | 0.008 | 0.007 | 0.01 | 0.01 | 0.011 | 0.01 | 0.009 | 0.011 | 0.01 | 0.01 | 0.005 | 0.016 | 0.008 | 0.009 |
| Mg | 0.324 | 0.398 | 0.358 | 0.316 | 0.411 | 0.457 | 0.415 | 0.406 | 0.481 | 0.35 | 0.369 | 0.39 | 0.432 | 0.384 | 0.457 | 0.471 | 0.476 | 0.466 | 0.58 | 0.482 | 0.554 | 0.502 | 0.414 | 0.409 |
| $Fe_2$+ | 0.655 | 0.578 | 0.600 | 0.638 | 0.569 | 0.544 | 0.536 | 0.574 | 0.517 | 0.653 | 0.629 | 0.564 | 0.552 | 0.588 | 0.493 | 0.495 | 0.526 | 0.537 | 0.418 | 0.52 | 0.443 | 0.503 | 0.585 | 0.592 |
| Ni | 0.002 | 0.002 | 0.002 | 0.002 | 0.003 | 0.001 | 0.002 | 0.003 | 0.003 | 0.003 | 0.001 | 0 | 0.003 | 0 | 0.004 | 0 | 0 | 0 | 0.005 | 0 | 0 | 0.004 | 0 | 0 |
| Mn | 0.007 | 0.006 | 0.008 | 0.010 | 0.007 | 0.006 | 0.008 | 0.006 | 0.008 | 0.01 | 0.01 | 0.008 | 0.009 | 0.008 | 0.007 | 0.008 | 0.007 | 0.008 | 0.007 | 0.008 | 0.008 | 0.008 | 0.009 | 0.009 |
| Totals | 3.025 | 2.984 | 3.041 | 3.039 | 3.021 | 3.000 | 3.047 | 3.022 | 3.001 | 3.001 | 3.001 | 3.046 | 3.014 | 3.029 | 3.049 | 3.037 | 3.000 | 3.001 | 3.000 | 2.999 | 3.001 | 3.001 | 3.000 | 3.001 |
| $Mg/(Mg+Fe^{2+})$ | 0.331 | 0.408 | 0.374 | 0.331 | 0.419 | 0.457 | 0.436 | 0.414 | 0.482 | 0.349 | 0.370 | 0.409 | 0.439 | 0.395 | 0.481 | 0.488 | 0.475 | 0.465 | 0.581 | 0.481 | 0.556 | 0.500 | 0.414 | 0.409 |
| Cr/(Cr + Al) | 0.779 | 0.775 | 0.745 | 0.726 | 0.592 | 0.679 | 0.745 | 0.726 | 0.684 | 0.700 | 0.745 | 0.726 | 0.695 | 0.681 | 0.745 | 0.726 | 0.708 | 0.710 | 0.745 | 0.726 | 0.642 | 0.656 | 0.745 | 0.726 |
| $Fe^{3}/(Fe_2^{2}+ Mg)$ | 0.669 | 0.592 | 0.626 | 0.669 | 0.581 | 0.543 | 0.564 | 0.586 | 0.518 | 0.651 | 0.630 | 0.591 | 0.561 | 0.605 | 0.519 | 0.512 | 0.525 | 0.535 | 0.419 | 0.519 | 0.444 | 0.500 | 0.586 | 0.591 |
| Ti/Cr | 0.009 | 0.005 | 0.006 | 0.004 | 0.009 | 0.006 | 0.004 | 0.007 | 0.007 | 0.011 | 0.006 | 0.005 | 0.007 | 0.007 | 0.008 | 0.007 | 0.007 | 0.008 | 0.007 | 0.007 | 0.004 | 0.013 | 0.006 | 0.006 |

## Individual Electron Microprobe Analyses of North Dyke A (Jester) Chromite Compositions

| Analysis No. | 1 | 2 | 3 | 4 | 1 | 2 | 3 | 4 | 1 | 2 | 3 | 4 | 1 | 2 | 3 | 4 | 1 | 2 | 3 | 4 |
|---|---|---|---|---|---|---|---|---|---|---|---|---|---|---|---|---|---|---|---|---|
| Sample No. | ND8 | | | | ND9 | | | | ND10 | | | | ND11 | | | | ND12 | | | |
| $SiO_2$ | 0.00 | 0.00 | 0.00 | 0.00 | 0.00 | 0.00 | 0.00 | 0.00 | 0.00 | 0.00 | 0.00 | 0.00 | 0.00 | 0.00 | 0.00 | 0.00 | 0.00 | 0.00 | 0.00 | 0.00 |
| $TiO_2$ | 0.24 | 0.23 | 0.41 | 0.15 | 0.39 | 0.27 | 0.30 | 0.28 | 0.33 | 0.34 | 0.27 | 0.37 | 0.21 | 0.32 | 0.21 | 0.35 | 0.29 | 0.39 | 0.41 | 0.30 |
| $Al_2O_3$ | 13.43 | 13.29 | 13.19 | 14.48 | 11.67 | 11.44 | 11.32 | 11.76 | 11.36 | 12.65 | 10.11 | 11.67 | 15.28 | 13.28 | 10.85 | 12.63 | 12.94 | 10.87 | 11.53 | 12.02 |
| $Cr_2O_3$ | 59.11 | 57.30 | 57.38 | 57.27 | 60.38 | 59.51 | 60.16 | 60.27 | 58.74 | 59.56 | 58.90 | 58.63 | 56.45 | 56.52 | 56.48 | 56.23 | 58.44 | 60.26 | 58.07 | 60.35 |
| $Fe_2O_3$ | 0.00 | 0.00 | 0.00 | 0.00 | 0.00 | 0.00 | 0.00 | 0.00 | 1.09 | 0.00 | 2.44 | 1.31 | 0.00 | 0.27 | 2.28 | 2.10 | 0.00 | 0.00 | 0.00 | 0.00 |
| FeO | 19.03 | 18.60 | 19.02 | 17.85 | 18.70 | 20.97 | 19.82 | 18.13 | 16.37 | 17.01 | 15.97 | 15.71 | 17.15 | 17.45 | 17.96 | 16.23 | 19.59 | 18.45 | 21.13 | 17.72 |
| NiO | 0.08 | 0.05 | 0.06 | 0.05 | 0.03 | 0.09 | 0.01 | 0.04 | 0.00 | 0.05 | 0.06 | 0.08 | 0.00 | 0.07 | 0.06 | 0.11 | 0.05 | 0.12 | 0.06 | 0.12 |
| MnO | 0.28 | 0.24 | 0.27 | 0.28 | 0.28 | 0.36 | 0.32 | 0.34 | 0.26 | 0.27 | 0.27 | 0.28 | 0.28 | 0.26 | 0.24 | 0.23 | 0.34 | 0.30 | 0.30 | 0.23 |
| MgO | 6.90 | 9.76 | 8.92 | 9.08 | 8.28 | 6.89 | 7.78 | 8.00 | 11.35 | 8.75 | 10.97 | 11.91 | 9.64 | 10.63 | 10.82 | 11.49 | 8.23 | 7.81 | 8.01 | 7.38 |
| Total | 99.07 | 99.47 | 99.25 | 99.16 | 99.73 | 99.53 | 99.71 | 98.82 | 99.50 | 98.63 | 98.99 | 99.96 | 99.01 | 98.80 | 98.90 | 99.37 | 99.86 | 98.20 | 99.51 | 98.12 |
| *Cations per 32 oxygens* | | | | | | | | | | | | | | | | | | | | |
| Al | 0.549 | 0.515 | 0.519 | 0.565 | 0.466 | 0.461 | 0.453 | 0.475 | 0.438 | 0.509 | 0.361 | 0.032 | 0.598 | 0.512 | 0.430 | 0.485 | 0.511 | 0.444 | 0.456 | 0.497 |
| Cr | 1.617 | 1.490 | 1.514 | 1.499 | 1.618 | 1.610 | 1.615 | 1.645 | 1.519 | 1.609 | 1.564 | 1.507 | 1.481 | 1.466 | 1.501 | 1.447 | 1.548 | 1.653 | 1.539 | 1.673 |
| $Fe_3^+$ | 0.000 | 0.000 | 0.000 | 0.000 | 0.000 | 0.000 | 0.000 | 0.000 | 0.027 | 0.000 | 0.062 | 0.032 | 0.000 | 0.007 | 0.058 | 0.051 | 0.000 | 0.000 | 0.000 | 0.000 |
| Ti | 0.006 | 0.006 | 0.100 | 0.004 | 0.010 | 0.007 | 0.008 | 0.007 | 0.008 | 0.009 | 0.007 | 0.009 | 0.005 | 0.008 | 0.005 | 0.009 | 0.007 | 0.010 | 0.010 | 0.008 |
| Mg | 0.356 | 0.478 | 0.444 | 0.448 | 0.418 | 0.351 | 0.394 | 0.409 | 0.553 | 0.446 | 0.549 | 0.574 | 0.477 | 0.520 | 0.492 | 0.557 | 0.411 | 0.404 | 0.400 | 0.385 |
| $Fe_2^+$ | 0.551 | 0.511 | 0.531 | 0.494 | 0.530 | 0.600 | 0.563 | 0.520 | 0.448 | 0.486 | 0.449 | 0.425 | 0.476 | 0.479 | 0.505 | 0.442 | 0.549 | 0.535 | 0.592 | 0.519 |
| Ni | 0.002 | 0.001 | 0.002 | 0.001 | 0.001 | 0.003 | 0.000 | 0.001 | 0.000 | 0.001 | 0.002 | 0.002 | 0.000 | 0.002 | 0.002 | 0.003 | 0.001 | 0.003 | 0.001 | 0.003 |
| Mn | 0.008 | 0.007 | 0.008 | 0.008 | 0.008 | 0.010 | 0.009 | 0.010 | 0.007 | 0.008 | 0.008 | 0.008 | 0.008 | 0.007 | 0.007 | 0.006 | 0.010 | 0.009 | 0.008 | 0.007 |
| Totals | 3.089 | 3.008 | 3.118 | 3.019 | 3.051 | 3.042 | 3.042 | 3.067 | 3.000 | 3.068 | 3.002 | 2.589 | 3.045 | 3.001 | 3.000 | 3.000 | 3.037 | 3.058 | 3.006 | 3.092 |
| $Mg/(Mg+Fe^{2+})$ | 0.393 | 0.483 | 0.455 | 0.476 | 0.441 | 0.369 | 0.412 | 0.440 | 0.552 | 0.479 | 0.550 | 0.575 | 0.501 | 0.521 | 0.493 | 0.558 | 0.428 | 0.430 | 0.403 | 0.426 |
| Cr/(Cr + Al) | 0.747 | 0.743 | 0.745 | 0.726 | 0.776 | 0.777 | 0.745 | 0.726 | 0.776 | 0.760 | 0.745 | 0.726 | 0.712 | 0.741 | 0.745 | 0.726 | 0.752 | 0.788 | 0.745 | 0.726 |
| $Fe^{2+}/(Fe^{2+}+Mg)$ | 0.607 | 0.517 | 0.545 | 0.524 | 0.559 | 0.631 | 0.588 | 0.560 | 0.448 | 0.521 | 0.450 | 0.425 | 0.499 | 0.479 | 0.507 | 0.442 | 0.572 | 0.570 | 0.597 | 0.574 |
| Ti/Cr | 0.004 | 0.004 | 0.066 | 0.003 | 0.006 | 0.004 | 0.005 | 0.004 | 0.005 | 0.006 | 0.004 | 0.006 | 0.003 | 0.005 | 0.003 | 0.006 | 0.005 | 0.006 | 0.006 | 0.005 |

## Individual Electron Microprobe Analyses of North Dyke B (Caesar) Chromite Compositions

| Analysis No. | 1 | 2 | 3 | 4 | 1 | 2 | 3 | 4 | 1 | 2 | 3 | 4 |
|---|---|---|---|---|---|---|---|---|---|---|---|---|
| Sample No. | ND16 | | | | ND17 | | | | ND18 | | | |
| $SiO_2$ | 0.00 | 0.00 | 0.00 | 0.00 | 0.00 | 0.00 | 0.00 | 0.00 | 0.00 | 0.00 | 0.00 | 0.00 |
| $TiO_2$ | 0.43 | 0.31 | 0.33 | 0.47 | 0.38 | 0.37 | 0.22 | 0.32 | 0.32 | 0.37 | 0.25 | 0.36 |
| $Al_2O_3$ | 13.77 | 13.01 | 12.9 | 12.93 | 14.62 | 14.66 | 12.65 | 15.35 | 12.71 | 12.69 | 13.64 | 13.36 |
| $Cr_2O_3$ | 55.16 | 56.33 | 56.38 | 56.14 | 57.98 | 59.8 | 58.64 | 57.67 | 57.32 | 57.65 | 57.50 | 55.87 |
| $Fe_2O_3$ | 0.59 | 2.55 | 1.05 | 0.64 | 0.00 | 0.00 | 0.00 | 0.00 | 0.00 | 0.00 | 0.00 | 2.34 |
| FeO | 20.72 | 16.39 | 17.54 | 18.33 | 16.31 | 19.21 | 18.77 | 17.81 | 19.42 | 19.24 | 19.24 | 16.09 |
| NiO | 0.11 | 0.02 | 0.13 | 0.05 | 0.05 | 0.09 | 0.05 | 0.04 | 0.04 | 0.08 | 0.04 | 0.09 |
| MnO | 0.3 | 0.28 | 0.29 | 0.27 | 0.31 | 0.29 | 0.31 | 0.28 | 0.29 | 0.38 | 0.24 | 0.28 |
| MgO | 8.81 | 11.68 | 10.58 | 10.17 | 8.81 | 7.5 | 9.34 | 8.14 | 8.92 | 9.61 | 9.80 | 11.81 |
| Total | 99.89 | 100.57 | 99.20 | 99.00 | 98.46 | 101.92 | 99.98 | 99.61 | 99.02 | 100.02 | 100.71 | 100.20 |
| *Cations per 32 oxygens* | | | | | | | | | | | | |
| Al | 0.533 | 0.493 | 0.498 | 0.501 | 0.59 | 0.596 | 0.493 | 0.628 | 0.5 | 0.49 | 0.524 | 0.506 |
| Cr | 1.431 | 1.431 | 1.46 | 1.46 | 1.568 | 1.604 | 1.531 | 1.582 | 1.512 | 1.493 | 1.48 | 1.42 |
| $Fe_3$+ | 0.015 | 0.062 | 0.026 | 0.016 | 0.000 | 0.000 | 0.000 | 0.000 | 0.000 | 0.000 | 0.000 | 0.057 |
| Ti | 0.011 | 0.007 | 0.008 | 0.012 | 0.01 | 0.01 | 0.005 | 0.008 | 0.008 | 0.009 | 0.006 | 0.009 |
| Mg | 0.431 | 0.559 | 0.516 | 0.499 | 0.45 | 0.334 | 0.46 | 0.369 | 0.443 | 0.469 | 0.466 | 0.566 |
| $Fe_2$+ | 0.569 | 0.44 | 0.48 | 0.504 | 0.461 | 0.555 | 0.519 | 0.517 | 0.542 | 0.527 | 0.524 | 0.433 |
| Ni | 0.003 | 0.001 | 0.003 | 0.001 | 0.001 | 0.002 | 0.001 | 0.001 | 0.001 | 0.002 | 0.001 | 0.002 |
| Mn | 0.008 | 0.008 | 0.008 | 0.007 | 0.009 | 0.009 | 0.009 | 0.008 | 0.008 | 0.011 | 0.007 | 0.008 |
| | 3.001 | 3.001 | 2.999 | 3 | 3.089 | 3.11 | 3.018 | 3.113 | 3.014 | 3.001 | 3.008 | 3.001 |
| $Mg/(Mg+Fe^{2+})$ | 0.431 | 0.560 | 0.518 | 0.498 | 0.494 | 0.376 | 0.470 | 0.416 | 0.450 | 0.471 | 0.471 | 0.567 |
| Cr/(Cr + Al) | 0.729 | 0.744 | 0.745 | 0.726 | 0.727 | 0.729 | 0.745 | 0.726 | 0.751 | 0.753 | 0.745 | 0.726 |
| $Fe^{2+}/(Fe_2^{+} + Mg)$ | 0.569 | 0.440 | 0.482 | 0.502 | 0.506 | 0.624 | 0.530 | 0.584 | 0.550 | 0.529 | 0.529 | 0.433 |
| Ti/Cr | 0.008 | 0.005 | 0.005 | 0.008 | 0.006 | 0.006 | 0.003 | 0.005 | 0.005 | 0.006 | 0.004 | 0.006 |

## Individual Average Electron Microprobe Analyses of Great Dyke Chromite Compositions

| | South Dyke | | | | Middle Dyke | | | | North Dyke A (JESTER) | | | | North Dyke B (CAESAR) | | | |
|---|---|---|---|---|---|---|---|---|---|---|---|---|---|---|---|---|
| Analysis No. | 1 | 2 | 3 | 4 | 5 | 6 | 7 | 8 | 9 | 10 | 11 | 12 | 13 | 14 | 15 | 16 |
| Sample No. | SD1 | | | | MD19 | | | | NDA8 | | | | NDB16 | | | |
| $SiO_2$ | 0.00 | 0.00 | 0.00 | 0.00 | 0.00 | 0.00 | 0.00 | 0.00 | 0.00 | 0.00 | 0.00 | 0.00 | 0.00 | 0.00 | 0.00 | 0.00 |
| $TiO_2$ | 0.53 | 0.23 | 0.36 | 0.28 | 0.33 | 0.36 | 0.46 | 0.27 | 0.24 | 0.23 | 0.41 | 0.15 | 0.43 | 0.31 | 0.33 | 0.47 |
| $Al_2O_3$ | 11.13 | 12.19 | 12.50 | 11.34 | 17.14 | 15.44 | 14.04 | 16.22 | 13.43 | 13.29 | 13.19 | 14.48 | 13.77 | 13.01 | 12.9 | 12.93 |
| $Cr_2O_3$ | 58.54 | 57.51 | 58.03 | 59.03 | 51.26 | 52.01 | 53.66 | 52.47 | 59.11 | 57.30 | 57.38 | 57.27 | 55.16 | 56.33 | 56.38 | 56.14 |
| $Fe_2O_3$ | 0.00 | 0.00 | 0.00 | 0.00 | 1.25 | 2.05 | 2.6 | 2.21 | 0.00 | 0.00 | 0.00 | 0.00 | 0.59 | 2.55 | 1.05 | 0.64 |
| FeO | 23.01 | 20.35 | 21.07 | 22.17 | 18.99 | 18.2 | 17.81 | 17.63 | 19.03 | 18.60 | 19.02 | 17.85 | 20.72 | 16.39 | 17.54 | 18.33 |
| NiO | 0.08 | 0.06 | 0.07 | 0.09 | 0.07 | 0.07 | 0.15 | 0 | 0.08 | 0.05 | 0.06 | 0.05 | 0.11 | 0.02 | 0.13 | 0.05 |
| MnO | 0.25 | 0.22 | 0.27 | 0.33 | 0.29 | 0.26 | 0.25 | 0.23 | 0.28 | 0.24 | 0.27 | 0.28 | 0.3 | 0.28 | 0.29 | 0.27 |
| MgO | 6.39 | 7.86 | 7.06 | 6.17 | 10.16 | 10.39 | 10.69 | 11.14 | 6.90 | 9.76 | 8.92 | 9.08 | 8.81 | 11.68 | 10.58 | 10.17 |
| Total | 99.93 | 98.42 | 99.36 | 99.41 | 99.49 | 98.78 | 99.66 | 100.17 | 99.07 | 99.47 | 99.25 | 99.16 | 99.89 | 100.57 | 99.20 | 99.00 |
| *Cations per 32 oxygens* | | | | | | | | | | | | | | | | |
| Al | 0.45 | 0.45 | 0.50 | 0.46 | 0.447 | 0.448 | 0.502 | 0.460 | 0.549 | 0.515 | 0.519 | 0.565 | 0.533 | 0.493 | 0.498 | 0.501 |
| Cr | 1.58 | 1.54 | 1.56 | 1.61 | 1.576 | 1.544 | 1.562 | 1.606 | 1.617 | 1.490 | 1.514 | 1.499 | 1.431 | 1.431 | 1.46 | 1.46 |
| $Fe_3$+ | 0.00 | 0.00 | 0.00 | 0.00 | 0.000 | 0.000 | 0.000 | 0.000 | 0.000 | 0.000 | 0.000 | 0.000 | 0.015 | 0.062 | 0.026 | 0.016 |
| Ti | 0.01 | 0.01 | 0.01 | 0.01 | 0.014 | 0.008 | 0.009 | 0.007 | 0.006 | 0.006 | 0.100 | 0.004 | 0.011 | 0.007 | 0.008 | 0.012 |
| Mg | 0.32 | 0.40 | 0.36 | 0.32 | 0.324 | 0.398 | 0.358 | 0.316 | 0.356 | 0.478 | 0.444 | 0.448 | 0.431 | 0.559 | 0.516 | 0.499 |
| $Fe_2$+ | 0.66 | 0.58 | 0.60 | 0.64 | 0.655 | 0.578 | 0.600 | 0.638 | 0.551 | 0.511 | 0.531 | 0.494 | 0.569 | 0.44 | 0.48 | 0.504 |
| Ni | 0.00 | 0.00 | 0.00 | 0.00 | 0.002 | 0.002 | 0.002 | 0.002 | 0.002 | 0.001 | 0.002 | 0.001 | 0.003 | 0.001 | 0.003 | 0.001 |
| Mn | 0.01 | 0.01 | 0.01 | 0.01 | 0.007 | 0.006 | 0.008 | 0.010 | 0.008 | 0.007 | 0.008 | 0.008 | 0.008 | 0.008 | 0.008 | 0.007 |
| Totals | 3.03 | 2.98 | 3.04 | 3.04 | 3.025 | 2.984 | 3.041 | 3.039 | 3.089 | 3.008 | 3.118 | 3.019 | 3.001 | 3.001 | 2.999 | 3 |
| $Mg/(Mg+Fe^{2+})$ | 0.331 | 0.408 | 0.374 | 0.331 | 0.331 | 0.408 | 0.374 | 0.331 | 0.393 | 0.483 | 0.455 | 0.476 | 0.431 | 0.560 | 0.518 | 0.498 |
| Cr/(Cr + Al) | 0.779 | 0.775 | 0.745 | 0.726 | 0.779 | 0.775 | 0.745 | 0.726 | 0.747 | 0.743 | 0.745 | 0.726 | 0.729 | 0.744 | 0.745 | 0.726 |
| $Fe^{2+}/(Fe_2^{+}$ + Mg) | 0.669 | 0.592 | 0.626 | 0.669 | 0.669 | 0.592 | 0.626 | 0.669 | 0.607 | 0.517 | 0.545 | 0.524 | 0.569 | 0.440 | 0.482 | 0.502 |
| Ti/Cr | 0.009 | 0.005 | 0.006 | 0.004 | 0.009 | 0.005 | 0.006 | 0.004 | 0.004 | 0.004 | 0.066 | 0.003 | 0.008 | 0.005 | 0.005 | 0.008 |

## Individual Average Electron Microprobe Analyses of Great Dyke Chromite Compositions

| | South Dyke | | | | Middle Dyke | | | | North Dyke A (JESTER) | | | | North Dyke B (CAESAR) | | | |
|---|---|---|---|---|---|---|---|---|---|---|---|---|---|---|---|---|
| Analysis No. | 1 | 2 | 3 | 4 | 13 | 14 | 15 | 16 | 5 | 6 | 7 | 8 | 9 | 10 | 11 | 12 |
| Sample No. | SD2 | | | | MD20 | | | | NDA9 | | | | NDB17 | | | |
| $SiO_2$ | 0.00 | 0.00 | 0.00 | 0.00 | 0.00 | 0.00 | 0.00 | 0.00 | 0.00 | 0.00 | 0.00 | 0.00 | 0.00 | 0.00 | 0.00 | 0.00 |
| $TiO_2$ | 0.31 | 0.31 | 0.39 | 0.32 | 0.44 | 0.32 | 0.20 | 0.39 | 0.39 | 0.27 | 0.30 | 0.28 | 0.38 | 0.37 | 0.22 | 0.32 |
| $Al_2O_3$ | 12.82 | 15.65 | 14.71 | 12.65 | 21.88 | 11.44 | 18.27 | 17.00 | 11.67 | 11.44 | 11.32 | 11.76 | 14.62 | 14.66 | 12.65 | 15.35 |
| $Cr_2O_3$ | 57.90 | 58.65 | 57.12 | 57.86 | 47.28 | 51.76 | 53.01 | 52.26 | 60.38 | 59.51 | 60.16 | 60.27 | 57.98 | 59.8 | 58.64 | 57.67 |
| $Fe_2O_3$ | 0.00 | 0.00 | 0.00 | 0.00 | 0 | 0.96 | 0.00 | 0.00 | 0.00 | 0.00 | 0.00 | 0.00 | 0.00 | 0.00 | 0.00 | 0.00 |
| FeO | 20.64 | 18.91 | 18.79 | 18.79 | 21.26 | 19.99 | 19.56 | 20.81 | 18.70 | 20.97 | 19.82 | 18.13 | 16.31 | 19.21 | 18.77 | 17.81 |
| NiO | 0.01 | 0.04 | 0.00 | 0.05 | 0.13 | 0.03 | 0.07 | 0.10 | 0.03 | 0.09 | 0.01 | 0.04 | 0.05 | 0.09 | 0.05 | 0.04 |
| MnO | 0.34 | 0.26 | 0.30 | 0.27 | 0.27 | 0.22 | 0.27 | 0.21 | 0.28 | 0.36 | 0.32 | 0.34 | 0.31 | 0.29 | 0.31 | 0.28 |
| MgO | 6.09 | 5.95 | 7.45 | 9.67 | 8.62 | 9.44 | 8.58 | 8.27 | 8.28 | 6.89 | 7.78 | 8.00 | 8.81 | 7.5 | 9.34 | 8.14 |
| Total | 98.11 | 99.77 | 98.76 | 99.61 | 99.88 | 94.16 | 99.96 | 99.04 | 99.73 | 99.53 | 99.71 | 98.82 | 98.46 | 101.92 | 99.98 | 99.61 |
| *Cations per 32 oxygens* | | | | | | | | | | | | | | | | |
| Al | 0.52 | 0.64 | 0.60 | 0.49 | 0.825 | 0.63 | 0.706 | 0.661 | 0.466 | 0.461 | 0.453 | 0.475 | 0.59 | 0.596 | 0.493 | 0.628 |
| Cr | 1.59 | 1.62 | 1.55 | 1.51 | 1.195 | 1.331 | 1.375 | 1.362 | 1.618 | 1.610 | 1.615 | 1.645 | 1.568 | 1.604 | 1.531 | 1.582 |
| $Fe_3$+ | 0.00 | 0.00 | 0.00 | 0.00 | 0 | 0.023 | 0 | 0 | 0.000 | 0.000 | 0.000 | 0.000 | 0.000 | 0.000 | 0.000 | 0.000 |
| Ti | 0.01 | 0.01 | 0.01 | 0.01 | 0.011 | 0.008 | 0.005 | 0.01 | 0.010 | 0.007 | 0.008 | 0.007 | 0.01 | 0.01 | 0.005 | 0.008 |
| Mg | 0.31 | 0.31 | 0.38 | 0.48 | 0.411 | 0.457 | 0.415 | 0.406 | 0.418 | 0.351 | 0.394 | 0.409 | 0.45 | 0.334 | 0.46 | 0.369 |
| $Fe_2$+ | 0.60 | 0.55 | 0.54 | 0.52 | 0.569 | 0.544 | 0.536 | 0.574 | 0.530 | 0.600 | 0.563 | 0.520 | 0.461 | 0.555 | 0.519 | 0.517 |
| Ni | 0.00 | 0.00 | 0.00 | 0.00 | 0.003 | 0.001 | 0.002 | 0.003 | 0.001 | 0.003 | 0.000 | 0.001 | 0.001 | 0.002 | 0.001 | 0.001 |
| Mn | 0.01 | 0.01 | 0.01 | 0.01 | 0.007 | 0.006 | 0.008 | 0.006 | 0.008 | 0.010 | 0.009 | 0.010 | 0.009 | 0.009 | 0.009 | 0.008 |
| Totals | 3.04 | 3.14 | 3.08 | 3.01 | 3.021 | 3.000 | 3.047 | 3.022 | 3.051 | 3.042 | 3.042 | 3.067 | 3.089 | 3.11 | 3.018 | 3.113 |
| $Mg/(Mg+Fe^{2+})$ | 0.344 | 0.359 | 0.414 | 0.479 | 0.419 | 0.457 | 0.436 | 0.414 | 0.441 | 0.369 | 0.412 | 0.440 | 0.494 | 0.376 | 0.470 | 0.416 |
| Cr/(Cr + Al) | 0.752 | 0.715 | 0.745 | 0.726 | 0.592 | 0.679 | 0.745 | 0.726 | 0.776 | 0.777 | 0.745 | 0.726 | 0.727 | 0.729 | 0.745 | 0.726 |
| $Fe^{2+}/(Fe_2^{+}+ Mg)$ | 0.656 | 0.641 | 0.586 | 0.521 | 0.581 | 0.543 | 0.564 | 0.586 | 0.559 | 0.631 | 0.588 | 0.560 | 0.506 | 0.624 | 0.530 | 0.584 |
| Ti/Cr | 0.005 | 0.005 | 0.006 | 0.005 | 0.009 | 0.006 | 0.004 | 0.007 | 0.006 | 0.004 | 0.005 | 0.004 | 0.006 | 0.006 | 0.003 | 0.005 |

## Individual Average Electron Microprobe Analyses of Great Dyke Chromite Compositions

| | South Dyke | | | | Middle Dyke | | | | North Dyke A (JESTER) | | | | North Dyke B (CAESAR) | | | |
|---|---|---|---|---|---|---|---|---|---|---|---|---|---|---|---|---|
| Analysis No. | 1 | 2 | 3 | 4 | 13 | 14 | 15 | 16 | 5 | 6 | 7 | 8 | 9 | 10 | 11 | 12 |
| Sample No. | SD3 | | | | MD21 | | | | NDA10 | | | | NDB18 | | | |
| $SiO_2$ | 0.00 | 0.00 | 0.00 | 0.00 | 0.00 | 0.00 | 0.00 | 0.00 | 0.00 | 0.00 | 0.00 | 0.00 | 0.00 | 0.00 | 0.00 | 0.00 |
| $TiO_2$ | 0.38 | 0.34 | 0.35 | 0.33 | 0.37 | 0.61 | 0.34 | 0.61 | 0.33 | 0.34 | 0.27 | 0.37 | 0.32 | 0.37 | 0.25 | 0.36 |
| $Al_2O_3$ | 11.18 | 11.59 | 14.04 | 13.92 | 16.34 | 15.00 | 15.04 | 16.23 | 11.36 | 12.65 | 10.11 | 11.67 | 12.71 | 12.69 | 13.64 | 13.36 |
| $Cr_2O_3$ | 57.89 | 58.02 | 57.66 | 58.11 | 52.84 | 52.15 | 52.87 | 52.22 | 58.74 | 59.56 | 58.90 | 58.63 | 57.32 | 57.65 | 57.50 | 55.87 |
| $Fe_2O_3$ | 0.00 | 0.00 | 0.00 | 0.00 | 0.00 | 0.00 | 0.26 | 0.00 | 1.09 | 0.00 | 2.44 | 1.31 | 0.00 | 0.00 | 0.00 | 2.34 |
| FeO | 22.21 | 19.67 | 20.20 | 20.75 | 19.01 | 23.55 | 22.64 | 20.57 | 16.37 | 17.01 | 15.97 | 15.71 | 19.42 | 19.24 | 19.24 | 16.09 |
| NiO | 0.10 | 0.14 | 0.12 | 0.12 | 0.12 | 0.10 | 0.05 | 0.08 | 0.00 | 0.05 | 0.06 | 0.08 | 0.04 | 0.08 | 0.04 | 0.09 |
| MnO | 0.30 | 0.24 | 0.27 | 0.31 | 0.28 | 0.37 | 0.35 | 0.29 | 0.26 | 0.27 | 0.27 | 0.28 | 0.29 | 0.38 | 0.24 | 0.28 |
| MgO | 7.04 | 9.02 | 6.87 | 6.55 | 9.94 | 7.09 | 7.45 | 7.99 | 11.35 | 8.75 | 10.97 | 11.91 | 8.92 | 9.61 | 9.80 | 11.81 |
| Total | 99.10 | 99.02 | 99.51 | 100.09 | 98.90 | 98.87 | 99.00 | 97.99 | 99.50 | 98.63 | 98.99 | 99.96 | 99.02 | 100.02 | 100.71 | 100.20 |
| *Cations per 32 oxygens* | | | | | | | | | | | | | | | | |
| Al | 0.49 | 0.46 | 0.57 | 0.56 | 0.626 | 0.586 | 0.589 | 0.619 | 0.438 | 0.509 | 0.361 | 0.032 | 0.5 | 0.49 | 0.524 | 0.506 |
| Cr | 1.56 | 1.53 | 1.56 | 1.57 | 1.357 | 1.366 | 1.388 | 1.458 | 1.519 | 1.609 | 1.564 | 1.507 | 1.512 | 1.493 | 1.48 | 1.42 |
| $Fe_3$+ | 0.00 | 0.00 | 0.00 | 0.00 | 0 | 0.018 | 0.007 | 0 | 0.027 | 0.000 | 0.062 | 0.032 | 0.000 | 0.000 | 0.000 | 0.057 |
| Ti | 0.01 | 0.01 | 0.01 | 0.01 | 0.009 | 0.015 | 0.008 | 0.007 | 0.008 | 0.009 | 0.007 | 0.009 | 0.008 | 0.009 | 0.006 | 0.009 |
| Mg | 0.36 | 0.45 | 0.35 | 0.33 | 0.481 | 0.35 | 0.369 | 0.39 | 0.553 | 0.446 | 0.549 | 0.574 | 0.443 | 0.469 | 0.466 | 0.566 |
| $Fe_2$+ | 0.63 | 0.55 | 0.58 | 0.59 | 0.517 | 0.653 | 0.629 | 0.564 | 0.448 | 0.486 | 0.449 | 0.425 | 0.542 | 0.527 | 0.524 | 0.433 |
| Ni | 0.00 | 0.00 | 0.00 | 0.00 | 0.003 | 0.003 | 0.001 | 0 | 0.000 | 0.001 | 0.002 | 0.002 | 0.001 | 0.002 | 0.001 | 0.002 |
| Mn | 0.01 | 0.01 | 0.01 | 0.01 | 0.008 | 0.01 | 0.01 | 0.008 | 0.007 | 0.008 | 0.008 | 0.008 | 0.008 | 0.011 | 0.007 | 0.008 |
| Totals | 3.06 | 3.00 | 3.07 | 3.07 | 3.001 | 3.001 | 3.001 | 3.046 | 3.000 | 3.068 | 3.002 | 2.589 | 3.014 | 3.001 | 3.008 | 3.001 |
| $Mg/(Mg+Fe^{2+})$ | 0.361 | 0.449 | 0.378 | 0.360 | 0.482 | 0.349 | 0.370 | 0.409 | 0.552 | 0.479 | 0.550 | 0.575 | 0.450 | 0.471 | 0.471 | 0.567 |
| Cr/(Cr + Al) | 0.760 | 0.770 | 0.745 | 0.726 | 0.684 | 0.700 | 0.745 | 0.726 | 0.776 | 0.760 | 0.745 | 0.726 | 0.751 | 0.753 | 0.745 | 0.726 |
| $Fe^{2}$+/($Fe_2$+ + Mg) | 0.639 | 0.551 | 0.622 | 0.640 | 0.518 | 0.651 | 0.630 | 0.591 | 0.448 | 0.521 | 0.450 | 0.425 | 0.550 | 0.529 | 0.529 | 0.433 |
| Ti/Cr | 0.006 | 0.006 | 0.006 | 0.005 | 0.007 | 0.011 | 0.006 | 0.005 | 0.005 | 0.006 | 0.004 | 0.006 | 0.005 | 0.006 | 0.004 | 0.006 |

## Individual Average Electron Microprobe Analyses of Great Dyke Chromite Compositions

| | South Dyke | | | | Middle Dyke | | | | North Dyke A (JESTER) | | | | North Dyke B (CAESAR) | | | |
|---|---|---|---|---|---|---|---|---|---|---|---|---|---|---|---|---|
| Analysis No. | 1 | 2 | 3 | 4 | 13 | 14 | 15 | 16 | 5 | 6 | 7 | 8 | 9 | 10 | 11 | 12 |
| Sample No. | | | | | MD22 | | | | NDA11 | | | | | | | |
| $SiO_2$ | 0.00 | 0.00 | 0.00 | 0.00 | 0.00 | 0.00 | 0.00 | 0.00 | 0.00 | 0.00 | 0.00 | 0.00 | | | | |
| $TiO_2$ | 0.31 | 0.34 | 0.34 | 0.38 | 0.42 | 0.42 | 0.44 | 0.39 | 0.21 | 0.32 | 0.21 | 0.35 | | | | |
| $Al_2O_3$ | 12.57 | 11.89 | 12.55 | 13.71 | 15.86 | 16.58 | 19.20 | 15.79 | 15.28 | 13.28 | 10.85 | 12.63 | | | | |
| $Cr_2O_3$ | 59.48 | 57.55 | 55.46 | 54.50 | 53.96 | 52.84 | 52.21 | 54.88 | 56.45 | 56.52 | 56.48 | 56.23 | | | | |
| $Fe_2O_3$ | 0.00 | 0.00 | 1.64 | 0.72 | 0.00 | 0.00 | 0.00 | 0.00 | 0.00 | 0.27 | 2.28 | 2.10 | | | | |
| FeO | 19.47 | 22.11 | 20.45 | 22.04 | 20.18 | 21.16 | 18.15 | 17.87 | 17.15 | 17.45 | 17.96 | 16.23 | | | | |
| NiO | 0.11 | 0.10 | 0.05 | 0.12 | 0.10 | 0.00 | 0.16 | 0.00 | 0.00 | 0.07 | 0.06 | 0.11 | | | | |
| MnO | 0.31 | 0.24 | 0.27 | 0.21 | 0.32 | 0.30 | 0.24 | 0.27 | 0.28 | 0.26 | 0.24 | 0.23 | | | | |
| MgO | 7.95 | 7.51 | 8.77 | 7.88 | 8.86 | 7.74 | 9.45 | 9.53 | 9.64 | 10.63 | 10.82 | 11.49 | | | | |
| Total | 100.2 | 99.74 | 99.53 | 99.56 | 99.70 | 99.04 | 99.85 | 98.73 | 99.01 | 98.80 | 98.90 | 99.37 | | | | |
| *Cations per 32 oxygens* | | | | | | | | | | | | | | | | |
| Al | 0.47 | 0.50 | 0.49 | 0.54 | 0.612 | 0.65 | 0.736 | 0.616 | 0.598 | 0.512 | 0.430 | 0.485 | | | | |
| Cr | 1.52 | 1.58 | 1.45 | 1.43 | 1.396 | 1.389 | 1.341 | 1.437 | 1.481 | 1.466 | 1.501 | 1.447 | | | | |
| $Fe_3$+ | 0.00 | 0.00 | 0.04 | 0.02 | 0 | 0 | 0 | 0 | 0.000 | 0.007 | 0.058 | 0.051 | | | | |
| Ti | 0.01 | 0.01 | 0.01 | 0.01 | 0.01 | 0.01 | 0.011 | 0.01 | 0.005 | 0.008 | 0.005 | 0.009 | | | | |
| Mg | 0.38 | 0.40 | 0.43 | 0.39 | 0.432 | 0.384 | 0.457 | 0.471 | 0.477 | 0.520 | 0.492 | 0.557 | | | | |
| $Fe_2$+ | 0.62 | 0.55 | 0.57 | 0.61 | 0.552 | 0.588 | 0.493 | 0.495 | 0.476 | 0.479 | 0.505 | 0.442 | | | | |
| Ni | 0.00 | 0.00 | 0.00 | 0.00 | 0.003 | 0 | 0.004 | 0 | 0.000 | 0.002 | 0.002 | 0.003 | | | | |
| Mn | 0.01 | 0.01 | 0.01 | 0.01 | 0.009 | 0.008 | 0.007 | 0.008 | 0.008 | 0.007 | 0.007 | 0.006 | | | | |
| Totals | 3.00 | 3.05 | 3.00 | 3.00 | 3.014 | 3.029 | 3.049 | 3.037 | 3.045 | 3.001 | 3.000 | 3.000 | | | | |
| $Mg/(Mg+Fe^{2+})$ | 0.377 | 0.421 | 0.433 | 0.389 | 0.439 | 0.395 | 0.481 | 0.488 | 0.501 | 0.521 | 0.493 | 0.558 | | | | |
| Cr/(Cr + Al) | 0.765 | 0.760 | 0.745 | 0.726 | 0.695 | 0.681 | 0.745 | 0.726 | 0.712 | 0.741 | 0.745 | 0.726 | | | | |
| $Fe^2_+/(Fe_2^+ + Mg)$ | 0.623 | 0.579 | 0.567 | 0.611 | 0.561 | 0.605 | 0.519 | 0.512 | 0.499 | 0.479 | 0.507 | 0.442 | | | | |
| Ti/Cr | 0.005 | 0.004 | 0.006 | 0.006 | 0.007 | 0.007 | 0.008 | 0.007 | 0.003 | 0.005 | 0.003 | 0.006 | | | | |

## Individual Average Electron Microprobe Analyses of Great Dyke Chromite Compositions

| | South Dyke | | | | Middle Dyke | | | | North Dyke A (JESTER) | | | | North Dyke B (CAESAR) | | | |
|---|---|---|---|---|---|---|---|---|---|---|---|---|---|---|---|---|
| Analysis No. | 1 | 2 | 3 | 4 | 13 | 14 | 15 | 16 | 5 | 6 | 7 | 8 | 9 | 10 | 11 | 12 |
| Sample No. | SD5 | | | | MD23 | | | | NDA12 | | | | | | | |
| $SiO_2$ | 0.00 | 0.00 | 0.00 | 0.00 | 0.00 | 0.00 | 0.00 | 0.00 | 0.00 | 0.00 | 0.00 | 0.00 | | | | |
| $TiO_2$ | 0.32 | 0.32 | 0.32 | 0.24 | 0.37 | 0.45 | 0.42 | 0.43 | 0.29 | 0.39 | 0.41 | 0.30 | | | | |
| $Al_2O_3$ | 12.15 | 11.56 | 10.30 | 12.97 | 14.92 | 14.51 | 13.29 | 15.05 | 12.94 | 10.87 | 11.53 | 12.02 | | | | |
| $Cr_2O_3$ | 57.00 | 57.21 | 57.23 | 57.76 | 53.91 | 52.91 | 53.02 | 51.94 | 58.44 | 60.26 | 58.07 | 60.35 | | | | |
| $Fe_2O_3$ | 0.02 | 0.00 | 2.42 | 0.00 | 1.19 | 2.74 | 5.43 | 2.72 | 0.00 | 0.00 | 0.00 | 0.00 | | | | |
| FeO | 22.01 | 22.37 | 19.57 | 21.77 | 19.38 | 19.79 | 15.58 | 19.12 | 19.59 | 18.45 | 21.13 | 17.72 | | | | |
| NiO | 0.06 | 0.00 | 0.17 | 0.09 | 0.00 | 0.00 | 0.18 | 0.00 | 0.05 | 0.12 | 0.06 | 0.12 | | | | |
| MnO | 0.31 | 0.30 | 0.27 | 0.36 | 0.26 | 0.31 | 0.25 | 0.30 | 0.34 | 0.30 | 0.30 | 0.23 | | | | |
| MgO | 7.68 | 7.35 | 8.97 | 6.20 | 9.85 | 9.63 | 12.13 | 9.95 | 8.23 | 7.81 | 8.01 | 7.38 | | | | |
| Total | 99.55 | 99.11 | 99.25 | 99.39 | 99.88 | 100.34 | 100.30 | 99.51 | 99.88 | 98.20 | 99.51 | 98.12 | | | | |
| *Cations per 32 oxygens* | | | | | | | | | | | | | | | | |
| Al | 0.48 | 0.46 | 0.41 | 0.53 | 0.57 | 0.555 | 0.503 | 0.577 | 0.511 | 0.444 | 0.456 | 0.497 | | | | |
| Cr | 1.51 | 1.52 | 1.52 | 1.57 | 1.383 | 1.357 | 1.346 | 1.336 | 1.548 | 1.653 | 1.539 | 1.673 | | | | |
| $Fe_3$+ | 0.00 | 0.00 | 0.06 | 0.00 | 0.029 | 0.067 | 0.131 | 0.066 | 0.000 | 0.000 | 0.000 | 0.000 | | | | |
| Ti | 0.01 | 0.01 | 0.01 | 0.01 | 0.009 | 0.011 | 0.01 | 0.01 | 0.007 | 0.010 | 0.010 | 0.008 | | | | |
| Mg | 0.38 | 0.37 | 0.45 | 0.32 | 0.476 | 0.466 | 0.58 | 0.482 | 0.411 | 0.404 | 0.400 | 0.385 | | | | |
| $Fe_2$+ | 0.62 | 0.63 | 0.55 | 0.62 | 0.526 | 0.537 | 0.418 | 0.52 | 0.549 | 0.535 | 0.592 | 0.519 | | | | |
| Ni | 0.00 | 0.00 | 0.01 | 0.00 | 0 | 0 | 0.005 | 0 | 0.001 | 0.003 | 0.001 | 0.003 | | | | |
| Mn | 0.01 | 0.01 | 0.01 | 0.01 | 0.007 | 0.008 | 0.007 | 0.008 | 0.010 | 0.009 | 0.008 | 0.007 | | | | |
| Totals | 3.00 | 3.00 | 3.00 | 3.05 | 3.000 | 3.001 | 3.000 | 2.999 | 3.037 | 3.058 | 3.006 | 3.092 | | | | |
| $Mg/(Mg+Fe^{2+})$ | 0.383 | 0.369 | 0.449 | 0.337 | 0.475 | 0.465 | 0.581 | 0.481 | 0.428 | 0.430 | 0.403 | 0.426 | | | | |
| Cr/(Cr + Al) | 0.759 | 0.768 | 0.745 | 0.726 | 0.708 | 0.710 | 0.745 | 0.726 | 0.752 | 0.788 | 0.745 | 0.726 | | | | |
| $Fe^{2}$+/($Fe_2$ + Mg) | 0.617 | 0.631 | 0.551 | 0.663 | 0.525 | 0.535 | 0.419 | 0.519 | 0.572 | 0.570 | 0.597 | 0.574 | | | | |
| Ti/Cr | 0.005 | 0.005 | 0.005 | 0.004 | 0.007 | 0.008 | 0.007 | 0.007 | 0.005 | 0.006 | 0.006 | 0.005 | | | | |

## Individual Average Electron Microprobe Analyses of Great Dyke Chromite Compositions

| | South Dyke | | | | Middle Dyke | | | | North Dyke A (JESTER) | | | | North Dyke B (CAESAR) | | | |
|---|---|---|---|---|---|---|---|---|---|---|---|---|---|---|---|---|
| Analysis No. | 1 | 2 | 3 | 4 | 13 | 14 | 15 | 16 | 5 | 6 | 7 | 8 | 9 | 10 | 11 | 12 |
| Sample No. | | | | | MD24 | | | | | | | | | | | |
| $SiO_2$ | | | | | 0.00 | 0.00 | 0.00 | 0.00 | | | | | | | | |
| $TiO_2$ | | | | | 0.20 | 0.66 | 0.34 | 0.37 | | | | | | | | |
| $Al_2O_3$ | | | | | 18.88 | 17.75 | 17.29 | 14.13 | | | | | | | | |
| $Cr_2O_3$ | | | | | 50.63 | 50.45 | 51.57 | 53.48 | | | | | | | | |
| $Fe_2O_3$ | | | | | 1.51 | 1.18 | 0.40 | 1.48 | | | | | | | | |
| FeO | | | | | 16.86 | 18.84 | 21.68 | 21.43 | | | | | | | | |
| NiO | | | | | 0.00 | 0.16 | 0.00 | 0.00 | | | | | | | | |
| MnO | | | | | 0.30 | 0.28 | 0.34 | 0.31 | | | | | | | | |
| MgO | | | | | 11.85 | 10.55 | 8.60 | 8.32 | | | | | | | | |
| Total | | | | | 100.23 | 99.87 | 100.22 | 99.52 | | | | | | | | |
| *Cations per 32 oxygens* | | | | | | | | | | | | | | | | |
| Al | | | | | 0.699 | 0.668 | 0.658 | 0.55 | | | | | | | | |
| Cr | | | | | 1.256 | 1.272 | 1.316 | 1.395 | | | | | | | | |
| $Fe_3+$ | | | | | 0.036 | 0.028 | 0.01 | 0.037 | | | | | | | | |
| Ti | | | | | 0.005 | 0.016 | 0.008 | 0.009 | | | | | | | | |
| Mg | | | | | 0.554 | 0.502 | 0.414 | 0.409 | | | | | | | | |
| $Fe_2+$ | | | | | 0.443 | 0.503 | 0.585 | 0.592 | | | | | | | | |
| Ni | | | | | 0 | 0.004 | 0 | 0 | | | | | | | | |
| Mn | | | | | 0.008 | 0.008 | 0.009 | 0.009 | | | | | | | | |
| Totals | | | | | 3.001 | 3.001 | 3.000 | 3.001 | | | | | | | | |
| $Mg/(Mg+Fe^{2+})$ | | | | | 0.556 | 0.500 | 0.414 | 0.409 | | | | | | | | |
| Cr/(Cr + Al) | | | | | 0.642 | 0.656 | 0.745 | 0.726 | | | | | | | | |
| $Fe^{2+}/(Fe_2{}^{+} + Mg)$ | | | | | 0.444 | 0.500 | 0.586 | 0.591 | | | | | | | | |
| Ti/Cr | | | | | 0.004 | 0.013 | 0.006 | 0.006 | | | | | | | | |

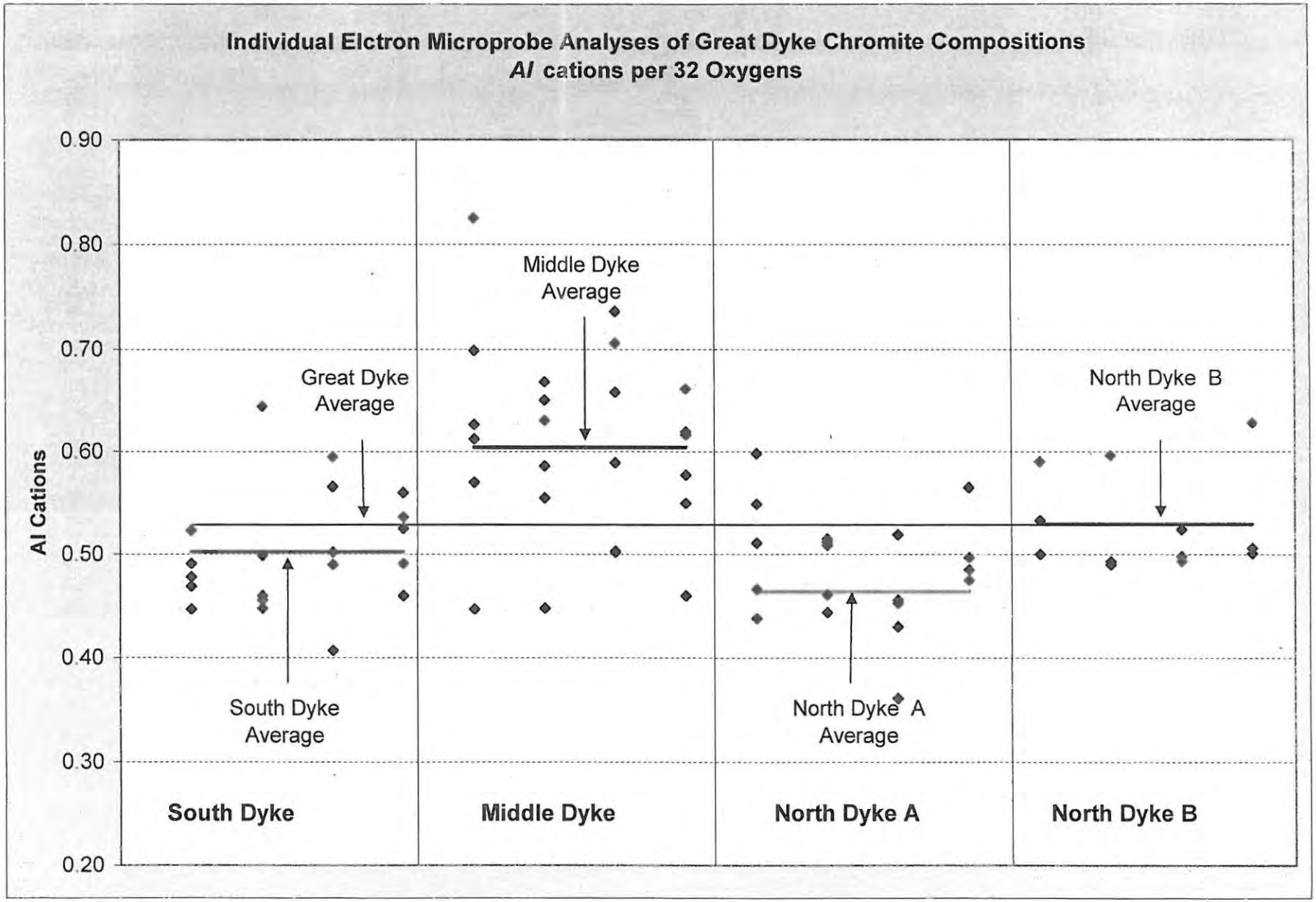
Individual Elctron Microprobe Analyses of Great Dyke Chromite Compositions
Al cations per 32 Oxygens
Al Cations
0.90
0.80
0.70
0.60
0.50
0.40
0.30
0.20
Middle Dyke Average
Great Dyke Average
North Dyke B Average
South Dyke Average
North Dyke A Average
South Dyke
Middle Dyke
North Dyke A
North Dyke B

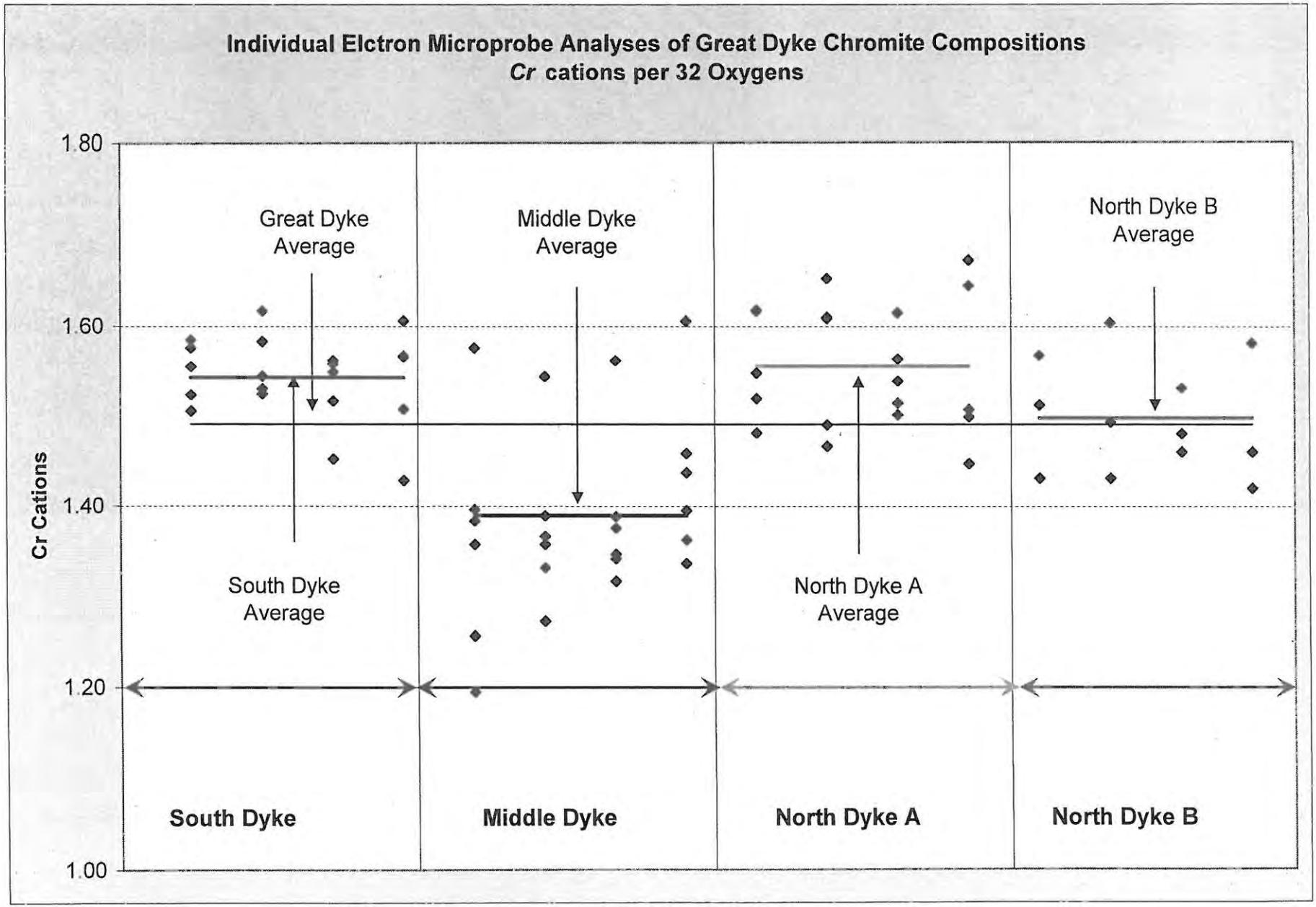
Individual Elctron Microprobe Analyses of Great Dyke Chromite Compositions
Cr cations per 32 Oxygens
Cr Cations
1.80
1.60
1.40
1.20
1.00
Great Dyke Average
Middle Dyke Average
North Dyke B Average
South Dyke Average
North Dyke A Average
South Dyke
Middle Dyke
North Dyke A
North Dyke B

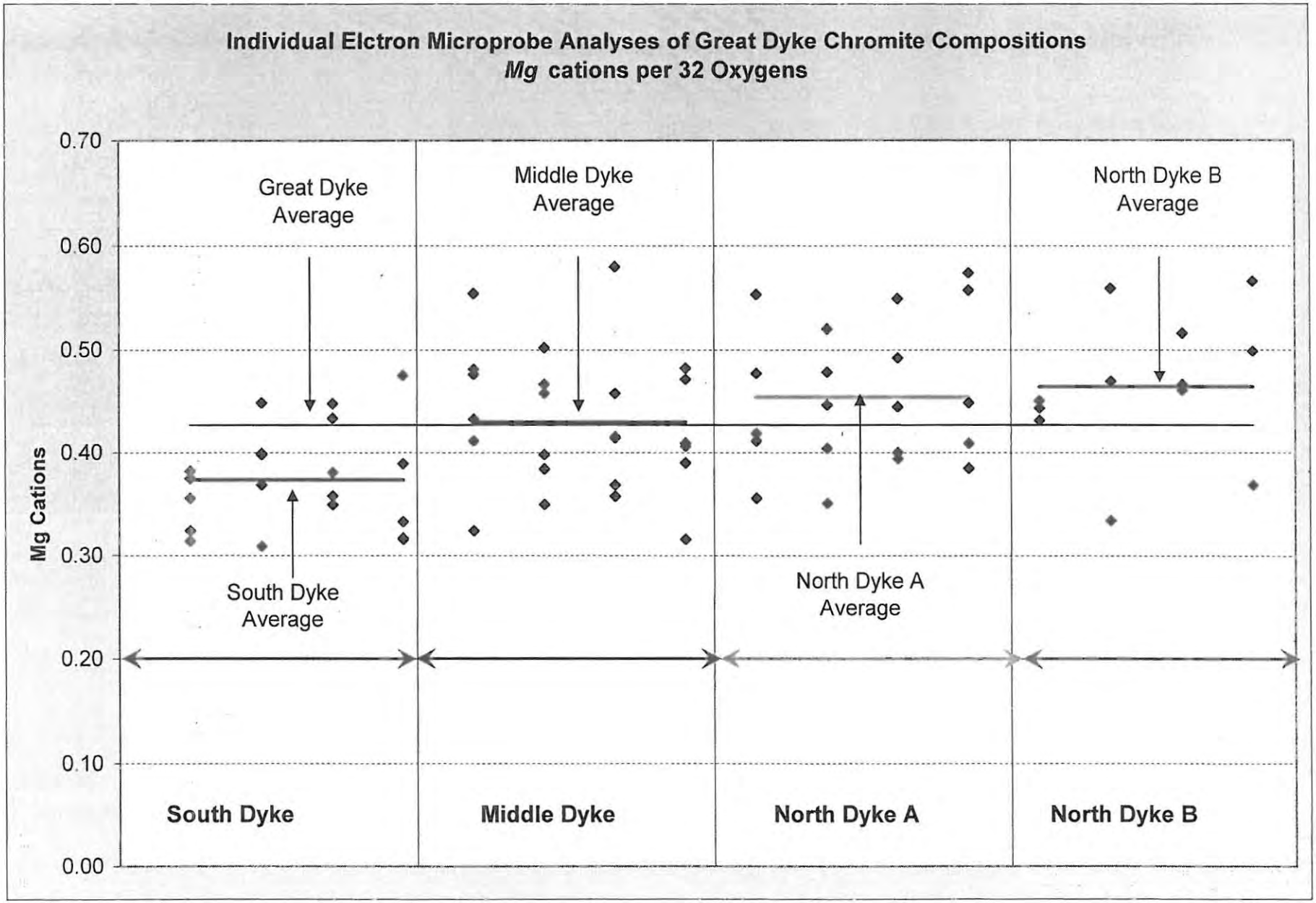
Individual Elctron Microprobe Analyses of Great Dyke Chromite Compositions
Mg cations per 32 Oxygens
Mg Cations
0.70
0.60
0.50
0.40
0.30
0.20
0.10
0.00
Great Dyke Average
Middle Dyke Average
North Dyke B Average
South Dyke Average
North Dyke A Average
South Dyke
Middle Dyke
North Dyke A
North Dyke B

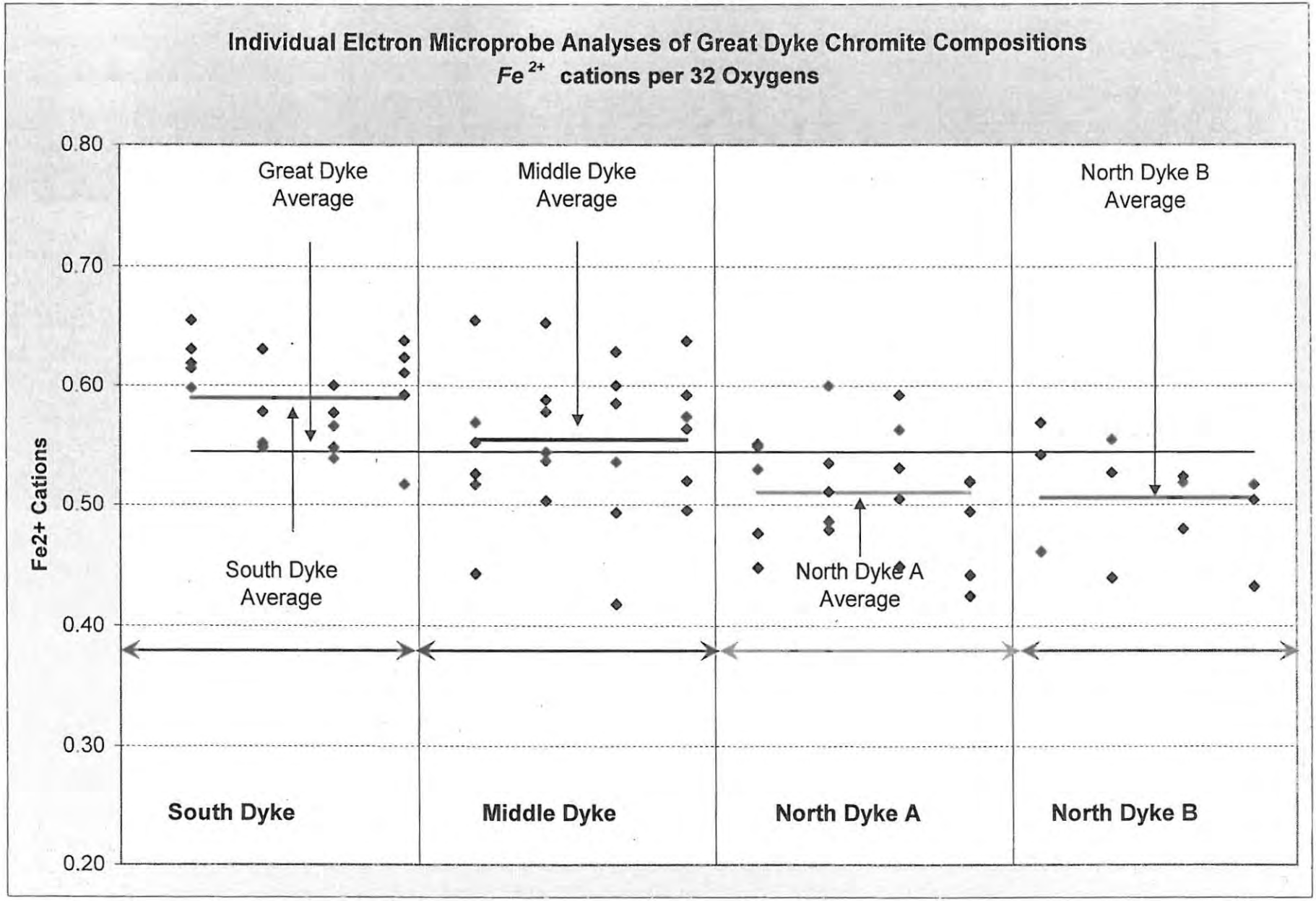
Individual Elctron Microprobe Analyses of Great Dyke Chromite Compositions
$Fe^{2+}$ cations per 32 Oxygens
Fe2+ Cations
0.80
0.70
0.60
0.50
0.40
0.30
0.20
Great Dyke Average
Middle Dyke Average
North Dyke B Average
South Dyke Average
North Dyke A Average
South Dyke
Middle Dyke
North Dyke A
North Dyke B